Understanding the Role of Vehicle Emissions as Part of Urban Air Pollution Source Complexity

Samuel Wilson

Doctor of Philosophy

University of York

Chemistry

March, 2025

Abstract

Air pollution is a major global challenge, with urban areas disproportionately affected due to high population densities and elevated pollutant concentrations. Despite advances in vehicle technology and stringent emissions legislation, road transport remains a significant source of urban air pollution. This thesis explores road transport emissions using individual vehicle measurements made with fast-response techniques to improve understanding of the complex relationship between these emissions and urban air quality. Analysis of over 600,000 remote sensing measurements from across the United Kingdom (UK) revealed decade-long trends in vehicular emissions of carbon monoxide, hydrocarbons, ammonia (NH_3), and nitrogen oxides (NO_x = NO + NO_2). The impact of national policies promoting diesel fuel use on air quality was evaluated, revealing that these policies led to an excess of 721 kt of NO_x emissions in the UK. Rising NH_3 emissions from an increasing number of gasoline and hybrid vehicles were also highlighted as a growing concern. Point sampling measurements demonstrated that vehicle exhaust location and aerodynamic properties influence near-road pollutant dispersion and concentrations, which suggests that targeting factors beyond direct emissions reduction could improve urban air quality. For example, relocating passenger car exhausts could reduce roadside pollutant concentrations by up to a third. Electric vehicles were found to disperse pollutants from fossil-fuelled vehicles, reducing near-road pollutant concentrations. Mobile monitoring in London, UK, showed that diesel and gasoline particulate filters effectively reduce particulate matter (PM) emissions, even under highly congested conditions. However, high-emitting vehicles and construction sites were identified as key sources of urban PM, indicating that non-vehicular sources are becoming increasingly important contributors to urban air pollution amidst a broader reduction in vehicle emissions.

Contents

List of Figures

List of Tables

Acknowledgements

The completion of this thesis required support from many people. First, I thank my supervisor, Professor David Carslaw, for his invaluable guidance, direction, and excellent conversation on long drives. I am also thankful to Dr Naomi Farren, my secondary supervisor, for her continued enthusiasm and support, whether at international conferences or by the roadside. I extend my thanks to Professor James Lee, also my secondary supervisor, for his encouragement throughout. I am grateful to Dr Andrew Rickard, my Independent Panel Member, for his guidance and for stepping in midway through my PhD. I have also received valuable input and insight from all members of my research group, especially Drs Jack Davison, Shona Wilde, and Rebecca Wagner.

I thank Ricardo Energy & Environment and the University of York for funding this PhD project. Ricardo Energy & Environment also played a key role in my training and the provision of data. I would like to thank Drs Louisa Kramer, Rebecca Rose, and Jasmine Wareham for their analytical support, and Alfie Nash for his technical support.

All of my colleagues at the Wolfson Atmospheric Chemistry Laboratories and the wider Chemistry Department at the University of York have made the last three and a half years very enjoyable. I am deeply grateful to my friends and family across the country for their encouragement in everything that I do.

Author's declaration

I declare that this thesis is a presentation of original work, and I am the sole author. This work has not previously been presented for an award at this University or any other. All sources are acknowledged as References. Chapters 2, 3, and 4 are based on peer-reviewed publications of which I am the lead author. Details of these articles are provided below.

Ch 2 Wilson, S., Farren, N. J., Rose, R. A., Wilde, S. E., Davison, J., Wareham, J. V., Lee, J. D., and Carslaw, D. C. **The impact on passenger car emissions associated with the promotion and demise of diesel fuel**. *Environment International* 128. (2023). p. 108330. DOI: 10.1016/j.envint.2023.108330

Ch 3 Wilson, S., Farren N. J., Bernard Y., Shaw M. D., Lee K., Crowe M., J. D. Lee, and Carslaw D. C. **Influence of Vehicle Design on Near-Road Concentrations of Traffic Related Air Pollutants**. *Environmental Science & Technology Air* 2. (2025). pp. 1089 – 1098. DOI: 10.1021/acsestair.5c00059

Ch 4 Wilson. S., Farren N. J., Wilde S. E., Wagner R. L., Lee J. D., Padilla L. E., Slater G., Peters D., and Carslaw D. C. **Mobile monitoring reveals the importance of non-vehicular particulate matter sources in London**. *Environmental Science: Processes and Impacts* 26. (2024). p. 2145. DOI: 10.1039/d4em00552j

In addition to the work presented in this thesis, I have contributed to three other publications, which are not included here but have informed and supported the development of this research. Details of these articles are provided below.

Farren N. J., Schmidt C., Juchem H., Pölher D., Wilde S. E., Wagner R. L., Wilson. S., Shaw D. S. and Carslaw D. C. **Emission ratio determination from road vehicles using a range of remote emission sensing techniques**. *Science of The Total Environment* 875. (2023). p. 162621. DOI: 10.1016/j.scitotenv.2023.162621

Wilde S. E., Padilla L. E., Farren N. J., Alvarez R. A., Wilson. S., Lee J. D., Wagner R. L., Slater G., Peters D. and Carslaw D. C. **Mobile monitoring reveals congestion penalty for vehicle emissions in London**. *Atmospheric Environment: X* 21. (2024). p. 100241. DOI: 10.1016/j.aeaoa.2024.100241

Farren N. J., Wilson. S., Bernard Y., Shaw M. D., Lee K., Crowe M. and Carslaw D. C. **An Ambient Measurement Technique for Vehicle Emission Quantification and Concentration Source Apportionment**. *Environmental Science & Technology* 58. (2024). pp. 20091 – 20100. DOI: 10.1021/acs.est.4c07907

Chapter 1

Introduction

1.1 Urban Air Pollution

Air pollution is the contamination of the environment by substances that alter the natural composition and characteristics of the atmosphere.[1] In addition to its wide-ranging environmental impacts, air pollution poses significant risks to human health, with both short- and long-term exposure linked to serious adverse effects.[2–6] In 2021, air pollution was attributed to 8.1 million deaths globally, a statistic that is dependent on a combination of pollutant concentrations and individual exposure levels.[7] Due to its largely anthropogenic origin, air pollution is present at the highest concentrations in densely populated urban areas, where the potential for human exposure is also highest. In 2022, 55% of the world's population resided in urban areas, with this value expected to rise to 70% by 2050.[8] As such, understanding and mitigating urban air pollution remains one of the most important global research priorities.

1.1.1 Pollutant Sources

Urban air pollution is a complex and dynamic problem shaped by the interactions between various pollutants, sources, and atmospheric processes. Air pollutants are classified as primary or secondary depending on their origin. Primary pollutants are emitted directly into the atmosphere from sources such as combustion and industrial processes. In contrast, secondary pollutants form in the atmosphere through chemical reactions involving primary pollutants and other atmospheric components. Research and mitigation efforts over the past few decades have primarily focused on a smaller number of major pollutants, which originate from both primary and secondary sources.[9–11] The following text describes these pollutants, their formation, and their anthropogenic sources.

Nitrogen Oxides (NO_x)

Nitrogen oxides (NO_x) refer collectively to nitrogen monoxide (NO) and nitrogen dioxide (NO_2). NO is a primary pollutant formed via high-temperature combustion, during which molecular nitrogen (N_2) in the air is oxidised. [12–14] The resulting NO molecule can then be further oxidised to NO_2, which may occur during combustion, producing primary NO_2, or later in the atmosphere, resulting in secondary NO_2.[15] This thermal NO_x formation pathway is dependent on combustion temperature and air-fuel ratio, giving different combustion sources varying NO_x emission rates.[14]

In urban areas, the primary sources of NO_x include internal combustion engines in road and other transport vehicles (Section 1.2.1), industrial combustion processes, and combustion for the generation of domestic and commercial energy, such as electricity and heat. Figure 1.1 illustrates how the total annual emissions of different NO_x sources in the United Kingdom (UK) have evolved over the past three decades using data from the UK National Atmospheric Emissions Inventory (NAEI).[16]

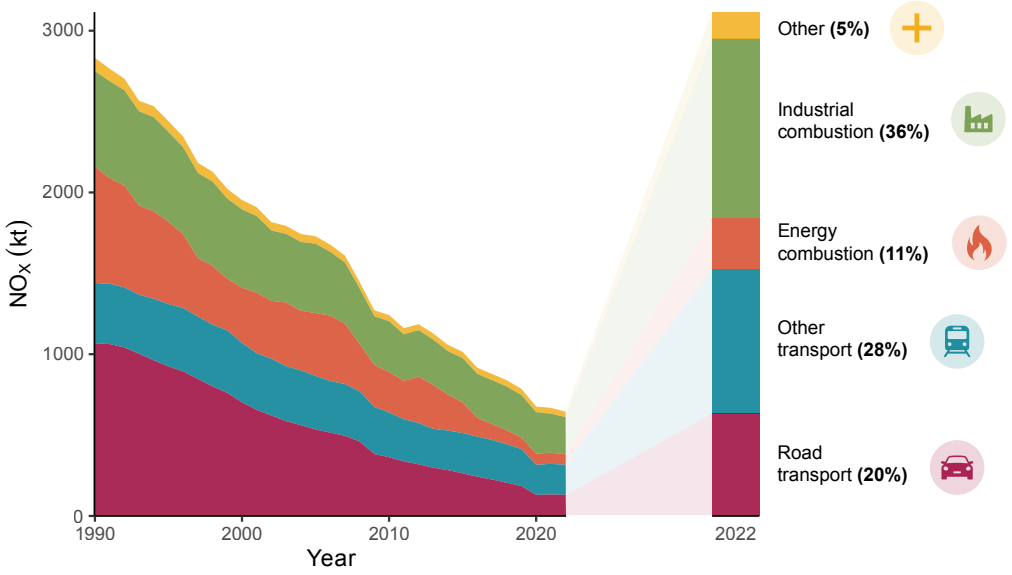

Figure 1.1: Annual UK NO_x emissions by source 1990 – 2022. The bar shows apportionment (%) for 2022. Data from the UK NAEI.[16].

Sulfur Dioxide (SO_2)

Sulfur dioxide (SO_2) is a primary pollutant produced during combustion from sulfur-containing compounds in fossil fuels. Many fuels, such as diesel, contain elemental sulfur (S) as an impurity, while others, such as coal or crude oil, contain sulfur in the form of compounds like pyrite (FeS_2) or sulfur-containing hydrocarbons (R – SH).[17]

Energy production and industrial combustion have historically been the most prevalent sources of SO_2 emissions in urban areas, with road and other transport making minor but significant contributions, as shown in Figure 1.2. [18]

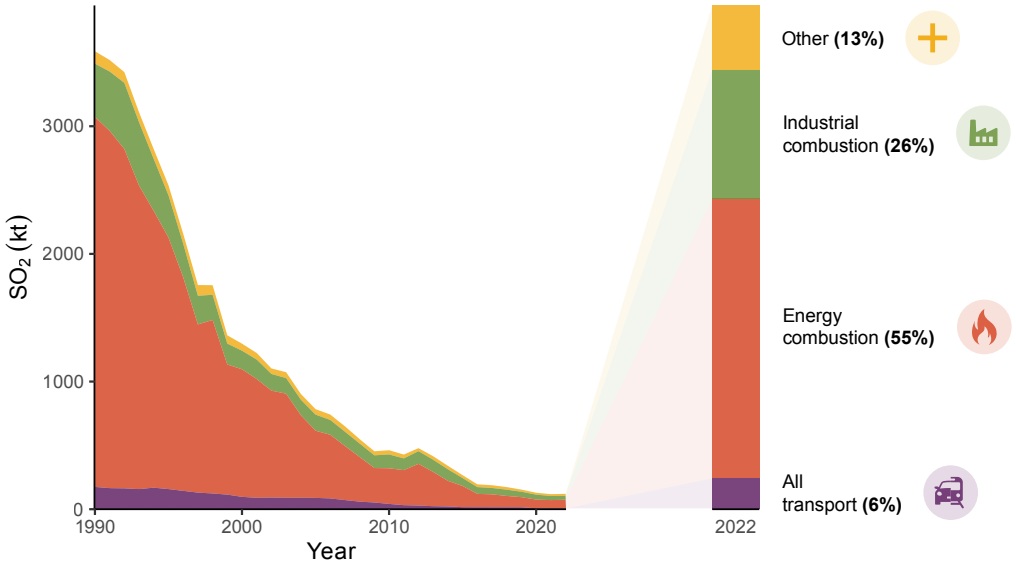

Figure 1.2: Annual UK SO_2 emissions by source 1990 – 2022. The bar shows apportionment (%) for 2022. Data from the UK NAEI.[18]

Carbon Monoxide (CO)

Carbon monoxide (CO) is a primary pollutant produced during incomplete combustion of fossil fuels. It forms when there is insufficient oxygen to fully oxidise carbon to carbon dioxide (CO_2). Given their mutual combustion origin, the major sources of CO in urban areas are similar to those of NO_x

and SO_2. Historically, road transport vehicles have been the dominant source of urban CO emissions. However, in the past two decades, as emissions from road transport have declined, combustion for energy generation has emerged as a significant contributor, shown in Figure 1.3.[19] Additional sources of CO include industrial combustion and biomass burning.[20]

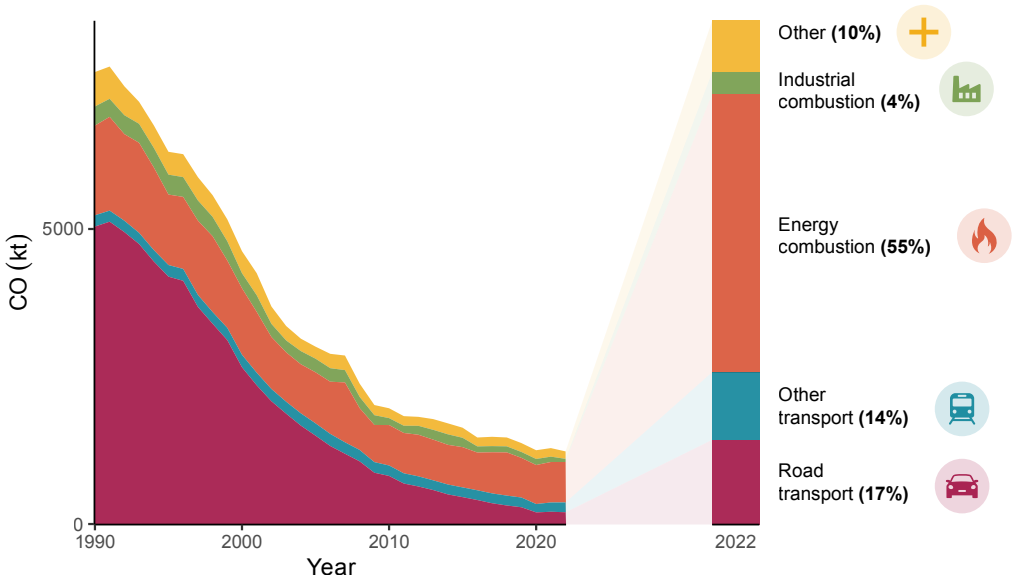

Figure 1.3: Annual UK CO emissions by source 1990 – 2022. The bar shows apportionment (%) for 2022. Data from the UK NAEI.[19]

Volatile Organic Compounds (VOCs)

Volatile organic compounds (VOCs) are a group of carbon-containing species (excluding CO_2 and methane) with high vapour pressures at room temperature, enabling them to evaporate into the atmosphere quickly. VOCs can be emitted as primary pollutants from a variety of anthropogenic and natural sources, with the former, shown in Figure 1.4, being particularly prominent in urban areas.[21, 22]

Industrial processes are the dominant source of VOC emissions in the UK. However, road transport and other internal combustion engine vehicles contribute significantly by releasing VOCs as unburnt hydrocarbons from

combustion and evaporative emissions from the fuel, screenwash, and de-icer liquids.[22–24]

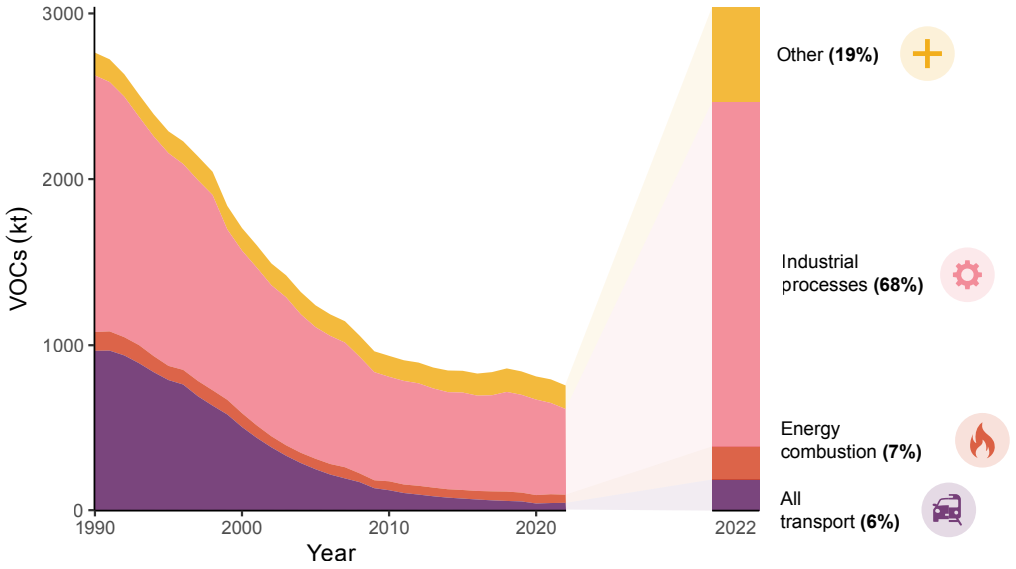

Figure 1.4: Annual UK VOC emissions by source 1990 – 2022. The bar shows apportionment (%) for 2022. Data from the UK NAEI.[22]

The diverse range of VOCs emitted in urban areas exhibit varying chemical reactivities. These reactions not only contribute to the formation of additional VOCs but also result in the production of other harmful secondary air pollutants. An important pathway for VOCs in the atmosphere is oxidation by the hydroxyl (OH) radical, which is produced from ozone in ultraviolet (UV) sunlight and reacts to form peroxy radicals (RO_2). In the presence of NO_x, this process can lead to net ozone production as discussed later in Section 1.2.3.[25, 26]

Ozone (O_3)

Tropospheric (ground-level) ozone (O_3), which is different to the stratospheric O_3 commonly referred to as the ozone layer, is a secondary air pollutant formed through photochemical reactions involving precursors such as NO_x and VOCs.[25, 26] The radical chain reaction process that results

in O_3 production is explored in detail later in this chapter (Section 1.2.3).

Urban concentrations of O_3 strongly depend on the relative balance of VOCs and NO_x in the local environment; two regimes can describe this balance. A NO_x-limited regime is one in which the rate of O_3 production increases with increasing NO_x concentrations, so the prevalent sources in Figure 1.1 are most important for O_3. In contrast, a VOC-limited regime is one in which the rate of O_3 production increases with increasing VOC concentrations, so the sources in Figure 1.4 are most important.

Ammonia (NH_3)

Ammonia (NH_3) emissions primarily originate from agricultural activities, as shown in Figure 1.5. In rural areas, NH_3 emissions result from the microbial decomposition of urea and manure, as well as volatilisation from ammonium-based fertilisers.[27, 28] In urban areas, road transport is an increasingly important source of NH_3, which is formed as an unintended by-product of the catalyst systems designed to reduce the emission of other pollutants, including NO_x, CO, and VOCs (Section 1.2.2).[29, 30] Non-vehicular sources of NH_3 in urban areas include industrial combustion catalysis, wastewater treatment plants, and waste decomposition from landfill.[31]

Although road transport is a relatively minor contributor to total UK NH_3 emissions compared to agriculture and is not reported separately in the UK NAEI, its significance is growing in urban areas. This is because NH_3 can readily react with other atmospheric species – often co-emitted from vehicle exhausts – to form particulate matter (Section 1.2.3).[32–34] Additionally, recent studies have highlighted the underestimation of NH_3 emissions in national inventories, particularly within urban environments.[35, 36] Emissions of NH_3 from road transport vehicles are explored in detail later in this chapter (Section 1.2.2).

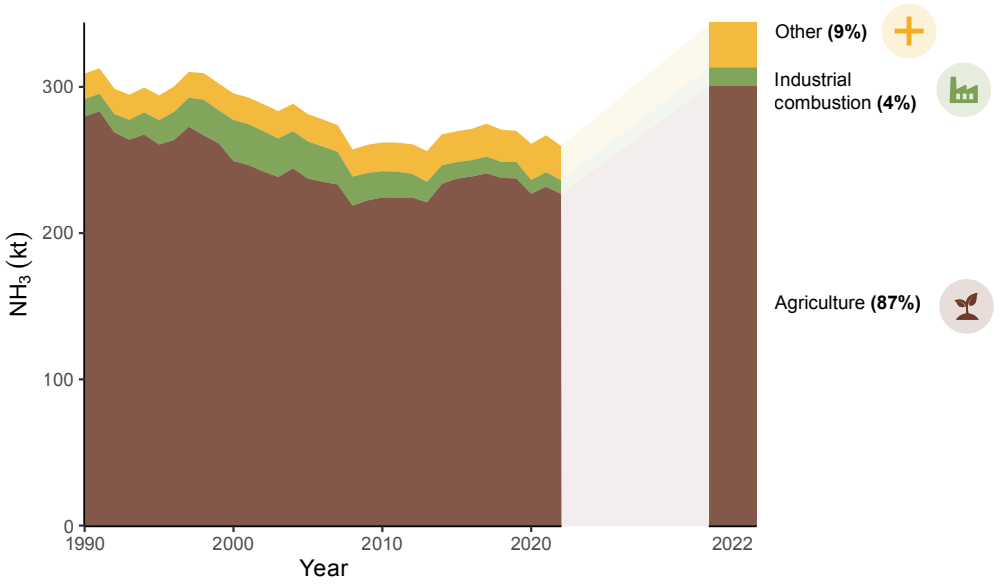

Figure 1.5: Annual UK NH_3 emissions by source 1990 – 2022. The bar shows apportionment (%) for 2022. Data from the UK NAEI.[27]

Particulate Matter (PM)

Atmospheric particulate matter (PM), also referred to as aerosol particles, consists of solid or liquid particles suspended in air. PM is typically classified based on particle diameter, with the most common size fractions being PM_{10} (particles with a diameter less than 10 µm) and $PM_{2.5}$ (particles with a diameter less than 2.5 µm). Urban PM emissions originate from both primary and secondary sources.

Primary PM is emitted directly from combustion processes, industrial activities, and construction work.[37] In urban environments, major sources include vehicle exhaust, tyre and brake wear, road dust resuspension, and emissions from domestic heating and industrial combustion.[38–40] Indoor activities, such as cooking, have also been identified as significant contributors to primary urban PM.[41, 42] Figure 1.6 shows how the total emissions of primary PM sources in the UK have evolved over the past three decades.

Secondary PM is produced in the atmosphere when gaseous precursors

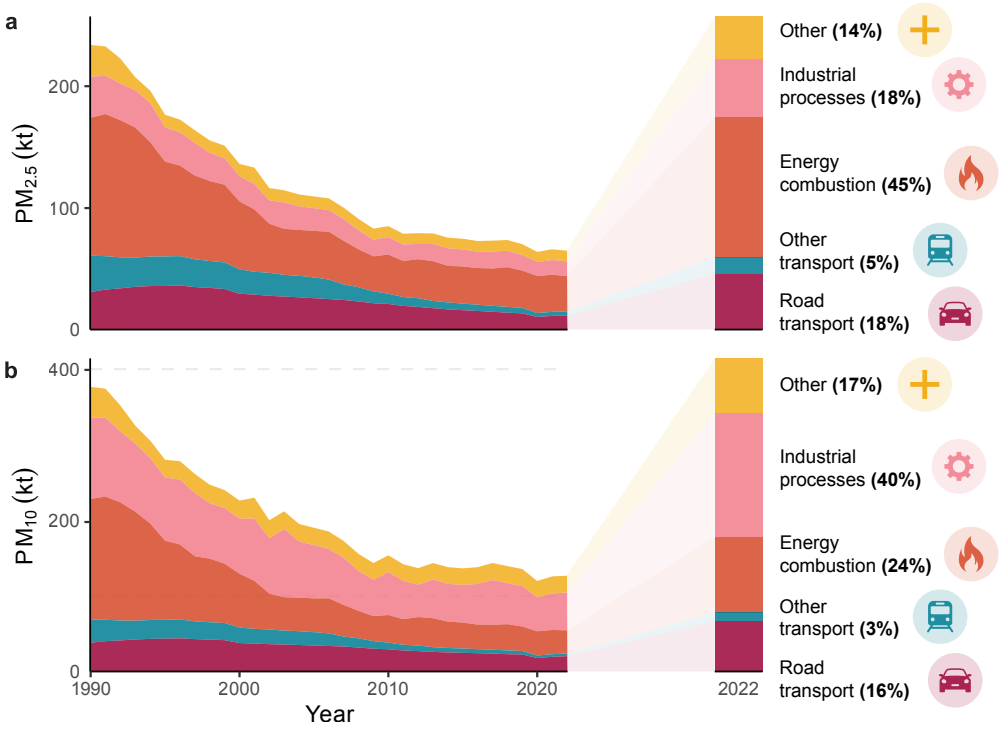

Figure 1.6: Annual UK $PM_{2.5}$ (**a**) and PM_{10} (**b**) emissions by source 1990 – 2022. The bar shows apportionment (%) for 2022. Data from the UK NAEI.[38, 39]

undergo chemical reactions, generating low-volatility compounds that form particles. Secondary organic aerosol (SOA) is produced through the multi-generational oxidation of VOCs. These oxidation products either nucleate to create new particles or integrate into existing ones.[43] Secondary inorganic aerosol (SIA) consists primarily of ammonium sulfate ($(NH_4)_2SO_4$) and ammonium nitrate (NH_4NO_3), which are formed from reactions involving NO_x, SO_2, and NH_3 (Section 1.2.3).[44]

Summary

The diverse range of primary sources and chemical interactions between major air pollutants and other atmospheric species make urban air pollution challenging to quantify and understand. Figure 1.7 provides an overview of the sources and interactions between these pollutants, highlighting their complexity. Over the past three decades, targeted research and effective

policy measures have significantly reduced the total annual emissions of major air pollutants in the UK. However, as society and technology evolve, further research on all sources of urban air pollution is essential to improve air quality.

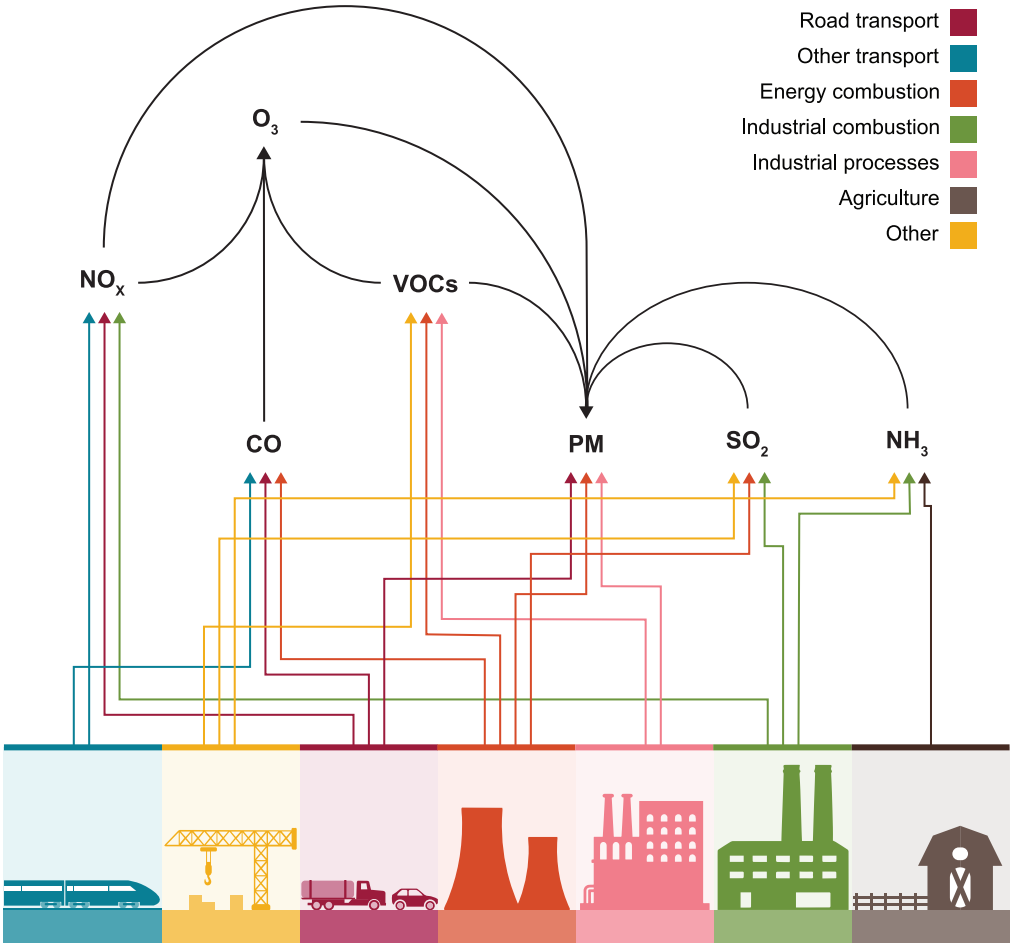

Figure 1.7: Diagram showing the three greatest sources of each major urban air pollutant in 2022 and their interactions in the atmosphere.

While the sources of urban air pollution play a significant role in determining ambient pollutant concentrations and exposure, meteorological and environmental conditions also heavily influence the dispersion and chemical transformation of pollutants in the atmosphere. Wind, temperature, humidity, and atmospheric stability can amplify or reduce pollutant emissions'

consequences.[45–47]. However, as these variables remain outside human control, the most effective strategy for improving air quality and mitigating the associated negative human health consequences is to target emissions reductions directly at their source.

1.1.2 Health and Environmental Importance

Air pollution primarily enters the body through inhalation. Once inside, the pollutant species can trigger various mechanisms that contribute to dysfunction and disease, including inflammation, oxidative stress, immunosuppression, and cellular mutagenicity.[48–53]

Many air pollutants act as irritants, affecting the eyes, upper airways, and respiratory tract. NO_2 is a potent respiratory irritant that can penetrate the lungs, triggering coughing and wheezing.[54] Although NO is less directly damaging, it reacts with O_3 in the atmosphere to form secondary NO_2. Some VOCs, such as benzene and isoprene, can cause serious eye and respiratory irritation.[55] Similarly, O_3, NH_3 and SO_2 irritate the eyes and the upper airways, increasing airway resistance.[56–58]

Long-term air pollution exposure (NO_2, SO_2, VOC, O_3, NH_3) is associated with reduced lung function, an increased risk of asthma development, and chronic obstructive pulmonary disease (COPD).[59, 60] PM, particularly $PM_{2.5}$ and $PM_{0.1}$ (ultra-fine particles with a diameter less than 0.1 μm), can penetrate deep into the lungs, causing inflammation and contributing to the progression of these conditions.[61, 62]

CO exposure uniquely causes hypoxia by binding to haemoglobin with a higher affinity than oxygen (O_2), reducing O_2 transport in the blood. Even at low concentrations, CO exposure can cause headaches due to reduced O_2 supply to the brain.[63] Long-term CO exposure is linked to cognitive decline and an increased risk of neurological diseases such as dementia and Alzheimer's disease.[64, 65] Other air pollutants also have implications for

neurological health; for example, NO_2, O_3, and $PM_{2.5}$ are associated with central nervous system dysfunction and increased incidence and progression of dementia, Alzheimer's disease and Parkinson's disease.[3, 4, 53, 65] Short-term exposure to $PM_{2.5}$ and NO_2 has also been associated with a reduction in executive cognitive function.[66, 67]

Air pollutants (NO_2, SO_2, VOCs, O_3, PM) significantly impact the cardiovascular system, with long-term exposure increasing the risk of cardiovascular disease through oxidative stress and inflammation.[60, 68–70] Air pollution exposure has been linked to diseases affecting nearly every organ system, including the liver, kidneys, pancreas, gastrointestinal system, and bones.[61] Figure 1.8 highlights a selection of medical conditions associated with air pollution exposure, as well as presenting the specific pollutants linked to each condition.[61, 71] PM is linked to conditions across multiple organ systems, largely due to its diverse chemical composition, which varies depending on its source and formation pathway.[72]

The conditions presented in Figure 1.8 are all correlated with an increase in all-cause mortality and directly affect society by decreasing life expectancy, reducing population productivity, and increasing healthcare costs. In the UK, it is estimated that outdoor air pollution is responsible for up to 43,000 annual deaths, with an associated health cost of £1.6 billion between 2017 and 2025.[73] Worldwide, these values rise to 4.1 million annual deaths and an associated health cost of £5.0 trillion in 2019, equivalent to 4.8% of the global gross domestic product (GDP).[7, 74]

Moreover, new evidence of the relationship and mechanisms by which air pollution is harmful to human health is consistently being reported. Recent research has shown that air pollution was associated with increased transmission rates of the SARS-CoV-2 virus during the COVID-19 global pandemic and that NO_x, O_3, and $PM_{2.5}$ are linked to the dysregulation of the human immune response to the virus.[75, 76] In other work, $PM_{2.5}$ has been

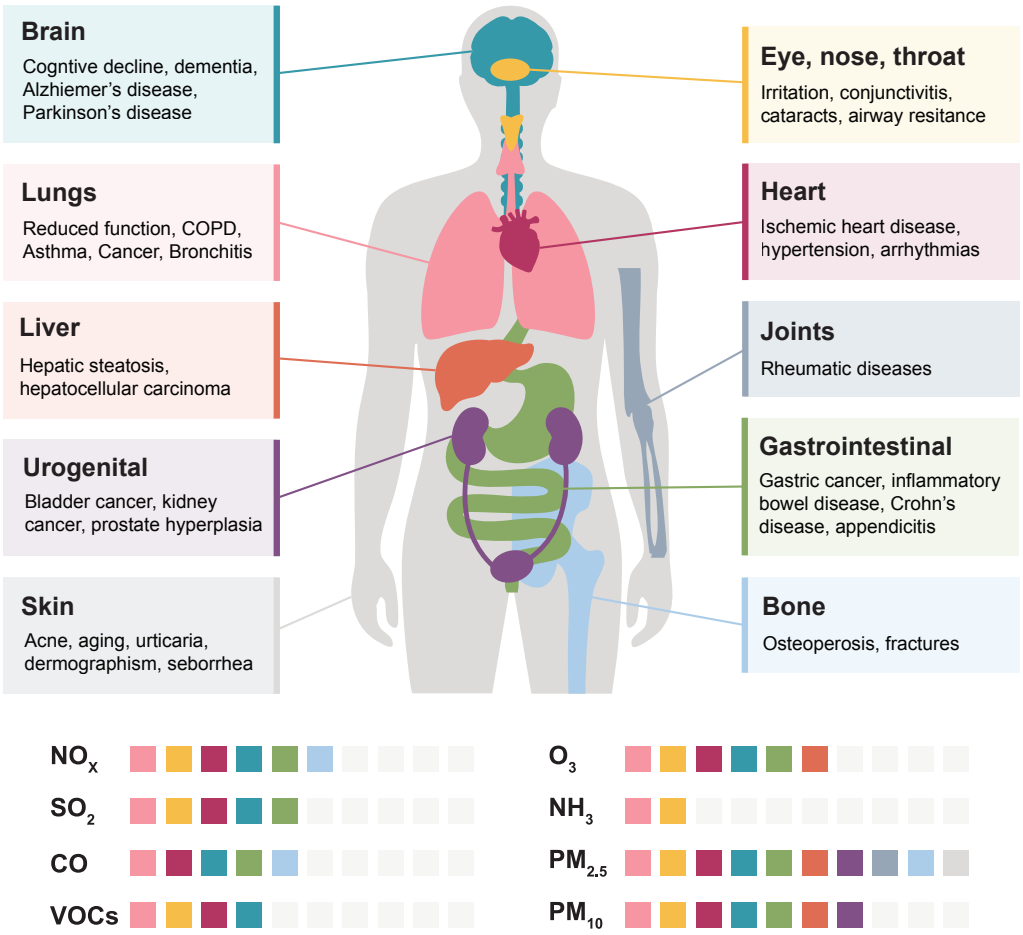

Figure 1.8: Medical conditions for different body systems associated with air pollution exposure. The coloured boxes indicate the organ systems reported to be affected by each air pollutant.

identified as a mechanism for the spread of antibiotic-resistant bacteria and genes, contributing to global antibiotic resistance.[77]

In addition to human health consequences, air pollution is responsible for a range of adverse environmental effects. NO_x and SO_2 can react with water vapour and other atmospheric species to form nitric acid (HNO_3) and sulfuric acid (H_2SO_4), major contributors to acid rain which causes ecosystem damage.[78] NO_x and NH_3 deposition in the environment, particularly in aquatic ecosystems, leads to nutrient imbalances and nitrogen enrich-

ment that can trigger eutrophication.[79, 80] O_3 directly inhibits plant growth by causing oxidative stress and damaging chloroplasts.[81, 82] This leads to vegetation damage, reducing diversity and lowering crop yields.[83]

Urban air pollution also has important implications for climate change, with many air pollutants sharing sources with greenhouse gases (GHGs) and either directly or indirectly influencing atmospheric heat retention. [84, 85] However, while climate change is a significant global challenge, the focus of this thesis is on the local air quality consequences of pollutant emissions. Understanding and addressing these localised effects is essential for protecting public health and preventing environmental harm.

The local air quality health and environmental impacts of air pollution are directly dependent on exposure, with sources that lead to higher concentrations or prolonged exposure posing the most significant risk. While advancing our understanding of the health effects of urban air pollution remains essential, it is equally important to continue to investigate the sources and interactions that ultimately determine human and environmental exposure. Research focusing on sources that contribute disproportionately to high-exposure scenarios offers the most effective pathway for immediate mitigation, particularly in urban environments where the majority of the world's population resides.

1.1.3 Current Trends

In the UK and many other regions worldwide, total annual emissions of many air pollutants have steadily declined over the past three decades.[86–89] This trend is reflected in ambient urban air pollution concentrations, which are measured through extensive global networks of monitoring sites.[90] These sites provide the most reliable indication of urban population exposure to air pollution. Figure 1.9 shows the annual mean urban background concentrations of six pollutants monitored by 140 sites in the UK's Ambient Urban

and Rural Network (AURN).[91] A decline in urban ambient concentrations of all pollutants except O_3 has been observed in the UK; O_3 is more difficult to mitigate due to its complex secondary formation (Section 1.2.3).

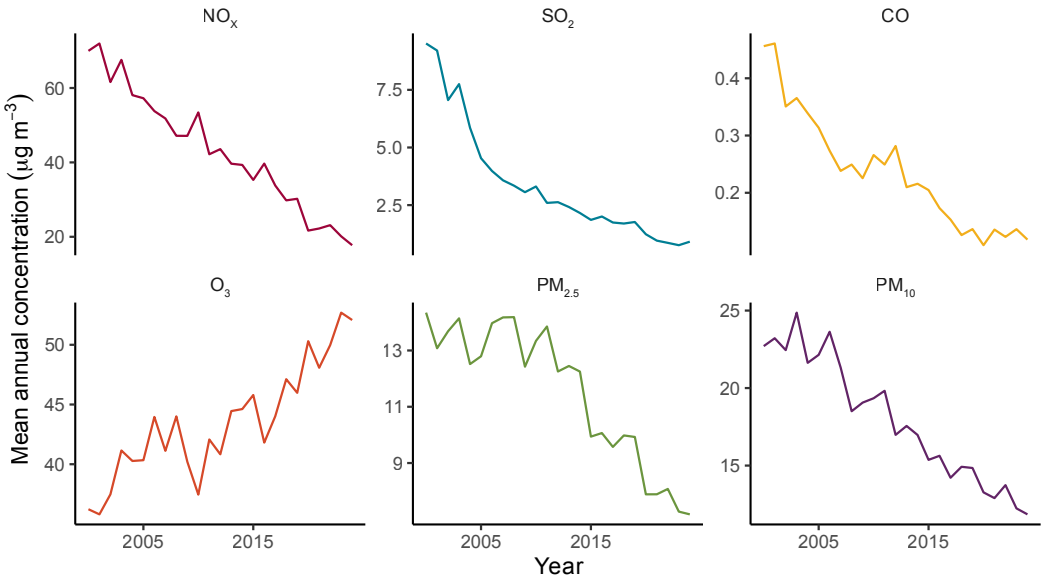

Figure 1.9: Mean annual concentrations of NO_x, SO_2, CO, O_3, $PM_{2.5}$, and PM_{10} at UK AURN urban background sites for the years 2000 – 2024.[91]

The decreasing ambient concentrations of many pollutants are a direct result of air pollution research, which has shaped policies and driven emissions reductions. However, no 'safe' air pollution level has been identified, and an ageing, growing population continues to amplify health impacts even as concentrations decline. The health benefits of further reductions in air pollution are therefore expected to increase more rapidly in the future, emphasising the need for continued research and policy advancements.[92]

The World Health Organization (WHO) published updated Air Quality Guidelines (AQGs) in 2021 for short-term (24-hour) and long-term (annual) exposure to six air pollutants: NO_2, SO_2, CO, O_3, $PM_{2.5}$, and PM_{10}. These guidelines, presented in Table 1.1, exclude VOCs and NH_3 because their health impacts are primarily indirect, contributing towards the formation of

secondary pollutants like O_3 and PM.

Table 1.1: Updated WHO 2021 Air Quality Guidelines.

Pollutant	**Averaging time**	**AQG value (µg m^{-3})**
NO_2	Annual	10
	24-hour	25
SO_2	24-hour	40
CO	24-hour	4000
O_3	Annual	60
	24-hour	100
$PM_{2.5}$	Annual	5
	24-hour	15
PM_{10}	Annual	15
	24-hour	45

The guideline limit values are evidence-based recommendations which reflect the lowest concentrations at which the guideline developers could be confident of an adverse health effect. It is estimated that 99% of the world's population currently live in areas that exceed these guideline concentration limits.[93] Moreover, there are many areas of the world in which emissions of air pollutants are increasing, particularly in developing lower- and middle-income nations.[88, 89] In 2019, 95% of the 4.1 million deaths attributed to outdoor air pollution occurred in these regions, where populations are exposed to 1.3 to 4 times higher pollutant concentrations.[7, 74]

1.1.4 The Role of Vehicle Emissions

Road transport plays an essential role in modern society, particularly in urban areas, where it facilitates the large-scale movement of passengers and freight. Unlike other modes of transport, road vehicles are resilient to weather conditions and not constrained by station or port access. Furthermore, their economic and practical accessibility makes private vehicle ownership feasible for the majority of the population. As of December 2023, there were 41.2 million licensed road vehicles in the UK, 81.6% of which were passenger cars.[94]

In addition to its role in society, road transport is a major contributor to urban air pollution, specifically traffic-related air pollution (TRAP). Since the mid-19th century, road vehicles have relied on fossil fuel combustion for power.[95] While the nature of the fuels, technologies, and pollutants of concern have evolved, as illustrated in Figure 1.10, the link between road vehicles and urban air pollution has remained significant.[96–104]

In 2025, road transport remains an important contributor to urban air pollution. As shown in Figure 1.7, it is among the top three sources for NO_x, CO, and PM. However, its impact extends beyond this, contributing to the emission or formation of all major air pollutants. This complexity is illustrated in Figure 1.11, which outlines the pathways through which road transport contributes to urban air pollution.

The importance of road transport in urban air pollution is amplified by its continuous and transient nature as an emission source, coupled with its proximity to the general population. Other significant sources, such as industrial plants and power stations, are relatively few in number, stationary, and subject to strict regulations.[105] These stationary sources can also often be located in remote areas to minimise human exposure. In contrast, the road transport sector in the UK alone comprises over 40 million individual, highly mobile emission sources that move unpredictably through space and

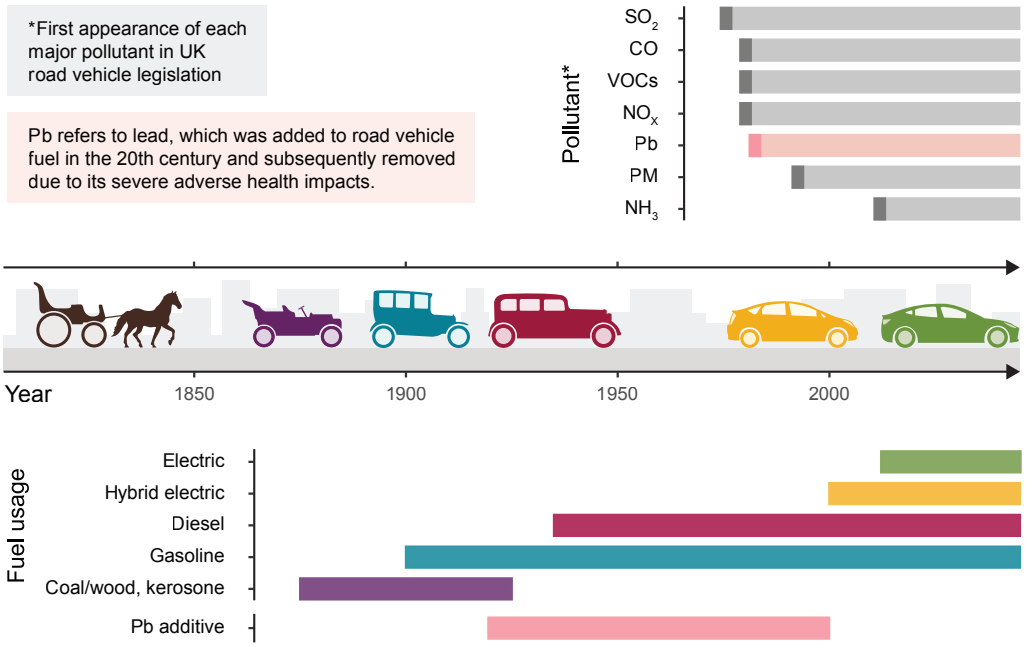

Figure 1.10: Timeline of road transport technology, fuel use, and associated air pollutants of concern. Pollutants are shown at their first appearance in UK motor vehicle legislation [100–104].

time, often through the nation's most densely populated regions. Even vehicles that appear identical - sharing the same manufacturer, engine model, and fuel type - can exhibit significant differences in their emissions output. These variations, which add considerable complexity to the quantification of road vehicle emissions, stem from factors such as traffic conditions, ambient environmental conditions, driver behaviour, and differences in vehicle maintenance.[106–109]

Many of the health and environmental effects outlined in Section 1.1.2 have been directly linked to TRAP.[110] These include damage to the respiratory and cardiovascular systems, the onset of asthma, and increased rates of acute respiratory infections in children.[5, 111] Given the widespread use and proximity of road vehicles to populations, their emissions pose a consistent and high exposure risk to surrounding pedestrians and residents, as well

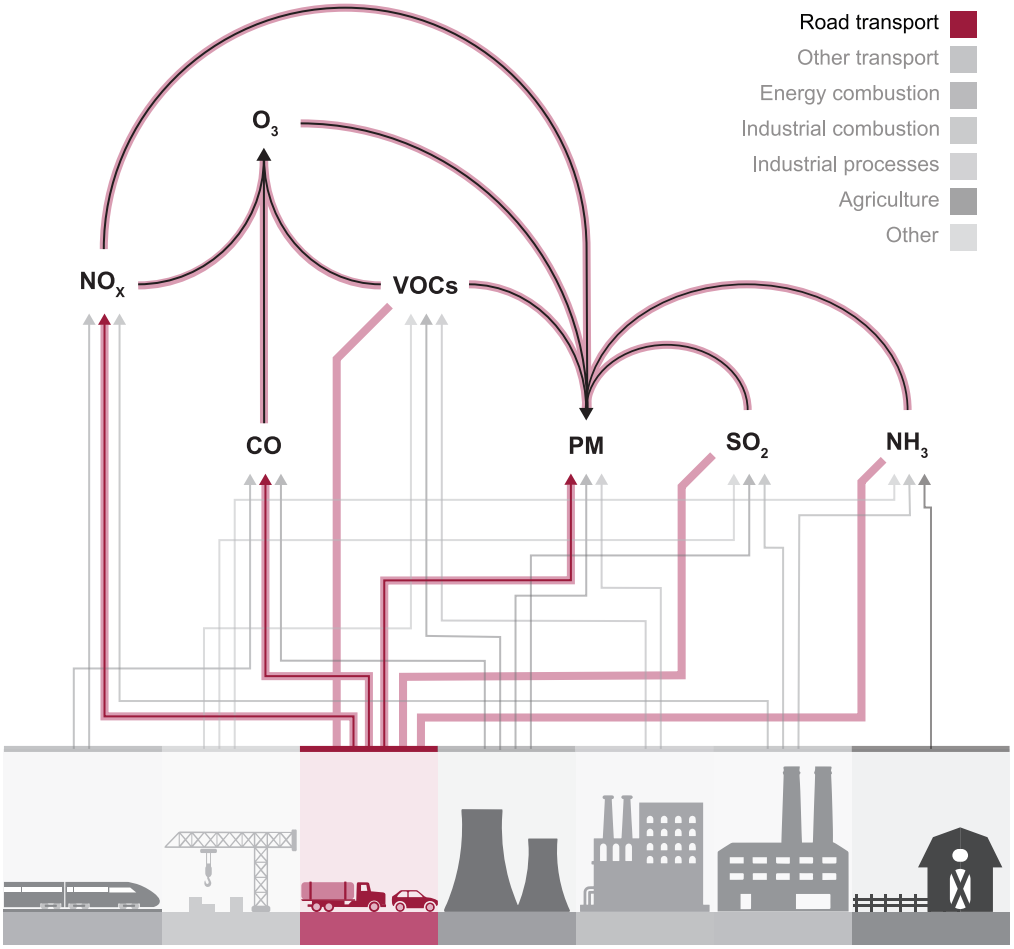

Figure 1.11: Modified diagram showing sources and interactions between air pollutants. The red lines highlight the pathways through which road transport contributes.

as vehicle drivers.[112–114] For these reasons, reducing emissions from road vehicles has been a key focus of urban air pollution mitigation efforts.

In the UK and other high-income nations, road transport emissions have steadily declined over the past three decades.[87, 90] Despite this, the rapid growth of urban populations and vehicle usage continues to exert pressure on air quality, necessitating innovative approaches to manage TRAP emissions effectively. Recent mitigation strategies in urban areas include investment in public transportation infrastructure to reduce total traffic volume, the

implementation of low-emission zones to remove the most polluting vehicles from urban centres (Section 1.3.2), and the promotion of electric vehicles (EVs).[115–119]

EVs eliminate exhaust emissions from road transport by replacing combustion engines with (locally) emission-free electric drivetrains. Although the electricity used to power EVs may still be generated via fossil fuel combustion, EVs have consistently been reported to offer efficiency advantages and lower GHG emissions overall.[120, 121] From an air quality perspective, EVs provide enormous benefits over combustion-powered vehicles, as they eliminate the exhaust portion of local road transport emissions.[120, 122] However, EVs still contribute to non-exhaust PM emissions, such as those from brake and tyre wear (Section 1.2.4). These emissions can sometimes exceed those of combustion-powered vehicles due to the added weight of the electric drivetrain.[123]

Despite the seemingly rapid adoption of EVs, only 3.2% of the UK vehicle fleet is currently electric-powered.[124] Even with a growing number of new EV registrations each year and the UK government's planned ban on new fossil-fuelled light-duty vehicle sales by 2035, the average passenger car lifespan (currently 18 years or 200,000 km and rising) means that a complete transition to an EV-dominated fleet will likely take several decades.[125, 126] Therefore, the air quality benefits associated with EVs may not be fully realised for many years. Moreover, during this transitional period, hybrid-electric drivetrains - combining electric and combustion power — are becoming increasingly common, currently accounting for 6.2% of the UK vehicle fleet.[124] It is essential that research on road transport emissions keeps pace with these evolving technologies to ensure that their air pollution implications are fully understood.

In low- and middle-income nations, the electrification of road transport is progressing at a significantly slower rate, if at all.[127] These regions face

a greater burden of TRAP, as older, more polluting vehicles retired from high-income nations are often exported to low- and middle-income countries. [128] Consequently, road transport emissions will remain a global concern for decades. Understanding the complex interactions between vehicle emission characteristics, urban environments, and atmospheric chemistry is, therefore, essential to developing targeted and sustainable solutions for reducing vehicle emissions and their associated adverse health consequences.

1.2 Chemistry of Vehicle Emissions

Modern road vehicles produce air pollutant emissions through a variety of mechanisms. Engine combustion generates emissions that are chemically transformed in exhaust after-treatment systems before being released into the atmosphere, where further reactions can take place. In addition to exhaust emissions, vehicles also emit pollutants through evaporative processes from onboard fluids and through abrasive wear of components like brakes, tyres, and road surfaces. Vehicle movement can also resuspend road dust, acting as an additional source of PM. The amount and composition of these emissions can vary widely depending on factors such as fuel type, operating conditions, ambient environment, and driving behaviour. This section examines the pathways through which road vehicles emit both primary and secondary air pollutants, with a focus on those described in Section 1.1.

1.2.1 Combustion Products

Fossil fuel combustion has been the primary energy source for road transport vehicles for over a century, with gasoline (petrol) and diesel serving as the dominant fuels in the UK. Both fuels are composed of hydrocarbon mixtures with minor differences in their compositions.[129] Engine-out emissions are pollutants generated directly by fuel combustion within the vehicle's internal combustion engine (ICE) before undergoing any processing in the exhaust system. Once treated by after-treatment technologies, these emissions are partially chemically transformed into what is released as exhaust emissions from the vehicle's tailpipe. Prior to the development of after-treatment systems, engine-out and exhaust emissions were identical.

ICEs operate by converting chemical energy in the fuel into mechanical energy. The basic principles involve compressing a fuel-air mixture within a cylinder and igniting it to produce high-pressure gases that drive

pistons, which in turn power the vehicle's drivetrain. ICE technology has evolved significantly over decades, with advancements in combustion control and engine-out emissions reduction, making them more efficient and less polluting than earlier generations.

Engine-out emissions from road vehicles are produced during the high-temperature combustion of hydrocarbon fuel in the presence of oxygen and nitrogen from the intake air. Most of the hydrocarbons are fully oxidised to CO_2 and water in complete combustion, illustrated for octane (C_8H_{18}) in Reaction 1.1. The products of complete combustion – CO_2 and water – along with unreacted oxygen and nitrogen from the intake air typically account for over 99.9% of the engine-out emissions.[130] The remaining fraction of the exhaust gases consists of various air pollutants.

$$2\ C_8H_{18} + 25\ O_2 \longrightarrow 16\ CO_2 + 18\ H_2O \tag{1.1}$$

If oxygen is insufficient for complete combustion, incomplete combustion results in the formation of CO and PM in the form of black carbon (BC), as illustrated in Reactions 1.2 and 1.3.

$$2\ C_8H_{18} + 17\ O_2 \longrightarrow 16\ CO + 18\ H_2O \tag{1.2}$$

$$2\ C_8H_{18} + 13\ O_2 \longrightarrow 8\ C\ (BC) + 8\ CO + 18\ H_2O \tag{1.3}$$

Under the high-temperature conditions of combustion, N_2, which constitutes the majority of the intake air, is oxidised via the *Zel'dovich mechanism*. This series of reactions involving molecular nitrogen, oxygen, and OH radicals results in the formation of NO, as shown in Reactions 1.4 to 1.6.[12–14]

$$N_2 + O \rightleftharpoons NO + N \tag{1.4}$$

$$N + O_2 \rightleftharpoons NO + O \tag{1.5}$$

$$N + OH \rightleftharpoons NO + H \tag{1.6}$$

Primary NO_2 can also be formed during combustion through the further reaction of NO with oxidant species, as shown in Reaction 1.7. However, the majority of NO_2 from road transport derived NO is produced after exhaust emission via secondary reactions in the atmosphere (Section 1.2.3).

$$NO + HO_2 \rightleftharpoons NO_2 + OH \tag{1.7}$$

Engine-out emissions may also include air pollutants derived from the hydrocarbon fuel, its additives, and impurities. The fuel itself is a complex mixture of thousands of alkane, alkene, and aromatic hydrocarbon (HC) species.[129] When these HC compounds are not fully oxidised during combustion, they can be emitted as unburnt or partially burnt hydrocarbons, serving as a source of VOCs.

Hydrocarbon fossil fuels, particularly diesel, often contain sulfur impurities, which produce SO_2 during combustion, as shown in Reaction 1.8. In the UK, legislation regulating sulfur content in road transport fuels during the 1990s and early 2000s has led to widespread use of sulfur-free fuels, resulting in a large reduction in SO_2 emissions from road transport.[131]

$$2\,C_8H_{18}S + 27\,O_2 \longrightarrow 16\,CO_2 + 18\,H_2O + 2\,SO_2 \tag{1.8}$$

Modern engines also require lubricants (engine oil) to operate. These lubricants are used within the engine to reduce friction, and small amounts are burnt during combustion. Unlike fuels, engine lubricants are less strictly regulated, and most formulations contain sulfur-based compounds, such as zinc dialkyl dithiophosphates (ZDDPs), to protect engine components and reduce wear.[132] Consequently, the combustion of engine lubricants can emit SO_2, amongst other air pollutants, including primary PM.[133, 134] This is particularly problematic when more significant amounts of lubricant are burned due to engine wear or malfunction.

One of the most infamous fuel additives from an air quality perspective is tetra-ethyl lead (TEL), which was introduced in the 1920s to enhance engine performance (Figure 1.10).[135] During combustion, TEL is converted into various lead-containing compounds that, when emitted into the atmosphere, have severe adverse effects on human health. Consequently, TEL was subjected to strict regulation and was banned entirely from road transport fuels in the UK by 2000.[103] While TEL's historical significance to road transport air quality is notable, its removal from road fuels has successfully mitigated its harmful impacts, and it is not a focus of this thesis.

More recently, biofuel blends containing part fossil fuel and part fuel derived from biomass have been introduced in the UK and globally to offset CO_2 GHG emissions from road transport and help mitigate climate change. These blends include E5 and E10 gasoline, which contain up to 5% and 10% bioethanol, respectively, and B7 diesel, which contains up to 7% bio-derived diesel.[136, 137] While biofuel blends have been reported to have a minor impact on the relative emissions of NO_x, PM (BC), and VOCs (HC) through differences in fuel chemistry and engine operation, research in this area remains inconclusive.[138–140] The addition of biomass-derived fuels further complicates the interactions between vehicle emissions and air quality.

In addition to gasoline and diesel, road vehicles can also utilise alternative fossil fuels such as Compressed Natural Gas (CNG) and Liquefied Petroleum Gas (LPG). These alternatives can be used in modified diesel and gasoline ICEs, respectively. In the UK, adoption of these fuels remains minimal, with CNG and LPG vehicles constituting less than 0.1% of the road vehicle fleet. [124] Similar to biofuel blends, alternative fossil fuels have been reported to have a negligible impact on the relative emissions of combustion-derived pollutants.[141, 142] While this thesis does not address alternative fossil fuels or biofuel blends directly, both areas require further exploration, particularly biofuel blends, as their global usage is expected to grow.

Engine-out emissions from diesel and gasoline vehicles differ significantly due to their combustion processes. Gasoline engines primarily operate using spark ignition (SI), where a spark plug ignites an air-fuel mixture maintained at or near a stoichiometric ratio, ensuring neither air nor fuel is in excess. [143] In practice, gasoline engines often operate slightly lean (excess air) or rich (excess fuel) as they regulate this balance using an intake air throttle. In contrast, diesel engines utilise compression ignition (CI), where air is compressed to high pressures and temperatures, and fuel is directly injected into the combustion chamber, auto-igniting upon contact with the hot air. [129] Unlike gasoline engines, diesel engines are un-throttled and always operate under lean conditions, regulating power through control of fuel injection. These differences result in distinct characteristics in engine design, operation, and emissions output.

Although diesel combustion occurs under overall lean conditions, localised regions of fuel-rich mixtures arise, resulting in a slower, diffusion-dominated combustion process.[139] This approach promotes high thermal efficiency but also generates high in-cylinder temperatures. Due to their high efficiency and the high torque associated with greater compression ratios, diesel ICEs are predominantly used in larger vehicles, such as heavy goods

vehicles (HGVs) and most light goods vehicles (LGVs); many passenger cars in the UK and Europe are also diesel-powered. In contrast, because gasoline combustion is optimised to maintain a stoichiometric air-fuel ratio, faster flame propagation and lower in-cylinder temperatures can be achieved.[143] However, this comes at the expense of efficiency due to throttling losses and the lower compression ratios necessary to ensure unwanted air-fuel autoignition (knock) does not occur. As a result, gasoline ICEs are primarily used in passenger cars and smaller vehicles, such as motorcycles.

With respect to engine-out emissions, diesel engines produce higher levels of NO_x and PM because of the heterogeneity of the air-fuel mixture and elevated in-cylinder temperatures.[144] Localised fuel-rich zones during combustion contribute to PM formation, while the high temperatures facilitate NO_x generation. Gasoline engines emit lower levels of NO_x and PM because of their stoichiometric combustion and more effective mixing of air and fuel. However, gasoline engines tend to produce higher levels of CO and HC/VOCs due to incomplete combustion at low loads when a stochiometric air-fuel ratio cannot be maintained.[145]

The differences in combustion technology and engine-out emissions have significant implications for the development of emission control systems. In gasoline engines, near-stoichiometric combustion ensures that exhaust gases consist of CO_2, water, engine-out pollutants, and a small amount of intake air. This composition allows for the effective integration of emission control systems and is the reason why gasoline combustion is optimised for stoichiometric air-fuel ratios, even though lean gasoline combustion is a more efficient alternative.[129] Diesel engines, however, must operate under lean conditions, where a significant portion of the exhaust gas includes oxygen from the intake air. This presents a considerable challenge for emission control systems, making the development of effective after-treatment technologies for diesel engines far more complex than for gasoline engines.

1.2.2 Emission Control Systems

To comply with increasingly stringent vehicle emission regulations (Section 1.3.1) over the past 50 years, manufacturers have developed a variety of systems to reduce engine-out emissions. These may be integrated into the ICE itself or installed downstream in the vehicle's exhaust as part of an exhaust after-treatment system. Due to differences in combustion technology and exhaust gas composition, gasoline and diesel ICEs employ different emission control systems, each relying on different chemical mechanisms to transform or capture engine-out pollutants.

1.2.2.1 Gasoline Technology

Emission control in gasoline vehicles has been achieved through catalytic converter technology. Catalysis accelerates chemical reactions using a catalyst - a substance that is not consumed and remains unchanged during the reaction. Catalytic converters contain precious metal catalysts such as platinum, palladium, and rhodium, which are coated onto a metal or ceramic substrate and contained within the exhaust system.[146] As exhaust gases pass over the catalyst, engine-out pollutants are chemically transformed.

Two-way Catalyst

Early gasoline catalytic converters, introduced in the 1970s, relied on oxidation to convert CO and HC into CO_2, as shown in Reactions 1.9 and 1.10, where HCs are represented by methane (CH_4). These two-way catalysts (oxidation catalysts) were named for their ability to oxidise both CO and HC.

$$2\,CO + O_2 \longrightarrow 2\,CO_2 \tag{1.9}$$

$$CH_4 + 2\,O_2 \longrightarrow CO_2 + 2\,H_2O \tag{1.10}$$

Three-way Catalyst (TWC)

In the late 1970s, three-way catalysts (TWCs) replaced two-way catalysts, adding the ability to reduce NO_x to nitrogen gas. The additional processes occurring in a TWC are outlined in Reactions 1.11 – 1.13, where HCs are represented by methane. The hydrogen in Reaction 1.13 is also produced in the TWC via hydrocarbon steam reformation and the water-gas shift reaction between CO and water.[146, 147]

$$2\ NO + 2\ CO \longrightarrow N_2 + 2\ CO_2 \tag{1.11}$$

$$2\ NO + CH_4 + O_2 \longrightarrow N_2 + CO_2 + 2\ H_2O \tag{1.12}$$

$$2\ NO + 2\ H_2 \longrightarrow N_2 + 2\ H_2O \tag{1.13}$$

TWCs require near-stochiometric combustion to function effectively. If the engine runs rich (excess fuel), there is insufficient oxygen in the exhaust gas to oxidise CO and HC. If the engine runs lean (excess air), oxygen binds to the catalyst surface, preventing the reduction of NO_x.[148] Achieving stochiometric combustion and the correct exhaust gas composition for optimum TWC operation requires precise control through a series of engine and exhaust sensors.

Since its introduction, TWC technology has evolved with more efficient catalyst materials and substrate structures, improving performance and durability.[149] TWCs have been a technological success story, substantially reducing exhaust emissions from gasoline vehicles for decades.[86] However, over time, catalyst surface and control system degradation can reduce TWC efficiency and, in some cases, lead to the formation of new pollutants.

Under rich combustion conditions, resulting from control system malfunction or degradation, TWCs can reduce NO_x to NH_3; one such pathway is shown in Reaction 1.14.[147, 150] This introduces NH_3 as an exhaust pollutant that was absent in the engine-out emissions. Gasoline TWCs are the largest source of urban NH_3, contributing to the formation of secondary PM (Section 1.2.3).

$$2\,NO + 2\,CO + 3\,H_2 \longrightarrow 2\,NH_3 + 2\,CO_2 \tag{1.14}$$

Gasoline Particulate Filter (GPF)

While TWCs address gaseous engine-out pollutants, they do not reduce PM emissions. Although gasoline ICEs typically produce less PM than their diesel counterparts, the growing adoption of gasoline direct injection (GDI) technology in the late 2000s, which improves performance and fuel economy, led to increased gasoline PM emissions.

Gasoline particulate filters (GPFs) were widely introduced in the early 2010s.[151] GPFs physically capture and trap PM emissions while allowing exhaust gases to pass through. The captured particles are then burned off through periodic passive or active regeneration, where high temperatures oxidise PM into CO_2.[151] GPFs can be installed downstream of the TWC or integrated within a single after-treatment system combining both technologies.[152] Figure 1.12 provides an overview of the engine-out and exhaust emissions from gasoline ICEs.

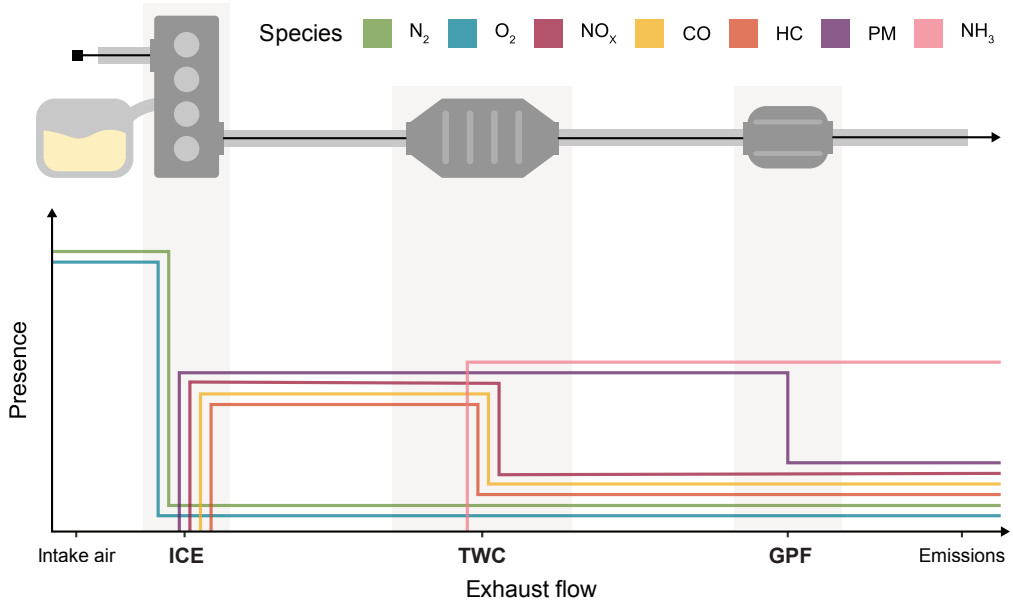

Figure 1.12: Gasoline ICE exhaust diagram showing the presence, creation, or removal of each pollutant throughout the different emission control systems. The presence is not quantitative and is intended only to illustrate the direction in which pollutant concentrations are likely to change.

1.2.2.2 Diesel Technology

Emission control in diesel vehicles presents unique challenges due to lean combustion, which produces exhaust gas with excess oxygen. As a result, the TWCs discussed in Section 1.2.2.1 are ineffective for diesel ICEs because oxygen in the exhaust prevents the chemical reduction of NO_x. As a result, alternative emission control technologies have been developed.

Diesel Oxidation Catalyst (DOC)

Similar to gasoline vehicles, diesel oxidation catalysts (DOCs) have been used since the 1970s to reduce CO and hydrocarbon (HC) emissions via Reactions 1.9 and 1.10.[148] However, because diesel combustion is lean, DOCs were not replaced by TWCs, and instead, DOCs persist as a key technology in modern diesel ICEs, with continued refinement over time. One drawback

of DOCs is their ability to oxidise NO to NO_2, increasing the fraction of the more harmful NO_2 in total NO_x emissions.[153]

Exhaust Gas Recirculation

The first dedicated NO_x control technology for diesel vehicles was exhaust gas recirculation (EGR), also introduced in the 1970s. EGR is an engine-based system designed to reduce engine-out NO_x emissions and not an after-treatment system. It functions by redirecting a portion of the exhaust gas back into the combustion chamber, displacing the intake air (and associated oxygen) and lowering peak combustion temperatures, which reduces NO_x formation.[154]

Similar to DOCs, EGR technology is still in use today, with many modern EGR systems incorporating heat exchangers to cool the exhaust gas before recirculation, improving efficiency.[154] However, EGR adds complexity to diesel ICEs, requiring additional moving parts and valves that can become blocked by carbon build-up over time.[155] Additionally, EGR can increase PM emissions due to lower combustion temperatures and incomplete combustion resulting from reduced oxygen availability.

Diesel Particulate Filter (DPF)

To control PM emissions, diesel particulate filters (DPFs) were introduced in the late 2000s.[29] DPFs operate on the same principles as GPFs but were developed and adopted earlier due to the higher PM emissions from diesel vehicles, particularly following the uptake of EGR technology (Section 1.2.2.1). In recent work, DOCs and DPFs have been combined into a single unit known as a particulate oxidation catalyst (POC), where NO_2 generated by the catalyst assists in the continuous oxidation of PM into CO_2.[156]

Lean NO_x Trap (LNT)

Despite advancements in EGR, DOCs, and DPFs, NO_x emissions from diesel vehicles remained higher than those from gasoline vehicles. In response to in-

creasingly stringent vehicle emissions regulations in the early 2010s (Section 1.3.1), two additional after-treatment technologies were introduced to target NO_x reduction: lean NO_x traps (LNTs) and selective catalytic reduction (SCR).

LNTs are installed downstream of the DOC and DPF and absorb NO_x under lean combustion conditions before releasing and chemically reducing it under rich conditions. These systems contain a precious metal catalyst similar to those found in TWCs and DOCs alongside metal carbonates and oxides. Under lean conditions, NO is oxidised to NO_2 and stored on a metal carbonate surface, as shown in Reactions 1.15 and 1.16, where barium (Ba) is the metal carbonate/oxide.[157, 158]

$$2\,NO + O_2 \rightleftharpoons 2\,NO_2 \tag{1.15}$$

$$4\,NO_2 + 2\,BaCO_3 + O_2 \rightleftharpoons 2\,Ba(NO_3)_2 + 2\,CO_2 \tag{1.16}$$

During periodic rich combustion phases, barium oxide is formed, and stored NO_2 is released and reduced by exhaust reductants (CO, HC, and hydrogen), catalysed by the precious metal catalyst.[157, 158] Simultaneously, barium carbonate is regenerated from barium oxide through reaction with exhaust gas CO_2. These process are outlined in Reactions 1.17–1.19.

$$2\,Ba(NO_3)_2 \rightleftharpoons 2\,BaO + 4\,NO_2 + O_2 \tag{1.17}$$

$$2\,NO_2 + 4\,CO \longrightarrow N_2 + 4\,CO_2 \tag{1.18}$$

$$BaO + CO_2 \longrightarrow BaCO_3 \tag{1.19}$$

Selective Catalytic Reduction (SCR)

SCR is another NO_x control technology widely adopted in the past decade. It relies on the injection of diesel exhaust fluid (DEF), typically urea, into the exhaust stream downstream of the DOC and DPF. At the high exhaust temperatures, urea decomposes into NH_3, which then reacts with NO and NO_2 over a precious metal catalyst to chemically reduce NO_x, as shown in Reactions 1.20 –1.22.[159]

$$4\,NO + 4\,NH_3 + O_2 \longrightarrow 4\,N_2 + 6\,H_2O \tag{1.20}$$

$$2\,NO_2 + 4\,NH_3 + O_2 \longrightarrow 3\,N_2 + 6\,H_2O \tag{1.21}$$

$$NO + NO_2 + 2\,NH_3 \longrightarrow 2\,N_2 + 3\,H_2O \tag{1.22}$$

Reaction 1.22, the faster SCR NO_x reduction pathway, benefits from a higher fraction (up to 50%) of NO_2 in the exhaust, improving overall NO_x reduction efficiency.[160] While both LNT and SCR technologies have been known since the late 20th century, their widespread adoption in diesel ICEs is relatively recent, and ongoing improvements continue to enhance their performance.

Although LNTs and SCR have reduced diesel NO_x emissions to levels comparable to gasoline vehicles, a significant drawback of both systems is the potential formation of ammonia as a by-product. This issue arises if after-treatment conditions are not precisely controlled. In SCR, excessive NH_3 injection relative to pre-SCR NO_x concentrations leads to unreacted NH_3 emissions, known as ammonia slip.[161] In LNTs, overly rich combustion conditions can cause excessive reductant (CO and hydrogen) exhaust gas concentrations, leading to NH_3 formation.[162]

Modern diesel vehicles integrate EGR, DOCs, DPFs, LNTs, and SCR to meet stringent emissions regulations. In recent years, to reduce ammonia slip emissions from SCR systems, ammonia oxidation catalysts have also been introduced.[163] The complexity of diesel emission control systems reflects the fundamental challenge posed by lean combustion and excess oxygen in the exhaust gas. Figure 1.13 provides an overview of the engine-out and exhaust emissions from diesel ICEs. As diesel emission control technologies continue to evolve, monitoring their long-term performance and degradation will be essential to ensure their continued effectiveness.

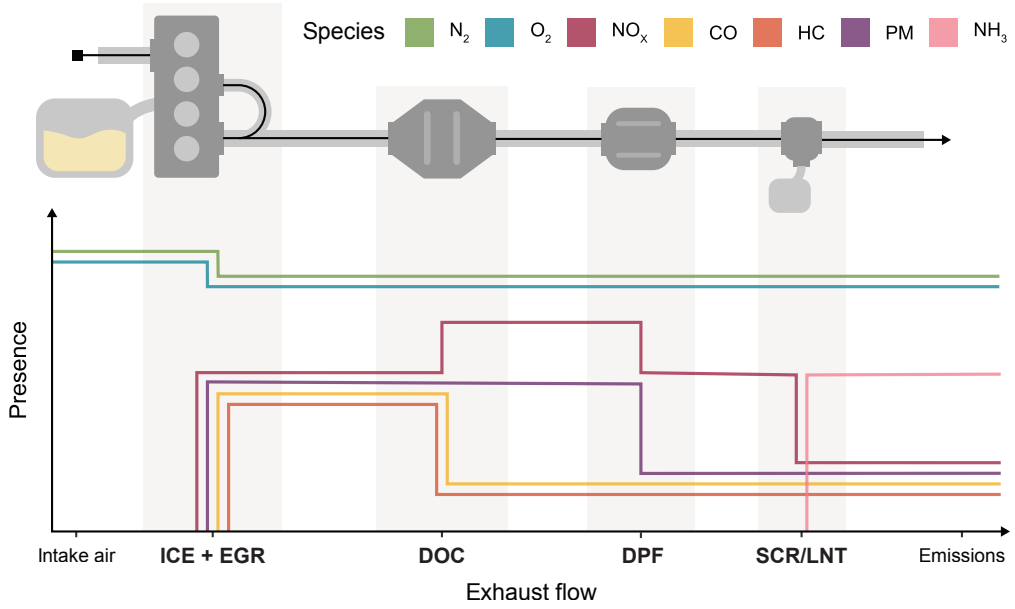

Figure 1.13: Diesel ICE exhaust diagram showing the presence, creation, or removal of each pollutant throughout the different emission control systems. The presence is not quantitative and is intended only to illustrate the direction in which pollutant concentrations are likely to change.

1.2.3 Secondary Pollutants

Once emitted from the tailpipe, primary exhaust pollutants from road transport can undergo atmospheric chemical transformations, forming harmful secondary pollutants. The rate and quantity of secondary pollutant formation are dependent on the concentrations of primary pollutants, co-pollutants, and existing atmospheric constituents, as well as meteorological conditions. Among the pollutants emitted from road vehicles, HCs exhibit the most complex secondary chemistry due to the wide range of species emitted. In addition to generating secondary VOCs, exhaust HCs contribute to the net production of tropospheric O_3.

O_3 formation is a radical chain process driven by interactions between NO_x and oxygen. NO, NO_2, and O_3 exist in a dynamic equilibrium described by the *Leighton relationship*, shown in Reactions 1.23 – 1.25.[164, 165] Photolysis of NO_2 produces NO and atomic oxygen, which reacts with molecular oxygen in the presence of a third molecule (M), to form O_3. M does not participate directly in the reaction but absorbs the excess energy released, stabilising the O_3 product, which can then react with NO, regenerating NO_2 and molecular oxygen, resulting in a null cycle with no net ozone production. The relative balance of NO and NO_2 depends on O_3 concentration and sunlight ($\lambda < 420$ nm) intensity, which is required for Reaction 1.23.[166]

$$NO_2 \xrightarrow{h\nu} NO + O \tag{1.23}$$

$$O + O_2 + M \longrightarrow O_3 + M \tag{1.24}$$

$$O_3 + NO \longrightarrow O_2 + NO_2 \tag{1.25}$$

Net ozone formation occurs when this equilibrium is disrupted by other pollutants, particularly VOCs. The process is initiated when a VOC (RH) is oxidised by the OH radical, producing a peroxy radical (RO_2). This radical oxidises NO to NO_2, perturbing the *Leighton relationship*, while forming an alkoxy radical (RO), which can further react to generate secondary VOCs, regenerate OH, and oxidise additional NO to NO_2. This cycle, illustrated in Figure 1.14, can involve numerous additional complex reactions but ultimately results in net O_3 production.

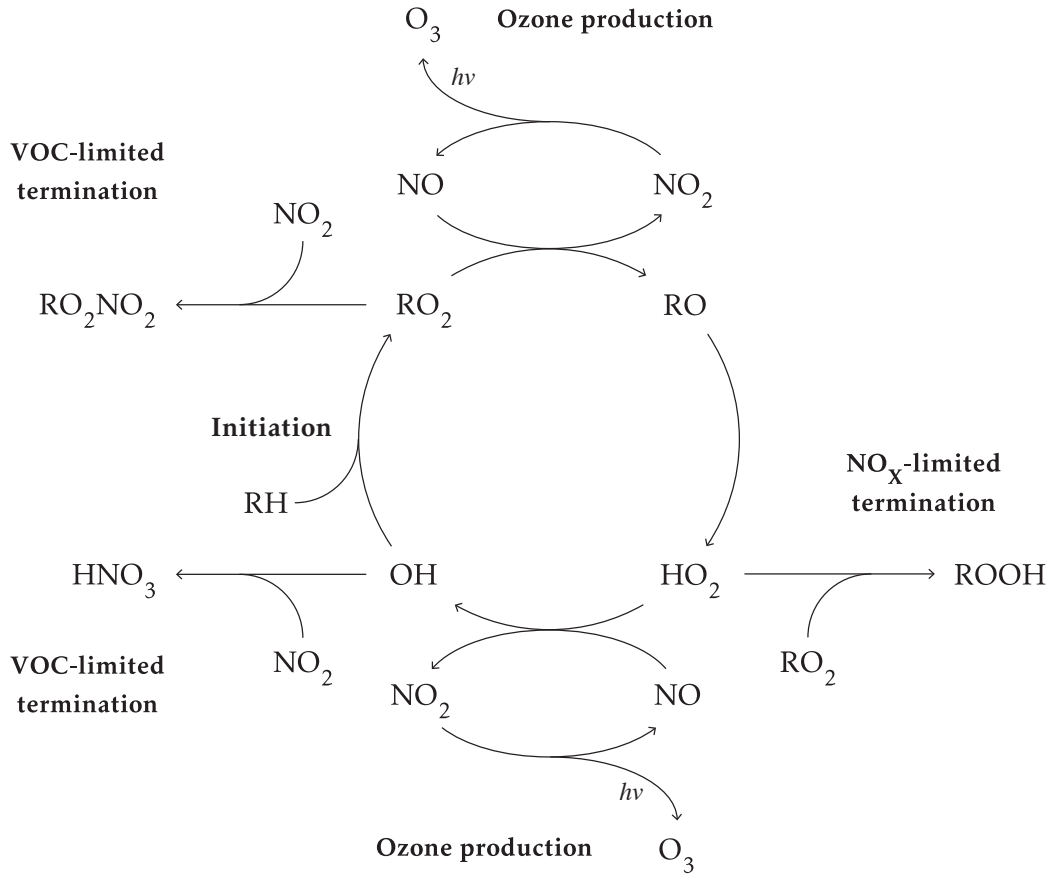

Figure 1.14: Reaction scheme for the net production of O_3 from NO_x and VOC chemistry.

Ozone formation is highly non-linear with respect to NO_x and VOC emissions. The rate of O_3 production depends on their relative local balance and the type of VOCs present, which are both strongly influenced by road transport, particularly in urban areas. As discussed in Section 1.1.1, whether O_3 formation is limited by NO_x or VOCs determines the dominant influence of vehicular emissions. In NO_x-limited regimes, NO_x emissions significantly impact O_3 concentrations, whereas in VOC-limited regimes, vehicular VOC emissions play a greater role, the dominant radical chain termination pathway for each regime is shown in Figure 1.14. Recently, a third regime referred to as the aerosol-inhibited regime has been proposed, where the uptake of hydroperoxy radicals (HO_2) onto aerosol particles is the dominant termination pathway.[167]

In addition to ozone formation, road transport-derived VOCs contribute to secondary PM, particularly SOA. The oxidation of VOCs during O_3 formation and wider atmospheric reactions produces lower-volatility products that can partition from the gas phase into particles. VOC emissions from road vehicles have been reported to comprise up to 21% of urban SOA, which account for anywhere from 20 to 70% of total urban $PM_{2.5}$.[168, 169]

Other road transport emissions also contribute to PM via SIA formation. NO_x and NH_3 emissions react in the atmosphere to form ammonium nitrate (NH_4NO_3) through Reactions 1.26 and 1.27.[170] Ammonium nitrate, along with other ammonium salts formed from reactions involving SO_2 and other pollutants, can nucleate to form PM or condense onto existing particles.[171]

$$NO_2 + OH \longrightarrow HNO_3 \tag{1.26}$$

$$HNO_3 + NH_3 \longrightarrow NH_4NO_3 \tag{1.27}$$

The full scope of the currently understood chemistry of secondary pollutant formation from vehicle emissions is extensive and cannot be fully covered here. One example of a species that plays a key role in both O_3 and PM formation is nitrous acid (HONO). It forms heterogeneously through the reaction of NO_2 with water vapour on surfaces near roads, as shown in Equation 1.28.[172] This process can also happen within vehicle exhaust systems, in which case the HONO produced is considered a primary pollutant.[173]

$$2\,NO_2 + H_2O \longrightarrow HONO + HNO_3 \tag{1.28}$$

Once formed, HONO undergoes rapid photolysis in sunlight, generating OH radicals that partake in the chemistry described earlier in this section. HONO represents just one example of the many air pollutants that could not be explored in this thesis but originate from vehicles and contribute significantly to urban air pollution.

1.2.4 Non-Exhaust Pollutants

As well as pollutants directly emitted and subsequently formed from exhaust emissions, road transport produces non-exhaust emissions. These originate from various intra-vehicular sources, with the most significant being particulate matter (PM) from frictional processes. Road vehicles rely on the friction between their tyres and the road to accelerate, decelerate, and change direction. Each of these processes causes abrasive wear of both the tyre and road surface, producing PM emissions. Similarly, braking systems function by creating friction between stationary and rotating components to convert the vehicle's kinetic energy into heat, a process that also releases PM.

Non-exhaust PM emissions, arising from tyre, road surface, and brake wear are similar to exhaust emissions in their complexity, varying with

material composition, driving behaviour, and ambient conditions.[174, 175] However, while exhaust emissions typically originate from a single source per vehicle, non-exhaust emissions are generated across multiple road contact and braking points, making them more challenging to quantify (Section 1.4). As a result, their measurement remains highly uncertain and largely unregulated.[176]

The composition and size distribution of non-exhaust PM emissions vary, and they predominantly contribute to PM_{10}, with a lesser but still important contribution to $PM_{2.5}$.[177] Brake wear PM emissions are composed primarily of heavy metals, including zinc (Zn), copper (Cu), iron (Fe), barium (Ba), and antimony (Sn), as well as organic compounds derived from braking surface materials.[178] Emissions from brake wear are particularly significant in urban areas where frequent braking increases PM generation.[179]

Tyres are composed of synthetic and natural rubber, carbon black, and various chemical additives. The wear process generates particles of varying sizes, with larger fragments remaining on the road and finer particles (PM_{10} and smaller) becoming airborne. The composition of these particles varies widely, often containing heavy metals and a range of organic compounds. [180] Road surface wear contributes additional mineral particles, including silica (SiO_2), Fe, and calcium (Ca), originating from asphalt and concrete breakdown.[181] The interaction between the tyre and road surface also influences particle formation, with factors such as vehicle load, speed, and road texture affecting emission rates.[182, 183]

In addition to intra-vehicular non-exhaust PM, road transport is capable of resuspending previously deposited road dust by shear forces from tyres and atmospheric turbulence in the vehicle wake.[184] Resuspended road dust represents the largest single contributor to vehicle non-exhaust PM_{10} emissions, exceeding direct brake, tyre, and road wear emissions in many urban environments.[177] Road dust is a heterogeneous mixture of materials, in-

cluding mineral particles from road wear, heavy metals from brake and tyre abrasion, and pollutants deposited from exhaust emissions. The chemical composition of resuspended dust can vary widely based on local ambient conditions, traffic intensity, and road maintenance practices.

Non-exhaust PM emissions from road transport occur regardless of power type, meaning that EVs are also a source. A key factor influencing these emissions is vehicle mass, as heavier vehicles generate more friction with the road surface, dissipate greater energy during braking, and resuspend more road dust.[175] Over time, road transport vehicles have become progressively larger and heavier due to growing consumer demand for more spacious vehicles with additional features. EVs often add even more weight because of their large batteries, further amplifying non-exhaust emissions.[185] However, EVs also utilise regenerative braking, which has been shown to reduce brake wear emissions by recovering kinetic energy and decreasing reliance on friction braking. This technology has the potential to mitigate one component of non-exhaust PM pollution.[123, 186] Despite this, tyre wear, road surface wear, and road dust resuspension remain significant sources of emissions, particularly for heavy EVs.

As exhaust emissions from ICE vehicles continue to decline due to stricter regulations (Section 1.3.1) and improved technology, non-exhaust sources are becoming the dominant contributor to traffic-related PM pollution.[175, 177] This shift has driven significant research over the past decade. Continued investigation into non-exhaust emissions is essential to reduce PM pollution in urban areas further and maximise the air quality benefits of fleet electrification.

Another source of non-exhaust emissions from road transport is evaporative fuel emissions, which arise from the volatilisation of fuel components, as opposed to combustion. These emissions can occur when refuelling or by permeating through fuel system components, releasing VOCs into the

atmosphere. Evaporative fuel emissions have been largely reduced in the UK and Europe through improvements in vehicle fuel system design, including sealed fuel tanks and onboard vapour recovery technologies, as well as through seasonal fuel reformulations.[187] These emissions do, however, remain a relevant source in many urban areas worldwide, particularly in warmer climates where higher temperatures increase fuel volatility.[188]

Recently, evaporative screen wash emissions have been reported to represent a significant and overlooked source of non-exhaust VOCs from road transport in the UK. Screenwash formulations contain high concentrations of VOCs like ethanol and methanol for antifreeze properties, which, when used in screen cleaning systems, evaporate into the atmosphere, contributing more VOC emissions than fuel evaporation and exhaust emissions combined.[23] Similar to non-exhaust PM emissions, VOCs from screenwash are independent of power type, and EVs contribute equally to this source. Ambient conditions strongly influence screen wash VOC emissions, with higher usage in the UK during winter due to seasonal formulation changes and increased road spray. While not a focus of this thesis, screen wash-related VOC emissions remain largely unregulated and will be increasingly important to address as the overall profile of road transport VOC emissions shifts with further exhaust emission reductions and fleet electrification.

1.2.5 Summary of Vehicle Emissions

The chemistry of vehicle emissions is complex, owing to the various pollutant sources within vehicles and their variations across the fleet. Matters are further complicated by the secondary reactions that occur in the atmosphere after emission, as well as the physical interaction of vehicles with their environment. Figure 1.15 summarises the chemistry of vehicle emissions.

Hybrid-electric vehicles, which combine an ICE with an electric drivetrain, are capable of emitting all the pollutants outlined in Figure 1.15 due

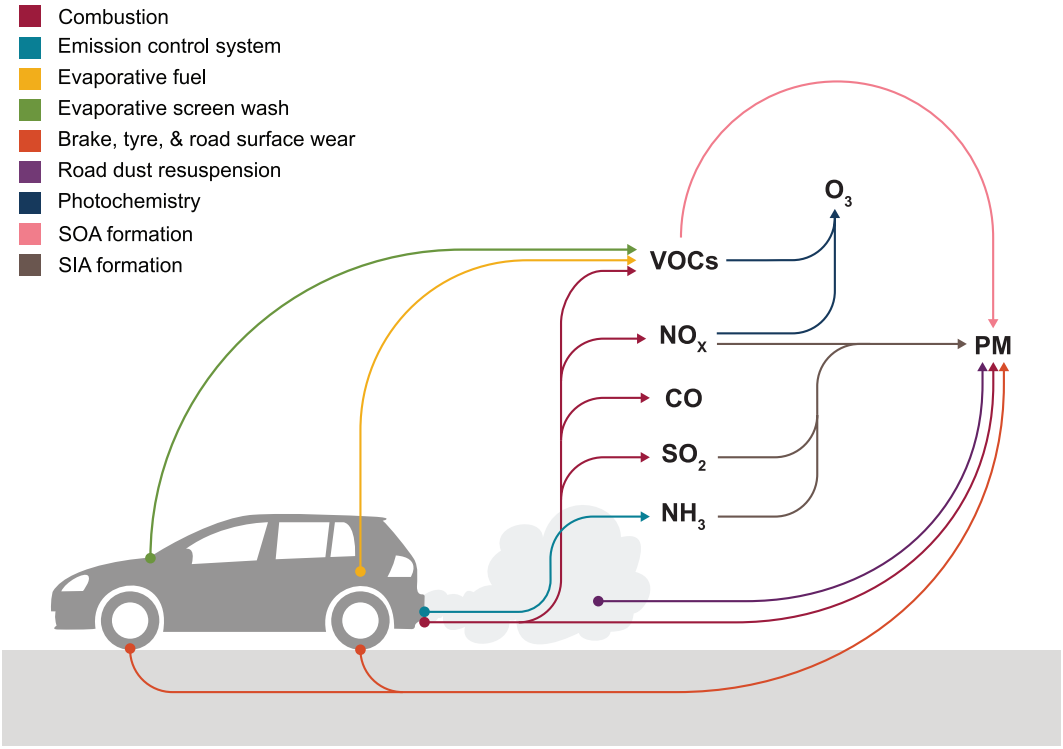

Figure 1.15: Diagram summarising the origin and chemistry of vehicle emissions.

to the combustion process and associated after-treatment systems. Primarily gasoline-powered, these vehicles generally produce lower emissions than those that are only fossil-fuelled by using the electric drivetrain to reduce engine load or, at times, power the vehicle entirely.[189, 190] However, the operation of hybrid drivetrain systems varies across manufacturers and models, influencing emission compositions by altering ICE temperature and the performance of emission control systems.[191] Given that hybrid vehicles now constitute the largest share of new road vehicle sales in the UK, fully understanding their emissions remains a research priority.[94]

The chemistry and emissions of road transport are influenced by factors such as driver behaviour, ambient conditions, and vehicle degradation. Cold-start emissions – those produced when a vehicle's engine is first started after being inactive – are consistently higher for all combustion-derived exhaust pollutants due to emission control systems operating below optimal

temperatures.[192, 193] Similarly, traffic congestion and stop-start driving can cause variation in exhaust gas flow, reducing the efficiency of these systems and leading to increased emissions of all pollutants.[176, 194, 195]

As vehicles age, emission control systems often degrade or fail before other ICE components, and their high replacement costs can lead to either unintentional malfunction or, in some cases, illegal tampering or removal. [35, 196, 197] Consequently, certain vehicles become disproportionately high emitters of pollutants. Research has consistently reported that the top ~10% of high-emitting vehicles contribute significantly to urban air pollution, accounting for over 50% of total vehicle emissions.[198–200] Effective mitigation strategies must therefore prioritise these vehicles to achieve meaningful reductions in emissions and subsequent improvements in urban air quality.

1.3 Mitigation of Vehicle Emissions

Mitigating the impact of road transport on urban air quality requires targeted strategies that directly address vehicle emissions. Over the past few decades, reducing emissions from road transport has been achieved through collective contributions from regulatory frameworks, technological advancements, and urban planning measures. These strategies have been most extensively implemented in high-income nations, but the pace and approach of adoption vary globally.

1.3.1 Emission Standards and Regulation

The primary method of vehicle emission mitigation is the implementation of emission standards, which set pollutant emission limits that new vehicle models must meet during Type Approval testing before they can be mass-produced and sold. In the UK and Europe, the Euro emission standards have played an important role in reducing exhaust emissions from new vehicles. [87, 90] Introduced in 1992, the Euro standards have undergone multiple revisions, with each stage imposing stricter limits on pollutants including NO_x, CO, HC, and PM. There are different pollutants and limits set for different vehicle categories and fuel types.

The most recent light-duty vehicle (passenger car and LGV) standard, Euro 6, introduced in 2015 and last updated in 2023, set significantly lower NO_x limits for diesel vehicles compared to previous iterations, driving the adoption of SCR and LNT emission control systems (Section 1.2.2.2). Further stages (Euro 7) are under development to address both exhaust and non-exhaust emissions.[201]

While emission standards have driven substantial reductions in vehicle exhaust emissions, their effectiveness has been limited by discrepancies between laboratory-based testing methods used for Type Approval and real-

world vehicle emissions.[202–204] Until 2015, emission limits were enforced using standardised laboratory drive cycles on chassis dynamometers (Section 1.4.1), which do not fully represent the range of real-world driving conditions. This issue gained widespread attention during the 2015 Dieselgate emissions scandal, where manufacturers were found to have fitted vehicles with defeat devices designed to detect laboratory testing conditions and manipulate emissions output.[205]

The Dieselgate emissions scandal, combined with growing evidence of the mismatch between laboratory and real-world emissions, led to the introduction of Real Driving Emissions (RDE) testing, which was added to the Euro 6 standard (Euro 6d). RDE requires vehicles to meet emissions limits for NO_x and PM under on-road driving conditions (Section 1.4.2) in addition to laboratory tests.[206] Despite these improvements, RDE testing remains subject to certain limitations, particularly in capturing emissions across the full range of driving behaviours and environmental conditions. RDE testing is enforced through conformity factors, which allow RDE emissions to exceed laboratory emissions by a specified margin. Conformity factors were initially set at 1.43 for NO_x and 1.5 for PM but have been progressively tightened, with Euro 6e reducing them to 1.10 and 1.34, respectively.[207] Further reductions are expected under Euro 7.

1.3.2 Low-Emission Zones

Low Emission Zones (LEZs) are an increasingly common urban air quality mitigation strategy that directly targets vehicle emissions. LEZs restrict access to certain areas based on vehicle emissions performance, determined by emission standards, with older, more polluting vehicles either prohibited or subject to financial charges. The UK's first LEZ was introduced in London in 2008, followed by the more stringent Ultra Low Emission Zone (ULEZ) in 2019.[208] The ULEZ operates alongside the Congestion Charge Zone

(CCZ) – a charge applied to all vehicles during peak hours – creating a combined system that encourages the use of less polluting vehicles and public transport.

Many other cities in the UK and worldwide have implemented similar systems, including Birmingham (UK), Leicester (UK), Berlin (Germany), Milan (Italy), and Santa Monica (United States).[209–213] Although the effectiveness of LEZs varies depending on their design and enforcement, studies have reported significant reductions in pollutant concentrations where they are applied.[214, 215] However, the potential for emissions displacement to areas outside the restricted zones, known as negative border or spillover effects, presents a challenge.[216]

Furthermore, recent work in London has shown that traffic congestion in urban areas can result in suboptimal NO_x emission control system (SCR and LNT) operation, even for the least polluting vehicles.[194] These findings demonstrate that other opposing variables can outweigh the benefits of LEZs and that addressing vehicle emissions in urban areas requires additional intervention.

Other traffic restriction strategies have also been implemented in the UK. In 2020, the Department for Transport (DfT) introduced Low-Traffic Neighbourhoods (LTNs). Unlike LEZs, which target vehicles based on emissions performance, LTNs use small-scale, area-based interventions to manage traffic flow in urban areas.[217] These interventions typically include modal filters such as planters, bollards, or camera gates to restrict traffic. While LTNs have been shown to reduce local air pollutant concentrations, they have also faced criticism from affected communities for imposed inconvenience. [218, 219]

1.3.3 Periodic Technical Inspections

Periodic technical inspections (PTIs) are mandatory vehicle checks designed to ensure roadworthiness and compliance with emissions standards. In the UK, the annual Ministry of Transport (MOT) test includes visual inspection of exhaust systems and emissions measurement for fossil-fuelled vehicles. However, the current testing regime is limited, relying on basic assessments where exhaust concentrations of NO_x, CO, and HC are measured while the vehicle is stationary and the engine is not under any load.[220] As a result, high-emitting vehicles – which contribute disproportionately to total vehicle emissions – may pass inspections. Additionally, MOT tests for hybrid vehicles may exclude emissions measurements altogether.

Expanding MOT requirements to include more comprehensive testing methods could help identify high-emitting vehicles more effectively, improving emissions compliance and improving urban air quality in the UK. It will also become increasingly important to include more stringent emissions testing for hybrid vehicles as their share of the fleet grows and ages, ensuring that emissions control systems maintain performance when operating on fossil fuel power. As the vehicle fleet evolves, robust emissions quantification methods are essential to evaluate mitigation measures and inform future policy developments.

1.4 Quantification of Vehicle Emissions

Quantifying vehicle emissions is essential for understanding their contribution to urban air pollution, assessing the effectiveness of existing mitigation strategies, and informing future policy decisions. Due to the range of pollutants emitted from vehicles and the variety of ways in which these emissions interact with the environment, accurate and representative quantification requires a combination of different measurement techniques. These techniques vary in their complexity, cost, and ability to replicate real-world driving conditions, with each offering unique advantages and limitations.

A common feature of all vehicle emission quantification methods is the production of emission factors, which express pollutant emissions per unit of an activity, such as distance travelled, fuel consumed, or time spent in operation.[221] Distance-based emission factors, or grammes of pollutant emitted per kilometre travelled ($g\,km^{-1}$), are widely used in national emissions inventories and for Type-Approval emissions testing.[222] Fuel-based emission factors, or grammes of pollutant emitted per kilogramme of fuel consumed ($g\,kg^{-1}$), are more easily derived from real-world vehicle emission measurements and offer a more consistent metric over a range of driving conditions.[223] Time-based emission factors, or grammes of pollutant emitted per second ($g\,s^{-1}$), are less common, although helpful in understanding emissions under transient conditions.

A range of measurement techniques are used to derive different emission factors. The following sections provide an overview of the five most widely used methods for vehicle emissions quantification, outlining their principles, applications, and associated strengths and limitations. Figure 1.16 presents these five techniques on a spectrum of control and real-world representativity.

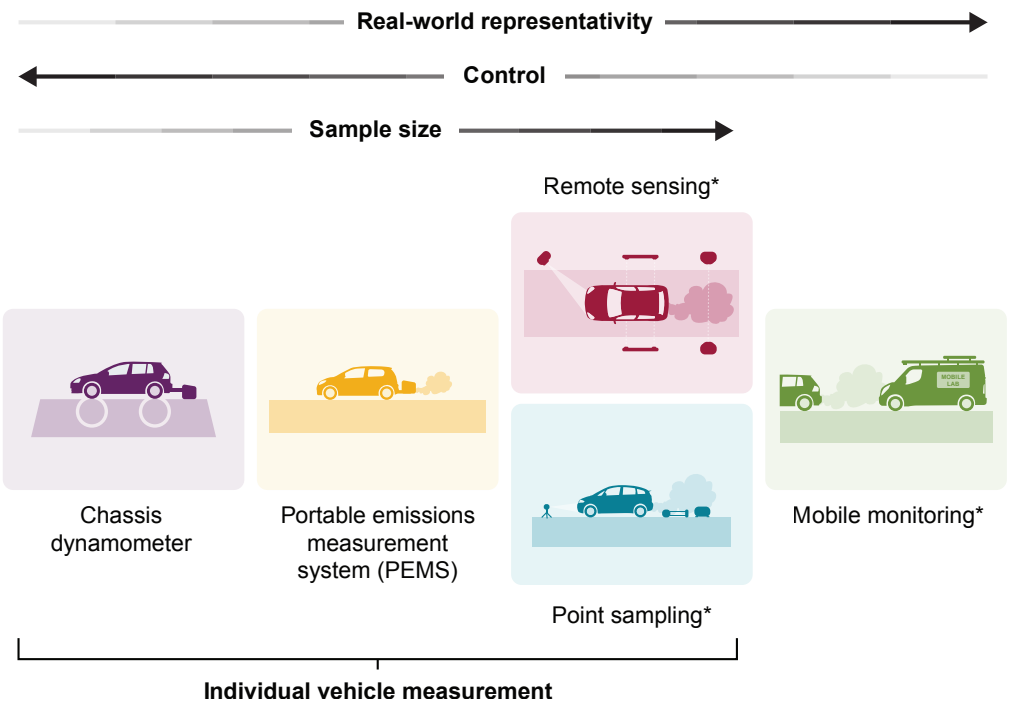

Figure 1.16: Five most widely used vehicle emission quantification techniques. * denotes techniques that are used in this thesis.

1.4.1 Chassis Dynamometer

Chassis dynamometer testing is a laboratory-based technique used to quantify vehicle emissions under controlled driving conditions. Vehicles are stationary, with their wheels driven on rollers that simulate road resistance, enabling them to be evaluated under engine load. Testing typically follows standardised drive cycles designed to replicate urban, rural, and motorway driving patterns. Exhaust emissions are measured directly at the tailpipe in real time, allowing distance-based, fuel-based, and time-based emission factors to be readily derived.[221]

This technique has been used since the 1970s and is still used for Type Approval emissions certification in the UK and Europe, with drive cycles such as the Worldwide Harmonised Light Vehicle Test Procedure (WLTP) representing modern regulatory standards.[201] The highly controlled nature

of chassis dynamometer testing ensures repeatability and allows emissions to be directly linked to vehicle activity. However, the controlled environment and standardised drive cycles often fail to capture the full range of real-world driving conditions.[202–204]

1.4.2 Portable Emissions Measurement Systems (PEMS)

Portable Emissions Measurement Systems (PEMS) have gained popularity since the early 2000s, enabling real-world emissions measurements by equipping vehicles with analytical instruments that measure pollutant emissions directly at the tailpipe during on-road driving.[224] PEMS emissions data are combined with GPS and engine performance data to calculate emission factors across different driving conditions. Similar to chassis dynamometer testing, the large amount of information obtained from PEMS allows for the derivation of distance-based, fuel-based, and time-based emissions factors.

PEMS testing was introduced as a regulatory tool for real-world emissions assessment under the 2015 Euro 6d RDE standard. While it offers high accuracy and the ability to capture emissions across a range of conditions, PEMS testing is time-consuming, costly, and typically limited to smaller sample sizes compared to other measurement techniques. PEMS studies often involve sample sizes of 5 – 20 vehicles, with more extensive reviews including up to hundreds of vehicles.[225–228] Consequently, PEMS testing is more suited to individual vehicle emissions assessments rather than large-scale fleet characterisation. However, as the volume of PEMS testing data grows globally, broader analyses may become increasingly feasible.

1.4.3 Remote Sensing

Remote sensing is a non-intrusive roadside technique developed in the late 1980s that measures a sub-one-second snapshot of pollutant concentrations in the exhaust plume of passing vehicles using open-path spectroscopy across the width of the road.[229] Pollutant concentration ratios to CO_2 are used to account for exhaust gas dispersion before measurement and derive fuel-based emission factors, which can be transformed into distance-based or time-based emission factors with additional information (Chapter 2). Remote sensing also captures vehicle movement information such as speed and acceleration, as well as registration number (license plate) photographs that can be used to obtain technical information for each passing vehicle.

Remote sensing enables the rapid measurement of large numbers of vehicles under real-world driving conditions, providing valuable insight into fleet-wide emissions distributions. The technique has been used globally to quantify vehicle emissions, and various commercial measurement systems have been developed. Figure 1.17 shows an example of a typical remote sensing measurement setup, and further details of the remote sensing equipment used in this thesis are provided in Section 1.4.6. Today, remote sensing is used regularly for emissions monitoring and mitigation strategy evaluation; it has also recently been considered for use in vehicle emission compliance enforcement.[230]

However, the technique's snapshot nature means that individual vehicle measurements only represent the exact conditions at the moment of measurement, and aggregation of thousands of measurements is required to obtain statistically robust emissions results. Moreover, because the technique uses open-path spectroscopy, it is not suitable for quantifying PM.

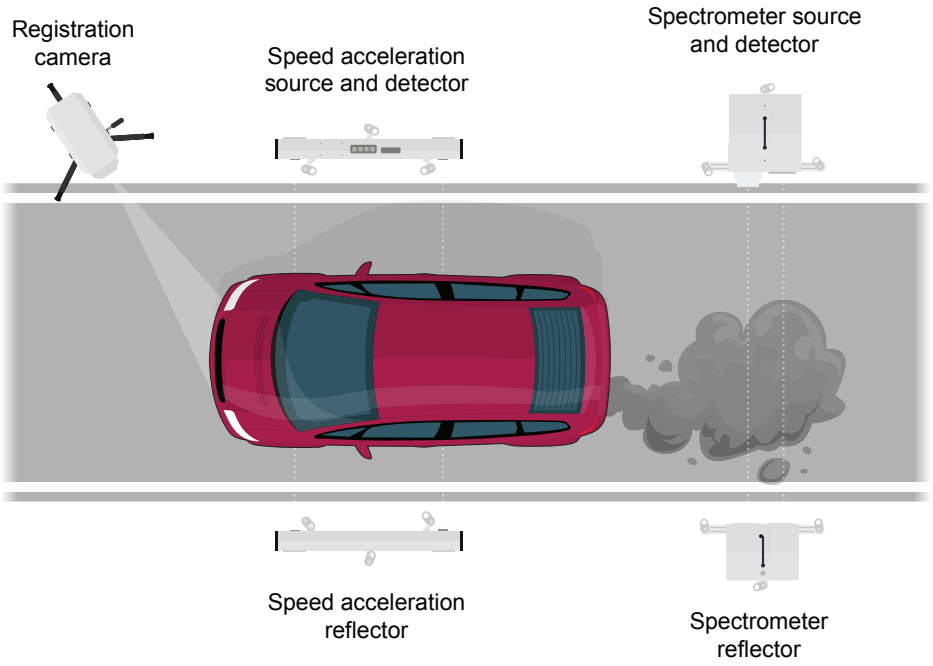

Figure 1.17: Remote sensing measurement setup.

1.4.4 Point Sampling

Point sampling is similar to remote sensing in that it is a non-intrusive roadside technique capable of measuring emissions from large quantities of vehicles.[231] However, instead of relying on snapshot open-path spectroscopy, point sampling is an extractive technique that employs a range of fast-response (~1 Hz) emissions measurement instruments that continuously sample roadside air as vehicles pass. This results in a continuous time series of pollutant concentrations that rise and fall as each vehicle's exhaust plume is measured.

Fuel-based emission factors can be derived from pollutant ratios to CO_2. Compared to remote sensing, point sampling provides more detailed insights into the transient emissions behaviour of passing vehicles, as it captures the entire duration of a vehicle's passage rather than a sub-second snapshot. However, this introduces additional complexity because the exhaust

plumes of closely spaced vehicles may overlap, complicating data interpretation. While the ability to use pollutant-specific instruments enhances sensitivity, time resolution, and the range of measurable pollutants, accurate background subtraction and precise time alignment between instruments are required to ensure robust data analysis, presenting additional and challenging processing steps.

Point sampling also records vehicle speed and acceleration, along with registration number photographs that can be used to retrieve technical information for each passing vehicle (Appendix A). This information is critical for attributing emissions to specific vehicles. Figure 1.18 shows a typical point sampling setup and further details on the emissions instrumentation used in this thesis are provided in Section 1.4.6.2.

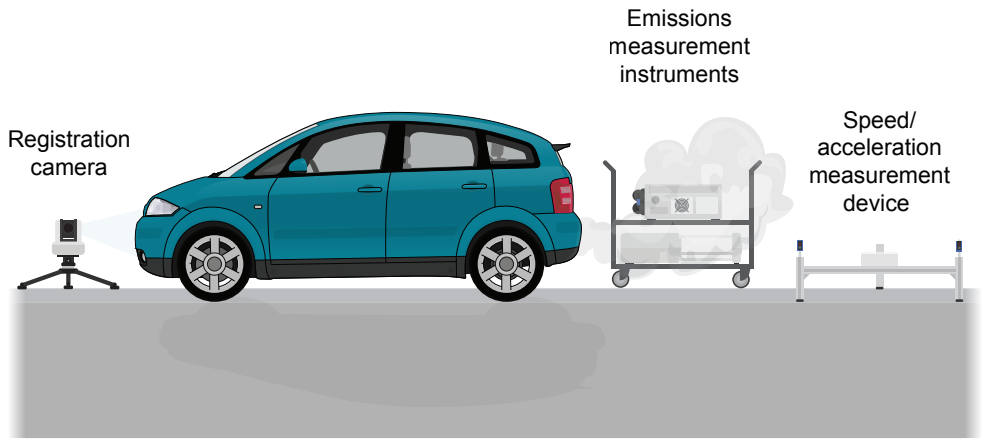

Figure 1.18: Point sampling measurement setup.

Although point sampling is a relatively new technique for vehicle emissions quantification, it has advanced significantly over the past decade. Earlier applications required filtering to isolate vehicle passes without interference from nearby vehicles, leading to substantial data loss.[232] However, advancements in statistical processing have greatly improved the utility of point sampling. For example, recent work has addressed instrument time

alignment using convolution functions, and a novel approach called *plume regression* has been developed.[233] This method uses robust linear regression to derive emission factors and apportion ambient pollutant concentrations to different vehicle types using data from all measured vehicles (Chapter 3).

While not classified as point sampling, near-road ambient air quality monitoring sites operate on similar principles (Section 1.1.3). These sites, which form part of the UK's AURN, use a range of extractive instruments to monitor vehicle emissions at hundreds of near-road locations across the country.[91] Similar air quality monitoring networks exist in other nations. [234, 235] The difference between these sites and vehicle emission point sampling is that they typically do not record individual vehicle data and have slower instrument response times, often averaged to one hour. Despite this limitation, these sites provide valuable insights into vehicle emissions and are frequently used to assess urban air quality trends relative to health guidelines, such as those set by the WHO (Section 1.1.3).[236]

1.4.5 Mobile Monitoring

Mobile monitoring involves mounting instruments on a vehicle, typically an LGV, to measure ambient pollutant concentrations while driving. Unlike PEMS testing, which measures emissions from the vehicle carrying the instruments, mobile monitoring captures pollution from the surrounding urban environment. This technique enables the measurement of spatial gradients in air pollution, providing valuable insights into traffic-related and other air pollution, which cannot be resolved through stationary monitoring. [237, 238] Mobile monitoring encompasses various measurement approaches, each suited to different objectives.

Typically, the instrumented vehicle follows predefined routes, repeated multiple times to build a comprehensive dataset containing information on how vehicle emissions vary spatially. While this method does not directly

quantify emissions from individual vehicles, it effectively assesses the combined impact of local traffic sources on air quality. The only constraint on emissions instrumentation is the vehicle's physical capacity, allowing a wide range of pollutants to be measured. Figure 1.19 shows a typical mobile monitoring setup, with details on the emissions instrumentation used in this thesis provided in Sections 1.4.6.2 – 1.4.6.4.

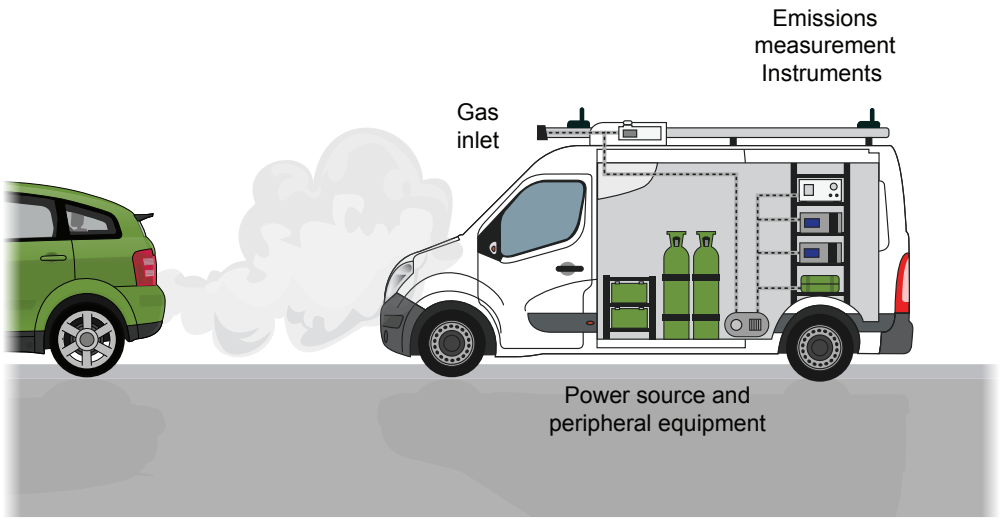

Figure 1.19: Mobile monitoring setup.

Similar to point sampling, mobile monitoring data is challenging to analyse, although mainly due to the additional spatial dimension. However, recent advancements in data processing have increased the insight that can derived from mobile monitoring data.[239] For example, in 2023, a distance-weighted approach was developed to improve the quantification of vehicle emissions in urban areas (Chapter 4).[194] While highly flexible, this method of mobile monitoring lacks the source attribution capabilities of other vehicle emission quantification techniques.

Another common mobile monitoring method is plume chasing, where the measurement vehicle follows another vehicle, continuously sampling its exhaust plume.[240] This approach functions as a non-intrusive but less

controlled alternative to PEMS testing and enables emissions measurement across a broader vehicle sample. While not included in this thesis, plume chasing is becoming increasingly common in vehicle emission research and has been used to characterise emissions from high-emitting vehicles.[241]

1.4.6 Analytical Techniques

This thesis focuses on real-world vehicle emissions measurements using remote sensing, point sampling, and mobile monitoring. Each method is based on distinct underlying principles, with point sampling and mobile monitoring adaptable to any sufficiently robust and portable emissions measurement instruments. This section provides a brief overview of the physical and chemical principles of operation behind the remote sensing equipment and the instruments selected for use in point sampling and mobile monitoring. Detailed experimental information is provided in the materials and methods section of each chapter.

1.4.6.1 FEAT/OPUS Accuscan RSD

Two remote sensing systems were used to collect data for Chapter 2: the Fuel Efficiency Automobile Test (FEAT), developed and supplied by the University of Denver, and the commercially available OPUS AccuScan Remote Sensing Device (RSD) 4600/5000. The principles underpinning the cross-road optical spectroscopy used in both systems have been described extensively in the literature, particularly in relation to the development of FEAT; a brief overview is provided here.[242–246]

The FEAT instrument measures CO_2, CO, and HC using using non-dispersive infrared (NDIR) spectroscopy. In this technique, infrared (IR) light is transmitted through vehicle exhaust plumes, where specific pollutants absorb light at characteristic wavelengths, allowing their concentrations to be determined. A single IR source, housed within a source module, is

focused across the road to a detector module, travelling through the exhaust plumes of passing vehicles. Upon entering the detector module, the IR beam is directed by a spinning mirror onto four IR detectors, each equipped with a passband filter to isolate the wavelengths corresponding to the target pollutants. The filtered wavelengths for each detector are:

- 2350 cm^{-1} (4.26 µm) for CO_2
- 2150 cm^{-1} (4.65 µm) for CO
- 2970 cm^{-1} (3.37 µm) for HC (targetting the C–H stretch)
- 2600 cm^{-1} (2.85 µm) as a reference wavelength, selected to be within the same spectral range as the target pollutants but not absorbed by any known pollutant

The concentration of each pollutant (c) is then calculated using the Beer-Lamber law (Equation 1.29), where the intensity of transmitted light (I) is measured at the corresponding detector, and the reference intensity (I_0) represents the initial light intensity before absorption. The equation also includes the molecular absorption coefficient of the pollutant gas (ϵ) and the effective path length across the road (l). For HC measurements, an experimentally determined scaling factor of 2 is applied to the calculated concentration to account for variation in IR absorbance across the wide range of species present in vehicle exhaust gas.[223, 247]

$$\epsilon\ c\ l\ =\ log(\frac{I_0}{I}) \tag{1.29}$$

UV absorption spectroscopy is used to measure NO, NO_2, NH_3, and SO_2. Similar to IR spectroscopy, a beam of UV light is directed across the road, co-linear with the IR beam. Upon returning to the detector, the UV

light is collected by a quartz UV fibre bundle and transmitted to two UV spectrometers.

- One spectrometer measures NO, NH_3, and SO_2 in the 200 – 226 nm spectral range.
- The other spectrometer measures NO_2 in the 430 – 447 nm spectral range.

These spectrometers use the UV light from the fibre bundle to calculate pollutant concentrations using the same Beer-Lambert law principles described for IR spectroscopy.

The exact operating principles of the OPUS AccuScan RSD are less well documented due to its commercial development. However, its measurement approach is generally similar to that of the FEAT system.[248] A key difference is the use of a single source-detector module on one side of the road that both transmits and receives a collinear IR and UV light beam. The beam is reflected by a corner cube mirror on the opposite side of the road, effectively doubling the instrument's path length and enhancing its sensitivity compared to the FEAT.

Earlier OPUS models featured only a single UV channel for measuring NO_x and NH_3, while more recent versions (including those used for the collection of data in this thesis) incorporate a second channel dedicated to NO_2.[249] The OPUS system also includes a feature for measuring PM using light opacity as a proxy for PM concentration. However, due to the low sensitivity of this method, PM measurements from the OPUS are not considered in this thesis.[250] Despite minor differences in the FEAT and OPUS instruments, a detailed comparison of the two in the literature suggests that the resulting gaseous pollutant concentrations from each are comparable.[251]

Both systems also contain peripheral modules housing simple optical sensors for measuring passing vehicles' speed and acceleration, as well as cameras for photographing vehicle registration numbers. Other commercial remote sensing systems have also been developed, including overhead-mounted systems capable of measuring exhaust temperature using thermal imaging.[252]

1.4.6.2 Airyx ICAD

The Airyx Iterative Cavity Enhance Differential Optical Absorption Spectroscopy (ICAD) NO_x analyser was used to measure CO_2, NO, and NO_2 through both point sampling and mobile monitoring for Chapters 3 and 4, respectively. This extractive instrument employs cavity-enhanced differential optical absorption spectroscopy (CE-DOAS) to achieve high-precision, high-time-resolution pollutant measurements.[253]

CE-DOAS operates on principles similar to those described in Section 1.4.6.1, but utilises narrowband light across multiple wavelengths to detect pollutant species. By leveraging the distinct absorption features of each gas, it effectively differentiates between pollutants absorbing within the same spectral region. The cavity-enhanced technique extends the optical path length by confining light within a high-reflectivity optical cavity, improving sensitivity to trace gas absorption. Additionally, an iterative approach corrects for non-linear absorption effects over the extended path length and accounts for light scattering from particulate matter.[254]

This method provides a direct, calibration-free measurement of NO_2 by detecting its characteristic absorption features in the 430 – 465 nm spectral range. Unlike traditional chemiluminescence analysers, which require chemical conversion and frequent calibrations, cavity-enhanced absorption spectroscopy enables robust and drift-free detection of NO_2.

The system incorporates an ozone-based gas phase converter that converts

NO to NO_2. The resulting increase in NO_2 concentration allows for the indirect determination of NO and, consequently, NO_x. Additionally, the ICAD system includes an NDIR sensor for CO_2 measurements, which detects IR absorption around 2350 cm^{-1} (4.26 µm). The high temporal resolution (0.5 Hz) and sensitivity of the instrument make it particularly well-suited for vehicle emissions monitoring, allowing for the detection of transient emission events from individual vehicles.[194, 255] In the standard configuration, this instrument has a 2 s response time. However, linear interpolation can applied to produce a 1 s (1 Hz) time series.

1.4.6.3 PALAS AQ Guard Ambient

The PALAS AQ Guard Ambient photometric particle number counter was used to measure PM during mobile monitoring for Chapter 5. This instrument operates on the principle of optical light scattering, a well-established technique for measuring airborne PM. Individual particles are illuminated with a polychromatic LED light source, and the instrument detects the light scattered at 90 °using photodetectors.[256] The intensity and angular distribution of the scattered light provide information used to determine PM concentration across different size fractions, up to 20,000 particles cm^{-3}.

Particles with aerodynamic diameters between 0.175–20 µm are measured at 1 Hz across 64 channels, with mass concentration (µg m^{-3}) calculated for different size fractions, including $PM_{2.5}$ and PM_{10}. Mass concentrations are derived using a mass conversion algorithm that accounts for the size and shape of the optical scattering signal. This algorithm was developed alongside the EN16450-certified (a European standard for the automated ambient monitoring of PM) FIDAS 200 instrument.[257]

The AQ Guard is an extractive instrument, sampling air at a constant flow rate of 1.0 L min^{-1}. This ensures controlled particle introduction into the measurement chamber, minimising losses due to deposition or turbulence.

Temperature, pressure, and humidity sensors correct for environmental factors, ensuring concentration measurements under varying conditions. This feature, combined with the instrument's ability to operate autonomously with low maintenance requirements, makes it well-suited for use in mobile monitoring. While the PALAS AQ Guard Ambient provides detailed PM size distribution data, it does not offer particle composition information.

1.4.6.4 Thermo Model 43i

The Thermo Model 43i SO_2 Analyzer was used to measure SO_2 during mobile monitoring for Chapter 5. This instrument, which operates on the principle of pulsed fluorescence, is highly sensitive and capable of detecting SO_2 down to concentrations of < 1.5 µg m^{-3}.[258] The technique relies on the ability of SO_2 molecules to absorb UV light and subsequently emit (fluoresce) light at a longer wavelength. The intensity of the emitted light is directly proportional to the concentration of SO_2 in the sampled air.

Sampled air is first filtered to remove hydrocarbons before entering the fluorescence chamber. Inside, a selective mirror assembly directs pulsed UV light at wavelengths (214, 220, 300 nm), specifically exciting SO_2 molecules in the air. As the air sample moves through the instrument, the excited SO_2 molecules fluoresce in the 240 – 420 nm range. This emitted light passes through a bandpass filter, ensuring that only the fluorescence signal reaches the photodetectors for measurement. The instrument manufacturer does not provide exact excitation and fluorescence detection wavelengths, but they are available in the literature.[259, 260]

By using pulsed fluorescence, the Thermo Model 43i provides highly sensitive measurements of SO_2 with a response time of 20 s. For use in mobile monitoring, an additional external sampling pump was used to increase the instrument flow rate, allowing for 1 Hz measurements of SO_2 through modification of the instrument software.

1.5 Thesis Structure

This thesis is presented in a journal-style format, comprising three stand-alone chapters based on published articles. Details of each article are provided in the author's declaration and at the beginning of each chapter. The content of each chapter remains faithful to the respective published article. Minor formatting adjustments have been made to section headings, figures, captions, citations, and reference styles for clarity and consistency. Supplementary material has been incorporated within each chapter, with additional references to other sections of the thesis added where appropriate for completeness. Each chapter includes a separate bibliography to ensure it functions as a self-contained unit without requiring additional document sections.

Chapter 2 examines the long-term air quality impacts of diesel passenger cars in the UK, with a focus on NO_x, using over 600,000 remote sensing vehicle emission measurements. The study considers two scenarios: one in which diesel was not promoted in the early 2000s and another where its decline post-Dieselgate did not occur. This work represents a novel application of remote sensing data and is the first to quantify the impact of diesel fuel use on UK vehicle emissions based on real-world measurements. A brief update section at the end of the chapter highlights relevant research released since its publication.

Chapter 3 explores how vehicle design influences near-road exposure to TRAP through point sampling measurements using the plume regression technique. This study is the first to analyse the effects of exhaust position and vehicle aerodynamics on roadside dispersion using real-world data, providing new insight into the dispersion processes occurring at the roadside. These processes directly influence human exposure to TRAP in urban areas and are currently poorly understood. Additionally, findings show that

EVs contribute to the dispersion of exhaust plumes from fossil-fuelled cars through vehicle-induced turbulence, revealing an unexpected air quality benefit of EV adoption. This chapter is based on a publication released in 2025; no updates were required at the time of writing this thesis.

Chapter 4 investigates both vehicular and non-vehicular sources of PM in Central and Outer London using mobile monitoring. The effects of the ULEZ are assessed and compared to recent research on NO_x emissions. While vehicular $PM_{2.5}$ levels in London are found to be well-controlled, isolated high-emission events from malfunctioning vehicles contribute disproportionately to local air pollution. The study also identifies key non-vehicular PM sources, including construction activities, which influence larger PM fractions and exhibit weather-dependent behaviour. A brief update section at the end of the chapter summarises relevant research developments since its publication.

1.6 References

[1] World Health Organization. *Air Pollution*. https://www.who.int/health-topics/air-pollution. Accessed: 2025-01-22. 2024 (cit. on p. 2).

[2] Manisalidis, I., Stavropoulou, E., Stavropoulos, A., and Bezirtzoglou, E. Environmental and health impacts of air pollution: a review. *Frontiers in public health* 8 (2020), p. 14. DOI: 10.3389/fpubh.2020.00014 (cit. on p. 2).

[3] Chen, H., Kwong, J. C., Copes, R., Hystad, P., Donkelaar, A. van, Tu, K., Brook, J. R., Goldberg, M. S., Martin, R. V., Murray, B. J., et al. Exposure to ambient air pollution and the incidence of dementia: a population-based cohort study. *Environment international* 108 (2017), pp. 271–277. DOI: 10.1016/j.envint.2017.08.020 (cit. on pp. 2, 12).

[4] Mortamais, M., Gutierrez, L.-A., Hoogh, K. de, Chen, J., Vienneau, D., Carrière, I., Letellier, N., Helmer, C., Gabelle, A., Mura, T., et al. Long-term exposure to ambient air pollution and risk of dementia: Results of the prospective Three-City Study. *Environment international* 148 (2021), p. 106376. DOI: 10.1016/j.envint.2020.106376 (cit. on pp. 2, 12).

[5] Health Effects Institure Panel on the Health Effects of Long-Term Exposure to Traffic-Related Air Pollution. *Systematic Review and Meta-analysis of Selected Health Effects of Long-Term Exposure to Traffic-Related Air Pollution*. https://www.healtheffects.org/publication/systematic-review-and-meta-analysis-selected-health-effects-long-term-exposure-traffic. 2022 (cit. on pp. 2, 18).

[6] Krewski, D. and Rainham, D. Ambient air pollution and population health: overview. *Journal of Toxicology and Environmental Health, Part A* 70.3-4 (2007), pp. 275–283. DOI: 10.1080/15287390600884859 (cit. on p. 2).

[7] Health Effects Institute. *State of Global Air 2024 Special Report*. https://www.stateofglobalair.org/resources/report/state-global-air-report-2024. 2024 (cit. on pp. 2, 12, 16).

[8] United Nations Statistics Division. *Sustainable Cities and Communitites*. https://unstats.un.org/sdgs/report/2023. Accessed: 2025-01-22. 2023 (cit. on p. 2).

[9] World Health Organization. *WHO global air quality guidelines*. https://www.who.int/publications/i/item/9789240034228. Accessed: 2025-02-04. 2021 (cit. on p. 2).

[10] United Kingdom National Atmospheric Emissions Inventory. *Air Pollutants*. https://naei.energysecurity.gov.uk/air-pollutants. Accessed: 2025-02-04. 2022 (cit. on p. 2).

[11] United Kingdom Government. *Health matters: air pollution*. https://www.gov.uk/government/publications/health-matters-air-pollution/health-matters-air-pollution. Accessed: 2025-02-04. 2018 (cit. on p. 2).

[12] Zeldovich, Y. B. *The Oxidation of Nitrogen in Combustion and Explosions*. Ed. by R. A. Sunyaev. Princeton: Princeton University Press, 1992, pp. 364–403. DOI: doi:10.1515/9781400862979.364 (cit. on pp. 3, 23).

[13] Lavoie, G. A., Heywood, J. B., and Keck, J. C. Experimental and theoretical study of nitric oxide formation in internal combustion engines. *Combustion science and technology* 1.4 (1970), pp. 313–326. DOI: 10.1080/00102206908952211 (cit. on pp. 3, 23).

[14] England, G., Heap, M., Pershing, D., Nihart, R., and Martin, G. Mechanisms of NO_X formation and control: Alternative and petroleum-derived liquid fuels. *Symposium (International) on Combustion*. Vol. 18. 1. Elsevier. 1981, pp. 163–174. DOI: 10.1016/S0082-0784(81)80021-5 (cit. on pp. 3, 23).

[15] Olsen, D. B., Kohls, M., and Arney, G. Impact of oxidation catalysts on exhaust NO_2/NO_X ratio from lean-burn natural gas engines. *Journal of the Air & Waste Management Association* 60.7 (2010), pp. 867–874. DOI: 10.3155/1047-3289.60.7.867 (cit. on p. 3).

[16] United Kingdom National Atmospheric Emissions Inventory. *Nitrogen Oxides*. https://naei.energysecurity.gov.uk/air-pollutants/nitrogen-oxides. Accessed: 2025-02-04. 2022 (cit. on p. 3).

[17] Smith, S. J., Aardenne, J. van, Klimont, Z., Andres, R. J., Volke, A., and Delgado Arias, S. Anthropogenic sulfur dioxide emissions: 1850–2005. *Atmospheric Chemistry and Physics* 11.3 (2011), pp. 1101–1116. DOI: 10.1073/pnas.1510743112 (cit. on p. 4).

[18] United Kingdom National Atmospheric Emissions Inventory. *Sulfur Dioxide*. https://naei.energysecurity.gov.uk/node/54. Accessed: 2025-02-04. 2022 (cit. on p. 4).

[19] United Kingdom National Atmospheric Emissions Inventory. *Carbon Monoxide*. https://naei.energysecurity.gov.uk/air-pollutants/carbon-monoxide. Accessed: 2025-02-04. 2022 (cit. on p. 5).

[20] Andreae, M. O. Emission of trace gases and aerosols from biomass burning–an updated assessment. *Atmospheric Chemistry and Physics* 19.13 (2019), pp. 8523–8546. DOI: 10.5194/acp-19-8523-2019 (cit. on p. 5).

[21] Kesselmeier, J. and Staudt, M. Biogenic volatile organic compounds (VOC): an overview on emission, physiology and ecology. *Journal of atmospheric chemistry* 33 (1999), pp. 23–88. DOI: 10.1023/a:1006127516791 (cit. on p. 5).

[22] United Kingdom National Atmospheric Emissions Inventory. *Non methane VOCs*. https://naei.energysecurity.gov.uk/air-pollutants/non-methane-voc. Accessed: 2025-02-04. 2022 (cit. on pp. 5, 6).

[23] Cliff, S. J., Lewis, A. C., Shaw, M. D., Lee, J. D., Flynn, M., Andrews, S. J., Hopkins, J. R., Purvis, R. M., and Yeoman, A. M. Unreported VOC emissions from road transport including from electric vehicles. *Environmental science & technology* 57.21 (2023), pp. 8026–8034. DOI: 10.1021/acs.est.3c00845 (cit. on pp. 6, 42).

[24] Harrison, R. M., Allan, J., Carruthers, D., Heal, M. R., Lewis, A. C., Marner, B., Murrells, T., and Williams, A. Non-exhaust vehicle emissions of particulate matter and VOC from road traffic: A review. *Atmospheric Environment* 262 (2021), p. 118592. DOI: 10.1016/j.atmosenv.2021.118592 (cit. on p. 6).

[25] Finlayson-Pitts, B. J. and Pitts Jr, J. N. Tropospheric air pollution: ozone, airborne toxics, polycyclic aromatic hydrocarbons, and particles. *Science* 276.5315 (1997), pp. 1045–1051. DOI: 10.1126/science.276.5315.1045 (cit. on p. 6).

[26] Atkinson, R. Atmospheric chemistry of VOCs and NO_X. *Atmospheric environment* 34.12-14 (2000), pp. 2063–2101. DOI: 10.1016/S1352-2310(99)00460-4 (cit. on p. 6).

[27] United Kingdom National Atmospheric Emissions Inventory. *Ammonia*. https://naei.energysecurity.gov.uk/air-pollutants/ammonia. Accessed: 2025-02-04. 2022 (cit. on pp. 7, 8).

[28] Van Damme, M., Clarisse, L., Franco, B., Sutton, M. A., Erisman, J. W., Kruit, R. W., Van Zanten, M., Whitburn, S., Hadji-Lazaro, J., Hurtmans, D., et al. Global, regional and national trends of atmospheric ammonia derived from a decadal (2008–2018) satellite record. *Environmental Research Letters* 16.5 (2021), p. 055017. DOI: 10.1088/1748-9326/abd5e0 (cit. on p. 7).

[29] Twigg, M. V. Controlling automotive exhaust emissions: Successes and underlying science. *Philosophical Transactions of the Royal Society A: Mathematical, Physical and Engineering Sciences* 363.1829 (2005), pp. 1013–1033. DOI: 10.1098/rsta.2005.1547 (cit. on pp. 7, 32).

[30] Kean, A., Littlejohn, D., Ban-Weiss, G., Harley, R., Kirchstetter, T., and Lunden, M. Trends in on-road vehicle emissions of ammonia. *Atmospheric Environment* 43.8 (2009), pp. 1565–1570. DOI: 10.1016/j.atmosenv.2008.09.085 (cit. on p. 7).

[31] Sutton, M., Dragosits, U., Tang, Y., and Fowler, D. Ammonia emissions from non-agricultural sources in the United Kingdom. *Atmospheric Environment*

34.6 (2000), pp. 855–869. DOI: 10.1016/S1352-2310(99)00362-3 (cit. on p. 7).

[32] Erisman, J. and Schaap, M. The need for ammonia abatement with respect to secondary PM reductions in Europe. *Environmental Pollution* 129.1 (2004), pp. 159–163. DOI: 10.1016/j.envpol.2003.08.042 (cit. on p. 7).

[33] Wang, M., Kong, W., Marten, R., He, X.-C., Chen, D., Pfeifer, J., Heitto, A., Kontkanen, J., Dada, L., Kürten, A., et al. Rapid growth of new atmospheric particles by nitric acid and ammonia condensation. *Nature* 581.7807 (2020), pp. 184–189. DOI: 10.1038/s41586-020-2270-4 (cit. on p. 7).

[34] Pan, Y., Tian, S., Liu, D., Fang, Y., Zhu, X., Zhang, Q., Zheng, B., Michalski, G., and Wang, Y. Fossil fuel combustion-related emissions dominate atmospheric ammonia sources during severe haze episodes: evidence from 15N-stable isotope in size-resolved aerosol ammonium. *Environmental science & technology* 50.15 (2016), pp. 8049–8056. DOI: 10.1021/acs.est.6b00634 (cit. on p. 7).

[35] Farren, N. J., Davison, J., Rose, R. A., Wagner, R. L., and Carslaw, D. C. Underestimated ammonia emissions from road vehicles. *Environmental Science & Technology* 54.24 (2020), pp. 15689–15697. DOI: 10.1021/acs.est.0c05839 (cit. on pp. 7, 44).

[36] Sun, K., Tao, L., Miller, D. J., Pan, D., Golston, L. M., Zondlo, M. A., Griffin, R. J., Wallace, H. W., Leong, Y. J., Yang, M. M., et al. Vehicle emissions as an important urban ammonia source in the United States and China. *Environmental Science & Technology* 51.4 (2017), pp. 2472–2481. DOI: 10.1021/acs.est.6b02805 (cit. on p. 7).

[37] Karagulian, F., Belis, C. A., Dora, C. F. C., Prüss-Ustün, A. M., Bonjour, S., Adair-Rohani, H., and Amann, M. Contributions to cities' ambient particulate matter (PM): A systematic review of local source contributions at global level. *Atmospheric environment* 120 (2015), pp. 475–483. DOI: 10.1016/j.atmosenv.2015.08.087 (cit. on p. 8).

[38] United Kingdom National Atmospheric Emissions Inventory. $PM_{2.5}$. https://naei.energysecurity.gov.uk/air-pollutants/PM2.5. Accessed: 2025-02-04. 2022 (cit. on pp. 8, 9).

[39] United Kingdom National Atmospheric Emissions Inventory. PM_{10}. https://naei.energysecurity.gov.uk/air-pollutants/PM10. Accessed: 2025-02-04. 2022 (cit. on pp. 8, 9).

[40] United Kingdom National Atmospheric Emissions Inventory. $PM_{0.1}$. https://naei.energysecurity.gov.uk/node/6609. Accessed: 2025-02-04. 2022 (cit. on p. 8).

[41] Song, R., Presto, A. A., Saha, P., Zimmerman, N., Ellis, A., and Subramanian, R. Spatial variations in urban air pollution: impacts of diesel bus traffic and restaurant cooking at small scales. *Air Quality, Atmosphere & Health* 14.12 (2021), pp. 2059–2072. DOI: 10.1007/s11869-021-01078-8 (cit. on p. 8).

[42] Saha, P. K., Presto, A. A., Hankey, S., Murphy, B. N., Allen, C., Zhang, W., Marshall, J. D., and Robinson, A. L. National exposure models for source-specific primary particulate matter concentrations using aerosol mass spectrometry data. *Environmental Science & Technology* 56.20 (2022), pp. 14284–14295. DOI: 10.1021/acs.est.2c03398 (cit. on p. 8).

[43] Srivastava, D., Vu, T. V., Tong, S., Shi, Z., and Harrison, R. M. Formation of secondary organic aerosols from anthropogenic precursors in laboratory studies. *Climate and Atmospheric Science* 5.1 (2022), p. 22. DOI: 10.1038/s41612-022-00238-6 (cit. on p. 9).

[44] Fine, P. M., Sioutas, C., and Solomon, P. A. Secondary particulate matter in the United States: insights from the particulate matter supersites program and related studies. *Journal of the Air & Waste Management Association* 58.2 (2008), pp. 234–253. DOI: 10.3155/1047-3289.58.2.234 (cit. on p. 9).

[45] Elminir, H. K. Dependence of urban air pollutants on meteorology. *Science of the total environment* 350.1-3 (2005), pp. 225–237. DOI: 10.1016/j.scitotenv.2005.01.043 (cit. on p. 11).

[46] Ramsey, N. R., Klein, P. M., and Moore III, B. The impact of meteorological parameters on urban air quality. *Atmospheric Environment* 86 (2014), pp. 58–67. DOI: 10.1016/j.atmosenv.2013.12.006 (cit. on p. 11).

[47] Perrino, C., Pietrodangelo, A., and Febo, A. An atmospheric stability index based on radon progeny measurements for the evaluation of primary urban pollution. *Atmospheric Environment* 35.31 (2001), pp. 5235–5244. DOI: 10.1016/S1352-2310(01)00349-1 (cit. on p. 11).

[48] Møller, P., Danielsen, P. H., Karottki, D. G., Jantzen, K., Roursgaard, M., Klingberg, H., Jensen, D. M., Christophersen, D. V., Hemmingsen, J. G., Cao, Y., et al. Oxidative stress and inflammation generated DNA damage by exposure to air pollution particles. *Mutation research/Reviews in mutation research* 762 (2014), pp. 133–166. DOI: 10.1016/j.mrrev.2014.09.001 (cit. on p. 11).

[49] Block, M. L. and Calderón-Garcidueñas, L. Air pollution: mechanisms of neuroinflammation and CNS disease. *Trends in neurosciences* 32.9 (2009), pp. 506–516. DOI: 10.1016/j.tins.2009.05.009 (cit. on p. 11).

[50] Mehta, M., Chen, L.-C., Gordon, T., Rom, W., and Tang, M.-s. Particulate matter inhibits DNA repair and enhances mutagenesis. *Mutation Research/-Genetic Toxicology and Environmental Mutagenesis* 657.2 (2008), pp. 116–121. DOI: 10.1016/j.mrgentox.2008.08.015 (cit. on p. 11).

[51] Glencross, D. A., Ho, T.-R., Camina, N., Hawrylowicz, C. M., and Pfeffer, P. E. Air pollution and its effects on the immune system. *Free Radical Biology and Medicine* 151 (2020), pp. 56–68. DOI: 10.1016/j.freeradbiomed.2020.01.179 (cit. on p. 11).

[52] Lodovici, M. and Bigagli, E. Oxidative stress and air pollution exposure. *Journal of toxicology* 2011.1 (2011), p. 487074. DOI: doi.org/10.1155/2011/487074 (cit. on p. 11).

[53] Genc, S., Zadeoglulari, Z., Fuss, S. H., and Genc, K. The adverse effects of air pollution on the nervous system. *Journal of toxicology* 2012.1 (2012), p. 782462. DOI: 10.1155/2012/782462 (cit. on pp. 11, 12).

[54] Hesterberg, T. W., Bunn, W. B., McClellan, R. O., Hamade, A. K., Long, C. M., and Valberg, P. A. Critical review of the human data on short-term nitrogen dioxide (NO_2) exposures: evidence for NO_2 no-effect levels. *Critical reviews in toxicology* 39.9 (2009), pp. 743–781. DOI: 10.3109/10408440903294945 (cit. on p. 11).

[55] Soni, V., Singh, P., Shree, V., and Goel, V. Effects of VOCs on human health. *Air pollution and control* (2018), pp. 119–142. DOI: 10.1007/978-981-10-7185-0_8 (cit. on p. 11).

[56] Kleinman, M. T. Sulfur dioxide and exercise: relationships between response and absorption in upper airways. *Journal of the Air Pollution Control Association* 34.1 (1984), pp. 32–37. DOI: 10.1080/00022470.1984.10465720 (cit. on p. 11).

[57] Shusterman, D. The effects of air pollutants and irritants on the upper airway. *Proceedings of the American Thoracic Society* 8.1 (2011), pp. 101–105. DOI: 10.1513/pats.201003-027RN (cit. on p. 11).

[58] Patocka, J. and Kuca, K. Irritant compounds: respiratory irritant gases. *Milit Med Sci Lett* 83.2 (2014), pp. 73–82. DOI: 10.31482/mmsl.2014.012 (cit. on p. 11).

[59] Achakulwisut, P., Brauer, M., Hystad, P., and Anenberg, S. C. Global, national, and urban burdens of paediatric asthma incidence attributable to ambient NO_2 pollution: estimates from global datasets. *The Lancet Planetary Health* 3.4 (2019), e166–e178. DOI: 10.1016/S2542-5196(19)30046-4 (cit. on p. 11).

[60] Chen, T.-M., Kuschner, W. G., Gokhale, J., and Shofer, S. Outdoor air pollution: nitrogen dioxide, sulfur dioxide, and carbon monoxide health effects. *The American journal of the medical sciences* 333.4 (2007), pp. 249–256. DOI: 10.1097/MAJ.0b013e31803b900f (cit. on pp. 11, 12).

[61] Schraufnagel, D. E., Balmes, J. R., Cowl, C. T., De Matteis, S., Jung, S.-H., Mortimer, K., Perez-Padilla, R., Rice, M. B., Riojas-Rodriguez, H., Sood,

A., et al. Air pollution and noncommunicable diseases: A review by the Forum of International Respiratory Societies' Environmental Committee, Part 2: Air pollution and organ systems. *Chest* 155.2 (2019), pp. 417–426. DOI: 10.1016/j.chest.2018.10.041 (cit. on pp. 11, 12).

[62] Kampa, M. and Castanas, E. Human health effects of air pollution. *Environmental pollution* 151.2 (2008), pp. 362–367. DOI: 10.1016/j.envpol.2007.06.012 (cit. on p. 11).

[63] Arngrim, N., Schytz, H. W., Hauge, M. K., Ashina, M., and Olesen, J. Carbon monoxide may be an important molecule in migraine and other headaches. *Cephalalgia* 34.14 (2014), pp. 1169–1180. DOI: 10.1177/0333102414534085 (cit. on p. 11).

[64] Townsend, C. L. and Maynard, R. L. Effects on health of prolonged exposure to low concentrations of carbon monoxide. *Occupational and Environmental Medicine* 59.10 (2002), pp. 708–711. DOI: 10.1136/oem.59.10.708 (cit. on p. 11).

[65] Peters, A. Ambient air pollution and Alzheimer's disease: The role of the composition of fine particles. *Proceedings of the National Academy of Sciences* 120.3 (2023), e2220028120. DOI: 10.1073/pnas.2220028120 (cit. on pp. 11, 12).

[66] Shehab, M. and Pope, F. Effects of short-term exposure to particulate matter air pollution on cognitive performance. *Scientific reports* 9.1 (2019), p. 8237. DOI: 10.1038/s41598-019-44561-0 (cit. on p. 12).

[67] Mallach, G., Shutt, R., Thomson, E. M., Valcin, F., Kulka, R., and Weichenthal, S. Randomized cross-over study of in-vehicle cabin air filtration, air pollution exposure, and acute changes to heart rate variability, saliva cortisol, and cognitive function. *Environmental Science & Technology* 57.8 (2023), pp. 3238–3247. DOI: 10.1021/acs.est.2c06556 (cit. on p. 12).

[68] Lee, B.-J., Kim, B., and Lee, K. Air pollution exposure and cardiovascular disease. *Toxicological research* 30.2 (2014), pp. 71–75. DOI: 10.5487/TR.2014.30.2.071 (cit. on p. 12).

[69] Sunyer, J., Ballester, F., Tertre, A. L., Atkinson, R., Ayres, J. G., Forastiere, F., Forsberg, B., Vonk, J. M., Bisanti, L., Tenías, J. M., et al. The association of daily sulfur dioxide air pollution levels with hospital admissions for cardiovascular diseases in Europe (The Aphea-II study). *European heart journal* 24.8 (2003), pp. 752–760. DOI: 10.1016/S0195-668X(02)00808-4 (cit. on p. 12).

[70] Bourdrel, T., Bind, M.-A., Béjot, Y., Morel, O., and Argacha, J.-F. Cardiovascular effects of air pollution. *Archives of cardiovascular diseases* 110.11 (2017), pp. 634–642. DOI: 10.1016/j.acvd.2017.05.003 (cit. on p. 12).

[71] European Environment Agency. *How air pollution affects our health*. https://www.eea.europa.eu/en/topics/in-depth/air-pollution/eow-it-affects-our-health. Accessed: 2025-02-08. 2024 (cit. on p. 12).

[72] Kelly, F. J. and Fussell, J. C. Size, source and chemical composition as determinants of toxicity attributable to ambient particulate matter. *Atmospheric environment* 60 (2012), pp. 504–526. DOI: 10.1016/j.atmosenv.2012.06.039 (cit. on p. 12).

[73] United Kingdom Parliment. *Research Briefing: Urban outdoor air quality*. https://post.parliament.uk/research-briefings. Accessed: 2025-02-08. 2023 (cit. on p. 12).

[74] World Bank. *The Global Health Cost of $PM_{2.5}$ Air Pollution: A Case for Action Beyond 2021*. https://openknowledge.worldbank.org/entities/publication/c96ee144-4a4b-5164-ad79-74c051179eee. 2022 (cit. on pp. 12, 16).

[75] Woodby, B., Arnold, M. M., and Valacchi, G. SARS-CoV-2 infection, COVID-19 pathogenesis, and exposure to air pollution: What is the connection? *Annals of the new York Academy of Sciences* 1486.1 (2021), pp. 15–38. DOI: 10.1111/nyas.14512 (cit. on p. 12).

[76] Ali, N. and Islam, F. The effects of air pollution on COVID-19 infection and mortality—a review on recent evidence. *Frontiers in public health* 8 (2020), p. 580057. DOI: 10.3389/fpubh.2020.580057 (cit. on p. 12).

[77] Zhou, Z., Shuai, X., Lin, Z., Yu, X., Ba, X., Holmes, M. A., Xiao, Y., Gu, B., and Chen, H. Association between particulate matter ($PM_{2.5}$) air pollution and clinical antibiotic resistance: a global analysis. *The Lancet Planetary Health* 7.8 (2023), e649–e659. DOI: 10.1016/S2542-5196(23)00135-3 (cit. on p. 13).

[78] Grennfelt, P., Engleryd, A., Forsius, M., Hov, Ø., Rodhe, H., and Cowling, E. Acid rain and air pollution: 50 years of progress in environmental science and policy. *Ambio* 49 (2020), pp. 849–864. DOI: 10.1007/s13280-019-01244-4 (cit. on p. 13).

[79] Bouwman, A., Van Vuuren, D., Derwent, R., and Posch, M. A global analysis of acidification and eutrophication of terrestrial ecosystems. *Water, Air, and Soil Pollution* 141 (2002), pp. 349–382. DOI: 10.1023/A:1021398008726 (cit. on p. 14).

[80] Khan, M. N. and Mohammad, F. Eutrophication: challenges and solutions. *Eutrophication: Causes, Consequences and Control: Volume 2* (2014), pp. 1–15. DOI: 10.1007/978-94-007-7814-6_1 (cit. on p. 14).

[81] Schraudner, M., Langebartels, C., and Sandermann, H. Changes in the biochemical status of plant cells induced by the environmental pollutant ozone. *Physiologia Plantarum* 100.2 (1997), pp. 274–280. DOI: 10.1111/j.1399-3054.1997.tb04783.x (cit. on p. 14).

[82] Grulke, N. and Heath, R. Ozone effects on plants in natural ecosystems. *Plant Biology* 22 (2020), pp. 12–37. DOI: 10.1111/plb.12971 (cit. on p. 14).

[83] Van Dingenen, R., Dentener, F. J., Raes, F., Krol, M. C., Emberson, L., and Cofala, J. The global impact of ozone on agricultural crop yields under current and future air quality legislation. *Atmospheric Environment* 43.3 (2009), pp. 604–618. DOI: 10.1016/j.atmosenv.2008.10.033 (cit. on p. 14).

[84] Myhre, G., Shindell, D., Bréon, F.-M., Collins, W., Fuglestvedt, J., Huang, J., Koch, D., Lamarque, J.-F., Lee, D., Mendoza, B., et al. Anthropogenic and natural radiative forcing. *Climate Change 2013-The Physical Science Basis* (2014), pp. 659–740. DOI: 10.1017/CBO9781107415324.018 (cit. on p. 14).

[85] Akasha, H., Ghaffarpasand, O., and Pope, F. Climate change and air pollution. *The Institute of Development Studies and Partner Organisations* (2021). DOI: 10.19088/K4D.2021.071 (cit. on p. 14).

[86] United Kingdom National Atmospheric Emissions Inventory. *United Kingdom Informative Inventory Report (1990 to 2021)*. https://uk-air.defra.gov.uk/assets/documents/reports/cat09/2303151609_UK_IIR_2023_Submission.pdf. Accessed: 2025-02-11. 2023 (cit. on pp. 14, 29).

[87] Koolen, C. D. and Rothenberg, G. Air pollution in Europe. *ChemSusChem* 12.1 (2019), pp. 164–172. DOI: 10.1002/cssc.201802292 (cit. on pp. 14, 19, 45).

[88] Sicard, P., Agathokleous, E., Anenberg, S. C., De Marco, A., Paoletti, E., and Calatayud, V. Trends in urban air pollution over the last two decades: A global perspective. *Science of The Total Environment* 858 (2023), p. 160064. DOI: 10.1016/j.scitotenv.2022.160064 (cit. on pp. 14, 16).

[89] Geddes, J. A., Martin, R. V., Boys, B. L., and Donkelaar, A. van. Long-term trends worldwide in ambient NO_2 concentrations inferred from satellite observations. *Environmental health perspectives* 124.3 (2016), pp. 281–289. DOI: 10.1289/ehp.1409567 (cit. on pp. 14, 16).

[90] Department for Environment, Food and Rural Affairs. *Emissions of air pollutants in the United Kingdom - Summary*. https://www.gov.uk/government/statistics/emissions-of-air-pollutants/emissions-of-air-pollutants-in-the-uk-summary. Accessed: 2025-02-10. 2024 (cit. on pp. 14, 19, 45).

[91] Department for the Environment Food and Rural Affairs. *Automatic Urban and Rural Network*. https://uk-air.defra.gov.uk/networks/network-info?view=aurn. Accessed: 2025-03-16. 2025 (cit. on pp. 15, 55).

[92] Li, C., Donkelaar, A. van, Hammer, M. S., McDuffie, E. E., Burnett, R. T., Spadaro, J. V., Chatterjee, D., Cohen, A. J., Apte, J. S., Southerland, V. A., et al. Reversal of trends in global fine particulate matter air pollution. *Nature*

Communications 14.1 (2023), p. 5349. DOI: 10.1038/s41467-023-41086-z (cit. on p. 15).

[93] World Health Organization. *WHO global air quality guidelines: particulate matter ($PM_{2.5}$ and PM_{10}), ozone, nitrogen dioxide, sulfur dioxide and carbon monoxide*. https://www.who.int/publications/i/item/9789240034228. Accessed: 2024-05-17. 2021 (cit. on p. 16).

[94] Department for Transport. *VEH1102: Licensed vehicles at the end of the year by body type and keepership (private and company): Great Britain and United Kingdom*. https://www.gov.uk/government/statistical-data-sets/vehicle-licensing-statistics-data. Accessed: 2025-02-11. 2024 (cit. on pp. 17, 43).

[95] Hård, M. and Jamison, A. Alternative cars: the contrasting stories of steam and diesel automotive engines. *Technology in Society* 19.2 (1997), pp. 145–160. DOI: 10.1016/S0160-791X(96)00061-9 (cit. on p. 17).

[96] United Kingdom Government. *Locomotive Act 1861*. https://www.legislation.gov.uk/ukpga/Vict/24-25/70/enacted. Accessed: 2025-02-11. 1861 (cit. on p. 17).

[97] Sturgess, J. The Case for the Steam Car. *SAE Transactions* 13 (1918), pp. 357–379 (cit. on p. 17).

[98] Van Basshuysen, R., Schäfer, F., et al. *Internal combustion engine handbook*. SAE International, 2016 (cit. on p. 17).

[99] Royal College of Physicians. *Every breath we take: the lifelong impact of air pollution*. https://www.rcp.ac.uk/improving-care/resources/every-breath-we-take-the-lifelong-impact-of-air-pollution/. Accessed: 2025-02-11. 2016 (cit. on p. 17).

[100] United Kingdom Government. *Road Traffic Act 1960*. https://www.legislation.gov.uk/ukpga/Eliz2/8-9/16/contents. Accessed: 2025-02-12. 1960 (cit. on pp. 17, 18).

[101] Henssler, H. and Gospage, S. The exhaust emission standards of the European community. *SAE transactions* (1987), pp. 159–173 (cit. on pp. 17, 18).

[102] European Union. *Council Directive 91/441/EEC of 26 June 1991 amending Directive 70/220/EEC on the approximation of the laws of the Member States relating to measures to be taken against air pollution by emissions from motor vehicles*. https://eur-lex.europa.eu/eli/dir/1991/441/oj/eng. Accessed: 2025-02-12. 1991 (cit. on pp. 17, 18).

[103] Von Storch, H., Costa-Cabral, M., Hagner, C., Feser, F., Pacyna, J., Pacyna, E., and Kolb, S. Four decades of gasoline lead emissions and control policies in Europe: a retrospective assessment. *Science of the Total Environment* 311.1-3 (2003), pp. 151–176. DOI: 10.1016/S0048-9697(03)00051-2 (cit. on pp. 17, 18, 25).

[104] Singh, S., Kulshrestha, M. J., Rani, N., Kumar, K., Sharma, C., and Aswal, D. An overview of vehicular emission standards. *Mapan* 38.1 (2023), pp. 241–263. DOI: 10.1007/s12647-022-00555-4 (cit. on pp. 17, 18).

[105] United Kingdom Government. *The Environmental Permitting (England and Wales) Regulations 2016*. https://www.legislation.gov.uk/uksi/2016/1154/contents. Accessed: 2025-02-11. 2016 (cit. on p. 17).

[106] Grange, S. K., Farren, N. J., Vaughan, A. R., Rose, R. A., and Carslaw, D. C. Strong temperature dependence for light-duty diesel vehicle NO_X emissions. *Environmental science & technology* 53.11 (2019), pp. 6587–6596. DOI: 10.1021/acs.est.9b01024 (cit. on p. 18).

[107] Xiang, J., Ghaffarpasand, O., and Pope, F. D. Assessing the Impact of Calendar Events upon Urban Vehicle Behaviour and Emissions Using Telematics Data. *Smart Cities* 7.6 (2024), pp. 3071–3094. DOI: 10.3390/smartcities7060120 (cit. on p. 18).

[108] Daham, B., Li, H., Andrews, G. E., Tate, J., Ropkins, K., and Bell, M. *Driver Variability Influences on Real World Emissions at a Road Junction using a PEMS*. Tech. rep. SAE Technical Paper, 2010 (cit. on p. 18).

[109] Davison, J., Rose, R. A., Farren, N. J., Wagner, R. L., Wilde, S. E., Wareham, J. V., and Carslaw, D. C. Gasoline and diesel passenger car emissions deterioration using on-road emission measurements and measured mileage. *Atmospheric Environment: X* 14 (2022), p. 100162. DOI: 10.1016/j.aeaoa.2022.100162 (cit. on p. 18).

[110] Bell, J., Honour, S. L., and Power, S. A. Effects of vehicle exhaust emissions on urban wild plant species. *Environmental Pollution* 159.8-9 (2011), pp. 1984–1990. DOI: 10.1016/j.envpol.2011.03.006 (cit. on p. 18).

[111] Boogaard, H., Patton, A., Atkinson, R., Brook, J., Chang, H., Crouse, D., Fussell, J., Hoek, G., Hoffmann, B., Kappeler, R., et al. Long-term exposure to traffic-related air pollution and selected health outcomes: A systematic review and meta-analysis. *Environment international* 164 (2022), p. 107262. DOI: 10.1016/j.envint.2022.107262 (cit. on p. 18).

[112] Levy, I., Mihele, C., Lu, G., Narayan, J., and Brook, J. R. Evaluating multipollutant exposure and urban air quality: pollutant interrelationships, neighborhood variability, and nitrogen dioxide as a proxy pollutant. *Environmental health perspectives* 122.1 (2014), pp. 65–72. DOI: 10.1289/ehp.1306518 (cit. on p. 19).

[113] Arter, C. A., Buonocore, J. J., Isakov, V., Pandey, G., and Arunachalam, S. Air pollution benefits from reduced on-road activity due to COVID-19 in the United States. *PNAS nexus* 3.1 (2024), pgae017. DOI: 10.1093/pnasnexus/pgae017 (cit. on p. 19).

[114] Matthaios, V. N., Kramer, L. J., Crilley, L. R., Sommariva, R., Pope, F. D., and Bloss, W. J. Quantification of within-vehicle exposure to NO_X and particles: Variation with outside air quality, route choice and ventilation options. *Atmospheric Environment* 240 (2020), p. 117810. DOI: 10.1016/j.atmosenv.2020.117810 (cit. on p. 19).

[115] Jonidi Jafari, A., Charkhloo, E., and Pasalari, H. Urban air pollution control policies and strategies: a systematic review. *Journal of Environmental Health*

Science and Engineering 19 (2021), pp. 1911–1940. DOI: 10.1007/s40201-021-00744-4 (cit. on p. 20).

[116] Cropper, M. and Suri, P. Measuring the air pollution benefits of public transport projects. *Regional Science and Urban Economics* 107 (2024), p. 103976. DOI: 10.1016/j.regsciurbeco.2023.103976 (cit. on p. 20).

[117] Transport for London. *Ultra Low Emission Zone*. https://tfl.gov.uk/modes/driving/ultra-low-emission-zone. Accessed: 2025-02-11. 2024 (cit. on p. 20).

[118] Bernard, Y., Miller, J., Wappelhorst, S., and Braun, C. Impacts of the Paris low-emission zone and implications for other cities. *TRUE–The Real Urban Emissions Initiative, United Kingdom, ISBN* 1744072 (2020) (cit. on p. 20).

[119] Park, D. and Lim, B. I. The effect of the ultra-low emission zone on $PM_{2.5}$ concentration in Seoul, South Korea. *Atmospheric Environment* 340 (2025), p. 120908. DOI: 10.1016/j.atmosenv.2024.120908 (cit. on p. 20).

[120] Requia, W. J., Mohamed, M., Higgins, C. D., Arain, A., and Ferguson, M. How clean are electric vehicles? Evidence-based review of the effects of electric mobility on air pollutants, greenhouse gas emissions and human health. *Atmospheric Environment* 185 (2018), pp. 64–77. DOI: 10.1016/j.atmosenv.2018.04.040 (cit. on p. 20).

[121] Das, P. K., Bhat, M. Y., and Sajith, S. Life cycle assessment of electric vehicles: a systematic review of literature. *Environmental Science and Pollution Research* 31.1 (2024), pp. 73–89. DOI: 10.1007/s11356-023-30999-3 (cit. on p. 20).

[122] Ferrero, E., Alessandrini, S., and Balanzino, A. Impact of the electric vehicles on the air pollution from a highway. *Applied energy* 169 (2016), pp. 450–459. DOI: 10.1016/j.apenergy.2016.01.098 (cit. on p. 20).

[123] Woo, S.-H., Jang, H., Lee, S.-B., and Lee, S. Comparison of total PM emissions emitted from electric and internal combustion engine vehicles: An experimental analysis. *Science of The Total Environment* 842 (2022), p. 156961. DOI: 10.1016/j.scitotenv.2022.156961 (cit. on pp. 20, 41).

[124] Department for Transport. *VEH1103: Licensed vehicles at the end of the quarter by body type and fuel type: Great Britain and United Kingdom*. https://www.gov.uk/government/statistical-data-sets. Accessed: 2025-02-11. 2024 (cit. on pp. 20, 26).

[125] United Kingdom Government. *Government sets out path to zero emission vehicles by 2035*. https://www.gov.uk/government/news/government-sets-out-path-to-zero-emission-vehicles-by-2035. Accessed: 2025-02-12. 2023 (cit. on p. 20).

[126] Nguyen-Tien, V., Elliott, R. J., Strobl, E., and Zhang, C. *Estimating the longevity of electric vehicles: What do 300 million MOT test results tell us?* https://cep.lse.ac.uk/_NEW/publications/abstract.asp?index=10626. 2024 (cit. on p. 20).

[127] Chanda, R. C., Vafaei-Zadeh, A., Hanifah, H., Ashrafi, D. M., and Ahmed, T. Achieving a sustainable future by analyzing electric vehicle adoption in developing nations through an extended technology acceptance model. *Sustainable Futures* 8 (2024), p. 100386. DOI: 10.1016/j.sftr.2024.100386 (cit. on p. 20).

[128] United Nations Environment Programme. *Used Vehicles and the Environment*. https://www.unep.org/resources/report/global-trade-used-vehicles-report. Accessed: 2025-02-12. 2020 (cit. on p. 21).

[129] Sarıkoç, S. Fuels of the diesel-gasoline engines and their properties. *Diesel and Gasoline Engines* 31 (2020). DOI: 10.5772/intechopen.89044 (cit. on pp. 22, 24, 26, 27).

[130] Air Quality Expert Group. *Exhaust Emissions from Road Transport*. https://uk-air.defra.gov.uk/assets/documents/reports/cat09/2112201014_1272021_Exaust_Emissions_From_Road_Transport.pdf. Accessed: 2025-02-17. 2021 (cit. on p. 23).

[131] United Kingdom Government. *The Oil Fuel (Sulphur Content of Gas Oil) Regulations 1990*. https://www.legislation.gov.uk/uksi/1990/1096/made. Accessed: 2025-02-17. 1990 (cit. on p. 24).

[132] Spikes, H. Low-and zero-sulphated ash, phosphorus and sulphur anti-wear additives for engine oils. *Lubrication science* 20.2 (2008), pp. 103–136. DOI: 10.1002/ls.57 (cit. on p. 25).

[133] Shao, H., Roos, J. W., and Remias, J. E. Evaluation of the Role of Lubricant Additives in Emission Control. *Lubricants* 10.12 (2022), p. 362. DOI: 10.3390/lubricants10120362 (cit. on p. 25).

[134] Xie, C., Toops, T. J., Lance, M. J., Qu, J., Viola, M. B., Lewis, S. A., Leonard, D. N., and Hagaman, E. W. Impact of Lubricant Additives on the Physicochemical Properties and Activity of Three-Way Catalysts. *Catalysts* 6.4 (2016), p. 54. DOI: 10.3390/cata16040054 (cit. on p. 25).

[135] Needleman, H. L. and Bellinger, D. C. Lead Hazards and Poisoning. *International Encyclopedia of Public Health (Second Edition)*. Ed. by S. R. Quah. Second Edition. Oxford: Academic Press, 2017, pp. 377–383. DOI: https://doi.org/10.1016/B978-0-12-803678-5.00249-6. URL: https://www.sciencedirect.com/science/article/pii/B9780128036785002496 (cit. on p. 25).

[136] United Kingdom Government. *E10 Petrol Explained*. https://www.gov.uk/guidance/e10-petrol-explained. Accessed: 2025-02-17. 2021 (cit. on p. 25).

[137] United Kingdom Government. *Road Fuel Labelling*. https://assets.publishing.service.gov.uk/media/5e70f58cd3bf7f269dbeef48/road-fuel-labelling-government-response-document.pdf. Accessed: 2025-02-17. 2019 (cit. on p. 25).

[138] Air Quality Expert Group and others. Road transport biofuels: impact on United Kingdom air quality. *Department for Environment, Food and Rural Affairs: London, UK* (2011) (cit. on p. 25).

[139] Anderson, L. G. Effects of using renewable fuels on vehicle emissions. *Renewable and Sustainable Energy Reviews* 47 (2015), pp. 162–172. DOI: 10.1016/j.rser.2015.03.011 (cit. on pp. 25, 26).

[140] Wallington, T. J., Anderson, J. E., Kurtz, E. M., and Tennison, P. J. Biofuels, vehicle emissions, and urban air quality. *Faraday discussions* 189 (2016), pp. 121–136. DOI: 10.1039/C5FD00205B (cit. on p. 25).

[141] Bielaczyc, P., Szczotka, A., and Woodburn, J. A comparison of exhaust emissions from vehicles fuelled with petrol, LPG and CNG. *IOP Conference Series: Materials Science and Engineering*. Vol. 148. 1. IOP Publishing. 2016, p. 012060. DOI: 10.1088/1757-899X/148/1/012060 (cit. on p. 26).

[142] Aosaf, M. R., Wang, Y., and Du, K. Comparison of the emission factors of air pollutants from gasoline, CNG, LPG and diesel fueled vehicles at idle speed. *Environmental pollution* 305 (2022), p. 119296. DOI: 10.1016/j.envpol.2022.119296 (cit. on p. 26).

[143] Leach, F., Kalghatgi, G., Stone, R., and Miles, P. The scope for improving the efficiency and environmental impact of internal combustion engines. *Transportation Engineering* 1 (2020), p. 100005. DOI: 10.1016/j.treng.2020.100005 (cit. on pp. 26, 27).

[144] Reşitoğlu, İ. A., Altinişik, K., and Keskin, A. The pollutant emissions from diesel-engine vehicles and exhaust aftertreatment systems. *Clean Technologies and Environmental Policy* 17 (2015), pp. 15–27. DOI: 10.1007/s10098-014-0793-9 (cit. on p. 27).

[145] IARC Working Group on the Evaluation of Carcinogenic Risks to Humans and International Agency for Research on Cancer. *Diesel and gasoline engine exhausts and some nitroarenes*. Vol. 46. World Health Organization, 1989 (cit. on p. 27).

[146] Kašpar, J., Fornasiero, P., and Hickey, N. Automotive catalytic converters: current status and some perspectives. *Catalysis today* 77.4 (2003), pp. 419–449. DOI: 10.1016/S0920-5861(02)00384-X (cit. on pp. 28, 29).

[147] Ramanathan, K., Sharma, C. S., and Kim, C. H. Global kinetics for ammonia formation and oxidation reactions in a commercial three-way catalyst. *Industrial & engineering chemistry research* 51.3 (2012), pp. 1198–1208. DOI: 10.1021/ie2017866 (cit. on pp. 29, 30).

[148] Twigg, M. V. Progress and future challenges in controlling automotive exhaust gas emissions. *Applied Catalysis B: Environmental* 70.1-4 (2007), pp. 2–15. DOI: 10.1016/j.apcatb.2006.02.029 (cit. on pp. 29, 31).

[149] Rood, S., Eslava, S., Manigrasso, A., and Bannister, C. Recent advances in gasoline three-way catalyst formulation: A review. *Proceedings of the Institution of Mechanical Engineers, Part D: Journal of Automobile Engineering* 234.4 (2020), pp. 936–949. DOI: 10.1177/0954407019859822 (cit. on p. 29).

[150] Heeb, N. V., Forss, A.-M., Brühlmann, S., Lüscher, R., Saxer, C. J., and Hug, P. Three-way catalyst-induced formation of ammonia—velocity-and acceleration-dependent emission factors. *Atmospheric Environment* 40.31 (2006), pp. 5986–5997. DOI: P10.1016/j.atmosenv.2005.12.035 (cit. on p. 30).

[151] Joshi, A. and Johnson, T. V. Gasoline particulate filters—A review. *Emission Control Science and Technology* 4.4 (2018), pp. 219–239. DOI: 10.1007/s40825-018-0101-y (cit. on p. 30).

[152] Richter, J. M., Klingmann, R., Spiess, S., and Wong, K.-F. Application of catalyzed gasoline particulate filters to GDI vehicles. *SAE International Journal of Engines* 5.3 (2012), pp. 1361–1370 (cit. on p. 30).

[153] Bishop, G. A. and Stedman, D. H. Emissions of nitrogen dioxide from modern diesel vehicles. *WIT Transactions on Ecology and the Environment* 116 (2008), pp. 247–254. DOI: 10.2495/AIR080261 (cit. on p. 32).

[154] Zheng, M., Reader, G. T., and Hawley, J. G. Diesel engine exhaust gas recirculation—-a review on advanced and novel concepts. *Energy conversion and management* 45.6 (2004), pp. 883–900. DOI: 10.1016/S0196-8904(03)00194-8 (cit. on p. 32).

[155] Synák, F. and Synák, J. Study of the Impact of Malfunctions of and Interferences in the Exhaust Gas Recirculation System on Selected Vehicle Characteristics. *SAE International Journal of Engines* 15.6 (2022), pp. 757–772 (cit. on p. 32).

[156] Feng, R., Hu, X., Li, G., Sun, Z., and Deng, B. A comparative investigation between particle oxidation catalyst (POC) and diesel particulate filter (DPF) coupling aftertreatment system on emission reduction of a non-road diesel engine. *Ecotoxicology and Environmental Safety* 238 (2022), p. 113576. DOI: 10.1016/j.ecoenv.2022.113576 (cit. on p. 32).

[157] Wang, Y., Raman, S., and Grizzle, J. W. Dynamic modeling of a lean NO/sub x/trap for lean burn engine control. *Proceedings of the 1999 American Control Conference (Cat. No. 99CH36251)*. Vol. 2. IEEE. 1999, pp. 1208–1212. DOI: 10.1109/ACC.1999.783232 (cit. on p. 33).

[158] Forzatti, P., Lietti, L., and Castoldi, L. Storage and Reduction of NO_X over LNT Catalysts. *Catalysis Letters* 145 (2015), pp. 483–504. DOI: 10.1007/s10562-014-1343-0 (cit. on p. 33).

[159] Forzatti, P. Present status and perspectives in de-NO_X SCR catalysis. *Applied catalysis A: general* 222.1-2 (2001), pp. 221–236. DOI: 10.1016/S0926-860X(01)00832-8 (cit. on p. 34).

[160] Koebel, M., Elsener, M., and Madia, G. Reaction pathways in the selective catalytic reduction process with NO and NO_2 at low temperatures. *Industrial & Engineering Chemistry Research* 40.1 (2001), pp. 52–59. DOI: 10.1021/ie000551y (cit. on p. 34).

[161] Börnhorst, M. and Deutschmann, O. Advances and challenges of ammonia delivery by urea-water sprays in SCR systems. *Progress in Energy and Combustion Science* 87 (2021), p. 100949. DOI: P10.1016/j.pecs.2021.100949 (cit. on p. 34).

[162] DiGiulio, C. D., Pihl, J. A., Choi, J.-S., Parks II, J. E., Lance, M. J., Toops, T. J., and Amiridis, M. D. NH_3 formation over a lean NO_X trap (LNT) system: Effects of lean/rich cycle timing and temperature. *Applied Catalysis B: Environmental* 147 (2014), pp. 698–710. DOI: 10.1016/j.apcatb.2013.09.012 (cit. on p. 34).

[163] Maunula, T., Tuikka, M., and Wolff, T. The reactions and role of ammonia slip catalysts in modern urea-SCR Systems. *Emission Control Science and Technology* 6.4 (2020), pp. 390–401. DOI: 10.1007/s40825-020-00171-1 (cit. on p. 35).

[164] Leighton, P. *Photochemistry of air pollution*. Elsevier, 2012 (cit. on p. 36).

[165] Crutzen, P. J. Tropospheric ozone: An overview. *Tropospheric ozone: regional and global scale interactions* (1988), pp. 3–32. DOI: 10.1007/978-94-009-2913-5_1 (cit. on p. 36).

[166] Madronich, S., Hastie, D., Ridley, B., and Schiff, H. Measurement of the photodissociation coefficient of NO_2 in the atmosphere: I. Method and surface measurements. *Journal of Atmospheric Chemistry* 1 (1983), pp. 3–25. DOI: 10.1007/BF00113977 (cit. on p. 36).

[167] Ivatt, P. D., Evans, M. J., and Lewis, A. C. Suppression of surface ozone by an aerosol-inhibited photochemical ozone regime. *Nature Geoscience* 15.7 (2022), pp. 536–540. DOI: 10.1038/s41561-022-00972-9 (cit. on p. 38).

[168] Sun, J., Wu, F., Hu, B., Tang, G., Zhang, J., and Wang, Y. VOC characteristics, emissions and contributions to SOA formation during hazy episodes. *Atmospheric Environment* 141 (2016), pp. 560–570. DOI: doi.org/10.1016/j.atmosenv.2016.06.060 (cit. on p. 38).

[169] Fan, L., Yan, X., Du, Q., Zhang, J., Liu, G., Yang, Y., Miao, Y., and Zhang, G. On the sources of ambient SOA in $PM_{2.5}$: An integrated analysis over Jinan city of China. *Atmospheric Pollution Research* 15.3 (2024), p. 102008. DOI: 10.1016/j.apr.2023.102008 (cit. on p. 38).

[170] Orel, A. E. and Seinfeld, J. H. Nitrate formation in atmospheric aerosols. *Environmental Science & Technology* 11.10 (1977), pp. 1000–1007. DOI: 10.1021/es60133a009 (cit. on p. 38).

[171] Peng, W., McCaffery, C., Kuittinen, N., Rönkkö, T., Cocker, D. R., and Karavalakis, G. Secondary organic and inorganic aerosol formation from a GDI

vehicle under different driving conditions. *Atmosphere* 13.3 (2022), p. 433. DOI: 10.3390/atmos13030433 (cit. on p. 38).

[172] Kurtenbach, R., Becker, K., Gomes, J., Kleffmann, J., Lörzer, J., Spittler, M., Wiesen, P., Ackermann, R., Geyer, A., and Platt, U. Investigations of emissions and heterogeneous formation of HONO in a road traffic tunnel. *Atmospheric Environment* 35.20 (2001), pp. 3385–3394. DOI: 10.1016/S1352-2310(01)00138-8 (cit. on p. 39).

[173] Kirchstetter, T. W., Harley, R. A., and Littlejohn, D. Measurement of nitrous acid in motor vehicle exhaust. *Environmental science & technology* 30.9 (1996), pp. 2843–2849. DOI: 10.1021/es960135y (cit. on p. 39).

[174] Thorpe, A. and Harrison, R. M. Sources and properties of non-exhaust particulate matter from road traffic: a review. *Science of the total environment* 400.1-3 (2008), pp. 270–282. DOI: 10.1016/j.scitotenv.2008.06.007 (cit. on p. 40).

[175] Piscitello, A., Bianco, C., Casasso, A., and Sethi, R. Non-exhaust traffic emissions: Sources, characterization, and mitigation measures. *Science of the Total Environment* 766 (2021), p. 144440. DOI: 10.1016/j.scitotenv.2020.144440 (cit. on pp. 40, 41).

[176] Air Quality Expert Group. *Non-Exhaust Emissions from Road Transport*. https://uk-air.defra.gov.uk/assets/documents/reports/cat09/1907101151_20190709_Non_Exhaust_Emissions_typeset_Final.pdf. Accessed: 2025-02-19. 2019 (cit. on pp. 40, 44).

[177] Pant, P. and Harrison, R. M. Estimation of the contribution of road traffic emissions to particulate matter concentrations from field measurements: A review. *Atmospheric environment* 77 (2013), pp. 78–97 (cit. on pp. 40, 41).

[178] Wåhlin, P., Berkowicz, R., and Palmgren, F. Characterisation of traffic-generated particulate matter in Copenhagen. *Atmospheric Environment* 40.12 (2006), pp. 2151–2159. DOI: 10.1016/j.atmosenv.2005.11.049 (cit. on p. 40).

[179] Grigoratos, T. and Martini, G. Brake wear particle emissions: a review. *Environmental science and pollution research* 22 (2015), pp. 2491–2504. DOI: 10.1007/s11356-014-3696-8 (cit. on p. 40).

[180] Zhang, M., Yin, H., Tan, J., Wang, X., Yang, Z., Hao, L., Du, T., Niu, Z., and Ge, Y. A comprehensive review of tyre wear particles: Formation, measurements, properties, and influencing factors. *Atmospheric Environment* 297 (2023), p. 119597. DOI: 10.1016/j.atmosenv.2023.119597 (cit. on p. 40).

[181] Lindgren, Å. Asphalt wear and pollution transport. *Science of the Total Environment* 189 (1996), pp. 281–286. DOI: 10.1016/0048-9697(96)05220-5 (cit. on p. 40).

[182] Gehrig, R., Zeyer, K., Bukowiecki, N., Lienemann, P., Poulikakos, L., Furger, M., and Buchmann, B. Mobile load simulators–A tool to distinguish between the emissions due to abrasion and resuspension of PM_{10} from road surfaces. *Atmospheric Environment* 44.38 (2010), pp. 4937–4943. DOI: 10.1016/j.atmosenv.2010.08.020 (cit. on p. 40).

[183] Gustafsson, M. and Johansson, C. *Road pavements and PM_{10}: summary of the results of research funded by the Swedish Transport Administration on how the properties of road pavements influence emissions and the properties of wear particles*. Trafikverket, 2012 (cit. on p. 40).

[184] Denby, B. R., Kupiainen, K. J., and Gustafsson, M. Review of road dust emissions. *Non-exhaust emissions*. Elsevier, 2018, pp. 183–203 (cit. on p. 40).

[185] Timmers, V. R. and Achten, P. A. Non-exhaust PM emissions from electric vehicles. *Atmospheric environment* 134 (2016), pp. 10–17 (cit. on p. 41).

[186] Antanaitis, D. B. Effect of regenerative braking on foundation brake performance. *SAE International Journal of Passenger Cars-Mechanical Systems* 3.2010-01-1681 (2010), pp. 14–30. DOI: 10.4271/2010-01-1681 (cit. on p. 41).

[187] Tipton, M. J., Lathem, T. L., Fu, J. S., and Tschantz, M. F. Effectiveness of emissions standards on automotive evaporative emissions in Europe under normal and extreme temperature conditions. *Environmental Research Communications* 4.8 (2022), p. 081003. DOI: 10.1088/2515-7620/ac8b69 (cit. on p. 42).

[188] Rubin, J. I., Kean, A. J., Harley, R. A., Millet, D. B., and Goldstein, A. H. Temperature dependence of volatile organic compound evaporative emissions from motor vehicles. *Journal of Geophysical Research: Atmospheres* 111.D3 (2006). DOI: 10.1029/2005JD006458 (cit. on p. 42).

[189] Ehsani, M., Gao, Y., and Miller, J. M. Hybrid electric vehicles: Architecture and motor drives. *Proceedings of the IEEE* 95.4 (2007), pp. 719–728. DOI: 10.1109/JPROC.2007.892492 (cit. on p. 43).

[190] Sher, F., Chen, S., Raza, A., Rasheed, T., Razmkhah, O., Rashid, T., Rafi-ul-Shan, P. M., and Erten, B. Novel strategies to reduce engine emissions and improve energy efficiency in hybrid vehicles. *Cleaner Engineering and Technology* 2 (2021), p. 100074. DOI: [10.1016/j.clet.2021.100074 (cit. on p. 43).

[191] Amini, M. R., Feng, Y., Wang, H., Kolmanovsky, I., and Sun, J. Thermal responses of connected HEVs engine and aftertreatment systems to eco-driving. *2019 IEEE Conference on Control Technology and Applications (CCTA)*. IEEE. 2019, pp. 724–729. DOI: 10.1109/CCTA.2019.8920520 (cit. on p. 43).

[192] Li, H., Andrews, G. E., Savvidis, D., Daham, B., Ropkins, K., Bell, M., and Tate, J. Study of thermal characteristics and emissions during cold start using an on-board measuring method for modern SI car real world urban driving. *SAE International Journal of Engines* 1.1 (2009), pp. 804–819 (cit. on p. 44).

[193] Matthaios, V. N., Kramer, L. J., Sommariva, R., Pope, F. D., and Bloss, W. J. Investigation of vehicle cold start primary NO_2 emissions inferred from ambient monitoring data in the UK and their implications for urban air

quality. *Atmospheric Environment* 199 (2019), pp. 402–414. DOI: 10.1016/j.atmosenv.2018.11.031 (cit. on p. 44).

[194] Wilde, S. E., Padilla, L. E., Farren, N. J., Alvarez, R. A., Wilson, S., Lee, J. D., Wagner, R. L., Slater, G., Peters, D., and Carslaw, D. C. Mobile monitoring reveals congestion penalty for vehicle emissions in London. *Atmospheric Environment: X* 21 (2024), p. 100241. DOI: 10.1016/j.aeaoa.2024.100241 (cit. on pp. 44, 47, 56, 61).

[195] Wu, L., Yu, F., Luo, H., Zhu, M., Liao, S., Liu, J., Wu, C., Horchler, E. J., Ristovski, Z., and Zheng, J. Characterization of ammonia emissions from light-duty gasoline vehicles based on real-world driving and dynamometer measurements. *Science of The Total Environment* 929 (2024), p. 172644. DOI: 10.1016/j.scitotenv.2024.172644 (cit. on p. 44).

[196] Park, G., Park, S., Hwang, T., Oh, S., and Lee, S. A Study on the Impact of DPF Failure on Diesel Vehicles Emissions of Particulate Matter. *Applied Sciences* 13.13 (2023), p. 7592. DOI: 10.3390/app13137592 (cit. on p. 44).

[197] Giechaskiel, B., Joshi, A., Ntziachristos, L., and Dilara, P. European regulatory framework and particulate matter emissions of gasoline light-duty vehicles: A review. *Catalysts* 9.7 (2019), p. 586. DOI: 10.3390/cata19070586 (cit. on p. 44).

[198] Bishop, G. A. and Stedman, D. H. A decade of on-road emissions measurements. *Environmental Science & Technology* 42.5 (2008), pp. 1651–1656. DOI: 10.1021/es702413b (cit. on p. 44).

[199] Park, S. S., Kozawa, K., Fruin, S., Mara, S., Hsu, Y.-K., Jakober, C., Winer, A., and Herner, J. Emission factors for high-emitting vehicles based on on-road measurements of individual vehicle exhaust with a mobile measurement platform. *Journal of the Air & Waste Management Association* 61.10 (2011), pp. 1046–1056. DOI: 10.1080/10473289.2011.595981 (cit. on p. 44).

[200] Ghaffarpasand, O., Ropkins, K., Beddows, D. C., and Pope, F. D. Detecting high emitting vehicle subsets using emission remote sensing systems. *Science*

of the Total Environment 858 (2023), p. 159814. DOI: 10.1016/j.scitotenv.2022.159814 (cit. on p. 44).

[201] European Commission. *Emissions in the automotive sector*. https://single-market-economy.ec.europa.eu/sectors/automotive-industry/environmental-protection/emissions-automotive-sector_en. Accessed 2025-03-01. 2024 (cit. on pp. 45, 50).

[202] Carslaw, D., Beevers, S., Westmoreland, E., Williams, M., Tate, J., Murrells, T., Stedman, J., Li, Y., Grice, S., Kent, A., et al. Trends in NO_X and NO_2 emissions and ambient measurements in the United Kingdom. *Version: July* 201.1 (2011) (cit. on pp. 46, 51).

[203] Mock, P., German, J., Bandivadekar, A., and Riemersma, I. Discrepancies between type-approval and "real-world" fuel-consumption and CO_2. *The International Council on Clean Transportation* 13 (2012). URL: https://theicct.org/wp-content/uploads/2021/06/ICCT_EU_fuelconsumption2_workingpaper_2012.pdf (cit. on pp. 46, 51).

[204] O'Driscoll, R., Stettler, M. E., Molden, N., Oxley, T., and ApSimon, H. M. Real world CO_2 and NO_X emissions from 149 Euro 5 and 6 diesel, gasoline and hybrid passenger cars. *Science of the total environment* 621 (2018), pp. 282–290. DOI: 10.1016/j.scitotenv.2017.11.271 (cit. on pp. 46, 51).

[205] Mujkic, E. and Klingner, D. Dieselgate: How hubris and bad leadership caused the biggest scandal in automotive history. *Public integrity* 21.4 (2019), pp. 365–377. DOI: 10.1080/10999922.2018.1522180 (cit. on p. 46).

[206] International Council on Clean Transportation. *Real-driving emissions test procedure for exhaust gas pollutant emissions of car and light commercial vehicles in Europe. International Council on Clean Transportation.* https://theicct.org/publication/real-driving-emissions-test-procedure-for-exhaust-gas-pollutant-emissions-of-cars-and-light-commercial-vehicles-in-europe/. 2017 (cit. on p. 46).

[207] International Council on Clean Transportation. *Euro 6e: Changes to the European Union light-duty vehicle type-approval procedure*. https://theicct.org/wp-content/uploads/2022/12/euro6e-type-approval-dec22.pdf. 2022 (cit. on p. 46).

[208] Transport for London. *Ultra Low Emission Zone*. https://tfl.gov.uk/modes/driving/ultra-low-emission-zone. Accesed: 2025-02-28. 2025 (cit. on p. 46).

[209] Birmingham City Council. *A clean air zone for Birmingham*. https://www.birmingham.gov.uk/info/20076/pollution/1763/a_clean_air_zone_for_birmingham. Accesed: 2025-02-28. 2025 (cit. on p. 47).

[210] Bristol City Council. *Bristol's Clean Air Zone*. https://www.bristol.gov.uk/residents/streets-travel/bristols-caz. Accesed: 2025-02-28. 2025 (cit. on p. 47).

[211] Senate Department for Urban Mobility, Transport, Climate Action and the Environment. *Berlin Low Emission Zone*. https://www.berlin.de/sen/uvk/en/environment/air/low-emission-zone/. Accesed: 2025-02-28. 2025 (cit. on p. 47).

[212] Urban Access Regulations in Europe. *Milan Area C Low Emission Zone*. https://urbanaccessregulations.eu/countries-mainmenu-147/italy-mainmenu-81/lombardia/milan-area-c-charging-scheme. Accesed: 2025-02-28. 2024 (cit. on p. 47).

[213] City of Santa Monica. *Zero Emission Delivery Zone*. https://www.santamonica.gov/zero-emission-delivery-zone. Accesed: 2025-02-28. 2025 (cit. on p. 47).

[214] Broster, S. and Terzano, K. A systematic review of the pollution and health impacts of low emission zones. *Case Studies on Transport Policy* (2024), p. 101340. DOI: 10.1016/j.cstp.2024.101340 (cit. on p. 47).

[215] Morfeld, P., Groneberg, D. A., and Spallek, M. F. Effectiveness of low emission zones: large scale analysis of changes in environmental NO_2, NO and NO_X concentrations in 17 German cities. *PloS one* 9.8 (2014), e102999. DOI: 10.1371/journal.pone.0102999 (cit. on p. 47).

[216] Zhai, M. and Wolff, H. Air pollution and urban road transport: Evidence from the world's largest low-emission zone in London. *Environmental Economics and Policy Studies* (2021), pp. 1–28. DOI: 10.1007/s10018-021-00307-9 (cit. on p. 47).

[217] United Kingdom Department for Transport. *Implementing low traffic neighbourhoods*. https://www.gov.uk/government/publications/implementing-low-traffic-neighbourhoods/implementing-low-traffic-neighbourhoods. Accessed: 2025-02-11. 2024 (cit. on p. 47).

[218] Yang, X., McCoy, E., Hough, K., and Nazelle, A. de. Evaluation of low traffic neighbourhood (LTN) impacts on NO_2 and traffic. *Transportation Research Part D: Transport and Environment* 113 (2022), p. 103536. DOI: 10.1016/j.trd.2022.103536 (cit. on p. 47).

[219] Whelan, I., Luiu, C., and Pope, F. D. Assessing the Polarising Impacts of Low-Traffic Neighbourhoods: A Community Perspective from Birmingham, UK. *International Journal of Environmental Research and Public Health* 21.12 (2024), p. 1638. DOI: 10.3390/ijerph21121638 (cit. on p. 47).

[220] United Kingdom Government. *MOT inspection manual: cars and passenger vehicles*. https://www.gov.uk/guidance/mot-inspection-manual-for-private-passenger-and-light-commercial-vehicles. Accesed: 2025-02-28. 2024 (cit. on p. 48).

[221] Franco, V., Kousoulidou, M., Muntean, M., Ntziachristos, L., Hausberger, S., and Dilara, P. Road vehicle emission factors development: A review. *Atmospheric Environment* 70 (2013), pp. 84–97. DOI: 10.1016/j.atmosenv.2013.01.006 (cit. on pp. 49, 50).

[222] Davison, J., Rose, R. A., Farren, N. J., Wagner, R. L., Murrells, T. P., and Carslaw, D. C. Verification of a National Emission Inventory and Influence of On-road Vehicle Manufacturer-Level Emissions. *Environmental Science & Technology* 55 (8 2021), pp. 4452–4461. DOI: 10.1021/acs.est.0c08363 (cit. on p. 49).

[223] Singer, B. C. and Harley, R. A. A fuel-based motor vehicle emission inventory. *Journal of the Air & Waste Management Association* 46.6 (1996), pp. 581–593. DOI: 10.1080/10473289.1996.10467492 (cit. on pp. 49, 58).

[224] Vlachos, T. G., Bonnel, P., Perujo, A., Weiss, M., Villafuerte, P. M., and Riccobono, F. In-use emissions testing with portable emissions measurement systems (PEMS) in the current and future European vehicle emissions legislation: overview, underlying principles and expected benefits. *SAE International Journal of Commercial Vehicles* 7.2014-01-1549 (2014), pp. 199–215. DOI: 10.4271/2014-01-1549 (cit. on p. 51).

[225] Weiss, M., Bonnel, P., Hummel, R., Manfredi, U., Colombo, R., Lanappe, G., Le Lijour, P., Sculati, M., et al. *Analyzing on-road emissions of light-duty vehicles with Portable Emission Measurement Systems (PEMS)*. Vol. 24697. Publications Office of the European Union Luxembourg, 2011 (cit. on p. 51).

[226] Giechaskiel, B., Riccobono, F., Vlachos, T., Mendoza-Villafuerte, P., Suarez-Bertoa, R., Fontaras, G., Bonnel, P., and Weiss, M. Vehicle emission factors of solid nanoparticles in the laboratory and on the road using portable emission measurement systems (PEMS). *Frontiers in Environmental Science* 3 (2015), p. 82. DOI: 10.3389/fenvs.2015.00082 (cit. on p. 51).

[227] Kousoulidou, M., Fontaras, G., Ntziachristos, L., Bonnel, P., Samaras, Z., and Dilara, P. Use of portable emissions measurement system (PEMS) for the development and validation of passenger car emission factors. *Atmospheric Environment* 64 (2013), pp. 329–338. DOI: 10.1016/j.atmosenv.2012.09.062 (cit. on p. 51).

[228] International Council on Clean Transportation. *Reassessment of Excess NO_X from European Diesel Cars following the Court of Justice of the European Union Rulings*. https://theicct.org/wp-content/uploads/2023/03/dieselgate-emissions-diesel-cars-Europe-mar23.pdf. 2023 (cit. on p. 51).

[229] Bishop, G. A. and Stedman, D. H. Measuring the emissions of passing cars. *Accounts of chemical research* 29.10 (1996), pp. 489–495. DOI: 10.1021/ar950240x (cit. on p. 52).

[230] Borken-Kleefeld, J. and Dallmann, T. Remote sensing of motor vehicle exhaust emissions. *The International Council on Clean Transportation* (2018) (cit. on p. 52).

[231] Knoll, M., Penz, M., Schmidt, C., Pöhler, D., Rossi, T., Casadei, S., Bernard, Y., Hallquist, A. M., Sjödin, A., and Bergmann, A. Evaluation of the point sampling method and inter-comparison of remote emission sensing systems for screening real-world car emissions. *Science of the Total Environment* 932 (2024), p. 171710. DOI: 10.1016/j.scitotenv.2024.171710 (cit. on p. 53).

[232] Knoll, M., Penz, M., Juchem, H., Schmidt, C., Pöhler, D., and Bergmann, A. Large-scale automated emission measurement of individual vehicles with point sampling. *Atmospheric Measurement Techniques* 17.8 (2024), pp. 2481–2505. DOI: 10.5194/amt-17-2481-2024 (cit. on p. 54).

[233] Farren, N. J., Wilson, S., Bernard, Y., Shaw, M. D., Lee, K., Crowe, M., and Carslaw, D. C. An Ambient Measurement Technique for Vehicle Emission Quantification and Concentration Source Apportionment. *Environmental Science & Technology* 58.45 (2024), pp. 20091–20100. DOI: 10.1021/acs.est.4c07907 (cit. on p. 55).

[234] United States Environmental Protection Agency. *AMTIC - Ambient Air Quality Monitoring Networks*. https://www.epa.gov/amtic/amtic-ambient-air-monitoring-networks. Accessed: 2025-03-16. 2025 (cit. on p. 55).

[235] European Environment Agency. *Up-to-date air quality data*. https://www.eea.europa.eu/en/analysis/maps-and-charts/up-to-date-air-quality-data. Accessed: 2025-03-16. 2023 (cit. on p. 55).

[236] Carslaw, D. C., Murrells, T. P., Andersson, J., and Keenan, M. Have vehicle emissions of primary NO_2 peaked? *Faraday discussions* 189 (2016), pp. 439–454. DOI: 10.1039/C5FD00162E (cit. on p. 55).

[237] Hu, S., Paulson, S. E., Fruin, S., Kozawa, K., Mara, S., and Winer, A. M. Observation of elevated air pollutant concentrations in a residential neighborhood of Los Angeles California using a mobile platform. *Atmospheric environment* 51 (2012), pp. 311–319. DOI: 10.1016/j.atmosenv.2011.12.055 (cit. on p. 55).

[238] Cummings, L. E., Stewart, J. D., Reist, R., Shakya, K. M., and Kremer, P. Mobile monitoring of air pollution reveals spatial and temporal variation in an urban landscape. *Frontiers in Built Environment* 7 (2021), p. 648620. DOI: 10.3389/fbuil.2021.648620 (cit. on p. 55).

[239] Padilla, L. E., Ma, G. Q., Peters, D., Dupuy-Todd, M., Forsyth, E., Stidworthy, A., Mills, J., Bell, S., Hayward, I., Coppin, G., et al. New methods to derive street-scale spatial patterns of air pollution from mobile monitoring. *Atmospheric environment* 270 (2022), p. 118851. DOI: 10.1016/j.atmosenv.2021.118851 (cit. on p. 56).

[240] Canagaratna, M. R., Jayne, J. T., Ghertner, D. A., Herndon, S., Shi, Q., Jimenez, J. L., Silva, P. J., Williams, P., Lanni, T., Drewnick, F., et al. Chase studies of particulate emissions from in-use New York City vehicles. *Aerosol Science and Technology* 38.6 (2004), pp. 555–573. DOI: 10.1080/02786820490465504 (cit. on p. 56).

[241] Pöhler, D., Schmidt, C., Horbanski, M., Schmitt, S., and Lampel, J. Identification of manipulated & defective truck NO_X emission reduction systems with plume chasing for authority inspections. *Transportation Research Procedia* 72 (2023), pp. 1661–1668. DOI: 10.1016/j.trpro.2023.11.638 (cit. on p. 57).

[242] Stedman, D. H., Bishop, G. A., Armstrong, J. A., and Maddox, J. *Fuel Efficiency Automobile Testing (FEAT)*. https://digitalcommons.du.edu/cgi/viewcontent.cgi?article=1218&context=feat_publications. 1988 (cit. on p. 57).

[243] Bishop, G. A., Starkey, J. R., Ihlenfeldt, A., Williams, W. J., and Stedman, D. H. IR long-path photometry: a remote sensing tool for automobile emissions. *Analytical Chemistry* 61.10 (1989), 671A–677A. DOI: 10.1021/ac00185a002 (cit. on p. 57).

[244] Guenther, P. L., Stedman, D. H., Bishop, G. A., Beaton, S. P., Bean, J. H., and Quine, R. W. A hydrocarbon detector for the remote sensing of vehicle exhaust emissions. *Review of Scientific Instruments* 66.4 (1995), pp. 3024–3029. DOI: 10.1063/1.1146498 (cit. on p. 57).

[245] Zhang, Y., Bishop, G. A., Beaton, S. P., Guenther, P. L., and McVey, l. F. Enhancement of remote sensing for mobile source nitric oxide. *Journal of the Air & Waste Management Association* 46.1 (1996), pp. 25–29. DOI: 10.1080/10473289.1996.10467437 (cit. on p. 57).

[246] Burgard, D. A., Bishop, G. A., and Stedman, D. H. Remote sensing of ammonia and sulfur dioxide from on-road light duty vehicles. *Environmental science & technology* 40.22 (2006), pp. 7018–7022. DOI: 10.1021/es061161r (cit. on p. 57).

[247] Stephens, R. D., Mulawa, P. A., Giles, M. T., Kennedy, K. G., Grobiicki, P. J., Cadle, S. H., and Knapp, K. T. An experimental evaluation of remote sensing-based hydrocarbon measurements: A comparison to FID measurements. *Journal of the Air & Waste Management Association* 46.2 (1996), pp. 148–158. DOI: 10.1080/10473289.1996.10467447 (cit. on p. 58).

[248] Opus Inspection. *Remote Sensing Device*. https://www.opusrse.com/technology/remote-sensing-device/. Accessed: 2025-03-08. 2025 (cit. on p. 59).

[249] Bernard, Y., Dallmann, T., Lee, K., Rintanen, I., and Tietge, U. Evaluation of real-world vehicle emissions in Brussels. *ICCT: Morgantown, WV, USA* (2021) (cit. on p. 59).

[250] Dallmann, T., Bernard, Y., Tietge, U., and Muncrief, R. Remote sensing of motor vehicle emissions in London. *ICCT Report* (2018) (cit. on p. 59).

[251] Rushton, C. E., Tate, J. E., Shepherd, S. P., and Carslaw, D. C. Interinstrument comparison of remote-sensing devices and a new method for calculating on-road nitrogen oxides emissions and validation of vehicle-specific power. *Journal of the Air & Waste Management Association* 68.2 (2018), pp. 111–122. DOI: 10.1080/10962247.2017.1296504 (cit. on p. 59).

[252] Hager Environmental and Atmospheric Technologies (HEAT). *Emission Detection And Reporting (EDAR)*. https://www.heatremotesensing.com/edar. Accessed: 2025-03-08. 2025 (cit. on p. 60).

[253] Airyx GmbH. *ICAD in situ NO_2-NO_X-NO Analyzer*. https://airyx.de/item/icad/. Accessed: 2025-03-08. 2025 (cit. on p. 60).

[254] Horbanski, M., Pöhler, D., Lampel, J., and Platt, U. The ICAD (iterative cavity-enhanced DOAS) method. *Atmospheric Measurement Techniques* 12.6 (2019), pp. 3365–3381. DOI: 10.5194/amt-12-3365-2019 (cit. on p. 60).

[255] Schmidt, C., Pöhler, D., Engel, T., Horbanski, M., Lampel, J., Schmitt, S., and Platt, U. Real Driving NO_X Emission Measurements of Vehicles with ICAD instruments for Plume Chasing. *EGU General Assembly Conference Abstracts*. 2021, EGU21–1646 (cit. on p. 61).

[256] PALAS. *AQ Guard System*. https://www.palas.de/en/product/aq-guard. Accessed: 2025-03-08. 2025 (cit. on p. 61).

[257] United Kingdom Environment Agency. *MCERTS performance standards for ambient monitoring equipment*. https://www.gov.uk/government/publications/mcerts-performance-standards-for-ambient-monitoring-equipment/mcerts-performance-standards-for-ambient-monitoring-equipment. Accessed: 2025-03-08. 2022 (cit. on p. 61).

[258] ThermoFischer Scientific. *Model 43i SO_2 Analyzer*. https://www.thermofisher.com/order/catalog/product/43I. Accessed: 2025-03-08. 2025 (cit. on p. 62).

[259] Manatt, S. L. and Lane, A. L. A compilation of the absorption cross-sections of SO_2 from 106 to 403 nm. *Journal of Quantitative Spectroscopy and Radiative Transfer* 50.3 (1993), pp. 267–276. DOI: 10.1016/0022-4073(93)90077-U (cit. on p. 62).

[260] Mettee, H. Fluorescence and phosphorescence of SO_2 vapor. *The Journal of Chemical Physics* 49.4 (1968), pp. 1784–1793. DOI: 10.1063/1.1670308 (cit. on p. 62).

Chapter 2

Impact of Policy on Passenger Car Emission Trends

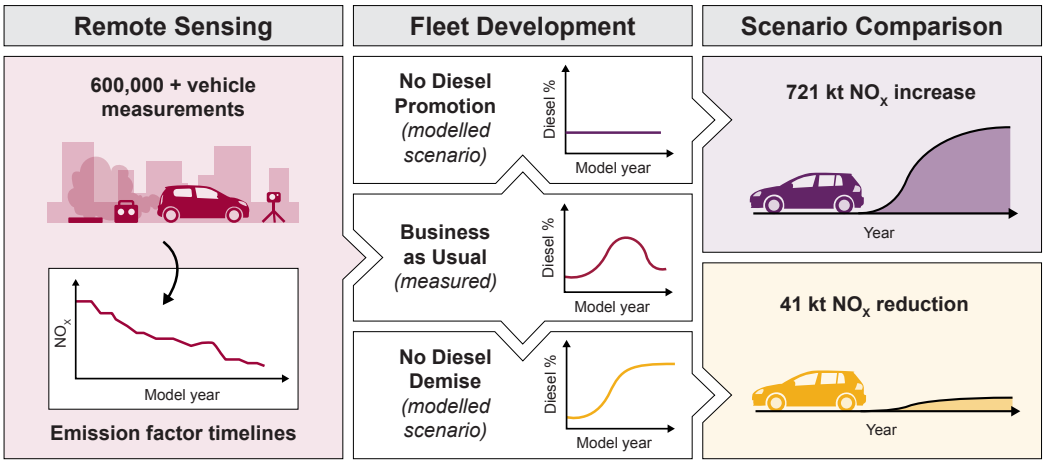

Wilson. S., Farren N. J., Rose R. A., Wilde S. E., Davison J., Wareham J. V., Lee J. D., and Carslaw D. C. **The impact on passenger car emissions associated with the promotion and demise of diesel fuel**. *Environment International* 128. (2023). p. 108330. DOI: 10.1016/j.envint.2023.108330

2.1 Abstract

The promotion and growth in the use of diesel fuel in passenger cars in the United Kingdom (UK) and Europe over the past two decades led to considerable adverse air quality impacts in urban areas and more widely. In this work, we construct a multi-decade analysis of passenger car emissions in the UK based on real-driving emissions data. An important part of the study is the use of extensive vehicle emissions remote sensing data covering multiple measurement locations, time periods, environmental conditions and consisting of over 600,000 measurements. These data are used to consider two scenarios: first, that diesel fuel use was not promoted in the early 2000s for climate mitigation reasons, and second, that there was not a dramatic decline in diesel fuel use following the Dieselgate scandal. The strong growth of diesel fuel use coincided with a time when diesel car nitrogen oxide (NO_x = NO + NO_2) emissions were high, and conversely, the strong decrease of diesel fuel use coincided with a time when diesel car after-treatment systems for NO_x control were effective. We estimate that the increase in diesel car use in the UK has resulted in excess NO_x emissions totalling 721 kt over three decades. This is equivalent to over seven times the total annual passenger car NO_x emissions and exceeds the total UK NO_x emissions of 681.8 kt in 2021. The associated damage cost is estimated at £5.875 billion. However, the sharp move away from diesel fuel post-Dieselgate only reduced NO_x emissions by 41 kt owing to the effectiveness of modern diesel after-treatment systems.

2.2 Introduction

2.2.1 Background and Context

Exhaust emissions from road vehicles are a dominant source of ambient air pollution, particularly in densely populated urban environments (Section 1.1.4). The proximity of road vehicles to the general population, particularly in urban areas, is a continued cause for concern given the myriad of health and wider environmental impacts associated with traffic-related air pollution (Section 1.1.2).[1–3] Over the past two decades the contribution of diesel-fuelled vehicles to adverse air pollution has been of particular concern. For light-duty vehicles in the early 2000s, diesel fuel offered fuel-efficiency and carbon (25 – 29% lower CO_2 emissions) advantages over gasoline.[4] While technology advancements and trends in passenger car characteristics (engine size, vehicle mass, etc.) have since reduced this advantage, its presence still resulted in the active promotion of diesel fuel in many countries.[5]. Furthermore, diesel vehicles are significant contributors to the emission of important air pollutants such as fine particulate matter ($PM_{2.5}$) and nitrogen oxides (NO_x = NO + NO_2) (Sections 1.2.1 and 1.2.2.2).

With respect to emissions of NO_x, the principal concern from a human health perspective is related to concentrations of nitrogen dioxide (NO_2), which resulted in the development of ambient limits in Europe and elsewhere.[6] The current limit for annual mean NO_2 concentrations in Europe is 40 μg m^{-3}, which has been widely exceeded across many European countries for the past two decades. However, the evidence surrounding the adverse health effects associated with NO_2 exposure has grown stronger over recent years, prompting the World Health Organization (WHO) to recommend an annual mean guideline of 10 μg m^{-3}.[7] Elevated concentrations of NO_2 are of particular concern to local air quality, especially in urban environments where there is close proximity of vehicular emissions to large populations.

For this reason, cities across the United Kingdom (UK) and Europe have adopted mitigation measures such as low-emission zones that seek to reduce emissions and concentrations of NO_2 and other traffic-related air pollutants, e.g., the Ultra Low Emission Zones in London, Paris, and Milan (Section 1.3.2).[8–10]

Emissions of NO_x also contribute to significant wider environmental damage. For example, NO_x is a key precursor in the formation of secondary particulate matter (PM) and tropospheric ozone (O_3), both of which are associated with a range of adverse health and environmental impacts (Section 1.1.2).[11–14] It is for these reasons that the past few decades have seen an increase in policy designed to mitigate the multiple impacts of NO_x and other pollutants. At a national level in Europe, total emission limits have been set as part of The National Emissions Ceiling Directive (NECD), which sets annual pollutant emission ceilings for member states for a range of pollutants such as $PM_{2.5}$, Volatile Organic Compounds (VOCs) and NO_x. [15, 16]

The promotion of diesel passenger cars in the UK corresponds to the time period from 2001 to 2015, during which company car tax (CCT), a benefit-in-kind tax applied to vehicles sold commercially, and vehicle excise duty (VED), a tax levied on vehicles for use on public roads, were restructured based on a vehicle's reported carbon dioxide (CO_2) emissions.[17, 18] These policies, which were initially introduced for CO_2 reduction and climate change mitigation reasons, provided a financial incentive to purchase a diesel car over one powered by gasoline. A combination of the restructured CCT and VED policies resulted in new diesel passenger car registrations increasing by 38% in one year from 2001 to 2002, and the total number of diesel passenger cars licensed in the UK increasing by a factor of 3 from 2001 to 2015.[19] While the air quality drawbacks associated with diesel fuel emissions were generally well understood at the inception of the restructured

CCT and VED policies, CO_2 reduction and climate mitigation reasoning took precedence, and full consideration was not given to the air quality implications of the adoption of diesel technology on a mass scale.[20] The significant increase in diesel car use was more generally observed across Europe.[21]

Following the 2015 'Dieselgate' scandal, diesel passenger car sales in the UK plummeted (the 'demise' of diesel fuel). The scandal was directly associated with emissions of NO_x and the discovery of deliberate tampering that led to excess emissions. In 2017, VED was further restructured such that only the first year of the tax was calculated based on reported CO_2 emissions before a fixed annual rate is applied for all internal combustion engine (ICE) powered passenger cars. This change removed much of the financial incentive to own a diesel vehicle, and when combined with the growing negative reputation of the fuel, resulted in the share of new diesel passenger car registrations in the UK falling from 48% in 2015 to 8% in 2022. [22]

2.2.2 Passenger Car Vehicle Emissions

Passenger car exhaust emissions have been regulated in the UK according to the European Type Approval emission standards (Euro standards) since 1992 (Section 1.3.1).[23, 24] Vehicle Type Approval is a Conformity of Production (CoP) process that all passenger cars must undergo before being eligible for sale in the UK.[25] Early Euro standards were enforced during Type Approval through predefined testing methods (drive cycles) under standardised laboratory conditions, with emissions limits set for each pollutant (Section 1.4.1). Over the following three decades, Euro standard emission limits and testing methods have become increasingly stringent and now extend from 'Euro 1' (1992) to 'Euro 6d' (2021) for passenger cars. The current Euro 6d standard regulates the exhaust emission of carbon monoxide (CO), hydrocarbons (HC),

NO_x, and PM, measured as the amount of pollutant emitted per unit distance travelled ($g\,km^{-1}$); a CO_2 emission factor is also reported in $g\,km^{-1}$ and used to determine the VED rate.[26] Different pollutant limits are set for diesel and gasoline fuels, Table 2.1 shows the pollutant emissions limits for each fuel type and Euro standard. In order to address the progressively demanding emissions limits, vehicle manufacturers have developed a variety of exhaust after-treatment system strategies (Section 1.2.2.1 and 1.2.2.2).

Table 2.1: European passenger car (Euro) standard emissions limits from Euro 1 (E1) to Euro 6 (E6).[24] PN is particle number, another metric used to quantify PM.

		Distance-specific emission ($g\,km^{-1}$)					(# km^{-1})
	Date	**CO**	**HC**	**HC + NO_x**	**NO_x**	**PM**	**PN**
Gasoline							
E1	1992	2.72	—	0.97	—	—	—
E2	1996	2.2	—	0.50	—	—	—
E3	2000	2.30	0.2	—	0.15	—	—
E4	2005	1.00	0.1	—	0.08	—	—
E5	2009	1.00	0.1	—	0.06	0.005	—
E6	2014	1.00	0.1	—	0.06	0.005	6×10^{11}
Diesel							
E1	1992	2.72	—	0.97	—	0.140	—
E2	1996	1.00	—	0.90	—	0.100	—
E3	2000	0.64	—	0.56	0.50	0.050	—
E4	2005	0.50	—	0.30	0.25	0.025	—
E5	2009	0.50	—	0.23	0.18	0.005	6×10^{11}
E6	2014	0.50	—	0.17	0.08	0.005	6×10^{11}

Gasoline passenger cars have used the three-way catalyst for emissions

control in Europe since the early 1990s due to the introduction of the Euro 1 standard.[24, 27] The three-way catalyst has remained the after-treatment system used by gasoline vehicles since this time but has been refined alongside developing Euro standards. By contrast, the technology used in diesel passenger cars has greatly evolved since the early 1990s, as shown in Figure 2.1. The principal technologies used to control diesel passenger NO_x emissions include exhaust gas recirculation (EGR), diesel oxidation catalysts (DOCs), and diesel particle filters (DPFs). EGR routes exhaust gases back into the combustion chamber, lowering combustion temperatures and reducing emissions of NO_x.[28] DOCs facilitate the high-temperature conversion of CO and HC into CO_2 and water, as well as oxidising NO to NO_2, the latter of which is necessary for the use in other forms of after-treatment.[29] DPFs physically capture exhaust PM during engine operation before oxidising stored material into CO_2. A major milestone in the reduction of NO_x emissions from diesel passenger cars was the introduction of selective catalytic reduction (SCR) and lean NO_x traps (LNTs) that were designed specifically to control NO_x emissions. These technologies were introduced on a mass scale following the increasingly stringent NO_x emissions limits that accompanied the Euro 6 standards (2014) for diesel passenger cars.

As a result of technological improvements, diesel passenger car exhaust systems have become increasingly complicated, often comprising a combination of different after-treatment components. Successful vehicle emission control, therefore, presents a significant engineering challenge for vehicle manufacturers. To ensure that passenger cars continue to meet emissions limits across a range of operating parameters, the Euro 6 standards introduced real-driving emissions (RDE) testing, during which vehicle emissions are measured using portable emissions measurement systems (PEMS) under real-driving conditions (Section 1.4.2). The introduction of RDE testing greatly expedited the integration of SCR and LNT systems, which were

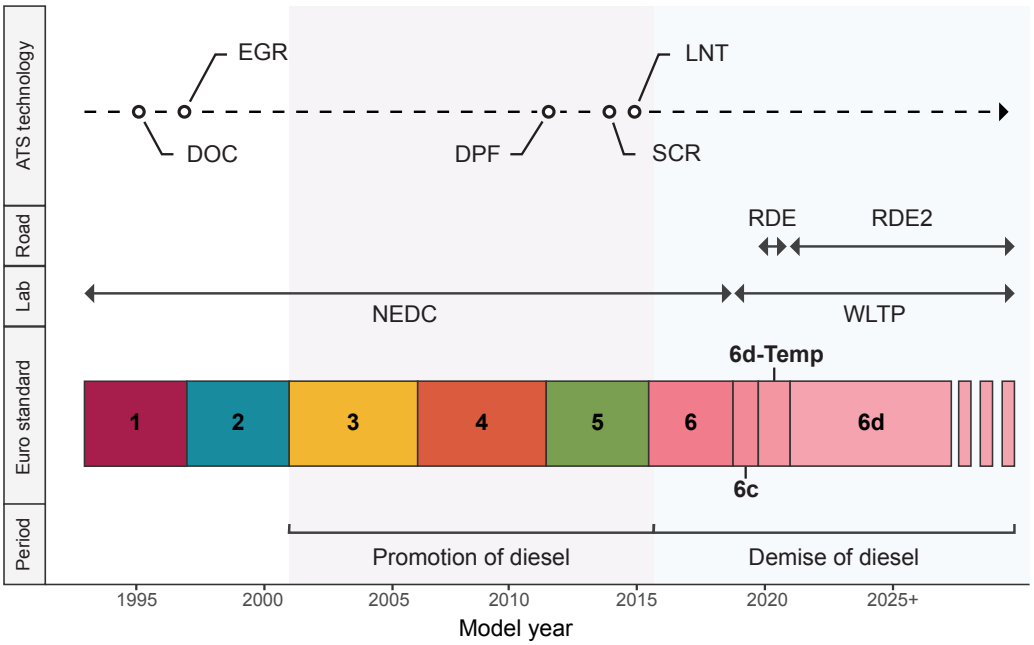

Figure 2.1: Timeline of diesel passenger car Euro standards, laboratory and road testing methods, and after-treatment technology adoption. ATS = After-treatment System. NEDC = New European Drive Cycle; WLTP = Worldwide Harmonised Light Vehicle Test Procedure; RDE = Real-Driving Emissions.

required to meet the lowered NO_x emission limits outside of traditional laboratory testing. While RDE legislation was under development prior to Dieselgate, the occurrence of the scandal increased awareness of passenger car NO_x emission issues and likely accelerated the implementation of the policy.[30, 31]

Vehicle emission remote sensing is an unobtrusive way of measuring emissions from vehicles under real-driving conditions, which has been extensively described elsewhere (Sections 1.4.3 and 1.4.6.1).[32–34] The instrumentation is deployed on the roadside. Individual measurements are less than one second in duration, and the measured emissions represent a single driving condition. However, a very large number of vehicles can be measured in a short period of time, allowing for measurements to be aggregated (e.g., by fuel type, vehicle category, Euro class) and used to provide detailed emissions

behaviour insight over a range of driving and ambient conditions.

2.2.3 Objectives

The aim of this paper is to quantify the impact of the promotion of diesel fuel usage in passenger cars on emissions of important air pollutants at a UK level, with a specific focus on the emission of NO_x. We also aim to quantify the impact of the rapid move away from diesel fuel on passenger car emissions in the wake of the Dieselgate scandal. An important aspect of our analysis is the use of real-driving emissions of NO_x and other pollutants based on comprehensive vehicle emission remote sensing measurements. The vehicle emission remote sensing data are used to construct a timeline of passenger car emissions over three decades, which is then used to evaluate the air quality impacts associated with the promotion and demise of diesel fuel. The results are compared with the UK National Atmospheric Emissions Inventory (NAEI) emissions to put their impacts into context, and the wider implications for urban and regional air quality are discussed.

2.3 Materials and Methods

2.3.1 Instrumentation

The measurements in this work were made with two remote sensing systems: the Fuel Efficiency Automobile Test (FEAT) research instrument supplied by the University of Denver and the commercially available Opus AccuScan RSD 4600/5000 (Section 1.4.6.1).[35, 36] Vehicle emission remote sensing instrumentation consists of three fundamental components: a spectroscopic unit for the measurement of exhaust gases, apparatus for measuring vehicle speed and acceleration, and a camera for photographing vehicle registration numbers (license plates).

Both systems operate perpendicular to the flow direction of a single lane of traffic and utilise collinear open-path infrared (IR) and ultraviolet (UV) spectroscopy. A remote sensing observation, which includes the emission measurement, speed and acceleration measurement, and registration number photograph, is made whenever the collinear light beam is obstructed by a passing vehicle. One hundred spectroscopic measurements are taken of each exhaust plume in half a second, and emission values are reported as molar volume ratios to CO_2, eliminating the variation associated with vehicle position and exhaust plume dispersion. All observations are preserved regardless of measurement validity, which is essential for deriving information about the vehicle fleet composition.

The FEAT instrument measures CO_2, CO, HC, and a background reference using four non-dispersive IR detectors, whereas ammonia (NH_3), nitrogen oxide (NO) and nitrogen dioxide (NO_2) measurements are obtained using two separate dispersive UV spectrometers. An extensive description of the development and operation of the FEAT instrument, as well as a detailed comparison of the two remote sensing systems, is available in the literature. [32, 33, 37]

2.3.2 Data Description

The remote sensing data set used in this work combines information from measurement campaigns conducted at 77 sites across the UK between 2012 and 2022. To ensure safe instrument operation and maximise measurement validity, data was collected only during dry daylight hours (0800 to 1800 h). The ambient temperature throughout the measurement campaigns ranged from -1 to 29 °C with a mean temperature of 14 °C.

The specific vehicle information for each remote sensing observation was obtained by cross-referencing the registration number photographs with vehicle technical databases. These data were supplied by CDL Vehicle Information Services Limited, which retrieved information from the Driver and Vehicle Licensing Agency (DVLA) and the Society of Motor Manufacturers and Traders (SMMT) Motor Vehicle Registration Information System. All measurements were assigned technical information relating to the fuel type, emission standard and registration date of the vehicle. Additional vehicle information was matched to approximately 70% of vehicles and included details on the manufacturer, vehicle dimensions and vehicle mass.

A total of 604,435 measurements of Euro 2 to 6 passenger cars are contained within the data in five different fuel classes: diesel vehicles, gasoline vehicles, gasoline full-hybrid electric vehicles (FHEVs), gasoline plug-in hybrid electric vehicles (PHEVs), and electric vehicles (EVs) – other fuel types were not measured in sufficient numbers to be included in this analysis. For the evaluation of passenger car fleet composition trends, all measurements were used, regardless of the validity of the emissions or speed/acceleration data or the presence of additional technical information; this was essential for ensuring that the composition information derived from the remote sensing data was an accurate representation of the on-road vehicle fleet. The calculation of distance-based emission factors requires valid emissions and speed/acceleration data, as well as additional technical information;

therefore, only observations with a complete measurement profile were used. [38] 56% of measurements were used to derive emission factors for CO and HC, 49% of measurements were used to derive emission factors for NO_x, and 34% of measurements were used to derive emission factors for NH_3. The lower proportion of valid NH_3 emissions measurements resulted from issues with instrument calibration. A statistical summary of the data set and the subsets used for emission factor calculation is provided in Table 2.2.

Table 2.2: Statistical summary of the remote sensing data set and subsets.

Characteristic	**Data subset**			
	All	**CO & HC**	**NH_3**	**NO_x**
# measurements	602280	321073	194544	281188
Diesel (%)	45	45	48	46
Gasoline (%)	51	52	50	52
FHEV (%)	3	2	2	2
PHEV (%)	0.5	0.3	0.2	0.3
EV (%)	0.5	0	0	0
Euro 2 (%)	2	1	1	1
Euro 3 (%)	13	11	12	9
Euro 4 (%)	24	23	25	22
Euro 5 (%)	30	33	35	33
Euro 6 (%)	31	32	27	35
Mean speed ($km\,h^{-1}$)	36.10	36.04	36.13	36.26
Mean acceleration ($km\,h^{-1}\,s^{-1}$)	1.22	1.33	1.44	1.36
Mean vehicle specific power ($kW\,t^{-1}$)	8.73	8.49	8.49	8.49
Mean temperature (°C)	14.54	14.37	14.61	14.14

2.3.3 Emission Factor Calculation

The conversion of remote sensing pollutant molar volume ratios to CO_2 into fuel-specific (also called fuel-based) emission factors (mass of pollutant emitted per mass of fuel consumed in $g\,kg^{-1}$) is straightforward and relies on stoichiometric assumptions about the composition and combustion of hydrocarbon fuels. This methodology has been described in detail elsewhere [32, 33]. While fuel-specific emission factors are often reported directly, their distance-based equivalents (mass of pollutant emitted per unit distance travelled in $g\,km^{-1}$) are more versatile and can be compared to the emission factors generated during vehicle Type Approval, as well as those used for emission inventory development (Section 1.4). Distance-based emission factors were calculated from the remote sensing data using a method developed by Davison et al.[38], a brief overview of which is provided here.

For each remote sensing observation, a physics-based approach was applied to calculate vehicle-specific power (VSP) in $kW\,t^{-1}$ from a combination of the speed and acceleration measurements as well as the vehicle technical information. Road load and aerodynamic drag coefficients provided by Davison et al.[38] were also used in this calculation. Next, fuel consumption in $kg\,s^{-1}$ was determined based on the linear relationship with VSP derived from the passenger car and heavy-duty emissions model.[39] The parameters used in this model were based on Euro 5 and 6 vehicles. Therefore, the fuel consumption for Euro 2 to 4 vehicles was increased by 5% to approximate poorer fuel efficiency. Fuel consumption values for gasoline hybrid vehicles (FHEVs and PHEVs), which comprised 2% of the remote sensing measurements, were reduced by 30% to approximate improved fuel efficiency resulting from electric power train utilisation.[40]

The fuel-specific emission factors from remote sensing measurements were then combined with the corresponding modelled fuel consumption values to generate time-specific emission factors (mass of pollutant emitted per

unit time in $g\,s^{-1}$). Next, the time-specific emission factors were aggregated and mapped to 1 Hz drive cycle data obtained from portable emission measurement system (PEMS) measurements undertaken by the UK Department for Transport (DfT). The PEMS data contained 4243 km of real-world urban, rural, and motorway driving, with individual test lengths ranging from 70.4 – 78.1 km. Further description of these drive cycles, as well the full details of this approach, are described extensively in the literature.[38].

Distance-based emission factors were calculated as the sum of the modelled 1 Hz time-specific emission factors divided by the total distance over 58 drive cycles. The output of this method was a distance-based emission factor for each vehicle model year and fuel type derived directly from on-road remote sensing measurements, reflecting a wide range of real-driving conditions. The method has been evaluated and compared with the UK national inventory, which demonstrated a carbon/energy balance within 1.5% when calculating total UK passenger car emissions.[41]

2.3.4 Timeline Construction

To evaluate UK passenger car emissions trends, a distance-based emission factor timeline was constructed as a function of vehicle model year for each measured pollutant. The model year was defined as the year in which a passenger car was first registered in the UK, obtained from the vehicle's technical information. Remote sensing measurements were grouped by model year before the ratio of different fuel types was calculated for each group (excluding EVs). This information was combined with the corresponding individual fuel type distance-based emission factor data to generate an average $g\,km^{-1}$ value for each vehicle model year. The total number of measurements available for each fuel type and model year are shown in Table 2.3. The actual number of measurements available for each pollutant was lower than these totals, owing to differing measurement validity rates; see Section 2.3.2.

Table 2.3: Remote sensing model year and fuel type group sample sizes.

	Fuel type			
Model year	**Diesel**	**Gasoline**	**FHEV**	**PHEV**
1998	1327	2137	—	—
1999	1625	3216	—	—
2000	1686	4638	—	—
2001	2445	7197	—	—
2002	3669	10236	—	—
2003	4964	11769	—	—
2004	6960	13196	—	—
2005	8954	14393	—	—
2006	10929	15845	314	—
2007	14500	17433	563	—
2008	14250	16183	733	—
2009	13864	16401	783	—
2010	16854	15779	1254	—
2011	19443	14298	1213	—
2012	20127	15409	1105	—
2013	19923	16783	930	—
2014	22089	17121	1099	—
2015	25066	19221	1386	339
2016	25849	20057	1611	522
2017	21177	20511	1744	586
2018	9004	14416	1046	374
2019	5536	10937	910	261
2020	2266	5701	673	340
2021	952	2877	511	379
2022	160	487	149	76

A major advantage of this approach is that it enables retrospective analysis of multi-decade emission trends predating the remote sensing measurement period (2012 to 2022). In this work, the data contained sufficient vehicle measurements to construct emissions timelines for diesel and gasoline vehicles with model years 1998 – 2022, gasoline FHEV vehicles with model years 2006 – 2022, and gasoline PHEV vehicles with model years 2015 – 2022. For the model years 2020, 2021, and 2022, no valid NH_3 measurements were reported as a result of an instrument calibration fault. To complete the emission factor data, the mean of the NH_3 distance-based emission factor for the model years 2017, 2018, and 2019 (Euro 6 vehicles) was calculated and applied to the missing period.

2.3.5 Scenario Development

The NO_x emission impact of the promotion and decline of diesel passenger cars in the UK was assessed through the development of three scenarios, for each of which a NO_x emission factor timeline was constructed. 'Business as Usual' (BAU) was defined as the baseline scenario, and average NO_x emission factors were derived from unmodified remote sensing emissions and fuel type composition data. A 'No Diesel Promotion' (NDP) scenario was constructed in which the fuel type composition data was adjusted such that the ratio of diesel and gasoline passenger cars remained unchanged from the mean value of the years 1998 to 2000. In this case, unmodified individual fuel type emission factor data were used, such that any differences in the scenario NO_x emission timelines were a direct result of the fuel type composition changes. Similarly, a 'No Diesel Demise' (NDD) scenario was constructed in which only the post-2015 model year fuel type composition data was adjusted such that the ratio of diesel and gasoline vehicles remained unchanged from the mean value of the years 2013 to 2015. A visualisation of the adjustments made to fuel type composition as a function of model

year for each scenario is presented in Figure 2.2. Only the ratio of diesel and gasoline vehicles was adjusted in the NDP and NDD scenarios; the proportion of the total of these fuel types combined (diesel + gasoline) to the total proportion of hybrid vehicles (gasoline FHEV + gasoline PHEV) was unchanged, as were the individual proportions of each hybrid vehicle type. EVs were excluded from this section of the analysis as they do not produce exhaust emissions.

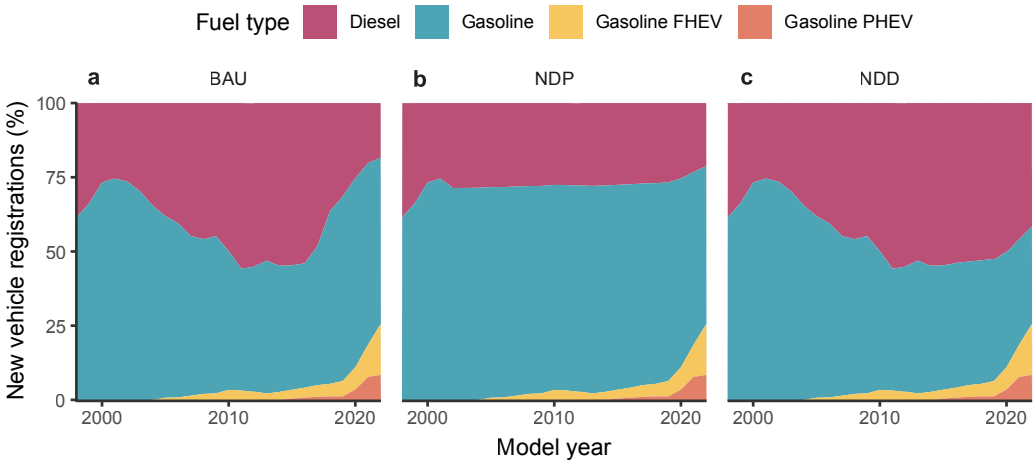

Figure 2.2: Passenger car fuel type composition (%) as a function of vehicle model year (1998 - 2022) for the (**a**) Business as Usual (BAU), (**b**) No Diesel Promotion (NDP), and (**c**) No Diesel Demise (NDD) scenarios.

2.3.6 Lifetime Emission Calculation

To further understand and contextualise the average NO_x emission factor values developed for each scenario, the data were combined with new passenger car registration and average annual mileage information. Total lifetime NO_x emissions from all passenger cars registered between 1998 and 2023 were calculated for each scenario, such that they could be disaggregated into annual values and compared.

First, the average operational life span of a passenger car in the UK was

assumed to be 14 years.[42] Because the data for each scenario contained information for vehicles registered between 1998 and 2022, the period over which lifetime NO_x emissions were calculated was 1999 (the year all 1998 model vehicles had been registered) to 2036 (the year all 2022 model vehicles had reached the end of their assumed lifespan). For each vehicle model year between 1998 and 2022 in each scenario, a total fleet NO_x emission factor (kt km^{-1}) was calculated to be the product of the corresponding average passenger car NO_x emission factor ($g\,km^{-1}$), and the number of new annual passenger car registrations. From here, these values were multiplied by the annual average total passenger car mileage data (km) for the years 1999 to 2036, yielding total NO_x emissions for each year (kt). Finally, the total NO_x emission values for each year between 1999 and 2036 were combined to produce an overall NO_x emission value (kt) for each year between 1999 and 2036 for each scenario. Summing all annual overall NO_x amounts within the three scenarios yielded a total lifetime NO_x emission value for each.

Annual new passenger car registration data were obtained from the DfT [43] and Northern Ireland Statistics and Research Agency[44], and annual average total passenger car mileage information was acquired from the National Travel Survey.[45] For the years 2023 – 2036, the annual average total passenger car mileage was assumed to be the mean of the years 2017, 2018, and 2019, which preceded the COVID-19 pandemic, during which travel restrictions reduced annual passenger car mileage.

2.4 Results and Discussion

2.4.1 Vehicle Emission Trends

Passenger car distance-based emission factors for CO, HC, NH_3, and NO_x are shown by fuel type and model year in Figure 2.3. The range of calculated emission factors is consistent with those reported in the literature.[38] For the pollutants that are regulated during passenger car Type Approval, the calculated emission factors align closely with the corresponding range of Euro standard emission limits displayed in Table 2.1. It should be noted that the trend in NO_x emissions from diesel cars includes the effect of hardware and software fixes on UK vehicles in the wake of the Dieselgate scandal. The effect of these fixes, which are implicit in the remote sensing measurements, was calculated to be a 30 – 36% reduction in NO_x affecting 1.6 and 2.0 litre Volkswagen Group diesel passenger cars.[46]

Overall, a steady decrease in emission factors with increasing model year is observed for all pollutants and fuel types. This trend is primarily attributed to continually improving internal combustion engine and exhaust after-treatment technology, driven by increasingly stringent emission standards and testing methods. It is important to consider that earlier-model passenger cars are older at the time of measurement, and the deterioration of these vehicles is likely to influence this observed trend partially. Vehicle model years before 2012 (the beginning of the remote sensing measurement period) were measured at an age that is equal to the difference between the measurement date and that of the vehicle's registration. While age is not a direct measure of accumulated vehicle usage and deterioration, these variables can be assumed to be correlated. The effect of passenger car deterioration on pollutant (CO, NH_3, NO_x) emission factors has been previously derived from remote sensing data and reported in the literature.[47] It is likely that the impact of the reported deterioration rates on the results of this work would

be small. However, it is important to acknowledge the contribution of this factor towards the trends seen in Figure 2.3 and recognise the limitations of the data. For passenger cars registered after 2012, the remote sensing measurement period spans their entire operational lifetime (up to and including 2022), and thus, the data set contains measurements of these vehicles across a range of ages and conditions, reducing the influence of deterioration on the results.

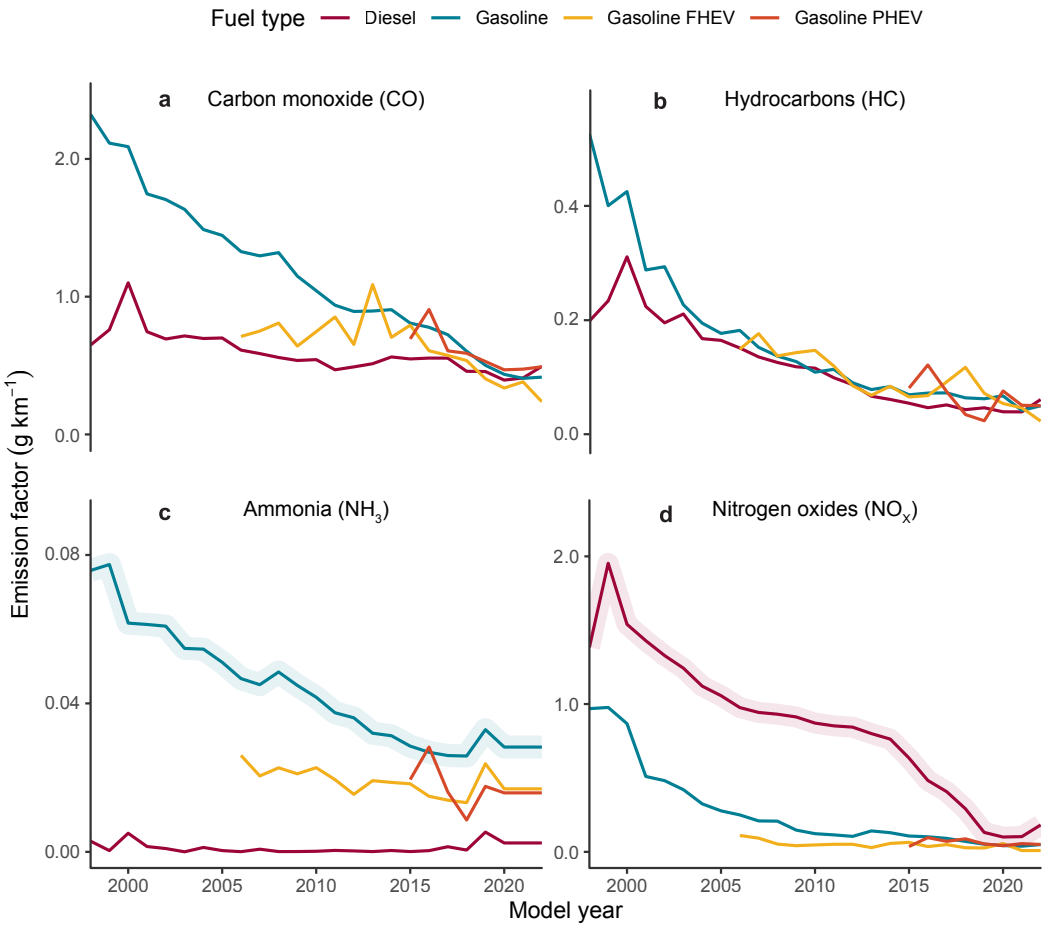

Figure 2.3: Passenger car distance-based emission factor values ($g\,km^{-1}$) for diesel, gasoline, gasoline FHEV, and gasoline PHEV vehicles as a function of model year (1998 – 2022), for (**a**) CO, (**b**) HC, (**c**) NH_3, and (**d**) NO_x. Gasoline and diesel fuel are highlighted for NH_3 and NO_x, respectively.

The diesel emission factor values differ considerably from those of gasoline across all pollutants in Figure 2.3, with the disparity being particularly prominent for NH_3 and NO_x. Gasoline NH_3 emissions, highlighted in blue in Figure 2.3, were 0.025 to 0.078 $g\,km^{-1}$ higher than those of diesel fuel, which can be attributed to NH_3 formation in the three-way catalytic converter systems fitted exclusively to gasoline fuelled passenger cars (Section 1.2.2.1). [48, 49] The increase in the NH_3 emission factors for the 2019 model year is likely a statistical feature arising from the low number of measurements for 2019 vehicles, owing to the missing NH_3 remote sensing data from 2020 onwards; see Section 2.3.4). Conversely, NO_x emission factor values for diesel, highlighted in red in Figure 2.3, were 0.057 to 0.926 $g\,km^{-1}$ higher than those of gasoline. The rapid decline in the diesel NO_x emission factor from 0.635 $g\,km^{-1}$ in 2015 to 0.182 $g\,km^{-1}$ in 2022 (71%) corresponds to the introduction of NO_x specific exhaust after-treatment systems (SCR and LNT), adopted for diesel passenger cars to meet Euro 6 NO_x limits and on-road RDE testing methods; see Figure 2.1.

From the remote sensing data, it is also possible to summarise information about changes in the fuel composition of a given property of the passenger car fleet as a function of model year. Figure 2.4 presents the change in vehicle fuel type share from 1998 to 2022. In both the combined plot panel (**a**) and the diesel plot panel (**b**), the rise and subsequent decline of diesel fuel with increasing passenger car model year are apparent. From the model year 2001 to 2015, the share of new diesel registrations increased from 24% to 54% before decreasing to 16% for the model year 2022.

The fuel-share statistics are generally consistent with statistics from the DfT, which report the share of new diesel passenger car registrations to be 18%, 48%, and 12% for the model years 2001, 2015, and 2021 (the most recent year for which data are available) respectively.[22] A distinct benefit of the remote sensing data is the direct measurements of vehicles in use. Only

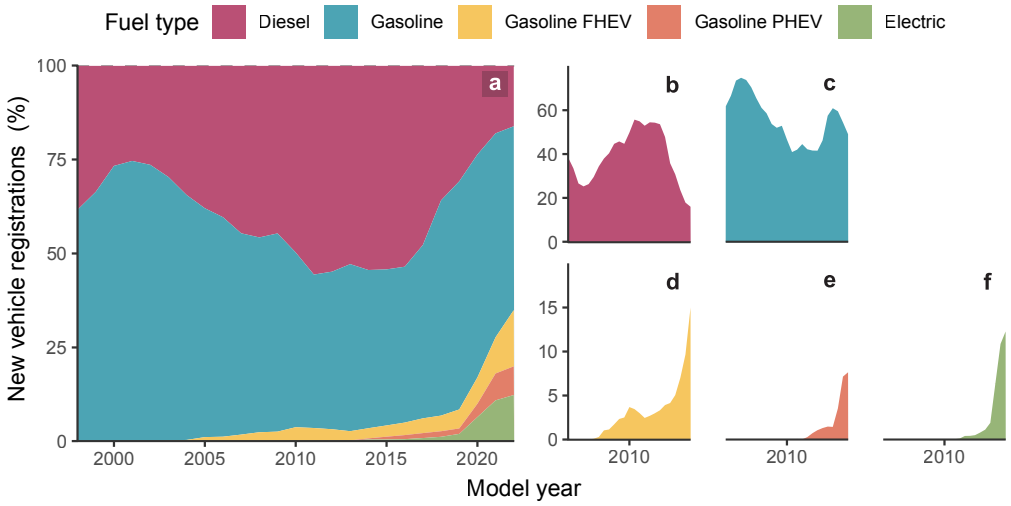

Figure 2.4: Passenger car fuel type composition (%) as a function of vehicle model year (1998 – 2022). The (**a**) combined total fuel type composition is displayed on the left and separate contributions from each fuel type: (**b**) Diesel, (**c**) Gasoline, (**d**) Gasoline FHEV, (**e**) Gasoline PHEV, (**f**) Electric, are shown on the right.

passenger cars that are being actively driven will be measured by remote sensing, and so the resulting data set reflects the on-road vehicle fleet as opposed to the total registered vehicle fleet represented in the DfT statistics. Diesel cars have higher annual mileage compared with gasoline cars, so their relative share is inflated in the on-road vehicle fleet compared to DfT statistics.[45] However, remote sensing measurements are typically collected in urban areas, where there are fewer diesel vehicles compared to rural and motorways, which would result in a conservative estimate of diesel car numbers.

Gasoline passenger car fleet composition trends generally contrast those described for diesel fuel. However, for later model years, the introduction of alternative fuel sources (FHEV, PHEV, and electric) resulted in a rate of gasoline share increase that was less than the rate of diesel share decrease. While electric and hybrid passenger cars operating in full electric mode do not produce exhaust emissions, they are still captured by the remote sensing

camera equipment, and all vehicle observations are preserved in the composition data set regardless of emissions measurement validity. This approach is essential for ensuring that the reported trends are representative of the on-road vehicle fleet and enables robust non-emissions related information such as that presented in Figure 2.4 to be derived from over 600,000 on-road vehicle observations.

For each vehicle model year and pollutant, the average of the distance-based emission factors for all fuel types was calculated, weighted by the fuel type composition data. The solid black lines in Figure 2.5 show these values as a function of model year for each pollutant and present a combination of the previously discussed emission factor and fleet fuel type composition results. The shaded areas beneath the black lines display the contribution towards the average value from each fuel type and assist in revealing the driving factors behind the observed trends.

Similar results are shown for both the CO and HC timelines in Figure 2.5; a general decrease in the average emission factor values of these pollutants is seen with increasing vehicle model year, resulting primarily from the decrease in the emissions from all fuel types seen in Figure 2.3. Additionally, the relative contribution towards the average from gasoline fuel increases from the model year 2015 onwards, corresponding to the period of the demise of diesel fuel in which the relative share of gasoline passenger cars in the fleet increased. For NH_3, the average emission factor value is dominated by the contribution from gasoline vehicles for all model years, and the increase seen from the model year 2017 onwards can be attributed to the increase in the relative share of gasoline passenger cars in the fleet.

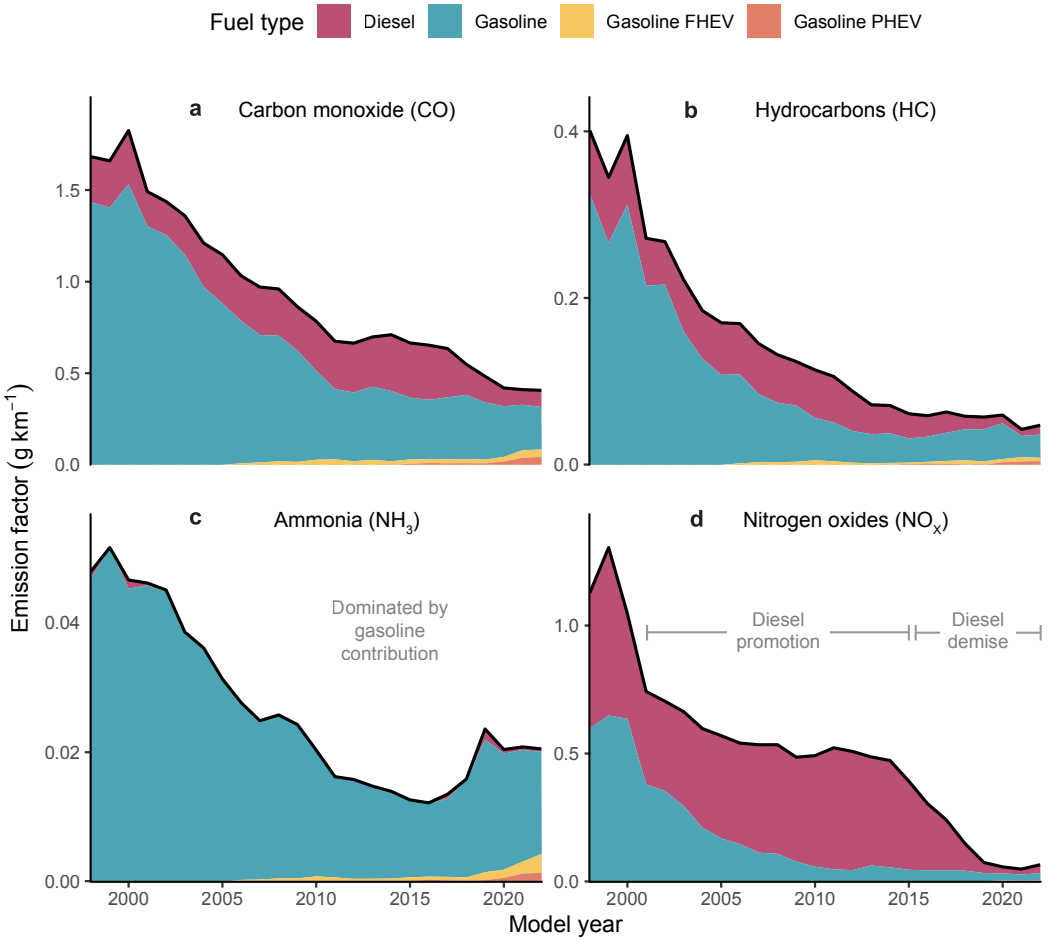

Figure 2.5: Average passenger car distance-based emission factor values ($g\,km^{-1}$) as a function of model year for (**a**) CO, (**b**) HC, (**c**) NH_3, and (**d**) NO_x. The solid black line represents the average distance-based emission factor values, and the shaded areas represent each fuel type's contribution to the average.

Diesel fuel contributions generally dominate the NO_x emissions following a period of growth between the model years 2001 and 2008. During this time, the rate of decrease of diesel and gasoline NO_x emission factors was similar (66% and 59% respectively, Figure 2.3), and thus this growth can be explained by the increase in the relative share of diesel passenger cars resulting from the promotion of diesel fuel. Another consequence arising from the increase in diesel vehicle share is the stagnation in the rate of

the average NO_x emission factor decrease with increasing model year, seen between 2005 and 2014 in Figure 2.5. During this period, despite both diesel and gasoline NO_x emission factors decreasing by 28% and 53%, respectively, the average NO_x emission factor only decreased by 17% because of the relative shift towards an increased proportion of newly registered diesel passenger cars. The implications of these results, which have been derived from on-road vehicle measurements, are very important: the rate of decrease of the average passenger car NO_x emission was diminished over a decade of vehicle model years as a direct consequence of the promotion of diesel fuel in the UK.

Following this period of NO_x emission factor stagnation, the rapid decrease (from 0.149 $g\,km^{-1}$ to 0.067 $g\,km^{-1}$, 83%) between model years 2015 to 2022 seen in Figure 2.5 is a result of the combination of two factors: a decrease in diesel vehicle NO_x emission factors resulting from the introduction of new exhaust after-treatment technology, and a decrease in relative diesel passenger car share due to reduced diesel fuel use. During this time, in addition to the decreasing average NO_x emission factor, the diesel contribution fell from 88% in 2015 to 50% in 2022. From the information reported, it is difficult to apportion the relative impact of reduced NO_x emissions and reduced use of diesel fuel.

2.4.2 Scenario Comparison

To disentangle the influences of improving vehicle technology and changes in the proportion of vehicle fuel types, this section explores three modelled scenarios, described in Section 2.3.5 and further evaluates the NO_x consequences of the promotion and demise of diesel fuel in the UK.

Using the fuel type composition data from Figure 2.2, an average NO_x emission factor timeline was produced for each scenario, as shown in Figure 2.6. Differences in the timeline average NO_x emission factor values

between scenarios can be attributed entirely to the changes in fuel type composition, considering that the individual fuel type emissions data used were identical. This approach effectively enables the evaluation of NO_x in modelled situations where the development of vehicle technology is consistent with BAU, but either the promotion (NDP) or the demise (NDD) of diesel fuel in the UK did not occur. Figure 2.7 shows the NO_x timelines for each scenario through two comparisons: BAU and NDP in panel (**a**), and BAU and NDD in panel (**b**).

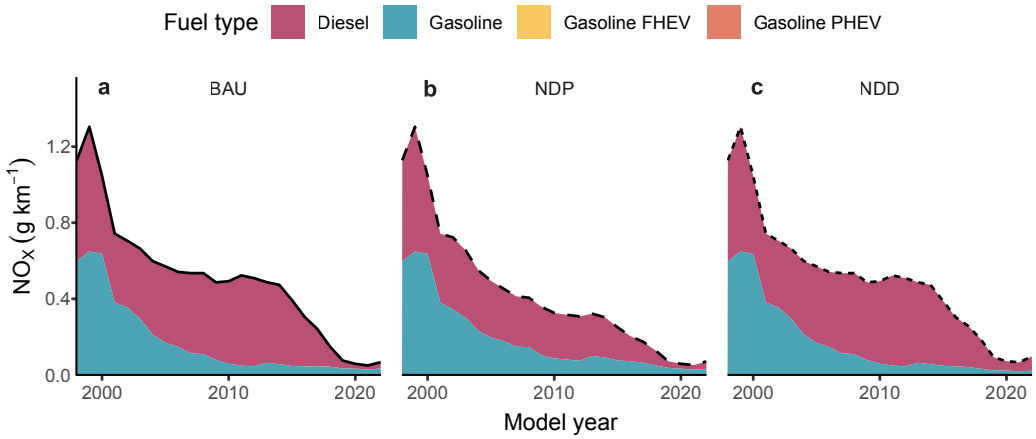

Figure 2.6: Average passenger car NO_x distance-based emission factor values ($g\,km^{-1}$) as a function of model year for the (**a**) Business as Usual (BAU), (**b**) No Diesel Promotion (NDP), and (**c**) No Diesel Demise (NDD) scenarios. The black lines represent the average distance-based emission factor values, and the shaded areas below represent each fuel type's contribution to the average.

The difference between the BAU and NDP scenarios (purple shaded region) represents the reduction in NO_x emission factors that could have been achieved had diesel fuel not been promoted in the UK, whereas the difference between the BAU and NDD scenarios (green shaded region) represents the increase in NO_x emission factors that may have been reported had the demise of diesel fuel not transpired. While the differences between scenarios within each comparison are a direct result of the modifications made to the fleet fuel

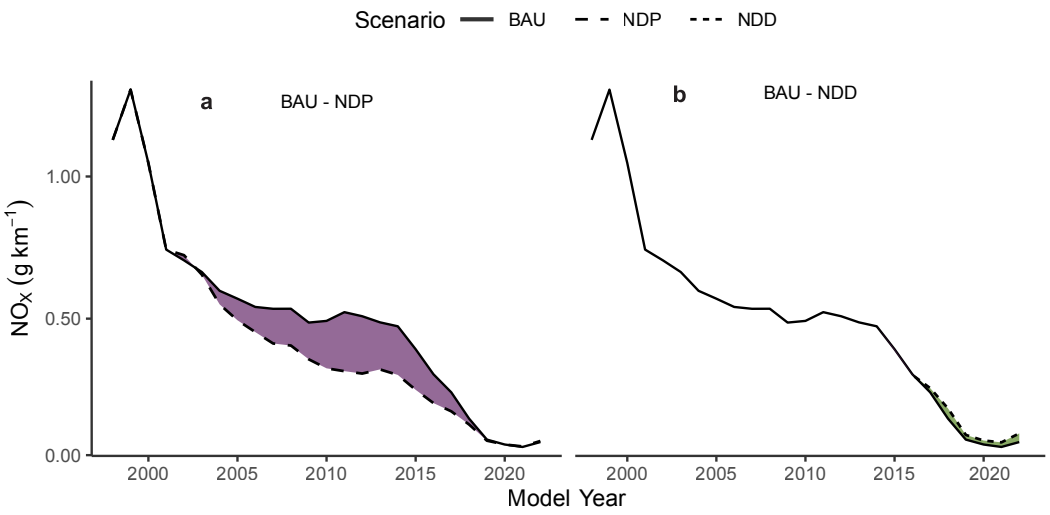

Figure 2.7: Average passenger car distance-based emission factor values ($g\,km^{-1}$) as a function of model year for each scenario. The purple shaded section in panel (**a**) represents the difference between the 'Business as Usual' and 'No Diesel Promotion' (BAU-NDP) scenarios. The green shaded section in panel (**b**) represents the difference between the 'Business as Usual' and 'No Diesel Demise' (BAU-NDD) scenarios.

type compositions to reflect different events, the disparity in the magnitude of these differences (and the sizes of the shaded regions) can be explained by the individual fuel NO_x distance-based emission factors shown in Figure 2.3. For the BAU-NDP comparison, the difference in fuel type composition reflects the promotion of diesel and occurs between model years 2001 and 2015, when diesel fuel NO_x emission factors were high. Conversely, for the BAU-NDD comparison, which reflects the demise of diesel, the difference in fuel type composition occurs between the model years 2015 and 2022, when diesel fuel NO_x emission factors were considerably lower due to effective after-treatment systems. Therefore, the fuel type composition differences between BAU and NDP have a larger influence than those between BAU and NDD, and the variation in the resulting average NO_x emission factors seen in Figure 2.7 is greater.

It is important to acknowledge that the development of vehicle technology is *not* entirely independent of events that influence vehicle fleet composition. The occurrence of Dieselgate is likely to have expedited the uptake of NO_x-specific after-treatment systems, resulting in post-2015 NO_x emission factors for an NDD scenario being higher than calculated in Figure 2.7. However, the exact impact of Dieselgate on the development of vehicle technology has not been quantified or considered in this analysis.

To further quantify and compare the relative NO_x impacts of the promotion and demise of diesel fuel, the estimated total lifetime NO_x emissions from all UK passenger cars with model years 1998 – 2022 was calculated for each scenario. These values were found to be 5480 kt, 4759 kt, and 5521 kt for BAU, NDP, and NDD, respectively. Figure 2.8 presents this information as the difference between the two modelled scenarios, and BAU disaggregated into an annual time-series in panel (**a**) and cumulative total in panel (**b**). The difference between the BAU and NDP scenarios (purple) represents the additional NO_x emission as a result of the promotion of diesel, whereas the difference between the BAU and NDD scenarios (green) represents the reduction in NO_x emissions as a result of the demise of diesel. The decrease in annual NO_x emissions for the years 2020 and 2021 is due to lower annual mileage values arising from the travel restrictions imposed during the COVID-19 pandemic.

The cumulative effect over three decades of promoting diesel fuel on total emissions of NO_x is calculated to be 721 kt. To put this total into perspective, it is equivalent to 7.38 times the total NO_x emitted by all passenger cars in the UK in 2021.[50] It is also greater than the total UK emissions of *all* NO_x *sources in 2021* of 681.8 kt.

The change in the total emission of NO_x is the principal impact that the growth in diesel use in passenger cars has had on air pollutant emissions. However, diesel vehicles are known to be important contributors to directly

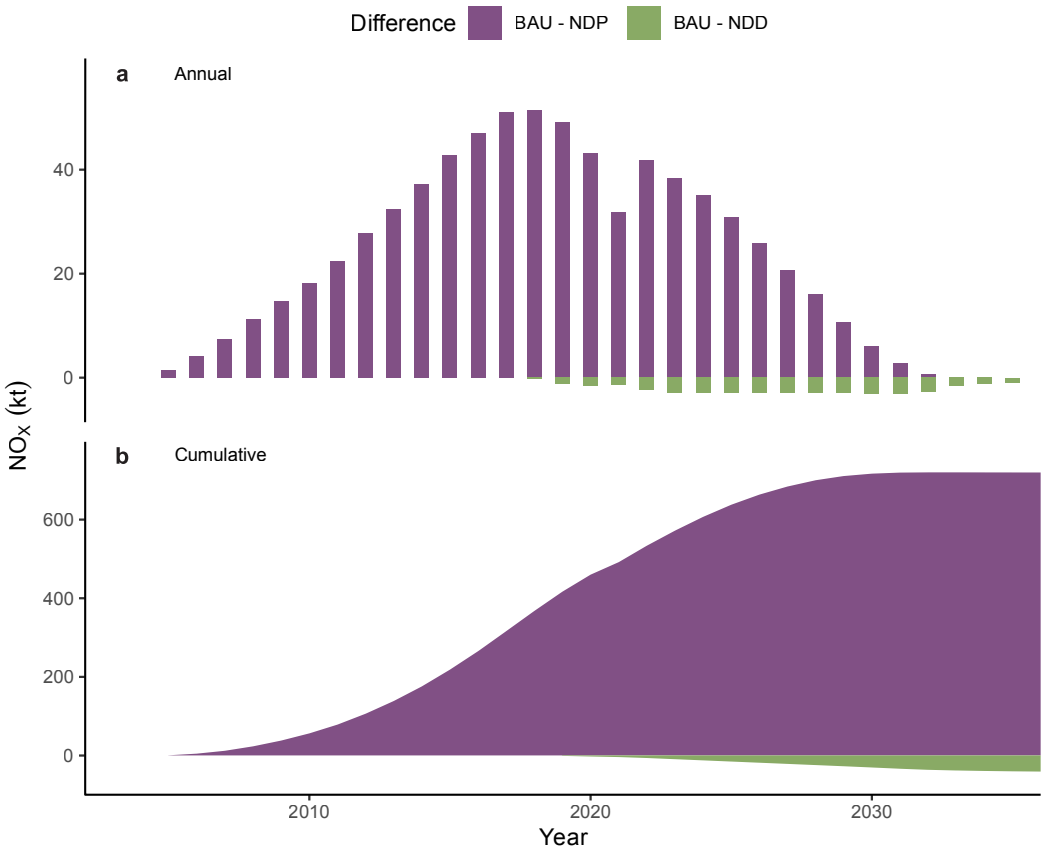

Figure 2.8: (**a**) Annual and (**b**) cumulative total lifetime NO_x emission difference from passenger cars registered between 1998 and 2022 for the 'Business as Usual' and 'No Diesel Promotion' (BAU-NDP) scenarios (purple), and the 'Business as Usual' and 'No Diesel Demise' (BAU-NDD) scenarios (green).

emitted (primary) NO_2. The use of diesel oxidation catalysts and particle filters, shown in Figure 2.1, led to large increases in directly emitted NO_2 emissions, making an important contribution to ambient NO_2 concentrations. [51] While the direct NO_2 emissions have not been quantified, the growth of diesel fuel use through the early 2000s would have led to considerably higher direct NO_2 emissions. The primary impact of directly emitted NO_2 is the contribution to local scale ambient NO_2 concentrations, which has been a major issue over the past two decades in Europe. Therefore, without diesel fuel promotion and growth, there would have been an additional benefit

beyond the reduction in total NO_x emissions.

While the move away from diesel fuel in the wake of Dieselgate resulted in a relatively small benefit in terms of NO_x emissions of 41 kt, there have been other consequences that could be important. As shown in Figure 2.4, a consequence of a move away from diesel was an increase in the use of gasoline, gasoline hybrid and electric vehicles. The relative increase in gasoline and gasoline hybrid vehicles led to a reduction in NO_x emissions but an increase in NH_3 emissions, as shown in Figure 2.5. Increased emissions of NH_3 would be expected to increase concentrations of $PM_{2.5}$ through the formation of ammonium nitrate (Section 1.2.3). The net impact of a reduction of NO_x emissions and an increase in emissions of NH_3 on concentrations of $PM_{2.5}$ is not known and would require a chemical transport model to establish effects on ambient $PM_{2.5}$ at a European scale. Nevertheless, the demise of diesel leading to increased vehicular NH_3 emissions is an unexpected outcome that requires further investigation.

2.5 Conclusions

The strong growth in diesel car use in the UK and Europe over the past two decades has been one of the most significant and profound factors influencing air quality from street level to a European scale. While there were likely benefits from policies encouraging diesel fuel from the perspective of carbon emissions, this benefit came at a significant cost to air quality and, in particular, urban air quality. It is clear that the climate and air quality impacts of different policies should be considered together. Vehicle technologies that aim to reduce important air pollutants such as NO_x have changed considerably over the past three decades. The emissions from gasoline passenger cars have been effectively controlled (and further refined) since the introduction of the three-way catalyst in 1992 in the UK. The situation for the control of air pollutants from diesel cars has evolved from very little control in the 1990s to the more recent use of complex but effective after-treatment systems such as selective catalytic reduction.

This work provides the first detailed evaluation and quantification of the impact that diesel car growth has had on the emission of important air pollutants. A novel and important component of the work is the use of extensive in-use vehicle emissions data from comprehensive remote sensing measurements. These measurements underpin the quantification of real-world emissions of pollutants, including NO_x and NH_3. We identify two principal changes to diesel car use over the past two decades: the steady growth of diesel fuel use from the early 2000s for climate mitigation reasons and the rapid decrease in diesel fuel use following the Dieselgate scandal in 2015. These two periods coincided with very different levels of NO_x emission control from diesel passenger cars.

The finding that the promotion of diesel fuel use in passenger cars resulted in excess emission of NO_x of 721 kt puts the impact of these policies

into context. This level of emission is over 7 times the total passenger car emissions of NO_x in the UK in 2021 and even exceeds UK total emissions of NO_x for the same year. Emissions of this magnitude were the result of the growth of diesel fuel use coinciding with a time when the control of diesel NO_x emissions was poor. Conversely, the rapid decrease in diesel fuel use has had a much lower impact than might have been expected (41 kt reduction in NO_x) because it occurred at a time when after-treatment systems used to control diesel NO_x were effective.

The full implications of such a large excess NO_x penalty are not known but are wide in nature. The most direct effect would have been related to urban concentrations of NO_2, which have proved to be highly challenging to control across Europe since the early 2000s. Exceedances of air quality limits of NO_2 have been most strongly associated with diesel NO_x emissions and also the direct emission of NO_2, which is much higher from diesel-fuelled vehicles compared with gasoline. Considering 2018, for example (the year with maximum NO_x contribution shown in Figure 2.8), our results show that if diesel cars had not been promoted, there would have been close to a 20% reduction in road transport NO_x emissions. A decrease in emissions of NO_x (and directly emitted NO_2) would likely have meant that many locations in Europe would not have exceeded legal air quality limits for NO_2.

However, because emissions of NO_x are directly linked to a wide range of other air quality problems, such as the formation of $PM_{2.5}$ and O_3, the impacts of diesel car growth would have extended well beyond urban air quality problems. An indication of the impacts of excess NO_x emissions can be gained from damage cost estimates that aim to quantify the human health and environmental impacts in terms of a financial amount, so-called externalities. The damage costs for NO_x include, for example, the impacts on human health associated with NO_x forming fine $PM_{2.5}$, which are estimated through the use of dispersion modelling and dose-response functions. In

the UK, for example, the damage cost estimates for NO_x are estimated to be £8,148 per tonne of NO_x.[52, 53] Given the total excess NO_x emission estimate of 721 kt, the total damage cost is estimated to be £ 5.875 billion.

Finally, an unintended consequence of the rapid move away from diesel car use post-Dieselgate is the growth in the use of gasoline and gasoline hybrid vehicles. The remote sensing data used in the current study suggests that the net effect is an increase in emissions of NH_3 associated with three-way catalysts. As gasoline vehicles age, emissions of NH_3 increase, which suggests that NH_3 emissions in future will be higher than expected.[40] Because NH_3 results in the formation of $PM_{2.5}$ and is strongly linked with problems associated with nitrogen deposition, this issue is of concern and deserves more attention.

2.6 Research Update

Since the publication of this work, new research has provided additional insight into the reported findings. Recent data suggest that the average operational lifespan of a passenger car in the UK exceeds the 14 years assumed in this study. This discrepancy is because the original value was based on average scrappage age and did not account for vehicles still in use. A new study using UK periodic technical inspection data, which corrects for this bias, estimates the average operational lifespan of a UK passenger car to be 18 years (Section 1.3.3).[54]

This change only affects the lifetime NO_x calculations in this work, as vehicle lifespan was used only in this context. Using the updated 18-year lifespan would increase the number of years over which a vehicle was active, and the total distance travelled per vehicle by approximately 30%. The total lifetime NO_x emissions for each scenario, and the differences between them, would therefore also increase by a similar amount. Consequently, the excess 721 kt of NO_x attributed to the promotion of diesel likely represents a conservative estimate, as does the 41 kt reduction associated with the decline of diesel. The impacts and message of this work remain unchanged.

Recent statistics from the 2023 National Travel Survey indicate that average annual passenger car mileage increased from 2022 but remained consistent with the 2017 – 2019 average, which was assumed in the lifetime NO_x calculations.[55] While future traffic patterns from 2023 to 2036 cannot be predicted, the 2023 data support the validity of the assumption used in this study.

UK-based real-world emissions measurements from the past two years reinforce this work's findings, with the latest data confirming continued low NO_x emissions from modern diesel vehicles.[56] Moreover, the introduction of Euro 6e standards for new light-duty vehicles at the end of 2023 further

increased the stringency of RDE testing, ensuring ongoing improvements in vehicle emissions performance.[57]

Ammonia from gasoline passenger cars, which was identified as a potential concern in this work, is becoming an increasingly important focus in vehicle emissions research, as new evidence suggests that they contribute significantly towards the formation of secondary $PM_{2.5}$ in urban areas.[58] Furthermore, the latest DfT data show a continued shift away from diesel towards gasoline and gasoline hybrid passenger cars, reinforcing the relevance of this issue.[59]

2.7 References

[1] Hoek, G., Krishnan, R. M., Beelen, R., Peters, A., Ostro, B., Brunekreef, B., and Kaufman, J. D. Long-term air pollution exposure and cardio-respiratory mortality: A review. *Environmental Health* 12 (2013). DOI: 10.1186/1476-069X-12-43 (cit. on p. 102).

[2] Bell, J., Honour, S. L., and Power, S. A. Effects of vehicle exhaust emissions on urban wild plant species. *Environmental Pollution* 159.8-9 (2011), pp. 1984–1990. DOI: 10.1016/j.envpol.2011.03.006 (cit. on p. 102).

[3] Anenberg, S., Miller, J., Henze, D., and Minjares, R. A global snapshot of the air pollution-related health impacts of transportation sector emissions in 2010 and 2015. *International Council on Clean Transportation* (2019), pp. 1–48 (cit. on p. 102).

[4] Sullivan, J., Baker, R., Boyer, B., Hammerle, R., Kenney, T., Muniz, L., and Wallington, T. CO_2 emission benefit of diesel (versus gasoline) powered vehicles. *Environmental Science and Technology* 38.12 (2004), pp. 3217–3223. DOI: 10.1021/es034928d (cit. on p. 102).

[5] Dornoff, J. and Rodríguez, F. Gasoline Versus Diesel: Comparing CO_2 Emission Levels of a Modern Medium Size Car Model under Laboratory and On-road Testing Conditions. *International Council on Clean Transportation* (2019) (cit. on p. 102).

[6] European Council. *Directive 2008/50/EC of the European Parliament and of the Council of 21 May 2008 on ambient air quality and cleaner air for Europe*. https://www.legislation.gov.uk/eudr/2008/50/contents. Accessed: 2023-05-04. 2008 (cit. on p. 102).

[7] World Health Organization. *Air Quality Guidelines — Update 2021. Copenhagen, Denmark: WHO Regional Office for Europe*. https://www.who.int/publications/i/item/9789240034228. Accessed: 2023-06-07. 2021 (cit. on p. 102).

[8] Transport for London. *Ultra Low Emission Zone*. https://tfl.gov.uk/modes/driving/ultra-low-emission-zone. Accessed: 2023-06-07. 2023 (cit. on p. 103).

[9] République Français. *Which vehicles can drive in Paris and the Greater Paris metropolis?* https://www.service-public.fr/particuliers/actualites/A14948?lang=en. Accessed: 2023-10-18. 2022 (cit. on p. 103).

[10] Comune di Milano. *Mobility: Area B*. https://www.comune.milano.it/aree-tematiche/mobilita/area-b. Accessed: 2023-10-18. 2023 (cit. on p. 103).

[11] Ngatia, L., Grace III, J. M., Moriasi, D., and Taylor, R. Nitrogen and phosphorus eutrophication in marine ecosystems. *Monitoring of marine pollution* 1 (2019), pp. 1–17. DOI: 10.5772/intechopen.81869 (cit. on p. 103).

[12] Selman, M., Greenhalgh, S., et al. Eutrophication: sources and drivers of nutrient pollution. *Renewable Resources Journal* 26.4 (2010), pp. 19–26. URL: https://www.wri.org/research/eutrophication-sources-and-drivers-nutrient-pollution (cit. on p. 103).

[13] Kroll, J. H., Ng, N. L., Murphy, S. M., Flagan, R. C., and Seinfeld, J. H. Secondary organic aerosol formation from isoprene photooxidation under high-NOx conditions. *Geophysical Research Letters* 32.18 (2005). DOI: doi.org/10.1021/es0524301 (cit. on p. 103).

[14] Ebi, K. L. and McGregor, G. Climate change, tropospheric ozone and particulate matter, and health impacts. *Environmental Health Perspectives* 116.11 (2008), pp. 1449–1455. DOI: 10.1289/ehp.1146 (cit. on p. 103).

[15] European Environment Agency. *NEC Directive reporting status 2015*. https://www.eea.europa.eu/publications/nec-directive-status-report-2015/nec-directive-reporting-status-2015. Accessed: 2023-06-07. 2015 (cit. on p. 103).

[16] European Environment Agency. *NEC Directive reporting status 2022*. https://www.eea.europa.eu/publications/national-emission-reduction-commitments-directive-2022/national-emission-reduction-commitments-directive. Accessed: 2023-06-07. 2022 (cit. on p. 103).

[17] United Kingdom Government. *United Kingdom Vehicle Excise Duty rates*. https://www.gov.uk/vehicle-tax-rate-tables/print. Accessed: 2023-02-17. 2023 (cit. on p. 103).

[18] HM Treasury. *Budget 2000*. https://www.gov.uk/government/uploads/system/uploads/attachment_data/file/265498/hc346.pdf. Accessed: 2023-06-07. 2000 (cit. on p. 103).

[19] United Kingdom Goverment Asset Publishing Service. *Road fuel consumption and the UL motor vehicle fleet*. https://assets.publishing.service.gov.uk/government/uploads/system/uploads/attachment_data/file/812622/Road_fuel_consumption_and_the_UK_motor_vehicle_fleet.pdf. Accessed: 2023-06-07. 2018 (cit. on p. 103).

[20] HM Treasury. *Consultation on reform of Vehicle Excise Duty to ensure a cleaner environment*. https://webarchive.nationalarchives.gov.uk/ukgwa/20090211145014/http:/www.hm-treasury.gov.uk/d/ConsultationOnReform.pdf. Accessed: 2023-06-07. 1998 (cit. on p. 104).

[21] Cames, M. and Eckard, H. Critical evaluation of the European diesel car boom - Global comparison, environmental effects and various national strategies. *Environmental Sciences Europe* 25 (1 2013). DOI: 10.1186/2190-4715-25-15 (cit. on p. 104).

[22] Department for Transport. *Vehicle Licensing Statistics Data Tables VEH1153*. https://www.gov.uk/government/statistical-data-sets/vehicle-licensing-statistics-data-tables. Accessed: 2023-05-04. 2022 (cit. on pp. 104, 120).

[23] European Commission. *Council Directive 91/441/EEC of 26 June 1991 amending Directive 70/220/EEC on the approximation of the laws of the Member States*

relating to measures to be taken against air pollution by emissions from motor vehicles. https://eur-lex.europa.eu/legal-content/EN/ALL/?uri=CELEX%3A31991L0441. Accessed: 2023-06-07. 1991 (cit. on p. 104).

[24] European Commission. *Emissions in the automotive sector*. https://single-market-economy.ec.europa.eu/sectors/automotive-industry/environmental-protection/emissions-automotive-sector_en. Accessed: 2023-06-07. 2022 (cit. on pp. 104–106).

[25] Vehicle Certification Agency. *Vehicle Type Approval*. https://www.vehicle-certification-agency.gov.uk/vehicle-type-approval/. Accessed: 2023-06-07. 2022 (cit. on p. 104).

[26] European Commission. *Commission Regulation (EU) 2016/646 of 20 April 2016 amending Regulation (EC) No 692/2008 as regards emissions from light passenger and commercial vehicles (Euro 6) (Text with EEA relevance)*. https://eur-lex.europa.eu/eli/reg/2016/646/oj. Accessed: 2023-06-07. 2016 (cit. on p. 105).

[27] Westerholm, R., Christensen, A., and Rosén, Å. Regulated and unregulated exhaust emissions from two three-way catalyst equipped gasoline fuelled vehicles. *Atmospheric Environment* 30.20 (1996), pp. 3529–3536. DOI: 10.1016/1352-2310(96)00048-9 (cit. on p. 106).

[28] Zheng, M., Reader, G. T., and Hawley, J. G. Diesel engine exhaust gas recirculation—-a review on advanced and novel concepts. *Energy conversion and management* 45.6 (2004), pp. 883–900. DOI: 10.1016/S0196-8904(03)00194-8 (cit. on p. 106).

[29] Twigg, M. V. Controlling automotive exhaust emissions: Successes and underlying science. *Philosophical Transactions of the Royal Society A: Mathematical, Physical and Engineering Sciences* 363.1829 (2005), pp. 1013–1033. DOI: 10.1098/rsta.2005.1547 (cit. on p. 106).

[30] International Council on Clean Transportation. *Real-driving emissions test procedure for exhaust gas pollutant emissions of car and light commercial vehicles*

in Europe. International Council on Clean Transportation. https://theicct.org/publication/real-driving-emissions-test-procedure-for-exhaust-gas-pollutant-emissions-of-cars-and-light-commercial-vehicles-in-europe/. 2017 (cit. on p. 107).

[31] European Commission. *Official Journal of the European Union. Amending Regulation (EC) No 692/2008 as regards emissions from light passenger and commercial vehicles (Euro 6)*. https://eur-lex.europa.eu/legal-content/EN/TXT/PDF/?uri=CELEX:32016R0646. 2016 (cit. on p. 107).

[32] Bishop, G. A. and Stedman, D. H. Measuring the emissions of passing cars. *Accounts of chemical research* 29.10 (1996), pp. 489–495. DOI: 10.1021/ar950240x (cit. on pp. 107, 109, 112).

[33] Burgard, D. A., Bishop, G. A., Stadtmuller, R. S., Dalton, T. R., and Stedman, D. H. Spectroscopy applied to on-road mobile source emissions. *Applied spectroscopy* 60.5 (2006), 135A–148A. DOI: 10.1366/000370206777412185 (cit. on pp. 107, 109, 112).

[34] Carslaw, D. C. and Rhys-Tyler, G. New insights from comprehensive on-road measurements of NO_x, NO_2 and NH_3 from vehicle emission remote sensing in London, UK. *Atmospheric Environment* 81.0 (2013), pp. 339–347. DOI: 10.1016/j.atmosenv.2013.09.026 (cit. on p. 107).

[35] University of Denver. *What is FEAT?* https://digitalcommons.du.edu/feat/#:~:text=What%20is%20FEAT%3F,to%20as%20a%20remote%20sensor. Accessed: 2023-03-07. 2023 (cit. on p. 109).

[36] Opus Inspection. *Remote Sensing Device*. https://www.opusrse.com/technology/remote-sensing-device/. Accessed: 2023-03-07. 2023 (cit. on p. 109).

[37] Rushton, C. E., Tate, J. E., Shepherd, S. P., and Carslaw, D. C. Interinstrument comparison of remote-sensing devices and a new method for calculating on-road nitrogen oxides emissions and validation of vehicle-specific power. *Journal of the Air & Waste Management Association* 68.2 (2018), pp. 111–122. DOI: 10.1080/10962247.2017.1296504 (cit. on p. 109).

[38] Davison, J., Bernard, Y., Borken-Kleefeld, J., Farren, N. J., Hausberger, S., Sjödin, Å., Tate, J. E., Vaughan, A. R., and Carslaw, D. C. Distance-based emission factors from vehicle emission remote sensing measurements. *Science of the Total Environment* 739 (2020), p. 139688. DOI: 10.1016/j.scitotenv.2020.139688 (cit. on pp. 111–113, 118).

[39] Hausberger, S. *Simulation of Real World Vehicle Exhaust Emission*. Vol. 82. Austria: Technische Universität Graz, 2003 (cit. on p. 112).

[40] Farren, N. J., Davison, J., Rose, R. A., Wagner, R. L., and Carslaw, D. C. Characterisation of ammonia emissions from gasoline and gasoline hybrid passenger cars. *Atmospheric Environment: X* 11 (2021). DOI: 10.1016/J.AEAOA.2021.100117 (cit. on pp. 112, 132).

[41] Davison, J., Rose, R. A., Farren, N. J., Wagner, R. L., Murrells, T. P., and Carslaw, D. C. Verification of a National Emission Inventory and Influence of On-road Vehicle Manufacturer-Level Emissions. *Environmental Science & Technology* 55 (8 2021), pp. 4452–4461. DOI: 10.1021/acs.est.0c08363 (cit. on p. 113).

[42] Society of Motor Manufacturers and Traders. *2022 Automotive Sustainability Report - Average Vehicle Age*. https://www.smmt.co.uk/industry-topics/sustainability/average-vehicle-age. Accessed: 2023-05-30. 2022 (cit. on p. 117).

[43] Department for Transport. *Vehicle Licensing Statistics Data Tables VEH0150*. https://www.gov.uk/government/statistical-data-sets/vehicle-licensing-statistics-data-tables. Accessed: 2023-03-19. 2022 (cit. on p. 117).

[44] Northern Ireland Statistics and Research Agency. *Driver and Vehicle Agency Statistics*. https://www.nisra.gov.uk/statistics/travel-and-transport/driver-vehicle-agency-statistics. Accessed: 2023-03-19. 2022 (cit. on p. 117).

[45] Department for Transport. *Vehicle Mileage and Occupancy NTS0901*. https://www.gov.uk/government/statistical-data-sets/nts09-vehicle-mileage-and-occupancy. Accessed: 2023-03-19. 2022 (cit. on pp. 117, 121).

[46] Grange, S. K., Grange, S. K., Farren, N. J., Vaughan, A. R., Davison, J., and Carslaw, D. C. Post-Dieselgate: Evidence of NO_X Emission Reductions Using On-Road Remote Sensing. *Environmental Science and Technology Letters* 7 (6 2020), pp. 382–387. DOI: 10.1021/acs.estlett.0c00188 (cit. on p. 118).

[47] Davison, J., Rose, R. A., Farren, N. J., Wagner, R. L., Wilde, S. E., Wareham, J. V., and Carslaw, D. C. Gasoline and diesel passenger car emissions deterioration using on-road emission measurements and measured mileage. *Atmospheric Environment: X* 14 (2022), p. 100162. DOI: 10.1016/j.aeaoa.2022.100162 (cit. on p. 118).

[48] Tagliaferri, S., Köppel, R., and Baiker, A. Influence of rhodium-and ceria-promotion of automotive palladium catalyst on its catalytic behaviour under steady-state and dynamic operation. *Applied Catalysis B: Environmental* 15.3-4 (1998), pp. 159–177. DOI: 10.1016/S0926-3373(97)00044-1 (cit. on p. 120).

[49] Heeb, N. V., Forss, A.-M., Brühlmann, S., Lüscher, R., Saxer, C. J., and Hug, P. Three-way catalyst-induced formation of ammonia—velocity-and acceleration-dependent emission factors. *Atmospheric Environment* 40.31 (2006), pp. 5986–5997. DOI: P10.1016/j.atmosenv.2005.12.035 (cit. on p. 120).

[50] United Kingdom National Atmospheric Emissions Inventory. *UK Informative Inventory Report (1990 to 2021)*. https://uk-air.defra.gov.uk/assets/documents/reports/cat09/2303151609_UK_IIR_2023_Submission.pdf. Accessed: 2023-08-03. 2023 (cit. on p. 127).

[51] Carslaw, D. C., Farren, N. J., Vaughan, A. R., Drysdale, W. S., Young, S., and Lee, J. D. The diminishing importance of nitrogen dioxide emissions from road vehicle exhaust. *Atmospheric Environment: X* 1 (2019). DOI: 10.1016/j.aeaoa.2018.100002 (cit. on p. 128).

[52] Department for Environment, Food, and Rural Affairs. *Air quality appraisal: damage cost guidance - Updated 2 March 2023*. https://www.gov.uk/government/publications/assess-the-impact-of-air-quality/air-quality-appraisal-damage-cost-guidance#damage-costs. Accessed: 2023-07-31. 2023 (cit. on p. 132).

[53] Brichby, D. *Air Quality damage cost update 2023 – FINAL Report*. https://uk-air.defra.gov.uk/assets/documents/reports/cat09/2301090900_Damage_cost_update_2023_Final.pdf. Accessed: 2023-08-01. 2023 (cit. on p. 132).

[54] Nguyen-Tien, V., Elliott, R. J., Strobl, E., and Zhang, C. *Estimating the longevity of electric vehicles: What do 300 million MOT test results tell us?* https://cep.lse.ac.uk/_NEW/publications/abstract.asp?index=10626. 2024 (cit. on p. 133).

[55] Department for Transport. *Vehicle Mileage and Occupancy NTS0901*. https://www.gov.uk/government/statistical-data-sets/nts09-vehicle-mileage-and-occupancy. Accessed: 2025-03-10. 2023 (cit. on p. 133).

[56] Farren, N. J., Wilson, S., Bernard, Y., Shaw, M. D., Lee, K., Crowe, M., and Carslaw, D. C. An Ambient Measurement Technique for Vehicle Emission Quantification and Concentration Source Apportionment. *Environmental Science & Technology* 58.45 (2024), pp. 20091–20100. DOI: 10.1021/acs.est.4c07907 (cit. on p. 133).

[57] International Council on Clean Transportation. *Euro 6e: Changes to the European Union light-duty vehicle type-approval procedure*. https://theicct.org/wp-content/uploads/2022/12/euro6e-type-approval-dec22.pdf. 2022 (cit. on p. 134).

[58] Wang, Y., Wen, Y., Zhang, S., Zheng, G., Zheng, H., Chang, X., Huang, C., Wang, S., Wu, Y., and Hao, J. Vehicular ammonia emissions significantly contribute to urban $PM_{2.5}$ pollution in two Chinese megacities. *Environmental science & technology* 57.7 (2023), pp. 2698–2705. DOI: 10.1021/acs.est.2c06198 (cit. on p. 134).

[59] Department for Transport. *VEH1103: Licensed vehicles at the end of the quarter by body type and fuel type: Great Britain and United Kingdom*. https://www.gov.uk/government/statistical-data-sets. Accessed: 2025-02-11. 2024 (cit. on p. 134).

Chapter 3

Influence of Vehicle Design on Near-Road Air Quality

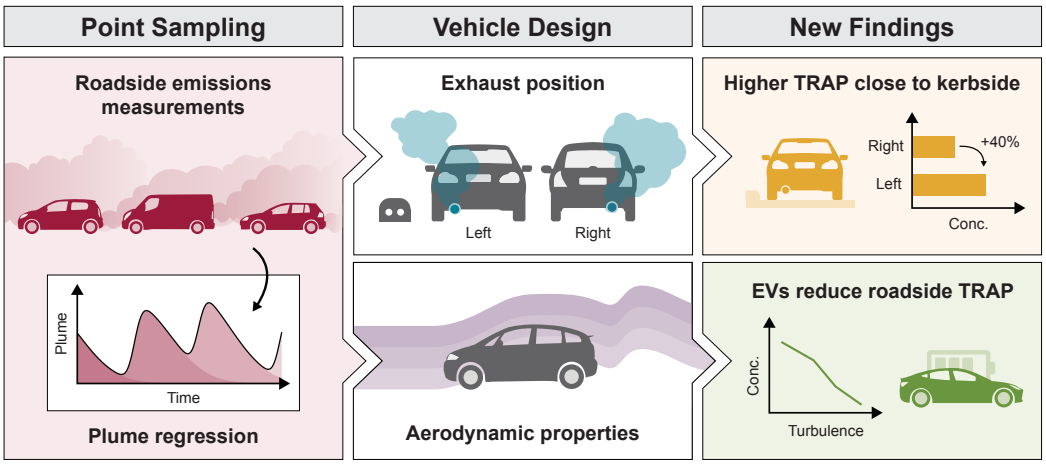

Wilson, S., Farren N. J., Bernard Y., Shaw M. D., Lee K., Crowe M., J. D. Lee, and Carslaw D. C. **Influence of Vehicle Design on Near-Road Concentrations of Traffic Related Air Pollutants**. *Environmental Science & Technology Air* 2. (2025). pp. 1089 – 1098. DOI: 10.1021/acsestair.5c00059

3.1 Abstract

Exposure to traffic-related air pollution (TRAP) is an ongoing health concern worldwide, particularly close to roads where concentrations are highest. Near-road exposure is influenced by complex processes such as the nature of vehicle emissions and the dispersion of vehicle exhaust plumes. In this work, we apply a recently developed technique called *plume regression* based on fast-response roadside measurements to better understand the factors affecting near-road TRAP concentrations. Of specific interest is determining the extent to which vehicle design and physical characteristics affect near-road exposure to important pollutants like nitrogen oxides (NO_x = NO + NO_2). We find that the position of a passenger car's exhaust (tailpipe) – whether on the left or right side – results in a 40% difference in pollutant concentration contribution at the kerbside. In the United Kingdom, only 20% of diesel passenger cars, the most significant vehicle class contributors to NO_x emissions, have their exhausts positioned on the right, the position associated with the lowest concentrations. If all diesel cars were equipped with right-positioned exhausts, kerbside TRAP concentrations from these vehicles could be reduced by one-third. We also find evidence that electric vehicles (EVs) act to dilute the exhaust plumes of proximate fossil-fuelled vehicles through vehicle-induced turbulence, reducing near-road TRAP exposure – a hitherto unrealised benefit of EVs.

3.2 Introduction

Traffic-related air pollution (TRAP) has long been recognised as having significant impacts on human health and the wider environment (Section 1.1.2).[1–3] An important way of studying TRAP is through ambient air quality measurements made close to roads. There are thousands of near-road ambient air quality measurement sites around the world that serve the primary purpose of monitoring the influence of road traffic on air pollution. Such sites typically report concentrations at an hourly resolution, which allows a comparison of measured concentrations with air quality standards and guidelines, many of which have an hourly mean averaging time.[4] Faster-response measurements of at least 1 Hz have increasingly been used for mobile measurements to map pollutant concentrations spatially and to estimate emission intensities (Section 1.4.6).[5–7] In part, this increase in the use of fast-response measurements reflect developments in instrumentation. However, far fewer studies have adopted similarly fast measurements at fixed locations.[8–10]

Reducing measurement sampling times offers the potential to develop an enhanced understanding of TRAP, which is important for informing strategies to mitigate air pollution and its health and environmental impacts, particularly in urban areas where exposure is highest (Section 1.3).[11] As instrument averaging times approach one or a few seconds, near-road measurements can resolve individual exhaust plumes from passing vehicles, greatly enhancing the potential to gain information on emission sources. At this temporal resolution, it is possible (but challenging) to quantify emissions from individual vehicles by integrating plume concentrations and using ratios to carbon dioxide (CO_2) to derive fuel-based emission factors (Section 1.4).[12] In related work, Farren et al. recently developed a new technique called *plume regression*, which greatly simplifies the quantification of vehicle

emissions.[13] This method leverages fast-response roadside measurements of dispersing vehicle exhaust plumes, eliminating the need to identify and extract individual vehicle plumes. Additionally, Farren et al. demonstrated that such measurements can be used for concentration source apportionment, enabling the quantification of total concentration contributions by vehicle type, which is valuable new information.

High temporal resolution roadside measurements, capable of resolving individual vehicle plumes, present an opportunity to investigate the factors that control near-road TRAP concentrations (Section 1.4.4). Critical data in this respect is information about the individual vehicles passing the measurement location. Automatic number plate recognition (ANPR) / license plate recognition (ALPR) systems enable the efficient capture of number plates for thousands of vehicles, which can then be used to query national vehicle databases. In the United Kingdom (UK), like many other countries, these databases provide comprehensive technical information, including fuel type and emission standard, as well as vehicle characteristics such as dimensions and mass. Coupling this technical information with techniques for analysing fast-response roadside measurements allows for a deeper investigation of the relationship between vehicle design characteristics and near-road concentrations of TRAP.

Previous work, including computational studies by Plogmann et al., has demonstrated that vehicle speed and design characteristics, such as exhaust position, are important factors influencing exhaust plume dispersion.[14, 15] In this paper, we apply the plume regression approach to real-world emissions measurements to understand better the vehicle-related factors that control near-road concentrations of TRAP. Of principal interest is the extent to which the physical design characteristics of vehicles affect measured concentration contributions. Specifically, we consider exhaust (tailpipe) position and vehicle aerodynamic properties. The proximity of the exhaust to

the kerb likely influences the degree of plume dilution, whereas the aerodynamic properties, such as physical size, are expected to affect vehicle-induced turbulence, thereby impacting near-road dispersion and concentrations. Additionally, we explore the growing role of electric vehicles (EVs) in the fleet and their influence on near-road TRAP concentrations, particularly how EVs contribute to the dilution of exhaust plumes from fossil-fuelled vehicles through vehicle-induced turbulence.

This study represents the first instance where individual vehicle measurements have been used to investigate these variables, offering a novel perspective on how vehicle design influences roadside TRAP concentrations. While the focus is on measurements made in the UK, the approach and findings are applicable to urban settings globally, providing transferable insights that could improve the quantification of TRAP at the thousands of near-road ambient air quality sites that exist worldwide.

3.3 Materials and Methods

3.3.1 Point Sampling

3.3.1.1 Instrumentation

Nitrogen oxides (NO_x = NO + NO_2) and CO_2 were measured at 1 Hz using an Airyx Iterative Cavity-Enhanced Differential Optical Absorption Spectrometer (ICAD).[16] The ICAD was placed on a trolley at the kerbside and sampled through a 30 cm length of 1/4" diameter perfluoroalkoxy tubing for continuous measurement of vehicle exhaust plumes. The instrument directly measures nitrogen dioxode (NO_2) in the 430 – 465 nm range through optical absorption, with an internal ozone-based gas phase titration system converting nitrogen oxide (NO) to NO_2, allowing for total NO_x and NO measurements. CO_2 is measured simultaneously via a non-dispersive infrared sensor. Further technical details are available in the literature (Section 1.4.6). [17]

A custom-built instrument was deployed approximately 1 m upstream of the ICAD instrument to record vehicle pass times. The instrument was named the Vehicle Measurement Device (VMD) and was based on a prototype built at Heidelberg University.[18] Optical sensors within the device measure vehicle speed and acceleration, triggering a camera positioned a further 5 – 10 m upstream of the device to capture rear images of passing vehicles. Additional information about the VMD is provided in Appendix A. All equipment was powered using two portable power stations with a capacity of 512 Wh and 256 Wh.

3.3.1.2 Measurement Surveys

Point sampling (PS) surveys were conducted at three sites in York, UK: two on the University of York campus (latitude 53.947, longitude −1.047) and

one in an industrial area near a large retail park (latitude 53.987, longitude −1.103). The locations were designated as sites A, B, and C respectively. Measurement surveys were carried out on weekdays between September and November 2023, during daylight hours and dry weather, with ambient temperatures ranging from 1.9 – 18.7 °C (12.9 °C mean). Photographs of the roadside measurement sites can be found in Figure 3.1.

Figure 3.1: Point sampling measurement sites (**a**) A, (**b**) B, and (**c**) C.

Registration (license plate) numbers were extracted from the vehicle images using ALPR software.[19] The registration numbers were sent to CDL Vehicle Information Services Limited to obtain vehicle technical data. CDL sources this information from the UK vehicle taxation system (DVLA) and the Society of Motor Manufacturers and Traders (SMMT) Motor Vehicle Registration Information System. The technical data includes a range of information, including, but not limited to, vehicle type, fuel type, mass, dimensions, make, model, registration date, and emission standard (Section 1.3.1).

In total, 11,264 vehicle passes (7,955 unique vehicles) were recorded over nine measurement days, with 14.7%, 23.9%, and 61.4% of measurements being made at sites A, B, and C, respectively. Technical information was obtained for 95% of vehicle passes. A summary of the measured vehicle fleet composition and driving conditions at each site is provided in Tables 3.1 and 3.2, respectively. Hybrid vehicles with different technologies (full hybrid,

plug-in hybrid, etc.) were grouped due to insufficient measurement numbers for separate groupings.

Table 3.1: Number of measurements and vehicle fleet composition (vehicle type, fuel type, and emission standard) at each measurement site. The total number of measurements across the sites (10,624) corresponds to the 95% of vehicle passes for which technical data was available.

Characteristic	**Site A**	**Site B**	**Site C**
# measurements	1565	2536	6523
Vehicle type			
Car (%)	75.0	74.5	78.0
LGV (%)	17.1	16.0	15.0
Bus (%)	2.7	4.1	0.3
HGV (%)	1.4	1.2	1.8
Motorcycle (%)	1.0	1.2	0.5
Unknown (%)	2.7	2.9	4.4
Fuel type			
Diesel (%)	42.0	41.3	44.2
Gasoline (%)	43.5	41.2	41.0
Hybrid (%)	7.9	10.1	7.5
Electric (%)	3.9	4.3	2.7
Unknown (%)	2.7	3.1	4.6
Emission standard			
Pre Euro 4 (%)	4.7	4.4	4.2
Euro 4 (%)	8.1	9.0	9.4
Euro 5 (%)	26.1	25.9	22.2
Euro 6 (%)	56.0	55.5	58.8
Unknown (%)	5.0	5.2	5.3

Table 3.2: Mean driving conditions at each measurement site.

Characteristic	Site A	Site B	Site C
Speed ($km\,h^{-1}$)	32.0	36.0	44.2
Acceleration ($km\,h^{-1}\,s^{-1}$)	3.1	−0.4	4.8
Vehicle gap (s)	15.0	15.7	7.0

3.3.2 Analysis Methods

3.3.2.1 Plume Regression

A *plume regression* technique is used to quantify the contribution from different types of vehicles that best explains the roadside concentration time series measurements.[13] For the NO_x and CO_2 concentration time series, the increments above a local background were determined for each pollutant. While various methods can be used, a simple rolling average low percentile approach was chosen, using a time window of 100 s.[6, 7, 20] This window was selected to comfortably encompass the typical width of an exhaust plume of ∼20 s while minimising the capture of contributions from sources other than passing vehicles.

Instead of attempting to isolate individual vehicle plumes, the technique uses a statistical approach to quantify concentration contributions for different categories of all passing vehicles. An average exhaust plume profile is derived from CO_2 measurements from isolated vehicles (where there is at least a 20 s gap between vehicle passes before and after, n = 306).[13] This plume profile represents the expected average rise and fall of concentrations after a vehicle passes. As noted by Farren et al., in some situations, different plume profiles could be used, for example, for different sites or for heavy vehicles with a vertically oriented exhaust. The effect of the plume profile shape is considered in more detail later in the text. Similar plume profiles

were observed at all three measurement sites, and one average plume profile was used for all vehicle groups.

In previous work by Farren et al., roadside concentration data were processed to provide emission factors by vehicle fuel and technology types, for example, a Euro 5 diesel passenger car.[13] The way in which the data are disaggregated is determined at the beginning of the analysis. In the current application, the interest is not the technologies but the design characteristics of a vehicle, such as the exhaust position for gasoline and diesel passenger cars. Each time a vehicle from a particular category passes (such as a gasoline vehicle with an exhaust positioned on the left-hand side), a normalised plume is added to the time series column for that category of vehicle. This process continues to cover all vehicle categories (determined by the initial disaggregation) of interest, and for all passing vehicles, the same averaged normalised plume profile determined from isolated vehicle measurements was used for all vehicle categories. The main aim of the analysis is to determine the optimal amount by which the vehicle category plumes must be multiplied to explain best the concentration increments of CO_2 and NO_x. The approach uses robust linear regression that relates the concentration of CO_2 or NO_x to the different vehicle category plumes.[21] The coefficients from the regression provide a direct estimate of the concentration contribution from each vehicle category. A useful benefit of the regression-based approach is that the standard errors are provided for each regression coefficient, from which 95% confidence intervals can be derived (using a Z-score of 1.96).

CO_2 was used as a tracer for TRAP in the plume regression technique due to its high concentration in exhaust gases, stability under ambient conditions, direct proportionality to fuel combustion, and independence from exhaust after-treatment systems (Section 1.2). These features make CO_2 an ideal tracer for assessing how vehicle design affects exhaust plume dispersion and subsequent roadside concentrations of TRAP, which can be assumed

to disperse similarly to CO_2.[14] CO_2 exhaust gas concentrations vary for diesel and gasoline fuels based on differences in the air/fuel ratio utilised for combustion. However, the differences in absolute CO_2 emissions output are small and discussed further in Section 3.4.1. NO_x was also analysed to provide direct evidence of the influence of vehicle design on roadside TRAP concentrations and to provide information that could be used to derive emission factors.

3.3.2.2 Vehicle Design Properties Assignment

Exhaust exit positions were assigned from the vehicle images for passenger cars only, as other vehicle types rarely show visible exhausts or did not exhibit varied placement. Of 8,643 car measurements, 44.4% were manually assigned as either 'left', 'right', 'centre', or 'split', while the 2.9% of EVs were assigned as 'none'. The assignments, based on the rear of the vehicle relative to UK traffic flow, define left as kerbside, right as offside, split for exhaust exits in both positions and centre for middle placement. Examples for each assignment are shown in Figure 3.2.

The remaining cars were not assigned manually due to non-visible down-turned exhaust exits, often hidden by the rear bumper. A random forest model was used to predict exhaust positions for these vehicles as either left or right, as split or centre exhausts are rarely down-turned or hidden by other design features.[22, 23] This machine learning algorithm, chosen for its ability to handle categorical data, was trained on the manually assigned data (80% training, 20% validation). Predictor variables included fuel type, Euro emission class, body type, manufacture year, number of doors, seat count, drive axle configuration, transmission type, and gear count. Features were selected to balance model robustness with the need for complete data; the model showed high classification accuracy with an F1-score of 0.94 and a Matthews correlation coefficient of 0.85. Following exhaust prediction,

Figure 3.2: Example photographs of the different manually assigned exhaust positions.

95.5% of cars (8597 measurements) had assigned exhaust positions, with the remaining unknowns due to insufficient predictor variable data. Tables 3.3 and 3.4 provide detailed model performance metrics and a summary of the number of manually assigned and predicted exhaust positions. To evaluate the influence of exhaust position on near-road TRAP concentrations, vehicles were grouped by type, fuel type, and exhaust position in the plume regression analysis.

Table 3.3: Passenger car exhaust position random forest prediction model training parameters and performance metrics.

Parameter	**Value**
ntree	500
mtry	2
Sensitivity (recall)	0.940
Specificity	0.907
Precision	0.940
Balanced accuracy	0.924
Area Under Curve (AUC)	0.978
F1 score	0.940
Matthews correlation coefficient	0.847

Table 3.4: Summary of the manually assigned and predicted passenger car exhaust positions.

	Manual		**Predicted**		**Total**	
Exhaust position	**n**	**%**	**n**	**%**	**n**	**%**
Left	1706	19.7	2446	54.3	4152	48.0
Right	1123	13.0	2062	45.7	3185	36.9
Centre	63	0.7	0	0	63	0.7
Split	944	10.9	0	0	944	10.9
None	253	2.9	0	0	253	2.9
Unknown	4554	52.7	0	0	46	0.5
Total	8643		4508		8643	

Aerodynamic drag coefficients (C_d) quantify a vehicle's air resistance and are directly proportional to vehicle-induced turbulence (Section 3.3.2.3). Vehicles were assigned a C_d value based on market segment classifications derived from their dimensions. Passenger cars were grouped into eight segments (A, B, C, D, E, F, J, S), while light goods vehicles (LGVs) formed a separate segment (V). Vehicles with missing dimension information, including heavy goods vehicles (HGVs) and buses, were classified as 'unknown'. Estimated C_d values from the literature were then assigned to each segment. [24, 25] Table 3.5 provides dimension classifications and C_d values for each segment.

Table 3.5: Dimension classifications and aerodynamic drag coefficients (C_d) for each vehicle segment. SUV* = sport utility vehicle, LGV* = light goods vehicle.

Segment	Description	Area (m^2)	Length (m)	height (m)	C_d	n
A	Mini	< 3.0	< 3.7	—	0.33	545
B	Small	< 3.0	< 4.2	—	0.32	2006
C	Medium	< 3.0	< 4.6	—	0.30	1876
D	Large	< 3.0	< 4.8	—	0.29	451
E	Executive	< 3.0	< 5.0	—	0.29	222
F	Luxury	< 3.0	≥ 5.0	—	0.29	25
J	SUV*	≥ 3.0	—	—	0.35	1834
S	Sport coupe	< 3.0	—	< 1.4	0.30	153
V	LGV*	–	–	–	0.34	1225

3.3.2.3 Vehicle-Induced Turbulence

Vehicle-induced turbulence plays an important role in exhaust gas dispersion and directly influences roadside TRAP concentrations. Turbulent kinetic energy (TKE), measured using a sonic anemometer, has been used to evaluate

the relationship between near-road TRAP and vehicle-induced turbulence. [15, 26, 27] In this study, we consider the power required to overcome aerodynamic drag, P_d, which is directly proportional to TKE and reflects the energy available for turbulence generation. P_d is calculated using Equation 3.1, where ρ is the air density (1.233 kg m^{-3} at the mean measurement temperature of 12.9 °C and 101.3 kPa), C_d is the drag coefficient (Section 3.3.2.2), A is the vehicle frontal area, and v is the measured vehicle speed.[25] A benefit of the vehicle technical information is the ability to calculate frontal area and P_d for individual vehicles from their dimension measurements.

$$TKE \propto P_d = \frac{1}{2} \rho C_d A v^3 \tag{3.1}$$

For assessing the impact of vehicle-induced turbulence and aerodynamic properties on near-road TRAP, vehicles were grouped by type, fuel type, exhaust position and losses due to aerodynamic drag, P_d. Drag losses were calculated using Equation 3.1 and expressed in categories as quantiles (Low < 0.25, $0.25 \leq$ Low-mid < 0.50, $0.50 \leq$ High-mid < 0.75, $0.75 \leq$ High), calculated independently for each vehicle type and fuel type subgroup. The calculation of quantiles was necessary as the plume regression method requires defined vehicle groupings.

3.3.2.4 Emission Rates

The CO_2 coefficients calculated from plume regression reflect the expected near-road concentration increment associated with each vehicle group and are influenced by both CO_2 emission rate and subsequent dispersion (related to exhaust position and aerodynamic properties). To isolate the contribution of dispersion and impact of vehicle design characteristics, two metrics for CO_2 emission rates were used in this study. Neither of the emission rate

values can be directly compared to the plume regression coefficients that provide concentration and not emission estimates. However, these emission factors are useful in understanding the extent to which roadside concentrations are associated with emissions rather than dispersion influences.

For the exhaust position analysis (Section 3.4.1), Type-Approval CO_2 emission rates based on laboratory test cycles ($g\,km^{-1}$), available from the vehicle technical information, were aggregated to calculate a mean value for each vehicle group. These emission rates are provided in Table 3.6. The mean Type-Approval CO_2 emission rate reflects an average value across a range of driving conditions and was chosen as it could be calculated for all vehicle types.

For the vehicle-induced turbulence and aerodynamic properties analysis (Section 3.4.4), which only included cars and LGVs, instantaneous CO_2 emission rates were modelled for individual vehicles. Instantaneous fuel consumption ($kg\,s^{-1}$) was calculated using the Passenger Car and Heavy Duty Emission Model (PHEM), incorporating vehicle speed, acceleration, road gradient, and technical data (e.g., mass, dimensions, engine specs). [28, 29] These rates were then converted into CO_2 emission rates ($g\,s^{-1}$) using standard emission factors: 3.16 $g\,kg^{-1}$ for gasoline and 3.17 $g\,kg^{-1}$ for diesel. [30] Finally, the values were aggregated for each vehicle group and used to normalise the plume regression CO_2 coefficients. Modelled instantaneous CO_2 emission rates provide a more accurate estimate of actual emission at the time of measurement than type-approval values but could not be calculated for all vehicle types due to missing technical data.

Table 3.6: Mean Type Approval CO_2 emission rates ($g\,km^{-1}$) for vehicle type, fuel type, and exhaust position groups.

Type	**Fuel**	**Exhaust**	**CO_2**	**Standard error**	**n**
Bus	Diesel	—	250.5	18.3	4
HGV	Diesel	—	227.9	5.9	42
LGV	Diesel	—	179.7	1.1	1278
Car	Diesel	All	132.8	0.6	2704
Car	Diesel	Split	144.8	1.5	448
Car	Diesel	Left	131.1	0.7	1713
Car	Diesel	Right	128.5	1.3	543
Car	Gasoline	All	134.5	0.5	4241
Car	Gasoline	Centre	154.0	4.4	51
Car	Gasoline	Left	133.0	0.5	2121
Car	Gasoline	Split	172.4	2.5	337
Car	Gasoline	Right	128.3	0.6	1732
Car	Hybrid	All	93.6	1.2	849
Car	Hybrid	Left	71.3	5.2	78
Car	Hybrid	Right	97.7	1.1	685
Car	Hybrid	Split	80.7	6.9	86
Motorcycle	Gasoline	—	77.8	10.1	9

3.4 Results and Discussion

3.4.1 Exhaust Position Effect on CO_2

The CO_2 concentration measurements were grouped by vehicle type, fuel type, and exhaust position (for passenger cars only) for plume regression. The resulting calculated CO_2 concentration coefficients are shown in Figure 3.3, with detailed values provided in Table 3.7. These coefficients represent the increase in roadside CO_2 concentrations associated with each vehicle group. It is important to note that these coefficients differ from vehicle emission factors, as roadside CO_2 concentrations are influenced by emission rates and factors such as exhaust proximity to the kerb and vehicle design features affecting plume dispersion. These measurements, therefore, offer direct insight into roadside TRAP emissions and dispersion under real-world conditions.

Figure 3.3 reveals clear trends driven by vehicle type, fuel type, and exhaust position. Larger vehicles, such as buses and HGVs, exhibit higher CO_2 coefficients due to their greater emission rates. Among passenger cars, gasoline hybrid vehicles are associated with the lowest CO_2 coefficients, reflecting their lower emission rates. Furthermore, left exhaust cars consistently produced higher CO_2 coefficients than right exhaust cars across all fuel types, highlighting the importance of exhaust proximity to the kerb for near-road TRAP concentrations.

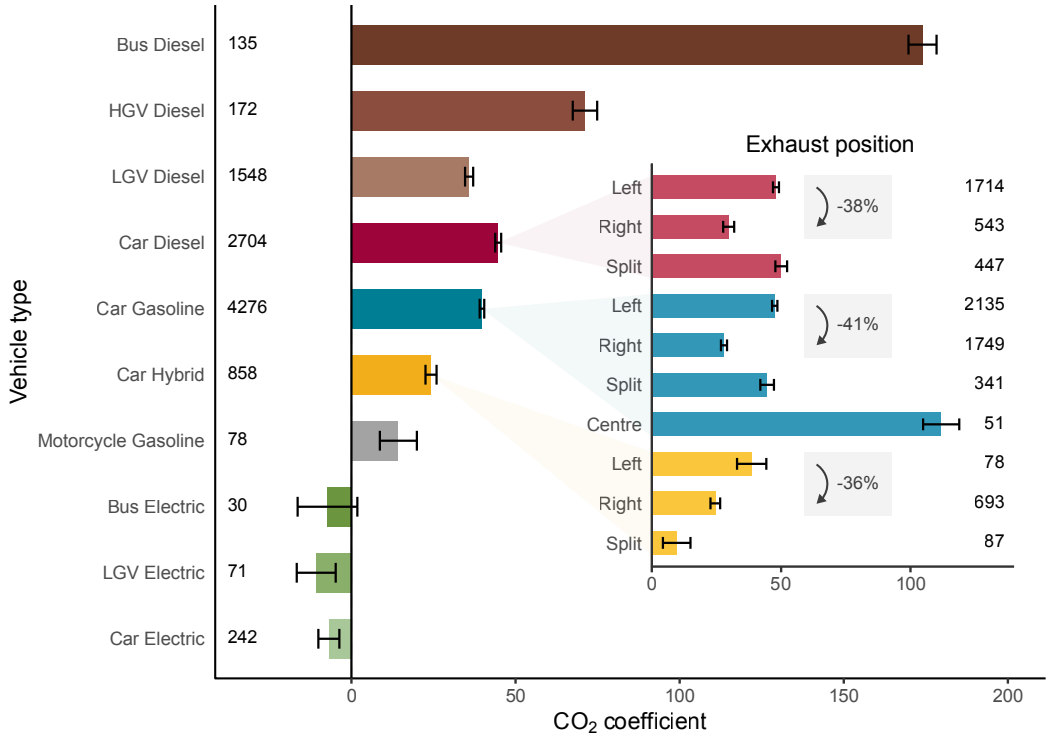

Figure 3.3: CO_2 coefficients for vehicle type and fuel type groups. The inset plot further separates passenger cars by exhaust position. Error bars represent 95% confidence intervals, and number labels denote vehicle group sample sizes. Grey boxes display the reduction in CO_2 coefficient for right exhaust positions compared to left for each fuel type. The exhaust locations include those manually assigned and predicted.

Specifically, CO_2 coefficients were reduced by 38%, 41%, and 36% for diesel, gasoline, and gasoline hybrid cars, respectively, when comparing right exhausts to left exhausts. These differences can confidently be attributed to exhaust location, as the mean vehicle speeds, aerodynamic properties, and Type Approval CO_2 emission rates (see Section 3.3.2.4 and Table 3.6) for left and right exhaust vehicles within each fuel type were very similar, with less than 5% variation across all comparisons. The only exception was for gasoline hybrid cars, where vehicles with right exhausts had a 37% higher mean Type Approval CO_2 emission rate than those with left exhausts.

This may explain why the difference in CO_2 coefficients was smallest for gasoline hybrid cars. However, it is important to note that Type Approval CO_2 emission rates do not perfectly represent real-world driving conditions and serve only as a guide.[31, 32]

Table 3.7: CO_2 concentration coefficients for vehicle type, fuel type, and exhaust position groups.

Type	Fuel	Exhaust	CO_2	Standard error	n
Bus	Diesel	—	174.8	2.2	135
HGV	Diesel	—	71.1	1.9	172
LGV	Diesel	—	36.0	0.6	1548
Car	Diesel	All	44.7	0.5	2704
Car	Diesel	Split	49.7	1.2	447
Car	Diesel	Left	48.0	0.6	1714
Car	Diesel	Right	29.7	1.1	543
Car	Gasoline	All	39.8	0.4	4276
Car	Gasoline	Centre	111.8	3.6	51
Car	Gasoline	Left	47.5	0.5	2135
Car	Gasoline	Split	44.6	1.3	341
Car	Gasoline	Right	27.9	0.6	1749
Car	Hybrid	All	24.3	0.9	858
Car	Hybrid	Left	38.6	5.7	78
Car	Hybrid	Right	24.6	1.9	693
Car	Hybrid	Split	44.6	2.6	87
Motorcycle	Gasoline	—	15.9	2.9	78
Bus	Electric	—	-8.3	4.6	30
LGV	Electric	—	-10.9	3.0	71
Car	Electric	None	-7.2	1.6	242

Diesel cars exhibited, on average, 12% higher CO_2 coefficients than gasoline cars despite having slightly lower Type Approval CO_2 emission rate values (Table 3.6). However, recent literature suggests that diesel cars may have higher real-world CO_2 emission rates than gasoline cars when adjusted for vehicle size, power output, and Type Approval CO_2 emission rate.[33]

To evaluate the machine learning algorithm used to assign exhaust positions for cars with non-visible exhausts in the images, a plume regression was performed, categorising car exhaust groups into manually assigned and predicted positions. The resulting CO_2 coefficients are shown in Figure 3.4 and Table 3.8. For manually assigned cars, CO_2 coefficients were reduced by 60%, 59%, and 75% for diesel, gasoline, and gasoline hybrid vehicles, respectively, when comparing right to left exhaust positions. In contrast, for predicted exhaust positions, the reductions were 23%, 34%, and 4%, respectively. While left-exhaust CO_2 coefficients were similar between manually assigned and predicted groups across all fuel types, right-exhaust CO_2 coefficients were approximately twice as high for predicted positions compared to manually assigned ones.

A likely explanation for these observations is exhaust *orientation*, which has been shown in the literature to influence plume dispersion and near-road exhaust gas concentrations.[14] Manually assigned exhausts are all horizontal, and predicted exhausts could all be assumed to be down-turned. Horizontal exhausts result in more dispersion and lower roadside concentrations, while down-turned exhausts result in less dispersion and higher roadside concentrations. Even though the predicted exhaust positions are not visible, these results show that there is a consistent left-right difference in CO_2 coefficients. However, hidden (down-turned) exhausts are associated with different dispersion characteristics compared with horizontal exhausts, likely resulting in a smaller left-right difference.[14]

While these effects explain the CO_2 coefficient trends for manually as-

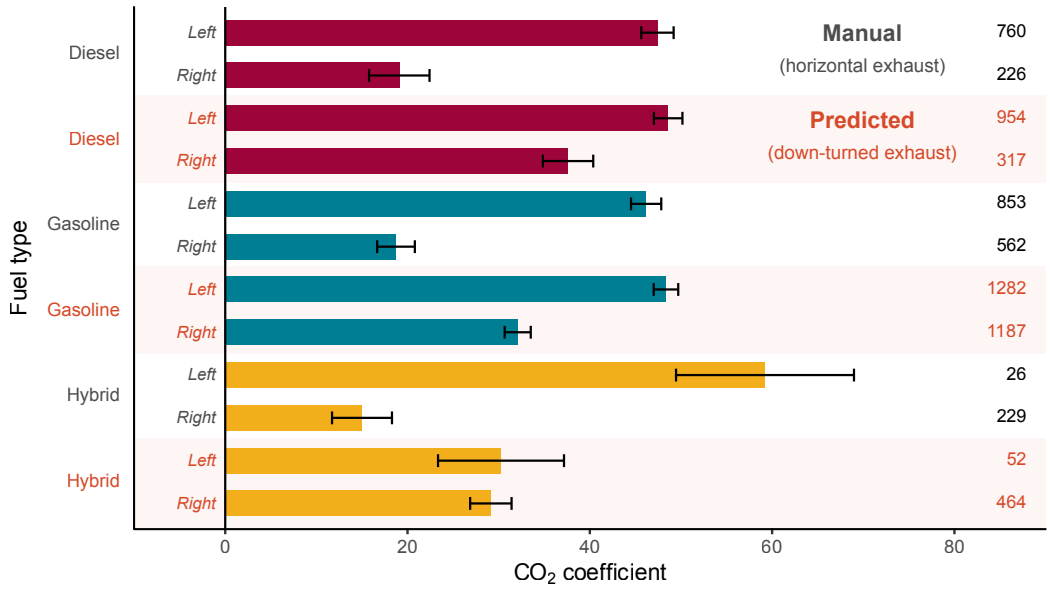

Figure 3.4: CO_2 coefficients for passenger cars with left and right exhaust positions, split into manually assigned and predicted groups. The error bars represent 95% confidence intervals, the text labels denote exhaust position, and the number labels show vehicle group sample sizes. The grey text represents manually assigned exhaust position vehicles, and the orange text and shading represent predicted exhaust position vehicles.

signed and predicted exhaust positions, other factors could be responsible for the discrepancy between these groups for right-exhaust cars. If exhaust orientation does not significantly influence near-road TRAP concentrations and the discrepancy instead arises from incorrect exhaust position predictions, then the manually assigned data in Figure 3.4 provide a more accurate representation of the impact of exhaust position on roadside CO_2 and TRAP concentrations. Notably, these manually assigned results show an even greater difference between left and right exhaust positions, reinforcing the implications discussed later in this section.

The consistency between trends in predicted and manually assigned exhaust positions, along with theoretical insights from simulation studies on near-road exhaust plume dispersion, suggests that the observed effects are in

Table 3.8: Passenger car CO_2 concentration coefficients for fuel type, exhaust position, and exhaust assignment source groups.

Fuel	Exhaust	Source	CO_2	Standard error	n
Diesel	Left	Manual	47.4	0.9	760
Diesel	Right	Manual	19.1	1.7	226
Diesel	Left	Predicted	48.6	0.8	954
Diesel	Right	Predicted	37.6	1.4	317
Gasoline	Left	Manual	46.2	0.8	853
Gasoline	Right	Manual	18.7	1.1	562
Gasoline	Left	Predicted	48.4	0.7	1282
Gasoline	Right	Predicted	32.1	0.7	1187
Hybrid	Left	Manual	59.2	5.0	26
Hybrid	Right	Manual	15.0	1.7	229
Hybrid	Left	Predicted	30.3	3.5	52
Hybrid	Right	Predicted	29.1	1.2	464

fact driven by exhaust orientation. To most accurately capture the impact of exhaust position across the entire passenger car fleet, which includes both horizontal and down-turned exhausts, the predicted exhaust positions should be incorporated into the analysis, as in Figure 3.3.

The CO_2 coefficient for gasoline cars with centre exhausts in Figure 3.3 was 1.4 and 3.0 times higher than for those with left and right exhausts, respectively. This increase is likely due to these vehicles being high-performance models with lower fuel efficiency and higher CO_2 emission rates, as confirmed by technical data showing all 51 centre-exhaust cars were classified as *sport* models with a 17.6% higher mean type-approval CO_2 emission rate. Additionally, centre exhausts release exhaust gases directly into the wake zone of the vehicle, where the interaction of turbulence and plume dispersion

could result in higher measured CO_2 concentrations when compared to exhaust positioned in other locations.[14] More research with direct turbulence measurements, such as using a sonic anemometer, is needed to understand these interactions better.

For split exhaust cars, CO_2 coefficients were similar to those with right exhausts for diesel and gasoline fuel but much lower than both left and right exhausts for gasoline hybrid fuel. Split exhaust diesel and gasoline cars exhibited mean Type Approval CO_2 emission rates that were 30 – 34% and 10 – 13% higher, respectively, compared to left and right exhaust cars. This difference may partially explain the observed results. Another contributing factor is the uneven distribution of exhaust gases in split exhaust systems, a characteristic that varies across manufacturers and models and could not be further discerned in this work.[34] Additionally, some vehicle manufacturers install fake split exhaust outlets to enhance vehicle aesthetics, even when the true exhaust is hidden on the left or right.[35] Where such fake exhausts were obvious, these vehicles were classified as unknown during exhaust position assignment. However, it is important to note that a small number of vehicles may have been incorrectly classified as split.

Exhaust position also likely explains the differences observed between diesel buses and HGVs. Despite similar Type Approval CO_2 emission rates, the CO_2 concentration coefficient for buses was 2.4 times higher than for HGVs. Diesel buses typically have exhausts located low at the rear, often visible on the right-hand side in vehicle images, whereas diesel HGV exhausts are more varied in placement, often higher on the vehicle toward the front and not visible in any images. This placement results in greater dispersion of exhaust gases before reaching the PS instruments for HGVs compared to buses, reducing their CO_2 concentration coefficients. Other factors influencing dispersion, such as vehicle speed and aerodynamic properties, were similar between the two vehicle groups.

For diesel LGVs, the CO_2 coefficient is lower than that of diesel cars with left exhausts but higher than those with right exhausts. LGVs have a Type Approval CO_2 emission rate 38% higher than cars with either left or right exhausts. While exhaust locations for LGVs could not be assigned, the CO_2 coefficient results suggest that most LGVs likely had right exhausts, based on their relative values when compared to diesel cars. LGVs had a greater mean frontal area but lower mean speed than diesel cars; these factors likely influence roadside exhaust dispersion in opposing ways, though the available data limit detailed conclusions.

These findings highlight the significant impact of vehicle design characteristics on near-road CO_2 and TRAP concentrations. Of all cars (excluding EVs), 38% had right-positioned exhausts, associated with the lowest CO_2 coefficients and roadside TRAP concentrations. If the remaining cars repositioned their exhausts to the right, the average CO_2 coefficient for cars — and thus roadside TRAP concentration contributions in the UK — could decrease by 29%. Achieving a comparable reduction through improvements in catalyst after-treatment systems would be far more challenging.

While it is unlikely that existing vehicles would be retrofitted with repositioned exhausts due to cost and engineering constraints, exhaust placement could be considered in the design of future vehicles. Although most vehicle models are built on global platforms, regional adaptation — such as steering column layout, headlight beam patterns, and emissions control settings — are already common.[36] In this context, exhaust position represents a feasible design consideration that could be aligned with local driving practices to reduce near-road TRAP exposure. Given the expected continued production of fossil-fuelled (particularly hybrid) vehicles over the coming decades, there remains scope for manufacturers to reduce near-road TRAP concentrations through design choices.[37]

The effect is particularly important for diesel cars in the UK, where only

20% of vehicles had right exhausts. Repositioning the exhausts of the remaining cars could reduce their roadside TRAP contributions by 33%, which is especially important given the historically higher NO_x and particulate emissions from diesel cars. It is important to note that exhaust repositioning does not reduce overall TRAP emissions. However, the primary concern with these pollutants is their harmful impacts on human health, and minimising roadside exposure by any means remains a priority.

Passenger car exhaust position often reflects the production region's left or right-hand traffic practices, with vehicles designed to position exhausts on the offside (furthest from the kerb). Of the measured cars, 76% were manufactured in regions that drive on the right-hand side of the road, opposite to the UK, explaining why the minority of vehicles had exhausts positioned on the right — the optimal position to minimise near road TRAP in the UK. Exhaust position is therefore disproportionately important in the UK, where vehicles drive on the left-hand side, but the passenger car fleet predominantly comprises models produced for right-hand driving regions.

The plume regression approach used in this study is based on the average CO_2 profile observed when any vehicle passes the point sampling set-up, using data with at least a 20 s between vehicles to avoid plume interference. As noted in Section 3.3.2.1, using different plume profiles for different sites and vehicle types and vehicle designs could be useful in some circumstances. It is, therefore, important to consider the extent to which the analysis results depend on the shape of the plume used.

Figure 3.5 compares three plume profiles: the base plume derived from measurements in this work, a square plume profile that broadly covers the same time range and a wide plume profile that has a width of approximately twice the base plume. The wide plume misses much of the rise and fall seen in the base plume, suggesting that it may not effectively capture emission and concentration differences between vehicle groups. The main interest is

in understanding how much the results in this work depend on the chosen plume profile.

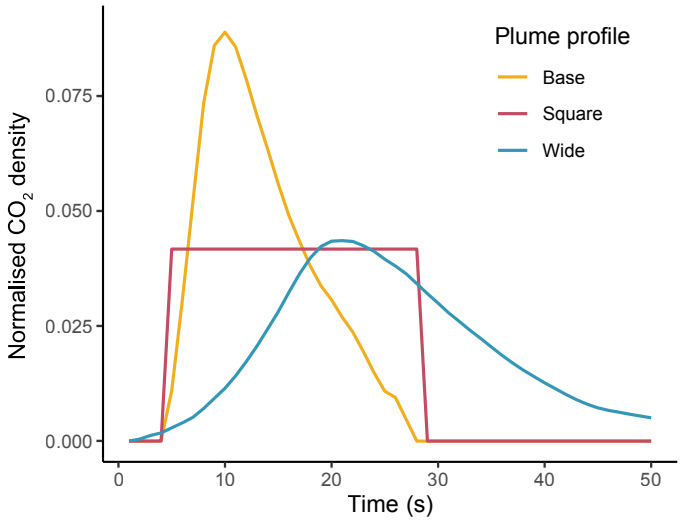

Figure 3.5: Three different plume profiles tested in the plume regression approach.

Figure 3.6 compares the CO_2 regression coefficients for different vehicle exhaust positions derived from the base, square, and wide plumes. Overall, the agreement between the three plume shapes is good, and the wide plume profile still yields reasonable results despite clear differences compared to the base plume - the wide plume maximum appears approximately 10 s after the base plume and continues well after the base plume reaches zero. The results suggest that the regression coefficients are not very sensitive to plume shape. One likely reason for this behaviour is that plumes for a particular type of vehicle are not correlated with other vehicle types. For example, a Euro 5 diesel car is not always followed by a Euro 6 gasoline car — the ordering is effectively random.

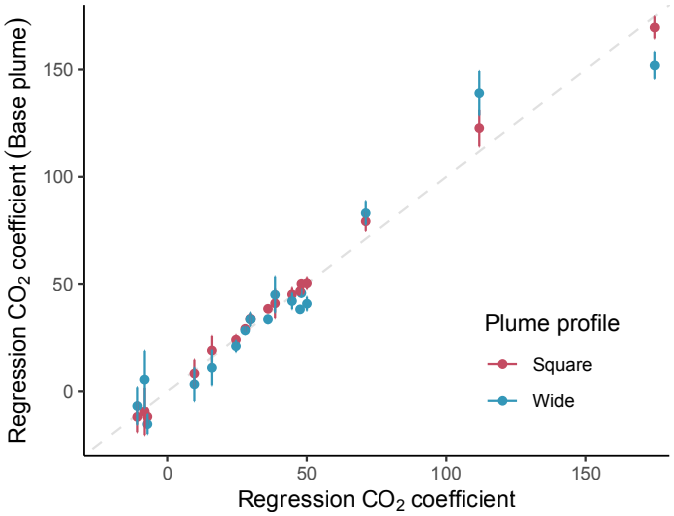

Figure 3.6: Scatter plot showing the relationship between calculated CO_2 coefficients comparing the base (measured) plume with a square plume profile and a wide plume profile.

To evaluate specifically how the results from plume regression varied with the differing geometries and characteristics of each measurement location in this study, additional analyses were conducted. First, the average plume profile for each site was calculated from isolated vehicle passes (n = 104, n = 173, and n = 29 for sites A, B, and C respectively), shown in Figure 3.7. Then, separate plume regressions were performed using data from each site individually, using the site's respective plume profile. Due to the further disaggregation required for this analysis, only passenger cars were included in the regression, as they provided sufficiently large sample sizes. Cars were grouped by fuel type and exhaust position; groups with sample sizes less than 25 were omitted, and incorporated into an 'other' category alongside other vehicle types for the regression. The results are shown in Figure 3.8.

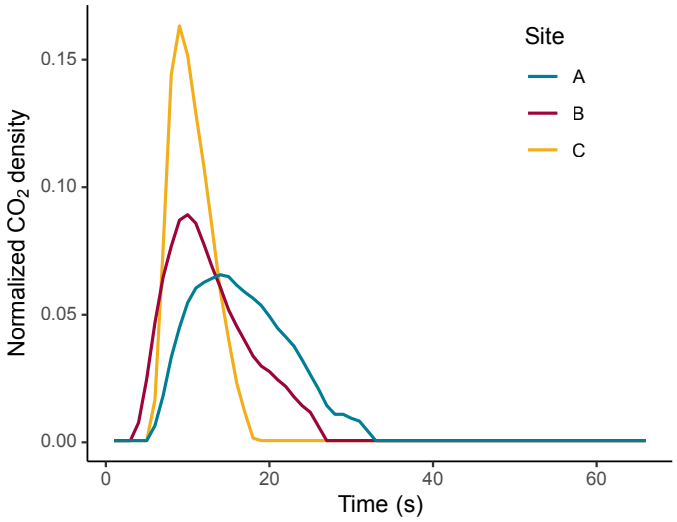

Figure 3.7: Plume profiles for each measurement site.

The plume profiles observed at sites A and B were similar in shape and duration. In contrast, the average plume profile at site C was approximately 10 seconds shorter, likely reflecting differences in site geometry and local characteristics. Despite these variations, individual plume regression analyses conducted separately for each site yielded results consistent with the main analysis. Across all fuel types for which a comparison could be made, vehicles with right-positioned exhausts consistently produced lower CO_2 concentration coefficients than those with left-positioned exhausts. The largest difference was observed for gasoline cars at site C (48%), while the smallest was seen for gasoline cars at site A (11%).

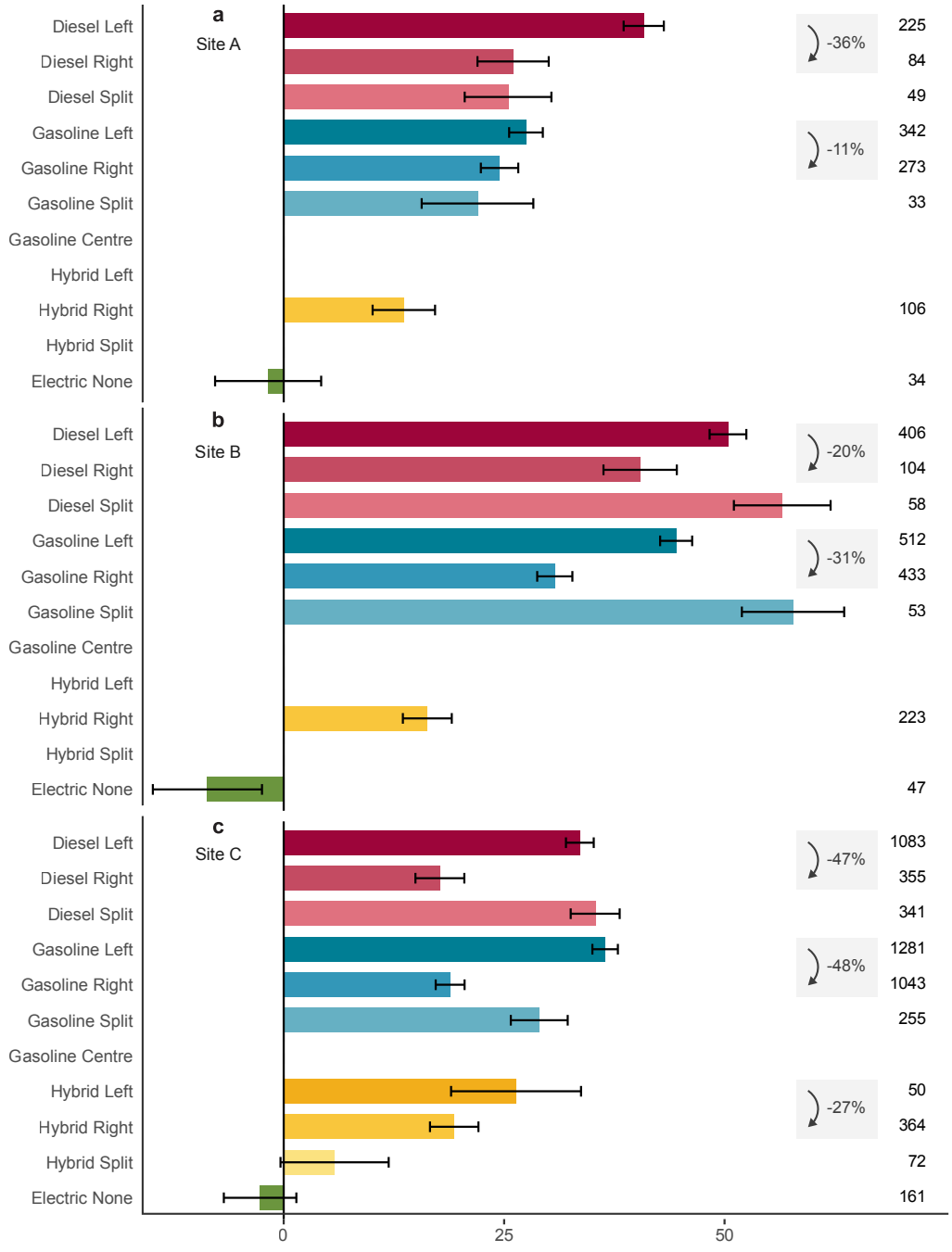

Figure 3.8: Passenger car CO_2 coefficients for fuel type, exhaust position, and measurement site (panels **a** – **c**) groups. Error bars represent 95% confidence intervals and number labels denote vehicle group sample sizes. Gray boxes display the reduction in CO_2 coefficient for right exhaust positions compared to left for each fuel type. The exhaust locations include those manually assigned and predicted.

Site B consistently produced CO_2 concentration coefficients for diesel and gasoline cars that were 22 – 162% higher than those observed at Sites A and C. This finding suggests that the physical characteristics of Site B, such as reduced dispersion or closer proximity to traffic, may have resulted in a greater fraction of vehicle exhaust reaching the measurement instrumentation.

Overall, these findings highlight that site-specific features can influence the magnitude of concentration coefficients derived from point sampling using the plume regression approach. However, the intra-site trends remain consistent with those observed in the aggregated analysis, and differences in site conditions do not change the conclusions of this study, but instead strengthen them further.

3.4.2 Exhaust Position Effect on NO_X

To more directly assess the impact of exhaust position on roadside TRAP concentrations, plume regression was performed for NO_x using the same vehicle groups analysed for CO_2. The NO_x concentration coefficient values for each group are presented in Figure 3.9 and Table 3.9. Unlike CO_2, NO_x emission rates vary significantly based on fuel type and after-treatment systems, adding complexity to vehicle group comparisons. For this reason, CO_2 was the primary focus of this analysis. However, the NO_x results provide valuable insight into near-road TRAP.

Diesel cars had NO_x concentration coefficients 5.2 and 6.5 times higher than those of gasoline cars for left and right exhaust positions, respectively, highlighting their significantly greater contribution to near-road NO_x concentrations, consistent with reported emission rates.[38, 39] For right exhaust cars, NO_x coefficients were 27.9%, 75.9%, and 34.0% lower than for left exhaust cars for diesel, gasoline, and gasoline hybrid vehicles, respectively, in agreement with the CO_2 findings (Section 3.4.1). The greater variability compared to CO_2 likely reflects the higher signal-to-noise ratio in the NO_x

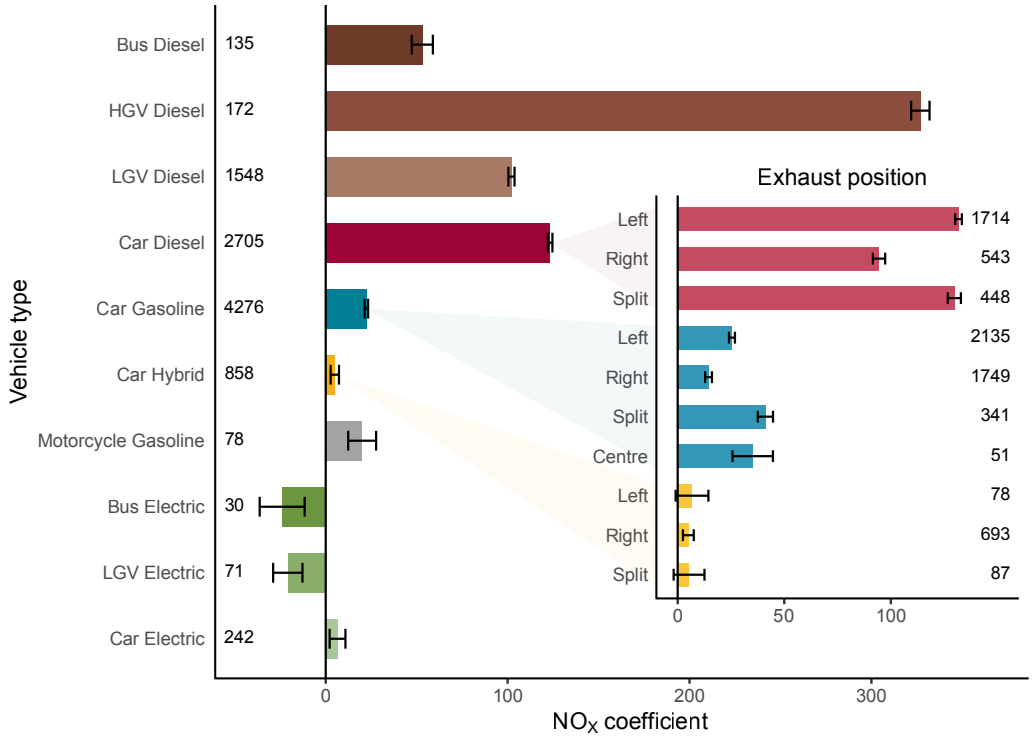

Figure 3.9: NO_x coefficients for vehicle type and fuel type groups. The inset plot further separates passenger cars by exhaust position. Error bars represent 95% confidence intervals, and number labels denote vehicle group sample sizes. The exhaust locations include those manually assigned and predicted.

increment data, especially for lower NO_x emitting gasoline and gasoline hybrid vehicles.

NO_x/CO_2 ratios (ppb ppm^{-1}) were calculated from the plume regression datasets to ensure differences in NO_x coefficients between left and right exhaust cars were due to exhaust position, rather than differences in NO_x emission rates due to variations in variables such as vehicle manufacturer, body type, or engine size. These ratios isolate NO_x emission rates by removing the influence of exhaust location and dispersion, assuming similar dispersion for CO_2 and NO_x.

Table 3.9: NO_x concentration coefficients for vehicle type, fuel type, and exhaust position groups.

Type	Fuel	Exhaust	NO_x	Standard error	n
Bus	Diesel	—	53.0	3.0	135
HGV	Diesel	—	326.7	2.6	172
LGV	Diesel	—	102.1	0.9	1548
Car	Diesel	Split	129.8	1.6	447
Car	Diesel	Left	131.7	0.8	1714
Car	Diesel	Right	94.4	1.5	543
Car	Gasoline	Centre	35.2	4.8	51
Car	Gasoline	Left	25.5	0.7	2135
Car	Gasoline	Split	41.1	1.8	341
Car	Gasoline	Right	14.5	0.8	1749
Car	Hybrid	Left	6.7	3.9	78
Car	Hybrid	Right	5.0	1.3	693
Car	Hybrid	Split	5.3	3.7	87
Motorcycle	Gasoline	—	21.3	3.9	78
Bus	Electric	—	-23.8	6.3	30
LGV	Electric	—	-20.4	4.1	71
Car	Electric	None	6.8	2.2	242

Vehicle emission remote sensing is another roadside measurement technique that uses cross-road spectroscopy to capture emissions from the entire vehicle plume (Sections 1.4.3 and 2.3.1). Emission ratios obtained from PS have previously been shown to agree well with those from remote sensing. [13] A representative sample of remote sensing measurements collected in 2022 was selected to match the PS data in terms of sample size, fuel type distribution, and Euro class distribution. The random forest machine learning algorithm (trained and used on the PS data) was applied to this remote

sensing sample to assign exhaust positions to vehicle measurements. The NO_x/CO_2 ratios from the remote sensing sample were then aggregated by fuel type and exhaust position, as shown in Table 3.10.

Table 3.10: NO_x/CO_2 ratios for cars grouped by fuel type and exhaust location, derived from point sampling and a representative sample of remote sensing data. Hybrid refers to gasoline hybrid vehicles. The uncertainty values represent 95% confidence intervals.

		NO_x/CO_2 (ppb ppm^{-1})	
Fuel Type	**Exhaust Position**	**Point Sampling**	**Remote Sensing**
Diesel	Left	2.74 ± 0.07	2.85 ± 0.17
Diesel	Right	3.18 ± 0.25	3.41 ± 0.35
Gasoline	Left	0.54 ± 0.03	0.46 ± 0.09
Gasoline	Right	0.52 ± 0.06	0.39 ± 0.08
Hybrid	Left	0.17 ± 0.20	0.59 ± 0.34
Hybrid	Right	0.20 ± 0.11	0.32 ± 0.08

The NO_x/CO_2 ratios derived from PS and the remote sensing sample align with values reported in the literature.[38] Strong agreement (all values within 95% confidence intervals) between the two data sets, summarised in Table 3.10, supports plume regression as a highly robust technique for assessing roadside vehicle emissions. Additionally, the similar NO_x/CO_2 ratio values for left and right exhaust vehicles indicate that the observed differences in NO_x coefficients are primarily due to exhaust position. Repositioning the exhausts of all cars to the right-hand side would reduce the average NO_x coefficient and, therefore, the average contribution of cars towards roadside NO_x increment concentrations in the UK by 26.1%, directly demonstrating the impact of vehicle design choices on near-road TRAP concentrations.

For NO_2, similar patterns to those observed for total NO_x were found across vehicle types and exhaust locations. The trends in NO_2 concentration coefficients mirrored those of NO_x, but were approximately five times smaller in magnitude. In the case of NO_2 concentrations there are two principal contributions to kerbside concentrations: the directly emitted (primary) NO_2 from vehicles and the contribution from NO reacting with ozone (O_3) to produce secondary NO_2 (Section 1.2.3). At other sites and for other conditions e.g. warm, sunny weather where secondary NO_2 formation could be enhanced, there could be differences in the behaviour of NO_2 and total NO_x, which would warrant further investigation.

3.4.3 Electric Vehicles

Plume regression produced *negative* CO_2 concentration coefficients for EVs (Figure 3.3), indicating that the passing of these vehicles is associated with a *decrease* in near-road CO_2 and TRAP concentrations. This finding was reinforced by a negative average plume profile for isolated EV measurements, shown in Figure 3.10. A likely explanation of this observation is that EVs disperse the plumes of nearby fossil-fuelled vehicles through vehicle-induced turbulence, which is influenced by the EV's aerodynamic properties (frontal area and drag coefficient), speed, and existing traffic TRAP concentrations due to fossil-fuelled vehicles.

Aerodynamic properties primarily depend on frontal area, which directly influences vehicle-induced turbulence (Equation 3.1). Larger, less aerodynamic EVs should, therefore, produce more turbulence and dispersion. Thus, electric buses are expected to have the most negative CO_2 coefficients, followed by electric LGVs and electric cars, given their relative sizes. However, CO_2 coefficients for EVs are also strongly influenced by vehicle speed (which has a cubic relationship with induced turbulence) and existing exhaust gas concentrations, both of which are dependent on traffic flow and measurement

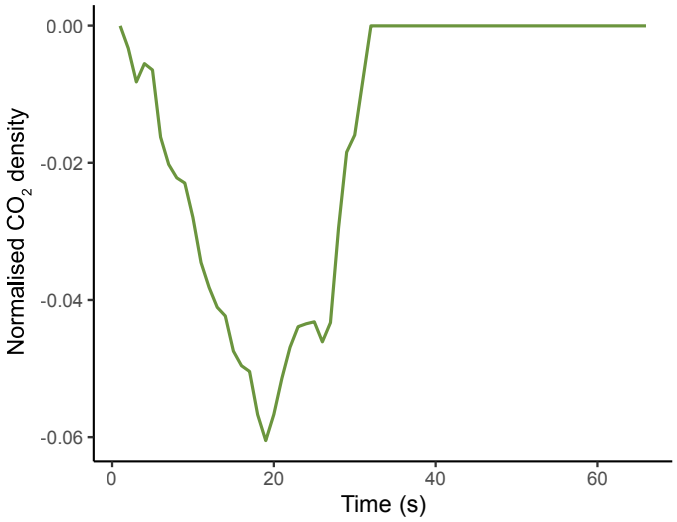

Figure 3.10: Plume profile for electric vehicles (n = 20).

location.

PS measurements were made at three sites: low-traffic sites A and B, with average vehicle gaps of 15.5 s and speeds of 34.5 $\mathrm{km\,h^{-1}}$, and high-traffic site C, with a 7.0 s gap and 44.2 $\mathrm{km\,h^{-1}}$ average speed. All electric buses, 80% of electric LGVs, and 34% of electric cars were measured at low-traffic locations, with the remainder sampled at the high-traffic site. Detailed driving conditions for each site are presented in Table 3.2. The low CO_2 coefficient for electric buses is likely due to their slower speeds and lower CO_2 concentrations at low-traffic sites A and B, with an average speed of 32.3 $\mathrm{km\,h^{-1}}$ and an average vehicle gap of 18.2 s. Although more electric LGVs were measured at low-traffic locations compared to electric cars, their more negative CO_2 coefficient suggests that the differences in frontal area and the resulting impact on turbulence dominate the results.

To further investigate EV impacts on near-road TRAP concentrations, the electric car group was divided by measurement location into low-traffic (sites A and B) and high-traffic (site C) categories, and plume regression was rerun for CO_2. The updated CO_2 coefficients for EVs are presented in Figure 3.11, while the coefficients for non-EVs remained unchanged. The CO_2 coefficients,

average speeds, frontal areas, and drag coefficients of the EV subgroups used in the revised plume regression are summarised in Table 3.11.

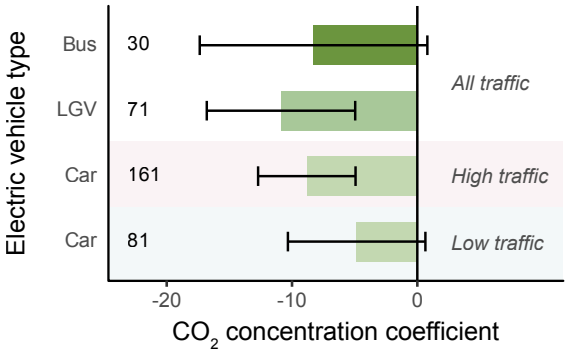

Figure 3.11: CO_2 concentration coefficients for EVs. Electric cars are disaggregated into those measured at the high- and low-traffic sites. The error bars represent 95% confidence intervals, and the text labels denote traffic conditions.

Table 3.11: CO_2 concentration coefficient, mean speed, mean frontal area, and mean drag coefficient for electric vehicles at the high and low traffic locations. No vehicle size data were available for buses in the technical information, and no drag coefficients were assigned.

Type	**Location**	**CO_2**	**Speed ($km\,h^{-1}$)**	**Gap (s)**	**Area (m^2)**	**C_d**	**n**
Car	High traffic	-8.8	45.6	7.3	2.9	0.32	161
Car	Low traffic	-4.8	35.3	18.2	2.8	0.32	81
LGV	All	-10.9	35.6	13.2	4.7	0.34	71
Bus	All	-8.3	32.3	18.2	–	–	30

The CO_2 concentration coefficient for electric cars at the high-traffic site was 83% more negative than at low-traffic sites, despite comparable frontal areas and drag coefficients. This difference is attributed to a 29% greater mean speed at the high-traffic site, which would act to enhance the dilution of exhaust plumes from other nearby vehicles. Indeed, the higher speed alone

may account for the observed CO_2 coefficient decrease, as vehicle-induced turbulence is proportional to the cube of speed ($1.29^3 = 2.15$, 115% increase in turbulence from speed). However, it is likely that existing concentrations of CO_2 at the high-traffic site were also greater, given the driving conditions and smaller average vehicle gap. The large 95% confidence intervals, due to relatively small sample sizes, highlight the need for further research to isolate these variables.

It is also important to consider differences in site characteristics that may influence the calculated CO_2 concentration coefficients, such as variations in geometry and local topography at each measurement location. These factors are explored in more detail in the individual site analyses presented in Section 3.4.1. At Site B (low-traffic), the CO_2 concentration coefficient for electric cars was four times more negative than at Sites A (low-traffic) and C (high-traffic). Consequently, the CO_2 concentration coefficient for cars at low-traffic sites in Figure 3.11 is likely more negative than would be expected under more uniform measurement conditions. This suggests that the true difference between high- and low-traffic sites may be greater than reported.

3.4.4 Aerodynamic Properties

To further investigate the role of vehicle-induced turbulence, we have considered the relationship between the CO_2 coefficient and P_d. For cars and LGVs, plume regression was run on four P_d quantile groups (Section 3.3.2.3). Cars were separated into fossil-fuelled and electric groups, and the resulting CO_2 concentration coefficients are shown in panels **a** and **b** of Figure 3.12. Exact coefficient values and additional information are provided in Table 3.12.

For fossil-fuelled cars, the relationship between vehicle-induced turbulence (P_d quantile) and measured CO_2 concentrations is complex. As P_d increases, both dispersion and CO_2 emission rates rise due to the impact of

P_d on engine load, which influences fuel consumption and emissions. Panel **a** of Figure 3.12 shows the CO_2 concentration coefficients for fossil-fuelled cars, reflecting the combined effect of the emission rate and near-road dispersion. Exhaust position distributions were similar across all four quantiles.

Panel **c** isolates the emission rate component of this relationship, presenting mean instantaneous modelled CO_2 emission rates for each P_d quantile (Section 3.3.2.4). With increasing P_d quantile (Low to High), the increasing drag force means that the vehicle's engine load is higher; thus, fuel consumption and CO_2 emission rate also increase.

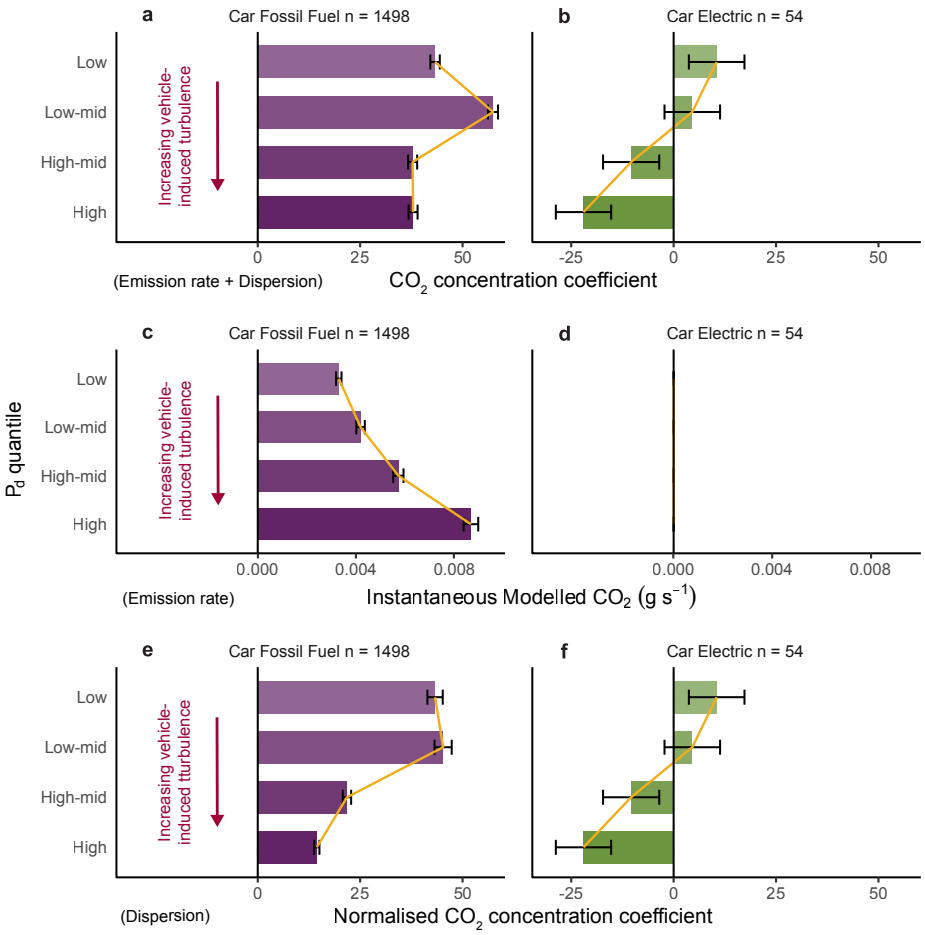

Figure 3.12: CO_2 concentration coefficient (**a** and **b**), instantaneous modelled CO_2 (**c** and **d**), and CO_2 concentration coefficient normalised by instantaneous modelled CO_2 (**e** and **f**) for fossil-fuelled and electric passenger cars, grouped by P_d quantile. The error bars represent 95% confidence intervals, and the yellow lines show the trends across quantiles.

To isolate the effect of vehicle-induced turbulence, the CO_2 concentration coefficients in panel **a** were normalised by the emission rates in panel **b**, using the Low P_d quantile emission rate as the baseline (1.0). While the normalised CO_2 concentration coefficients, shown in panel **e**, do not show a perfect decrease with increasing P_d, normalisation does shift the results towards expectation, eliminating the initial increase from Low to Low-mid P_d (likely due to rising CO_2 emissions) and revealing a clear downward

Table 3.12: CO_2 concentration coefficient, mean power of drag P_d, mean vehicle speed V, mean frontal area A, and mean drag coefficient C_d for each vehicle group in the plume regression run to investigate the influence of vehicle-generated turbulence.

Type	**Fuel**	**Quantile**	**CO_2**	**P_d (W)**	**V ($km\,h^{-1}$)**	**A (m^2)**	**C_d**	**n**
Car	Fossil fuel	Low	43.3	324.3	30.1	2.74	0.32	1498
Car	Fossil fuel	Low-mid	57.4	648.6	38.1	2.78	0.32	1498
Car	Fossil fuel	High-mid	37.8	1100.2	45.5	2.80	0.32	1498
Car	Fossil fuel	High	37.9	1897.9	52.9	2.94	0.33	1498
Car	Electric	Low	10.5	366.0	30.7	2.85	0.32	54
Car	Electric	Low-mid	4.6	744.2	39.8	2.89	0.31	54
Car	Electric	High-mid	-10.4	1122.2	45.3	2.92	0.32	54
Car	Electric	High	-22.0	1989.1	54.0	2.93	0.32	54
LGV	Diesel	Low	34.1	380.7	27.2	4.07	0.34	288
LGV	Diesel	Low-mid	76.0	714.5	33.3	4.42	0.34	288
LGV	Diesel	High-mid	28.5	1214.3	40.2	4.26	0.34	288
LGV	Diesel	High	20.8	2536.7	50.1	4.49	0.34	288

trend from Low-mid to High P_d. Similar findings for LGVs are presented in Figure 3.13.

Because electric cars do not emit CO_2, they serve as an ideal baseline for evaluating the effects of vehicle-induced turbulence on near-road TRAP concentrations. From P_d quantile Low to High, the electric car CO_2 coefficient becomes increasingly negative, highlighting the role of EV-induced turbulence in dispersing CO_2 and reinforcing the findings in the previous section. Over this range, mean vehicle speed increased by 75%, while frontal area increased by 2.8%. Because speed and frontal area are the primary drivers of turbulence, the stronger correlation with speed suggests that it is

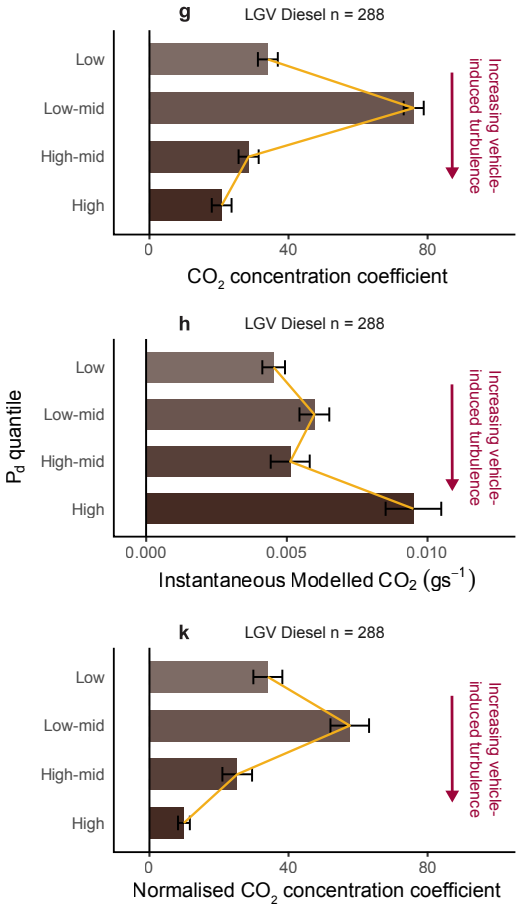

Figure 3.13: CO_2 concentration coefficient (**g**), instantaneous modelled CO_2 (**h**), and CO_2 concentration coefficient normalised by instantaneous modelled CO_2 (**k**) for diesel LGVs, grouped by P_d quantile. The error bars represent 95% confidence intervals, and the yellow lines show the trends across quantiles.

the dominant factor behind the increasingly negative CO_2 coefficients.

Positive CO_2 coefficients for electric cars in the lower P_d quantiles can be attributed to two factors. First, low turbulence in these quantiles may not effectively disperse CO_2 from other traffic, leading the plume regression to attribute residual CO_2 to electric cars. Second, low P_d electric cars represent the smallest CO_2 concentration increments, so minor deviations from local background concentrations have a larger impact on coefficient variability.

Emission rates were not calculated for electric cars, so no normalisation

was applied, making panels **f** and **a** identical. If the modelled CO_2 emission rates for fossil-fuelled cars perfectly captured the true emissions during vehicle measurements, the normalised CO_2 coefficients in panel **e** would isolate the dispersion effects on roadside CO_2 concentrations and closely match the trend observed for electric cars in panel **f**. However, modelling inaccuracies and variability in the PS data introduce discrepancies, and additional research is required to draw further conclusions.

These findings demonstrate that vehicle-induced turbulence directly affects roadside CO_2 and TRAP concentrations, with the impact increasing with P_d. While aerodynamic properties such as frontal area and drag coefficient contribute, vehicle speed plays a more significant role due to its greater variation and cubed relationship with P_d. For fossil-fuelled vehicles, turbulence and dispersion effects on roadside CO_2 and TRAP concentrations are closely linked to emission rates, which also rise with increasing P_d.

3.5 Conclusions

Fast-response point sampling coupled with individual vehicle information is an effective method of understanding the processes that influence roadside concentrations of TRAP. The findings of this study provide transferable insights that have the potential to improve the quantification of TRAP at thousands of near-road ambient air quality sites worldwide.

Furthermore, the global implications of the findings are directly significant. In all regions, the international vehicle market ensures that a portion of the fleet will have exhausts positioned closest to the kerb, regardless of left or right-hand driving practices. This results in higher-than-necessary roadside concentrations of TRAP. Future research should prioritise quantifying how the effects of exhaust position diminish with increasing lateral and vertical distance from the road. One approach to achieve this is through controlled release experiments, where a tracer gas is emitted from various points on a vehicle to simulate different exhaust positions.

With respect to the influence of vehicle-induced turbulence on near-road TRAP concentrations, this work demonstrates the existence of such an effect and highlights key influencing variables. Future studies should explore the interaction between vehicle-induced turbulence and TRAP concentrations using sonic anemometers to measure TKE directly.

An unexpected finding of this study was the ability of EVs to reduce near-road CO_2 and TRAP concentrations from fossil-fuelled vehicles. This reduction is primarily influenced by existing emissions from fossil-fuelled vehicles and EV-induced turbulence, which are determined by their design and speed. As a result, this effect is likely greatest in areas with high existing TRAP concentrations and for faster, larger EVs. Further research using sonic anemometers to measure TKE directly will be important in advancing our understanding of these interactions.

3.6 References

[1] Anenberg, S., Miller, J., Henze, D., and Minjares, R. A global snapshot of the air pollution-related health impacts of transportation sector emissions in 2010 and 2015. *International Council on Clean Transportation: Washington, DC, USA* (2019), pp. 1–48 (cit. on p. 146).

[2] Institute, H. E. *Traffic-Related Air Pollution: a Critical Review of the Literature on Emissions, Exposure, and Health Effects. Health Effects Institute. Panel on the Health Effects of Traffic-Related Air Pollution*. https://www.healtheffects.org/system/files/SR17TrafficReview.pdf. Date accessed: 2024-12-19. 2010 (cit. on p. 146).

[3] Bell, J., Honour, S. L., and Power, S. A. Effects of vehicle exhaust emissions on urban wild plant species. *Environmental Pollution* 159.8-9 (2011), pp. 1984–1990. DOI: 10.1016/j.envpol.2011.03.006 (cit. on p. 146).

[4] Xie, P., Zhang, C., Wei, Y., Zhu, R., Chu, Y., Chen, C., Wu, Z., and Hu, J. Status of near-road air quality monitoring stations and data application. *Atmospheric Environment: X* 23 (2024), p. 100292. DOI: 10.1016/j.aeaoa.2024.100292 (cit. on p. 146).

[5] Apte, J. S., Messier, K. P., Gani, S., Brauer, M., Kirchstetter, T. W., Lunden, M. M., Marshall, J. D., Portier, C. J., Vermeulen, R. C. H., and Hamburg, S. P. High-Resolution Air Pollution Mapping with Google Street View Cars: Exploiting Big Data. *Environ. Sci. Technol.* 51.12 (2017), pp. 6999–7008. DOI: 10.1021/acs.est.7b00891 (cit. on p. 146).

[6] Wilde, S. E., Padilla, L. E., Farren, N. J., Alvarez, R. A., Wilson, S., Lee, J. D., Wagner, R. L., Slater, G., Peters, D., and Carslaw, D. C. Mobile monitoring reveals congestion penalty for vehicle emissions in London. *Atmospheric Environment: X* 21 (2024), p. 100241. DOI: 10.1016/j.aeaoa.2024.100241 (cit. on pp. 146, 152).

[7] Wilson, S., Farren, N. J., Wilde, S. E., Wagner, R. L., Lee, J. D., Padilla, L. E., Slater, G., Peters, D., and Carslaw, D. C. Mobile monitoring reveals the importance of non-vehicular particulate matter sources in London. *Environmental Science: Processes & Impacts* 26.12 (2024), pp. 2145–2157. DOI: 10.1039/D4EM00552J (cit. on pp. 146, 152).

[8] Brimblecombe, P., Chu, M., Liu, C.-H., Fu, Y., Wei, P., and Ning, Z. Roadside NO_2/NO_X and primary NO_2 from individual vehicles. *Atmospheric Environment* 295 (2023), p. 119562. DOI: doi.org/10.1016/j.atmosenv.2022.119562 (cit. on p. 146).

[9] Chu, M., Brimblecombe, P., Gali, N. K., Ghadikolaei, M. A., Wei, P., Li, X., Yang, S., Wei, Y., and Ning, Z. Roadside measurement of N_2O and CH_4 emissions from vehicles in Hong Kong. *Science of The Total Environment* 956 (2024), p. 177241. DOI: 10.1016/j.scitotenv.2024.177241 (cit. on p. 146).

[10] Preble, C. V., Dallmann, T. R., Kreisberg, N. M., Hering, S. V., Harley, R. A., and Kirchstetter, T. W. Effects of Particle Filters and Selective Catalytic Reduction on Heavy-Duty Diesel Drayage Truck Emissions at the Port of Oakland. *Environmental Science & Technology* 49 (14 2015). DOI: 10.1021/acs.est.5b01117 (cit. on p. 146).

[11] Khreis, H., Warsow, K. M., Verlinghieri, E., Guzman, A., Pellecuer, L., Ferreira, A., Jones, I., Heinen, E., Rojas-Rueda, D., Mueller, N., et al. The health impacts of traffic-related exposures in urban areas: Understanding real effects, underlying driving forces and co-producing future directions. *Journal of Transport & Health* 3.3 (2016), pp. 249–267. DOI: 10.1016/j.jth.2016.07.002 (cit. on p. 146).

[12] Knoll, M., Penz, M., Juchem, H., Schmidt, C., Pöhler, D., and Bergmann, A. Large-scale automated emission measurement of individual vehicles with point sampling. *Atmospheric Measurement Techniques* 17.8 (2024), pp. 2481–2505. DOI: 10.5194/amt-17-2481-2024 (cit. on p. 146).

[13] Farren, N. J., Wilson, S., Bernard, Y., Shaw, M. D., Lee, K., Crowe, M., and Carslaw, D. C. An Ambient Measurement Technique for Vehicle Emission Quantification and Concentration Source Apportionment. *Environmental Science & Technology* 58.45 (2024), pp. 20091–20100. DOI: 10.1021/acs.est.4c07907 (cit. on pp. 147, 152, 153, 176).

[14] Plogmann, J., Stauffer, C., Dimopoulos Eggenschwiler, P., and Jenny, P. URANS Simulations of Vehicle Exhaust Plumes with Insight on Remote Emission Sensing. *Atmosphere* 14.3 (2023), p. 558. DOI: 10.3390/atmos14030558 (cit. on pp. 147, 154, 164, 167).

[15] Xiang, S., Zhang, S., Brimblecombe, P., Yu, Y. T., Noll, K. E., Liu, H., Wu, Y., and Hao, K. An Integrated Field Study of Turbulence and Dispersion Variations in Road Microenvironments. *Environmental Science & Technology* (2024). DOI: 10.1021/acs.est.4c04217 (cit. on pp. 147, 158).

[16] Airyx. *ICAD In Situ NO_X Monitor*. https://airyx.de/item/icad/. Accessed: 2024-10-17. 2023 (cit. on p. 149).

[17] Horbanski, M., Pöhler, D., Lampel, J., and Platt, U. The ICAD (iterative cavity-enhanced DOAS) method. *Atmospheric Measurement Techniques* 12.6 (2019), pp. 3365–3381. DOI: 10.5194/amt-12-3365-2019 (cit. on p. 149).

[18] Juchem, H. P. S. Straßenrand-Messungen der NO_X-Emissionen von Fahrzeugen mit einem ICAD-Messgerät. B.S. thesis. University of Heidelberg, 2021 (cit. on p. 149).

[19] Rekor OpenALPR. *Rekor CarCheck Vehicle Recognition API*. https://www.openalpr.com/software/carcheck. Accessed: 2023-12-10. 2023 (cit. on p. 150).

[20] Padilla, L. E., Ma, G. Q., Peters, D., Dupuy-Todd, M., Forsyth, E., Stidworthy, A., Mills, J., Bell, S., Hayward, I., Coppin, G., Moore, K., Fonseca, E., Popoola, O. A., Douglas, F., Slater, G., Tuxen-Bettman, K., Carruthers, D., Martin, N. A., Jones, R. L., and Alvarez, R. A. New methods to derive street-scale spatial patterns of air pollution from mobile monitoring. *Atmospheric En-*

vironment 270 (2022), p. 118851. DOI: 10.1016/j.atmosenv.2021.118851 (cit. on p. 152).

[21] Venables, W. N. and Ripley, B. D. *Modern Applied Statistics with S*. Fourth. ISBN 0-387-95457-0. New York: Springer, 2002. URL: https://www.stats.ox.ac.uk/pub/MASS4/ (cit. on p. 153).

[22] Breiman, L. and Cutler, A. *randomForest: Breiman and Cutlers Random Forests for Classification and Regression*. https://CRAN.R-project.org/package=randomForest. Accessed: 2024-06-20. 2024 (cit. on p. 154).

[23] Kuhn, M. *caret: Classification and Regression Training*. https://CRAN.R-project.org/package=caret. Accessed: 2024-06-20. 2023 (cit. on p. 154).

[24] Kühlwein, J. Driving resistances of light-duty vehicles in Europe: present situation, trends, and scenarios for 2025. *International Council on Clean Transportation* 49.30 (2016). URL: https://theicct.org/publication/driving-resistances-of-light-duty-vehicles-in-europe-present-situation-trends-and-scenarios-for-2025/ (cit. on p. 157).

[25] Schuetz, T. C. *Aerodynamics of road vehicles*. Sae International, 2015 (cit. on pp. 157, 158).

[26] Vachon, G., Louka, P., Rosant, J., Mestayer, P., and Sini, J. Measurements of traffic-induced turbulence within a street canyon during the Nantes' 99 experiment. *Water, Air and Soil Pollution: Focus* 2 (2002), pp. 127–140. DOI: 10.1023/A:1021323031600 (cit. on p. 158).

[27] Thaker, P. and Gokhale, S. The impact of traffic-flow patterns on air quality in urban street canyons. *Environmental pollution* 208 (2016), pp. 161–169. DOI: 10.1016/j.envpol.2015.09.004 (cit. on p. 158).

[28] Hausberger, S. *Simulation of Real World Vehicle Exhaust Emission*. Vol. 82. Austria: Technische Universität Graz, 2003 (cit. on p. 159).

[29] Davison, J., Bernard, Y., Borken-Kleefeld, J., Farren, N. J., Hausberger, S., Sjödin, Å., Tate, J. E., Vaughan, A. R., and Carslaw, D. C. Distance-based emission factors from vehicle emission remote sensing measurements. *Science of the Total Environment* 739 (2020), p. 139688. DOI: 10.1016/j.scitotenv.2020.139688 (cit. on p. 159).

[30] Bernard, Y., Tietge, U., German, J., and Muncrief, R. *Determination of real world emissions from passenger vehicles using remote sensing data*. https://theicct.org/wp-content/uploads/2021/06/TRUE_Remote_sensing_data_20180606.pdf. 2018 (cit. on p. 159).

[31] Mock, P., German, J., Bandivadekar, A., and Riemersma, I. Discrepancies between type-approval and "real-world" fuel-consumption and CO_2. *The International Council on Clean Transportation* 13 (2012). URL: https://theicct.org/wp-content/uploads/2021/06/ICCT_EU_fuelconsumption2_workingpaper_2012.pdf (cit. on p. 163).

[32] Fontaras, G., Zacharof, N.-G., and Ciuffo, B. Fuel consumption and CO_2 emissions from passenger cars in Europe–Laboratory versus real-world emissions. *Progress in energy and combustion Science* 60 (2017), pp. 97–131. DOI: 10.1016/j.pecs.2016.12.004 (cit. on p. 163).

[33] Dornoff, J. and Rodríguez, F. Gasoline Versus Diesel: Comparing CO_2 Emission Levels of a Modern Medium Size Car Model under Laboratory and On-road Testing Conditions. *Internation Council on Clean Transportation* (2019). URL: https://theicct.org/wp-content/uploads/2021/06/Gas_v_Diesel_CO2_emissions_FV_20190503_1.pdf (cit. on p. 164).

[34] United Kingdom Government. *MOT inspection manual: cars and passenger vehicles, 8.2 Exhaust emissions*. https://www.gov.uk/guidance/mot-inspection-manual-for-private-passenger-and-light-commercial-vehicles/8-nuisance. 2024 (cit. on p. 167).

[35] Exhaust molded trim, part no. 80A807834ET94. *Audi Genuine Parts and Accessories*. https://parts.audiusa.com/p/Audi__/Trim-molding

/ 131887603 / 80A807834ET94 . html. Accessed: 2025-01-28. 2024 (cit. on p. 167).

[36] Ravi, S. S., Osipov, S., and Turner, J. W. Impact of modern vehicular technologies and emission regulations on improving global air quality. *Atmosphere* 14.7 (2023), p. 1164. DOI: 10.3390/atmos14071164 (cit. on p. 168).

[37] Conway, G., Joshi, A., Leach, F., García, A., and Senecal, P. K. A review of current and future powertrain technologies and trends in 2020. *Transportation Engineering* 5 (2021), p. 100080. DOI: 10.1016/j.treng.2021.100080 (cit. on p. 168).

[38] Carslaw, D. C., Beevers, S. D., Tate, J. E., Westmoreland, E. J., and Williams, M. L. Recent evidence concerning higher NO_X emissions from passenger cars and light duty vehicles. *Atmospheric Environment* 45.39 (2011), pp. 7053–7063. DOI: 10.1016/j.atmosenv.2011.09.063 (cit. on pp. 174, 177).

[39] Wilson, S., Farren, N. J., Rose, R. A., Wilde, S. E., Davison, J., Wareham, J. V., Lee, J. D., and Carslaw, D. C. The impact on passenger car emissions associated with the promotion and demise of diesel fuel. *Environment International* 182 (2023), p. 108330. DOI: 10.1016/j.envint.2023.108330 (cit. on p. 174).

Chapter 4

Importance of Non-Vehicular Emissions in Urban Areas

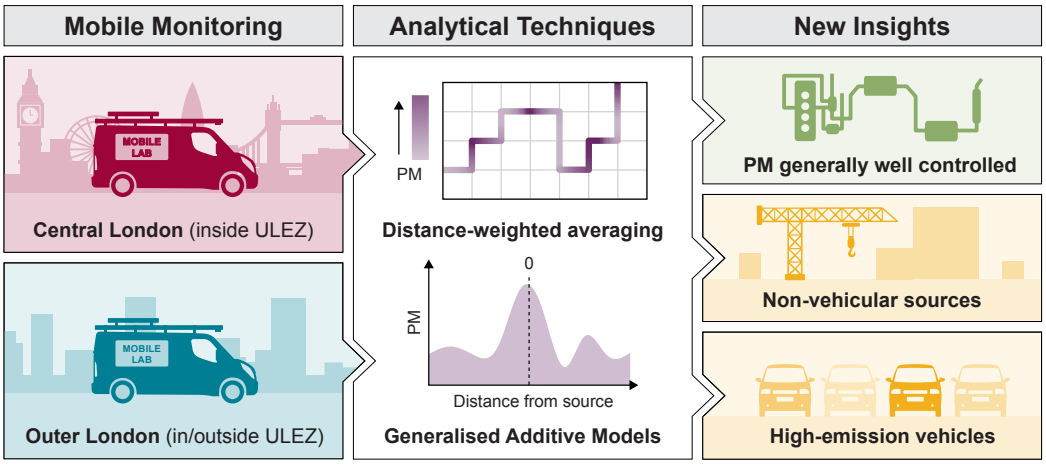

Wilson. S., Farren N. J., Wilde S. E., Wagner R. L., Lee J. D., Padilla L. E., Slater G., Peters D, and Carslaw D. C. **Mobile monitoring reveals the importance of non-vehicular particulate matter sources in London**. *Environmental Science: Processes and Impacts* 26. (2024). p. 2145. DOI: 10.1039/d4em00552j

4.1 Abstract

This study uses mobile monitoring to gain a better understanding of particulate matter (PM) sources in two areas of Central and Outer London, UK. We find that, unlike emissions of nitrogen oxides (NO_x = NO + NO_2), which are elevated in Central London due to the high number of diesel vehicles and congestion, fine particulate matter ($PM_{2.5}$) emissions are well-controlled. This finding provides evidence for the effectiveness of vehicle particulate filters, supporting the view that their widespread adoption has mitigated $PM_{2.5}$ emissions, even in the highly dieselised area of Central London. However, mobile monitoring also reveals infrequent elevated $PM_{2.5}$ concentrations caused by malfunctioning vehicles. These events were confirmed through simultaneous measurements of $PM_{2.5}$ and sulfur dioxide (SO_2), the latter being a strong tracer of engine lubricant combustion. A single event from a gasoline car, representing just 0.15% of the driving distance in Outer London, was responsible for 7% of the $\Delta PM_{2.5}$ concentration above background levels, highlighting the ongoing importance of addressing high-emission vehicles. In a novel application of mobile monitoring, we demonstrate the ability to identify and quantify non-vehicular sources of PM. Among the sources unambiguously identified are construction activities, which result in elevated concentrations of coarse particulate matter ($PM_{coarse} = PM_{10} - PM_{2.5}$). The mobile measurements clearly highlight the spatial extent of the influence of such sources, which would otherwise be difficult to determine. Furthermore, these sources are shown to be weather-dependent, with PM_{coarse} concentrations reduced by 62% during wet conditions compared to dry ones.

4.2 Introduction

4.2.1 Background and Context

Considerable progress has been made in reducing particulate matter (PM) emissions in the UK and many other parts of the world over the past three decades.[1] However, exposure to fine PM is the leading environmental risk factor for the global burden of disease, with emissions continuing to rise in certain regions (Section 1.1.2).[2] The reduction of PM in the atmosphere remains a major challenge, and further efforts are necessary to reduce emissions and protect human health. From 1990 to 2021, UK emissions of fine particulate matter ($PM_{2.5}$) declined by 66%, and emissions of the larger size fraction of particulate matter (PM_{10}) decreased by 63% over the same period.[3, 4] Despite this progress, the health evidence related to PM has strengthened over this period, and in September 2021, the World Health Organization (WHO) published updated Air Quality Guidelines (Section 1.1.3). The revised guideline for annual average concentrations of $PM_{2.5}$ was reduced from 10 $\mu g\ m^{-3}$ to 5 $\mu g\ m^{-3}$, while the corresponding value for PM_{10} was reduced from 20 $\mu g\ m^{-3}$ to 15 $\mu g\ m^{-3}$.[5] These new WHO guidelines for long-term exposure to pollutants reflect the lowest levels at which the guideline developers could be confident of an adverse health effect.

Meeting the WHO PM guidelines is very challenging for most countries, especially in urban areas where there is a diverse range of PM sources and high complexity associated with identifying those of the greatest importance. In 2023, the UK annual mean concentrations of $PM_{2.5}$ and PM_{10} were 7.7 $\mu g\ m^{-3}$ and 15.2 $\mu g\ m^{-3}$, respectively.[6] Furthermore, 79% of the UK exceeded the WHO $PM_{2.5}$ guidelines, and it is estimated that in the UK, over 48,000 premature deaths are attributable to $PM_{2.5}$ exposure annually.[7] The continued effort to reduce PM concentrations requires a comprehensive quantitative understanding of the contributions of different sources.

The enduring concern over PM health effects has led to a variety of emission reduction strategies, both for the precursor emissions of $PM_{2.5}$, including nitrogen oxides (NO_x = NO + NO_2), sulfur dioxide (SO_2), and ammonia (NH_3), as well as direct reduction of primary particles. A major focus of emissions reduction has been the mitigation of PM from road transport, which has historically been a major source in urban areas (Section 1.1.4). PM emissions from road transport comprise both exhaust and non-exhaust contributions. Non-exhaust PM emissions, which are becoming increasingly significant, arise from brake wear, tyre wear, road surface wear, and re-suspension of road dust, producing a variety of particle sizes, predominantly in the PM_{10} size fraction (Section 1.2.4). In contrast, exhaust PM emissions originate from fuel combustion, particularly in diesel engines, producing $PM_{2.5}$, which has been the target of reduction strategies in the past two decades (Section 1.2.1).

The introduction of diesel particulate filters (DPFs) for light and heavy-duty vehicles in the UK was a pivotal step to address $PM_{2.5}$ emissions from road transport (Section 1.2.2.2). Mandated under increasingly stringent emission standards, DPFs serve as highly efficient technologies designed to physically trap particles and burn off accumulated material.[8] Following their widespread adoption in the late 2000s, DPFs have contributed largely to the 50% reduction in UK $PM_{2.5}$ emissions from road transport between 2008 and 2021.[3] Moreover, during this period, vehicle emission standards and control technologies have continued to develop, with gasoline vehicles in the UK requiring particulate filters from 2019 onwards, further reducing $PM_{2.5}$ emissions from road transport (Section 1.2.2.1).[9]

As road transport emissions of PM have been reduced, the relative importance of other sources has increased. The number and type of non-vehicular sources are vast, including industrial processes, construction and demolition activities, residential heating and cooking activities.[10] $PM_{2.5}$ and PM_{10} emis-

sions from these sources are challenging to quantify due to their transient and unpredictable nature, and there are very few primary emission factor measurements available in the literature. Efforts to mitigate PM in urban areas must encompass a broader range of sources, with a developing focus on those of non-vehicular origin.

In order to reduce $PM_{2.5}$ and PM_{10} concentrations in an urban area such as London, the concept of the *controllable fraction* of PM concentrations is important. Recent measurements of $PM_{2.5}$ show that a significant fraction originates outside the UK in the form of secondary inorganic and organic aerosol (Section 1.2.3).[11] Therefore, at the city level, there is limited scope to reduce PM concentrations by controlling emissions in London itself. Nevertheless, it is important for London and other cities to quantify the PM that is locally controllable and take appropriate action to reduce concentrations further. In this respect, considering the increment in PM concentrations above the regional background provides a more meaningful metric, as it is more closely related to the controllable fraction of PM compared to absolute concentrations.

Mobile monitoring, which involves the use of fast-response air quality analysers contained within a mobile laboratory, is well suited to evaluate PM emissions in urban areas due to its ability to provide high-resolution spatial and temporal information (Section 1.4.5).[12, 13] Unlike stationary monitoring sites, which offer limited geographical coverage, mobile laboratories can traverse the urban environment, measuring a diverse range of emission sources. This approach allows for the detection of transient PM emission events that might be otherwise missed and reveals spatial patterns in PM concentrations through repeated driving routes.[14] However, working with mobile monitoring data is challenging, and new analytical techniques are required to successfully derive useful information from data with high spatial and temporal variability.

In recent research by Wilde et al., a new framework for analysing mobile measurements was developed[15]. Higher NO_x increments were measured in Central London compared to Outer London, and the road transport fleet-averaged emission intensity for NO_x in Central London was double that of Outer London as a consequence of high levels of dieselisation and congested traffic conditions. These findings demonstrate that the comprehensive spatial information that can be derived from mobile monitoring is essential for understanding the complex dynamics of urban air pollution, identifying emission sources, and informing targeted mitigation strategies to improve air quality.

4.2.2 Objectives

This study aims to use fast response mobile measurements of PM_{10} and $PM_{2.5}$, together with gaseous measurements of NO_x, SO_2 and carbon dioxide (CO_2), to improve understanding of PM sources in London. The main objectives are (i) to evaluate PM emissions in Central and Outer London and determine whether there is a diesel congestion penalty - elevated pollutant emissions due to the inefficient operation of emission control systems in congested traffic conditions - which has previously been observed for NO_x emissions in Central London; (ii) to identify and quantify the contribution made by infrequent high-emission vehicles; and (iii) to develop methods to identify and quantify non-vehicular sources of PM, considering different PM size fractions and the influence of meteorology and dispersion characteristics.

4.3 Materials and Methods

4.3.1 Mobile Monitoring

4.3.1.1 Instrumentation

Mobile measurements were made using an instrumented mobile laboratory (Nissan NV400SE transit van). A detailed description of the mobile laboratory is available in the literature; a summary is provided in this text. [15, 16] Air was sampled from a forward-facing inlet mounted 2.25 m above the ground at the front of the vehicle to minimise self-sampling of exhaust emissions. The risk of exhaust self-sampling is greatest when reversing and during stationary intervals. Instances, where the van was reversing, were excluded from the analysis, and preliminary stationary tests indicated minimal self-sampling of the exhaust, with all observed test measurements corresponding to passing vehicles.

Multiple air pollutants, including PM, NO_x, SO_2, CO_2, carbon monoxide (CO), methane (CH_4), and ozone (O_3), were measured using a variety of fast-response analysers contained within the mobile laboratory. Flame ignition tests were performed daily prior to monitoring, and the resulting concentration peaks characterised instrument response times.

The data from each instrument were time-aligned by calculating the optimal offset for each species using a cross-correlation procedure relative to the fastest-responding instrument. The time series for each species was shifted to produce the maximum correlation coefficient with CO_2, which was chosen as the reference measurement. A 5 s offset was applied to the data to account for the delay caused by air travelling from the sample inlet to the instruments; for typical vehicle speeds of 30 – 45 $km\,h^{-1}$, this offset corresponds to a distance of 50 m.

Geographic location, vehicle speed, and vehicle direction were mea-

sured using a Garmin GPS 18x computer mounted externally 2.5 m above the ground. Front-facing video footage was recorded using a dashboard-mounted VANTRUE X4S 4K camera. All data were collected at 1 Hz using custom DAQFactory software, and air pollutant measurements were merged with the corresponding geographic information after the time alignment adjustments. A 'snapping' procedure was applied to correct inaccurate location measurements resulting from the loss of GPS signal. Each location measurement was projected to the nearest point on a network that contained only the road links included in the mobile monitoring route. Measurements transformed more than 200 m were excluded from the analysis. This procedure was most necessary in Central London due to the high density of tall buildings near the road.

This analysis primarily considers PM, which was measured using a PALAS Air Quality Guard Ambient photometric particle number counter, which was mounted to the roof of the mobile laboratory (Section 1.4.6.3).[17] The instrument sampled air directly and was mounted approximately 0.2 m above and 1.5 m behind the forward-facing inlet used to supply the other onboard instrumentation. Direct sampling with no sample line minimises inertial and gravitational particle losses at the instrument inlet, which are particularly relevant for larger PM size fractions. Additionally, the instrument's 360° inlet design helps to mitigate the effects of vehicle turbulence.

The instrument has a response time of 1 s and measures particles with aerodynamic diameters between 0.175 – 20 µm over 64 channels via single-particle optical light scattering. The mass concentrations of PM (in µg m^{-3}) are calculated for a variety of size fractions (PM_1, $PM_{2.5}$, PM_4, PM_{10}) using a mass conversion algorithm that considers the shape and duration of the signal and was developed alongside the EN16450 certified Fidas 200 instrument. While the PALAS Air Quality Guard Ambient offers detailed information on PM size distribution, it does not provide any data on particle

composition.

Other species considered in this analysis include NO_x, CO_2, and SO_2. An Airyx Iterative Cavity-Enhanced Differential Optical Absorption Spectrometer (ICAD) was used to measure both NO_x and CO_2 (Section 1.4.6.2).[18] This instrument directly measures NO_2 in the spectral range between 430 and 465 nm, and an internal gas phase O_3 titration system converts NO to NO_2, allowing measurement of total NO_x. Parallel CO_2 measurements are made using a smartGAS non-dispersive infra-red gas sensor. In the standard configuration, this instrument has a 2 s response time; linear interpolation was applied to produce a 1 s time series.

A Thermo Model 43i Analyzer was used to measure SO_2 (Section 1.4.6.4).[19] This instrument operates on the principle of pulsed fluorescence detection and has a standard configuration with a detection limit of < 1.5 μg m^{-3} and a response time of 20 s. An additional external sampling pump was employed to increase the instrument flow rate, and modifications to the software enabled 1 s measurements of SO_2. For this study, minor changes to the detection limit resulting from these modifications are negligible, as only situations involving high SO_2 emissions (> 20 μg m^{-3}) are considered.

4.3.1.2 Measurement Locations

Mobile monitoring was performed in September 2022 at two locations within London, UK (Figure 4.1). Fixed driving routes were defined for each location prior to the monitoring campaign. The routes were driven continuously in alternate directions and were designed to cover a range of road types, traffic conditions and vehicle fleet compositions, both inside and outside the Ultra Low Emission Zone (ULEZ) (Section 1.3.2). A summary of the driving routes at each location is provided in Table 4.1. The experiment was designed to contrast two areas of London: the highly dieselised area of Central London that suffers from congestion and an Outer London location with a vehicle

fleet that is more reflective of the composition of the UK-wide vehicle fleet.

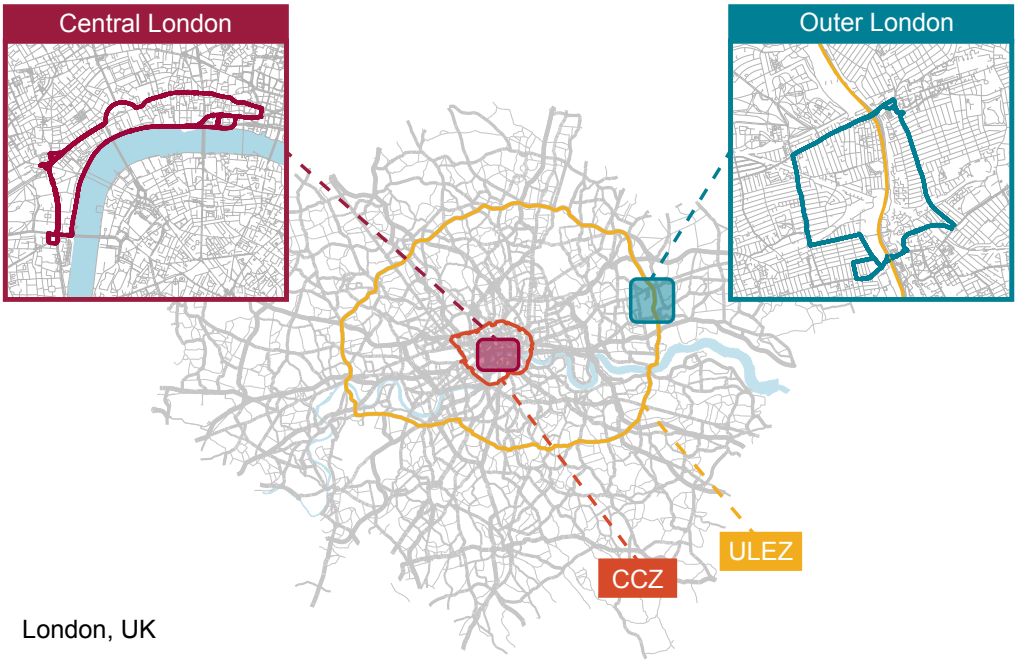

Figure 4.1: Central and Outer London measurement locations. The yellow and orange lines represent the boundaries of the Ultra Low Emission Zone (ULEZ) and Congestion Charge Zone (CCZ) at the time of the monitoring campaign (September 2022), respectively. Map data courtesy of OpenStreetMap® contributors, distributed under the Open Data Commons Open Database License v1.0.

The Central London route was close to the River Thames, featured major roads, and was located within the Congestion Charge Zone (CCZ) and ULEZ. The CCZ is an area where drivers of all vehicles must pay a daily fee to reduce traffic congestion, whereas the ULEZ imposes a daily charge only on vehicles that do not meet specified stringent emission standards. The Outer London route straddled the ULEZ and featured primarily arterial and residential roads, as well as two high streets, one of which was inside the ULEZ. It should be noted that the half of the Outer London route contained within the ULEZ boundary is officially considered Inner London; for simplicity in this text, the entire route is referred to as Outer London.[20] A 2.5 km elevated section

Table 4.1: Summary information for each measurement location.

Variable	Central London	Outer London
Routes completed	47	41
Route length (km)	6.2	8.0
Mean van speed ($km h^{-1}$)	10.3	16.6
Mean temperature (°C)	25.2	24.5
Measurement start date	04 SEP	12 SEP
Measurement end date	09 SEP	15 SEP
Total raw measurements (1 Hz)	103,928	72,118

of the North Circular Road, which is a highway that surrounds London, was initially part of the Outer London route. However, since the driving conditions on this road differed significantly from those on the rest of this route and the Central London route, data from this section were excluded from the analysis.

4.3.2 Analysis Methods

4.3.2.1 Background Subtraction

Background subtraction isolates the local emission component of the measurements by separating the most recent, 'fresh' emissions from the urban background. The subtracted urban background concentrations represent well-mixed pollution consisting of both 'aged' local emissions, emitted long before the time of measurement, and emissions that have been transported to the measurement location from elsewhere. For a species X, once the background is subtracted, the remaining increment (ΔX) can be attributed to local emissions from nearby sources. In this work, a method described by Padilla et al. was implemented to achieve background subtraction.[21]

First, a centred 5-minute rolling window was applied to the mobile time series, which included all data 2.5 minutes before and after each 1 s measurement. Next, the background concentrations for each measurement were taken as the 1st percentile value within the frame of the measurement's 5-minute window. Finally, the calculated background concentration was subtracted from the measurement value to determine the emission increment.

The 1st percentile was chosen to ensure that the smallest emission plumes were not excluded from the analysis, and sensitivity tests revealed that the choice of rolling window length did not significantly impact the calculated emission increments. Additional information about the background subtraction method can be found in the literature.[15]

4.3.2.2 PM Size Fractions

The PM component of this analysis considers the mass concentration values, in µg m^{-3}, of two particle size fractions. Fine PM (PM_{fine}) was defined as PM with an aerodynamic diameter less than 2.5 µm, and coarse PM (PM_{coarse}) was defined as PM with an aerodynamic diameter between 2.5 and 10 µm. The value of PM_{fine} was taken as the $PM_{2.5}$ value reported by the PALAS Air Quality Guard instrument (Equation 4.1), while PM_{coarse} was calculated by subtracting this value from the reported PM_{10} value (Equation 4.2). Background subtraction was applied to the time series for PM_{fine} and PM_{coarse} after this calculation to derive the increment values ΔPM_{fine} and ΔPM_{coarse} (Section 4.3.2.1).

$$PM_{fine} = PM_{2.5} \tag{4.1}$$

$$PM_{coarse} = PM_{10} - PM_{2.5} \tag{4.2}$$

Both PM_{fine} and PM_{coarse} originate from a variety of sources in urban areas. Primary PM_{fine} typically comes from combustion sources such as motor vehicle engines, industrial processes, and domestic/commercial activities, in particular, cooking.[22–24] The atmospheric transformation of gases such as SO_2 and NO_x into fine particles (secondary aerosol formation) is a secondary source of urban PM_{fine}.[23, 25] PM_{coarse} is primarily emitted from abrasive mechanical sources such as motor vehicle tyre and brake wear, road dust re-suspension, and construction and demolition activities.[25–29] However, it is important to note that many of these sources emit a range of particles spanning both size fractions, and while these general descriptions are useful for data interpretation, the exact apportionment of PM_{fine} and PM_{coarse} to specific sources is not always possible.

Due to instrument limitations, this work does not consider ultra-fine PM with an aerodynamic diameter smaller than 0.1 µm. There is increasing evidence indicating that these particles pose significant health risks.[30] However, this analysis primarily considers PM mass concentrations, which have been shown to be largely independent of ultra-fine PM emissions due to their negligible mass, even at high particle number concentrations.[31, 32] To mitigate the negative health consequences of urban PM effectively, both particle mass concentrations for PM_{fine} and PM_{coarse}, and the particle number concentration of ultra-fine PM should be considered in combination.

4.3.2.3 Distance-Weighted Mean Calculation

Distance-weighted mean concentration values were calculated using a Gaussian kernel within a continuously moving window.[15] The Gaussian kernel assigns higher weights to measurements that are closer to the data point, decreasing the weights as the distance from the point increases. The standard deviation σ, which controls the width of the Gaussian curve, influences the degree to which the measurements are weighted. This method reflects

real-world concentration measurements, which are more strongly influenced by nearby emission sources and less by those that are distant.

This method has two main purposes: first, to provide a concentration aggregation of multiple mobile measurement circuits (47 and 41 for Central and Outer London as shown in Table 4.1), and second, to provide a way in which to smooth the data spatially at a predetermined scale through the choice of σ.

The driving routes in Central and Outer London were converted into networks of equally spaced 10 m points, containing 1092 and 1138 points, respectively. For each species measured, mean concentrations were calculated using a two-step approach. First, the data were separated into individual complete circuits of the route, and the distance-weighted mean was determined (σ = 100 m) at each 10 m point. This is similar to the drive-pass mean outlined elsewhere in the literature [13, 33], but prevents over-weighting of measurements made at locations where the mobile laboratory was moving at low speeds or stationary. Second, these values were averaged across all circuits using the arithmetic mean to determine an overall distance-weighted mean concentration for each 10 m point.

All processing was carried out using the R programming language, and the functions used to perform distance-weighted mean calculations are available in the `mobilemeasr` R package.[34, 35] A σ value of 100 m was chosen for distance-weighted calculations to represent a near-field distance scale, over which direct exposure to urban source emissions is likely.[36]

4.3.2.4 Non-Vehicular PM Source Characterisation

A novel analytical method was developed to identify and quantify PM emissions from non-vehicular sources. In this work, the method is applied to two major construction sites located in Central and Outer London.

For each site, a 1 km segment of the driving route was selected, centred

on the construction site. The exact midpoint of each segment represented the point on the road network closest to the geographical centre of the construction site, as identified using onboard camera data from the mobile laboratory. Next, the mobile monitoring increment measurements for both locations across all driving circuits within these 1 km segments were isolated, and the distance along the road network between each measurement and the respective construction site centre point was calculated. It is important to note that individual mobile monitoring increment concentrations (1 Hz) were used for this analysis, and not the equally spaced 10 m distance-weighted mean values discussed in Section 4.4.2. Generalised additive models (GAMs), which are capable of fitting non-linear relationships between variables, were then employed to evaluate the relationship between PM concentrations and the calculated distances, using the `mgcv` R package.[37]

The Central London data in this section of the analysis were subdivided into two categories based on the weather conditions during mobile monitoring. Onboard camera footage was used to assign each driving circuit as wet or dry, depending on the presence of precipitation and the condition of the road surface. Circuits where the weather condition changed or was unclear were omitted. All mobile monitoring in Outer London was conducted in dry weather conditions. The total number of measurements within the 1 km segments for Central London (Wet), Central London (Dry) and Outer London were 6349, 5563, and 6145, respectively.

4.4 Results and Discussion

4.4.1 Measurement Location Comparison

Pollutant measurements from all driving circuits in Central and Outer London were aggregated, and the mean increments of PM_{fine}, PM_{coarse}, NO_x, CO_2 and SO_2 for each location are presented in Table 4.2. While these PM values represent averages, there were periods of significantly higher concentrations of PM_{fine} and PM_{coarse} within the data set. Specifically, the maximum increments of PM_{fine} reached 92.0 µg m^{-3} in Central London and 271.8 µg m^{-3} in Outer London, whereas PM_{coarse} peaked at 207.8 µg m^{-3} in Central London and 221.7 µg m^{-3} in Outer London. These episodic peaks in PM are important as they increase short-term human exposure, potentially leading to acute health effects.

A direct comparison of these values and those in Table 4.2 with WHO guidelines is not appropriate, as the reported values are concentration increments rather than absolute concentrations. However, these increments represent the controllable fraction of PM, which is critical for informing future PM reduction strategies for London. A limitation of this study is a lack of PM composition information, which, if available, would enable a more in-depth apportionment of the measured PM increments to different urban sources, such as road transport (exhaust and non-exhaust), industrial processes, and domestic/commercial activities. Previous research indicates that PM in urban areas has traditionally been dominated by road transport emissions; however, recent studies have highlighted the importance of other non-vehicular sources, including commercial and domestic cooking, as well as construction activities.[22–24, 28, 38] The focus of this section, road transport PM emissions, are generally controlled by three main factors: total traffic volume, traffic congestion, and vehicle fleet composition.

Table 4.2: Mean increment concentrations of PM_{fine}, PM_{coarse}, NO_x, CO_2, and SO_2 at each measurement location, presented with 95% confidence intervals. Mean values were calculated from all 1 Hz increment measurements at each location. 95% confidence intervals were calculated using the standard error of the mean and a Z-score = 1.96. Percentage differences were calculated relative to the Outer London data.

	Concentration (µg m^{-3})		
Species	**Central London**	**Outer London**	**% difference**
ΔPM_{fine}	2.83 ± 0.02	3.62 ± 0.05	− 22
ΔPM_{coarse}	5.93 ± 0.05	5.35 ± 0.05	+ 11
ΔNO_x	175.8 ± 1.8	101.9 ± 1.6	+ 73
ΔCO_2 ($\times 10^3$)	51.0 ± 0.3	45.0 ± 0.3	+ 13
ΔSO_2	2.72 ± 0.01	3.04 ± 0.07	− 11

Combustion is the primary source of CO_2 in urban environments, with vehicle exhaust emissions as the main contributor.[39] Therefore, the mean ΔCO_2 concentrations likely reflect vehicle combustion activity, suggesting that total traffic volume was slightly higher in Central London compared to Outer London. This is supported by the mean ΔPM_{coarse} concentration, which was 11% higher in Central London, aligning with the 13% difference in ΔCO_2 values. PM_{coarse} in urban areas can be largely attributed to non-exhaust vehicle emissions such as tyre and brake wear, road surface wear, and dust re-suspension, and therefore also act as a tracer species for total traffic volume.[28] It is important to note that the emissions of CO_2 and PM_{coarse} are not entirely independent of traffic congestion and vehicle fleet composition, and the differences in these variables between locations will influence the results. However, total traffic volume is still likely to dominate the trends observed in mean increment concentrations.

In contrast, both NO_x and PM_{fine} emissions are much more sensitive to vehicle fleet composition due to the variability of the emission control systems fitted to vehicles of different types and ages (Section 1.2.2.1 & 1.2.2.2). NO_x emissions are also highly sensitive to traffic congestion because of the complexity of the emissions control systems that reduce NO_x. Typically, exhaust NO_x from diesel vehicles – the highest NO_x emitters – is controlled using selective catalytic reduction (SCR) or a lean NO_x trap (LNT); both operate on the principle of chemical reduction and are highly dependent on the operating parameters of the engine and traffic conditions (Section 1.2.2.2).[8] Exhaust PM, which consists mainly of PM_{fine}, is controlled using particulate filters that physically trap particles and burn off accumulated material.[8]

Differences in traffic congestion and vehicle fleet composition at each measurement location arise from the nature and position of the chosen driving routes and explain the observed NO_x and PM_{fine} increment concentrations. The Central London measurement location was a busy urban centre inside the CCZ and ULEZ, and so the vehicle fleet was comprised mostly of newer vehicles conforming to the most stringent emission standards. However, traffic flow was poor, and congestion was frequent, as evidenced by the mean van speed shown in Table 4.1. In contrast, the Outer London measurement location was partially outside of the ULEZ, with approximately half of the driving route extending beyond the boundary. This portion of the route included older vehicles, with greater wear and less effective or deteriorated emission control systems (Section 4.4.3). However, traffic at the Outer London location was more free-flowing than in Central London, and congestion was less frequent, resulting in an increase of over 60% in the mean speed of the van at this location (Table 4.1).

The ΔNO_x concentrations presented in Table 4.2 are likely dominated by the impact of traffic congestion; the mean in Central London was 73% higher

than in Outer London. This increase is consistent with the results reported by Wilde et al. and can be attributed to the congestion penalty associated with the inefficient operation of SCR and LNT emission control systems.[15] Conversely, the mean ΔPM_{fine} concentration in Central London was 22% lower than in Outer London. This result is important, indicating that there is no congestion penalty for PM_{fine} in Central London and that the composition of the vehicle fleet predominantly influences concentrations. Furthermore, unlike NO_x emission control systems, these data provide evidence for the success of particulate filters, which remain efficient even under congested conditions.

However, it is still important to acknowledge the impact of vehicle fleet composition on PM_{fine} emissions. The higher mean ΔPM_{fine} concentration in Outer London can be attributed to the non-ULEZ portion of the driving route, which includes non-ULEZ compliant vehicles. Many of these older vehicles are not fitted with particulate filters, and those that are have accumulated wear, reducing their effectiveness. Moreover, as vehicles age, they can develop engine faults that increase pollutant emissions, which, when coupled with the lack of an effective emission control system, may contribute to the episodic high-concentration peaks contained within the mobile monitoring data.

To quantify the effects of the ULEZ and vehicle fleet composition, mobile monitoring data from Outer London were split into two groups: measurements taken inside the ULEZ (n = 43,957) and outside the ULEZ (n = 28,161). Mean pollutant increments for each group were recalculated and are presented in Table 4.3. The mean ΔPM_{fine} concentration was 38% higher outside the ULEZ than inside, while the mean ΔPM_{coarse} concentration was 7% lower. This difference in ΔPM_{fine} highlights the strong impact of the ULEZ and vehicle fleet composition on urban PM_{fine} emissions. A comparison of mean ΔPM_{fine} and ΔNO_x concentrations for the inside ULEZ data for Outer Lon-

don with the Central London data (which was collected entirely within the ULEZ) showed increases of 15% and 63%, respectively. The relatively small increase in ΔPM_{fine}, consistent with the ΔCO_2 increase of 17% for the same comparison, supports the absence of a congestion penalty for PM_{fine}. For ΔNO_x in Outer London, the mean concentration was 14% lower outside the ULEZ than inside, suggesting that while vehicle fleet composition is a dominant factor in urban PM_{fine} emissions, it has less impact on NO_x emissions.

Table 4.3: Mean increment concentrations of PM_{fine}, PM_{coarse}, NO_x, CO_2, and SO_2 in Central London and inside/outside of the Ultra Low Emission Zone (ULEZ) in Outer London. The entire Central London driving route was inside of the ULEZ. Mean values were calculated from all 1 Hz measurement data. The values in brackets represent the mean increment concentrations outside of the ULEZ with the high-emission vehicle R event removed.

	Concentration ($\mu g\ m^{-3}$)		
Species	**Central London**	**Inside ULEZ**	**Outside ULEZ**
ΔPM_{fine}	3.62	3.15	4.36 (3.72)
ΔPM_{coarse}	5.93	5.49	5.13 (5.15)
ΔNO_x	175.8	107.8	92.7 (92.6)
ΔCO_2 ($\times 10^3$)	51.0	43.5	47.4 (47.2)
ΔSO_2	2.72	2.51	3.87 (2.49)

Also shown in brackets in Table 4.3 are mean pollutant increments outside of the ULEZ in Outer London, with data removed corresponding to an individual high-emission vehicle event, discussed in detail in Section 4.4.3. Although this vehicle may represent an example of ULEZ-driven changes in fleet composition, its removal ensures that the observed trends are robust. Excluding this event reduced the ΔPM_{fine} concentration, but

the value outside the ULEZ was still 18% higher than that inside the ULEZ. However, the exclusion markedly lowers the ΔSO_2 concentration outside the ULEZ, aligning it with that inside the ULEZ; this is also discussed later in the text. To further reduce PM_{fine} in Outer London and more widely, it is critical to consider ageing and deteriorated vehicles, especially those with exceptionally high emissions.

4.4.2 Distance-Weighted PM Concentrations

A key feature of mobile monitoring is the spatial information it can provide. Distance-weighted mean concentrations of ΔPM_{fine} and ΔPM_{coarse} were calculated for 10 m points along each driving circuit in Central and Outer London, and the values at each point across all driving circuits were aggregated (Section 4.3.2.3). A statistical summary of these data is provided in Table 4.4, and Figure 4.2 presents a spatial distribution for each PM size fraction at each measurement location.

The results in Table 4.4 differ from those in Table 4.2 in that they were calculated from the mobile data after 10 m distance-weighted aggregation. The statistics presented in Table 4.4 therefore reflect the distribution of the distance-weighted spatial averages and not the raw measurements. Although the mean values of ΔPM_{fine} and ΔPM_{coarse} in Table 4.4 for each location follow the same trends as discussed in Section 4.4.1, their exact values are not identical to those in Table 4.2 because the spatial variability of the mobile measurements influences them.

The magnitude of the difference between ΔPM_{fine} for Outer and Central London increases when moving from the minimum (2%) through the 25^{th} quantile (3%), median (6%), 75^{th} quantile (35%), to the maximum (69%). This trend is visualised in Figure 4.3 and shows that the difference in ΔPM_{fine} between locations is biased toward the upper end of the distribution, likely due to deteriorated vehicles within the on-road fleet.

Table 4.4: Statistical summary of distance-weighted increment concentrations at each equally spaced 10 m point in Central and Outer London. The values represent the arithmetic mean of the distance-weighted increments calculated for each 10 m point across all driving routes. Sample sizes are n = 1092 for Central London and n = 1138 for Outer London.

Species	**Mean**	**Min**	**Q25**	**Med**	**Q75**	**Max**
Central London (µg m^{-3})						
ΔPM_{fine}	2.74	1.43	2.56	2.74	2.89	4.78
ΔPM_{coarse}	5.74	2.34	5.10	5.69	6.14	11.29
Outer London (µg m^{-3})						
ΔPM_{fine}	3.65	1.46	2.73	3.45	4.42	15.57
ΔPM_{coarse}	5.27	1.27	4.53	5.34	5.93	10.33

The four panels in Figure 4.2 visually show the trends discussed in PM concentrations, as well as additional variation along driving routes, with elevations near busy intersections with increased traffic. These features of the spatial distributions, particularly for ΔPM_{fine}, suggest that most measurements along each route were dominated by road traffic emissions rather than other sources. If sources such as industrial activities or residential and commercial cooking had consistently contributed to the measurements, the spatial distributions in Figure 4.2 would likely display localised enhancements corresponding to their locations. Panel (**b**) of Figure 4.2 shows elevated ΔPM_{fine} concentrations around an area of the road that contained an individual high-emission vehicle. This transient event, which occurred on a single driving circuit, produced ΔPM_{fine} concentrations high enough to influence the average aggregate values across all 47 circuits in Outer London and is discussed in more detail in Section 4.4.3.

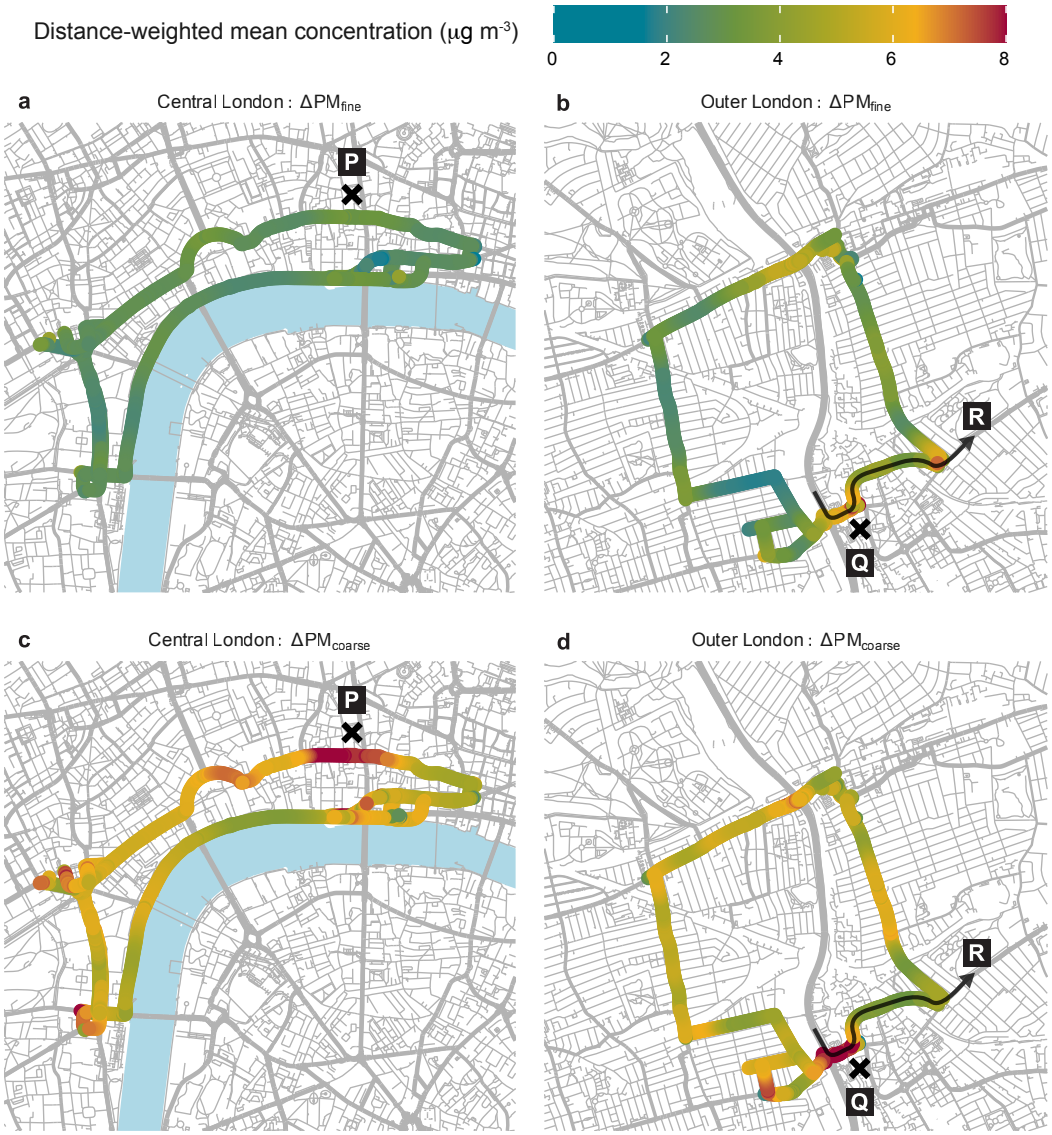

Figure 4.2: Spatial distributions of the distance-weighted mean concentrations of PM_{fine} (panels **a** & **b**) and PM_{coarse} (panels **c** & **d**) in Central and Outer London. The points labelled P and Q denote the positions of major construction sites in Central and Outer London, respectively. The black arrow labelled R shows the route of a high-emission vehicle in Outer London. Map data courtesy of OpenStreetMap® contributors, distributed under the Open Data Commons Open Database License v1.0.

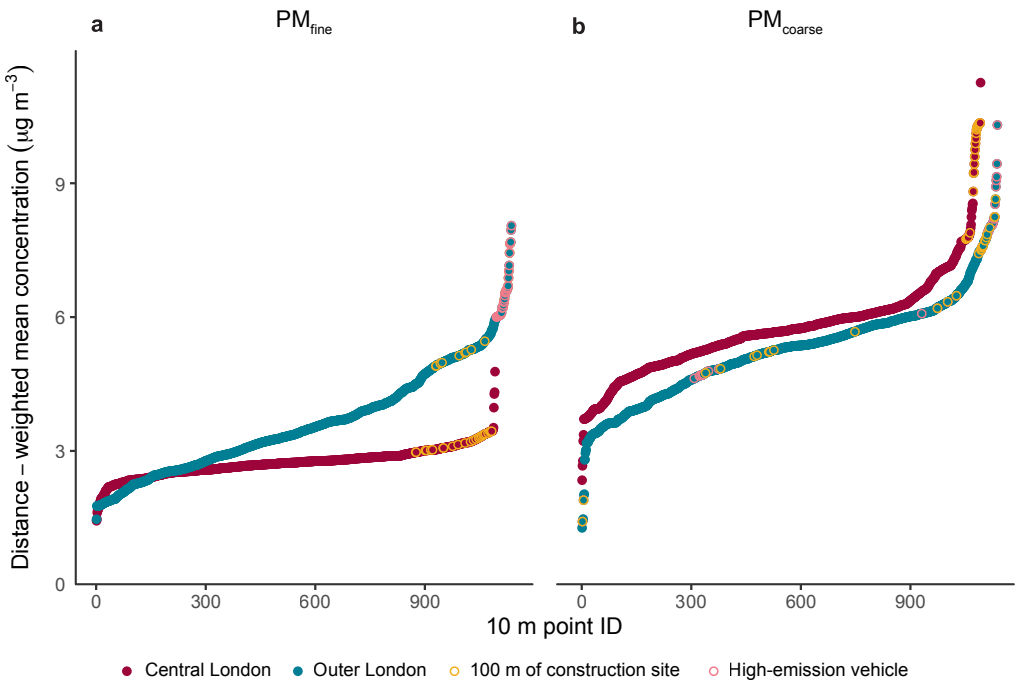

Figure 4.3: Distribution of distance-weighted mean concentration enhancement values for PM_{fine} (**a**) and PM_{coarse} (**b**) for each measurement location. The x-axis represents the identifier for each (10 m spaced) point arranged in ascending order of concentration. Points highlighted in yellow were within 100 m of construction sites P and Q, and points highlighted in pink were on the road section that contained the high-emission vehicle.

Labels P and Q in Figure 4.2 indicate two areas of highly elevated concentrations of ΔPM_{fine} and ΔPM_{coarse}, with an emphasis on the latter. The increased concentrations at locations P and Q were consistent across all driving circuits and, therefore, could not be attributed to transient one-off events. Inspection of the mobile laboratory's onboard camera footage revealed positions P and Q corresponded exactly with major construction sites in Central and Outer London, photographs of which are shown in Figure 4.4. Construction sites P and Q featured non-road mobile machinery and extended 78 m and 104 m, respectively, alongside the driving route at each location. The mean concentrations of raw ΔPM_{coarse} measurements within 100 m of the

centre points of P and Q were 9.56 µg m^{-3} and 6.42 µg m^{-3} respectively, 67% and 22% higher than the overall location mean values reported in Table 4.4. It should be noted that in Outer London, the section of road containing an individual high-emission vehicle overlapped with the position of construction site Q (Section 4.4.3). However, the ΔPM_{coarse} contribution from the high-emission vehicle was relatively low (Figure 4.5) and insufficient to explain the observed increase. Many of the data points within 100 m of the construction sites populated the upper end of the distance-weighted concentration increment distributions for both measurement locations and PM size fractions, as shown in Figure 4.3. The reported results provide evidence for the increasing importance of non-vehicular PM sources amidst the successful control of vehicle emissions, which is discussed further in Section 4.4.4.

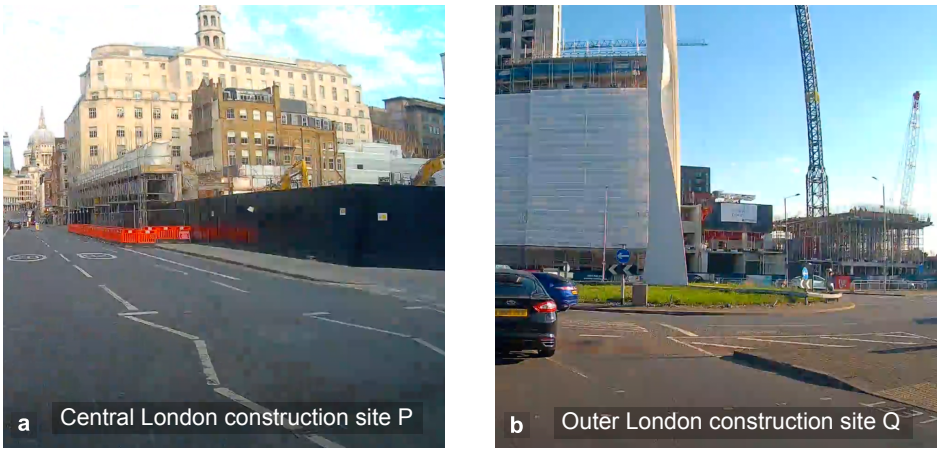

Figure 4.4: Photographs of (**a**) construction site P in Central London and (**b**) construction site Q in Outer London, captured by the mobile laboratory's onboard camera.

4.4.3 High-Emission Vehicles

Mobile monitoring data from Outer London demonstrate the substantial impact that individual high-emission vehicles can have on PM concentrations. While measuring in the non-ULEZ section of the driving route, a car emitting visible blue/white smoke from its exhaust joined the road two vehicles ahead of the mobile laboratory. This vehicle, which was designated the label R, was tracked for 1.2 km along the section of driving route highlighted with a black arrow in Figure 4.2. A photograph of high-emission vehicle R and the concentration increments of PM_{fine}, PM_{coarse}, and SO_2 during the period following it are shown in Figure 4.5.

During the approximately 10-minute period following high-emission vehicle R, elevated concentrations of PM_{fine} were observed, with frequent peaks ranging from 100 to 200 μg m^{-3}, corresponding to the vehicle's acceleration at traffic lights and roundabouts. The average measured ΔPM_{fine} concentration while tracking this vehicle was 51.27 μg m^{-3}, more than 17 times higher than the average for the rest of the measurements on the same driving circuit (3.00 μg m^{-3}). Moreover, despite occurring only on a section of a single driving circuit, the impact of high-emission vehicle R is visible in the spatial distribution of distance-weighted mean concentrations presented in panel (**b**) of Figure 4.2.

In addition to identifying high PM emissions from individual vehicles, mobile monitoring provides multi-pollutant information. The co-emission of SO_2 (Figure 4.5) is indicative of an engine malfunction resulting in lubricant combustion (Section 1.2.1). Outside of this high-emission event, measured SO_2 increment concentrations were consistently low with mean values of 2.5 and 2.7 μg m^{-3} in Central and Outer London, respectively. These results are expected given that vehicle fuel in the UK is regulated and must have a sulfur content lower than 10 ppm.[40] Engine lubricant, however, often contains sulfur in greater quantities to improve anti-wear properties.[41, 42] Although

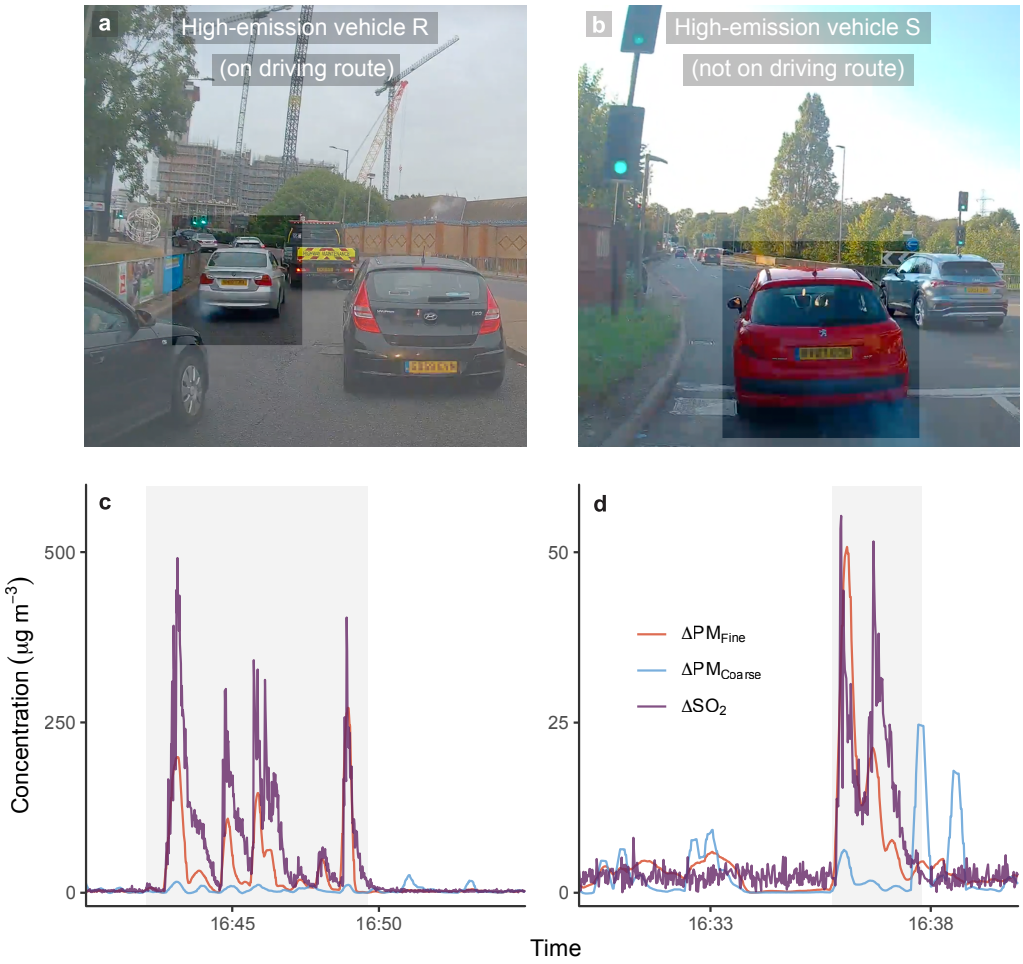

Figure 4.5: Photographs captured by the mobile laboratory's onboard camera of (**a**) high-emission vehicle R and (**b**) high emission vehicle S. Pollutant concentration time series tracking (**c**) high-emission vehicle R and (**d**) high-emission vehicle S. The grey shaded areas represent the time period during which the vehicles were being measured.

this lubricant is not designed to be burnt in a vehicle's engine, deterioration or malfunction can result in combustion of the lubricant and subsequent elevated emission of both SO_2 and PM through a variety of mechanisms. [42–44]

The registration number of high-emission vehicle R was captured by the onboard camera of the mobile laboratory and cross-referenced with the

Driver and Vehicle Licensing Agency (DVLA) vehicle database to access its technical specifications and vehicle safety inspection information.[45] Registered in 2006, the Euro 4 gasoline car had covered approximately 116,000 miles at its safety inspection in January 2023, 4 months after the mobile monitoring campaign. This vehicle model was not fitted with a particulate filter, which, when combined with lubricant combustion, increases PM emission and explains the measured ΔPM_{fine} concentrations. Furthermore, the vehicle failed the aforementioned safety inspection due to a warning light indicating an engine malfunction, and additional notes from the inspection state that blue smoke was emitted during acceleration.[45]

Filtering the mobile monitoring data ΔPM_{fine} and ΔSO_2 to include only values above the 99th percentile (11.90 and 9.41 µg m^{-3} respectively) revealed a second high-emission vehicle, assigned the label S, which was measured during a transit period within Outer London, outside of the designated measurement route. The mobile laboratory tracked behind this vehicle on a road outside of the ULEZ for 0.5 km over 2 minutes. The resulting increment concentrations of up to 50 µg m^{-3} for PM_{fine} and SO_2, as well as those for PM_{coarse}, are presented in Figure 4.5. This vehicle was a 2007 Euro 4 gasoline car without a particulate filter, and the co-emission of SO_2 and PM_{fine} suggest engine malfunction and subsequent lubricant combustion. As the vehicle was not measured on the specified driving route, it was not included in the primary analysis.

Although the two high-emission vehicles observed during this study represent outliers in terms of their malfunctioning status and associated PM_{fine} emissions, their potential contribution to overall fleet emissions is significant. High-emission vehicle R measured on the driving route was present for less than 0.15% of the total distance driven in Outer London; however, its presence increased the overall mean ΔPM_{fine} concentration (Table 4.2) by 7%. The mean increment concentrations in Outer London

with high-emission vehicle R removed are provided in Table 4.5, and the same values for outside the ULEZ in Outer London are presented in brackets in Table 4.3; all previously discussed trends remained consistent. Other research using a range of stationary measurement techniques reports that high-emission vehicles representing a small fraction of the total vehicle fleet are responsible for a disproportionate share of total PM emissions, particularly for gasoline vehicles.[46, 47] The results of this study agree with these findings and demonstrate the suitability of mobile monitoring for the detection, quantification, and explanation of high-emission vehicles, which must be targeted to control PM in urban areas effectively.

Table 4.5: Mean increment concentrations of PM_{fine}, PM_{coarse}, NO_x, CO_2, and SO_2 at each measurement location, presented with 95% confidence intervals. The Outer London location has the high-emission vehicle event removed. Mean values were calculated from all 1 Hz increment measurements at each location. 95% confidence intervals were calculated using the standard error of the mean and a Z-score = 1.96. Percentage differences were calculated relative to the Outer London data.

	Concentration (µg m^{-3})		
Species	**Central London**	**Outer London**	**% difference**
ΔPM_{fine}	2.83 ± 0.02	3.37 ± 0.02	− 16
ΔPM_{coarse}	5.93 ± 0.05	5.36 ± 0.05	+ 11
ΔNO_x	175.8 ± 1.8	102.0 ± 1.6	+ 72
ΔCO_2 ($\times 10^3$)	51.0 ± 0.3	44.9 ± 0.3	+ 14
ΔSO_2	2.72 ± 0.01	2.50 ± 0.01	+ 9

4.4.4 Non-Vehicular PM Sources

To further characterise and quantify PM emissions from construction sites P and Q, a 1 km segment of the driving route at each location was isolated, centred on the respective site. The PM increment measurements within each segment were used in combination with GAMs to calculate the average concentrations of ΔPM_{fine} and ΔPM_{coarse} as a function of the distance from the construction site (Section 4.3.2.4). In Outer London, measurements that corresponded with the nearby high-emission vehicle comprised 5% of the data and were excluded from this part of the analysis to ensure that the influence of construction site Q on ΔPM_{fine} could be better evaluated. The data from Central London were divided into two categories, 'Wet' or 'Dry', based on weather conditions; the results for these two categories and those for Outer London, where the weather condition was always dry, are presented in Figure 4.6.

Panel (**b**) in Figure 4.6 shows a clear Gaussian peak centred on construction site P, with concentrations of ΔPM_{fine} and ΔPM_{coarse} reaching maximum values of 5.21 µg m^{-3} and 22.50 µg m^{-3} respectively. Both ΔPM_{fine} and ΔPM_{coarse} concentrations rapidly decayed with increasing distance from the origin in both directions. The two smaller peaks adjacent to the primary peak associated with construction site P could be attributed to other minor construction activities within the 1 km road segment; this was confirmed by footage from the onboard camera, and photographs are shown in Figure 4.7 These minor construction activities did not contain non-road mobile machinery and extended much smaller distances along the driving route (25 m and 15 m). The peaks associated with these activities were not obvious when examining the spatial distributions of overall PM increments in Section 4.3.2.3; however, they became apparent when using a more targeted analytical approach.

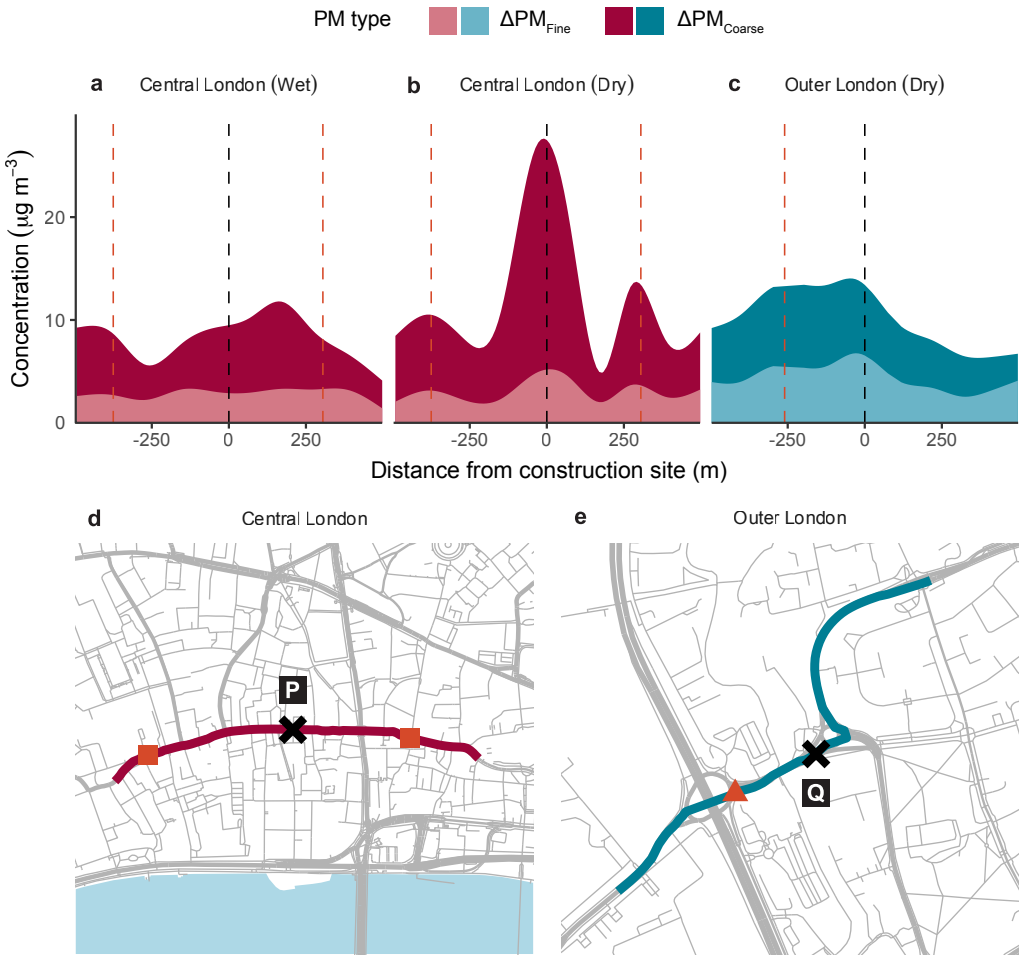

Figure 4.6: Concentrations of ΔPM_{fine} and ΔPM_{coarse} within a 1 km road segment centred on major construction sites P and Q, calculated using GAMs. Panels (**a**), (**b**), and (**c**) show PM mass concentration as a function of distance from the construction site, with PM_{coarse} concentrations stacked on PM_{fine} concentrations. The Central London data are separated into wet and dry weather conditions; all measurements for Outer London were made in dry conditions. Panels (**d**) and (**e**) show spatially the respective 1 km road segment for each site. The two orange dashed lines and orange squares in panels (**a**), (**b**), and (**d**) denote the position of smaller secondary construction work in Central London. The orange dashed line and triangle in panels (**c**) and (**e**) denote the position of a large multi-lane roundabout in Outer London. Map data courtesy of OpenStreetMap® contributors, distributed under the Open Data Commons Open Database License v1.0.

The footage from the onboard camera was reviewed to identify other possible (false-negative) construction activities that were not apparent in the mobile monitoring data. There were no other major construction activities (containing non-road mobile machinery and extending more than 50 m along the driving route), highlighting the effectiveness of distance-weighted mobile monitoring techniques for detecting large, non-transient, non-vehicular PM sources. There were 4 and 2 additional minor construction activities identified in Central and Outer London, respectively. Similar to the minor construction activities presented in Figure 4.6, these sites were not obvious in the overall spatial distribution data. Repeating the same targeted analytical approach that was used to investigate construction sites A and B, but with a 250 m segment of road centred on each minor construction site, revealed that each activity was associated with a concentration peak of ΔPM_{fine} and ΔPM_{coarse}, with maximum values ranging between 2.48 – 5.19 μg m^{-3} and 6.25 – 15.76 μg m^{-3} respectively. As well as further demonstrating the utility of combining mobile measurements with a targeted analytical approach, these results highlight the benefit of recording camera footage when performing mobile monitoring.

Figure 4.7: Photos of the minor construction sites within 1 km of major construction site P in Central London, captured by the mobile laboratory's onboard camera.

Comparison of PM increment distributions for the different meteorological conditions in Central London, shown in Figure 4.6: panel (**a**) and (**b**), revealed that wet weather was correlated with a reduction in PM emissions from construction site P. This effect was particularly prominent for PM_{coarse}, with the peak increment concentration reduced by 62%. The exact reason for this observation could not be determined conclusively and was likely the result of a combination of factors. Precipitation has been shown to reduce PM concentrations through scavenging and wet deposition, and wet road conditions can decrease the mobility of settled PM, suppressing emissions from re-suspension.[48, 49] It is also possible that the observed decline in PM was attributable to a reduction in construction activity arising from unfavourable wet weather conditions that made outdoor work difficult.

Although meteorological variations in Central London significantly impacted PM levels near construction site P, their effect on the rest of the driving route was much smaller. Table 4.6 presents the average concentrations of PM increments under each meteorological condition for the entire Central London driving route, excluding measurements within 100 m of the construction site P. There was a 14% difference in increments of PM_{fine} and a 15% difference in increments of PM_{coarse} between wet and dry conditions. Additionally, when comparing the dry Central London data with the Outer London data, all previously discussed trends and observations remained consistent.

The influence of construction site Q on the Outer London observations in Figure 4.6 was less obvious than the influence of construction site P on the dry Central London observations, despite similar weather conditions. This difference was likely the result of variations in the types of construction activities on sites P and Q, as well as differences in the surrounding urban environment. The maximum average concentration of ΔPM_{fine} and ΔPM_{coarse} around construction site Q in Outer London were 6.76 $\mu g\ m^{-3}$

Table 4.6: Mean PM enhancement concentrations for wet and dry weather conditions in Central London, presented with 95% confidence intervals. Measurements made within 100 m of construction site P were excluded.

	Concentration (µg m^{-3})	
Species	**Dry**	**Wet**
ΔPM_{fine}	2.48 ± 0.02	2.88 ± 0.03
ΔPM_{coarse}	5.85 ± 0.10	4.96 ± 0.07

and 8.07 µg m^{-3}, respectively, much lower than those around construction site P in Central London during dry weather. Furthermore, the relative contributions from each PM size fraction at the maximum were different, with PM_{fine} accounting for only 19% of total PM (PM_{fine} + PM_{coarse}) in dry Central London but accounting for 46% of total PM in Outer London. This observation may have been a result of increased combustion activity producing more PM_{fine} at construction site Q when compared to site P; however, no correlation was observed between PM and gaseous combustion species such as CO_2 or NO_x. It is more likely that within the increments of PM_{fine} in Outer London, there was a greater contribution from road transport vehicles compared to Central London, for the reasons outlined previously in the text (Section 4.4.1). Furthermore, there was a large multi-lane roundabout located 250 m from construction site Q, as highlighted in panels (**c**) and (**e**) of Figure 4.6. The heavy traffic and congestion on this part of the driving route were likely responsible for the additional PM peak in Outer London, arising from a mix of primary vehicle exhaust and non-exhaust emissions, as well as re-suspended particles from construction activities at the nearby site Q. No elevated ΔSO_2 concentrations were observed at either construction site.

In addition to local meteorological conditions, other aspects of the mobile

monitoring data can help to characterise non-vehicular PM sources, such as considering the driving direction in dry Central London. This location and meteorological condition were chosen for further analysis due to the distinct peak observed for construction site P and the fact that there was minimal interference from the surrounding environment. Mobile measurements were grouped by the direction in which the mobile laboratory was travelling on the driving route (clockwise or anticlockwise). Vehicles in the UK drive on the left-hand side of the road, so measurements from the anticlockwise driving route will be closer to construction site P than those from the clockwise driving route. Figure 4.8 presents the concentrations of PM increments in dry Central London, separated by the direction of travel of the mobile laboratory and, therefore, the distance relative to construction site P.

The maximum average ΔPM_{fine} and ΔPM_{coarse} values were 64% and 82% higher, respectively, when travelling on the side of the road closest to the construction site compared to maximum values on the side of the road further away. Moreover, comparing the lower bound of the 95% confidence interval for the closer side of the road to the upper bound for the further side, the absolute difference in maximum ΔPM_{fine} and ΔPM_{coarse} values were 1.81 $\mu g\ m^{-3}$ and 8.62 $\mu g\ m^{-3}$ respectively, highlighting the statistical significance of the observed differences. The decrease in ΔPM_{coarse} across the road is strongly indicative of a local source where concentration gradients change dramatically over short distances. Similarly to the along-road fall-off in the concentration of ΔPM_{coarse} (shown in Figure 4.6), the perpendicular decrease across the road in ΔPM_{coarse} concentration is also strong. The stronger concentration gradients observed for ΔPM_{coarse} compared to ΔPM_{fine} are expected, as larger particles have greater mass and are more susceptible to gravitational settling, limiting their transport distance from the source.

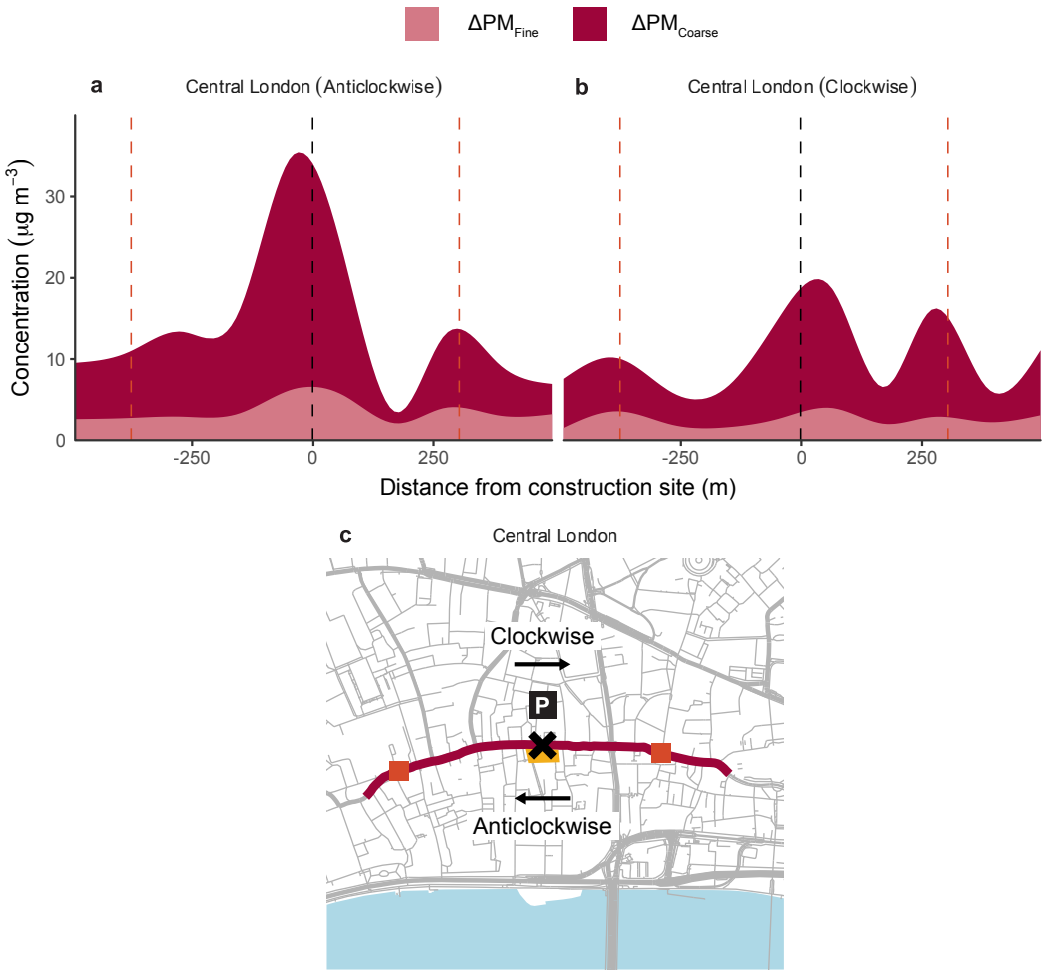

Figure 4.8: Concentrations of ΔPM_{fine} and ΔPM_{coarse} within a 1 km road segment centred on construction site P during dry conditions in Central London, calculated using GAMs. The data are separated by direction of travel along the driving route. The two orange dashed lines and squares denote the position of other minor construction activities, the yellow shaded area represents the footprint of construction site P, and the arrows indicate the clockwise and anticlockwise directions on the Central London driving route.

These results highlight a distinct advantage of performing the mobile monitoring driving routes in both directions. Measuring across the full width of the carriageway ensures that proximate non-vehicular emission sources on both sides of the road are included in the measurements and

enables the gradient of their fall-off in concentration to be quantified. Furthermore, driving in both directions provides a more accurate representation of the spatial variability of emissions along the road network, especially at junctions, where traffic conditions upon approach are often different from those after exit.

The identification, quantification, and characterisation of construction sites P and Q were only possible due to the unique information provided by mobile monitoring. Moreover, the campaign from which the data were obtained was not originally designed to target non-vehicular PM sources; their discovery was possible through robust spatial analysis of the mobile measurements and subsequent development of novel techniques. Furthermore, the developed techniques can be easily extended to investigate non-vehicular PM sources in various locations and from different origins. For instance, cooking emissions from restaurants have recently been identified as a significant contributor to urban PM_{fine} concentrations.[24, 38] This study highlights the increasing importance of non-vehicular sources in urban areas amidst the successful control of vehicular PM emissions and provides a foundation upon which to develop future research and inform mitigation strategies.

4.5 Conclusions

Fast-response mobile measurements provide excellent opportunities to understand the nature of emission sources in urban environments. However, they introduce complexities for data analysis because they vary in both space and time. Nevertheless, this work demonstrates robust strategies that can be adopted to maximise the insights that can be obtained from such measurements. First, the repeated measurement of road links (in this study, approximately 50) in both traffic directions maximises the opportunity to detect 'persistent' rather than transient sources. Second, simultaneous measurement of multiple pollutants greatly improves the ability to link concentration measurements with specific types of emission sources. In this study, SO_2 was shown to be a key tracer compound that can be used to identify the few high-sulfur combustion emission sources remaining in a city such as London. Similarly, the measurement of both PM_{fine} and PM_{coarse} enables non-combustion sources of PM to be unambiguously identified.

As historically dominant sources of PM in urban areas, such as road vehicle exhaust emissions, continue to decline, the need to better understand and quantify various poorly characterised sources, such as construction activities and individual high-emission vehicles, becomes increasingly important. Often, these sources are transient in nature or have an uncertain spatial distribution, making it difficult to evaluate their impact using fixed-site stationary measurements. Mobile monitoring offers a dynamic approach to address these challenges. As PM measurement techniques advance, the ability to obtain highly disaggregated measurements of particle composition will further assist in this goal.

4.6 Research Update

In March 2025, a report reviewing the London ULEZ was released.[50] The ULEZ was expanded in 2023, extending beyond the boundary that existed during the 2022 measurement campaign for this publication. While the report primarily discusses the impact of this expansion, it also covers the ULEZ pre-expansion, and the findings remain relevant to this work.

The report found that the ULEZ contributed to a reduction in vehicle exhaust $PM_{2.5}$ emissions of 29 % since its introduction in 2019. This aligns with the findings of this work, supporting the conclusion that a newer, cleaner vehicle fleet with fewer high-emitting vehicles improves ambient air quality. Furthermore, the report confirms that ULEZ compliance is high and increasing, with over 90% of vehicles driving within the pre-expansion ULEZ meeting emissions standards (the remainder pay a charge for non-compliance). These high compliance rates validate the conclusions from this work, which assumed that the vehicle fleet in Inner London was newer and cleaner than in Outer London - parts of which were outside the ULEZ at the time of measurement.

The report also found that the ULEZ reduced $PM_{2.5}$ concentrations in Outer London, beyond the ULEZ boundary, confirming positive border effects. Border effects, which were not discussed in this publication, occur when changes in the vehicle fleet within a Low Emission Zone (LEZ) influence air quality in adjacent areas (Section 1.3.2).[51] These effects can be positive (improving air quality) or negative (worsening air quality). The positive border effects observed for London likely result from many vehicles driving near the ULEZ boundary also being used within the ULEZ, making them compliant with emissions standards and thus newer and cleaner than they would be without the ULEZ. This suggests that the concentrations measured in Outer London in this work may have been lower than those in

similar urban areas without a nearby LEZ, because many vehicles in outer London are ULEZ-compliant. It is therefore expected that the $PM_{2.5}$ benefits associated with a cleaner and newer vehicle fleet may be even greater than implied by this work.

It is important to note that the report used a different methodology, analysing annual trends from a network of stationary monitoring sites across London and the wider UK. The reported PM reductions are relative to an estimated no-ULEZ scenario rather than direct comparisons from comprehensive monitoring inside and outside the ULEZ. A key difference in the report was the finding that NO_x concentrations were successfully reduced by the ULEZ, likely reflecting the differences in analysis methods. This work, along with a similar previous study, used extensive mobile monitoring on highly congested Inner London roads, where the influence of traffic congestion and the performance of after-treatment systems are more pronounced. [15] In contrast, the report's findings are based on a distributed network of stationary monitoring sites, where these localised traffic effects are less significant, and broader city-wide trends dominate.

These findings underscore the importance of using a range of quantification techniques to assess vehicle emissions in urban areas. Combining comprehensive mobile measurements with broader stationary monitoring data provides a more complete understanding of the impact and nuances of vehicle emission mitigation strategies like the ULEZ.

4.7 References

[1] Hammer, M. S., Donkelaar, A. van, Li, C., Lyapustin, A., Sayer, A. M., Hsu, N. C., Levy, R. C., Garay, M. J., Kalashnikova, O. V., Kahn, R. A., et al. Global estimates and long-term trends of fine particulate matter concentrations (1998–2018). *Environmental Science & Technology* 54.13 (2020), pp. 7879–7890. DOI: 10.1021/acs.est.0c01764 (cit. on p. 196).

[2] Klimont, Z., Kupiainen, K., Heyes, C., Purohit, P., Cofala, J., Rafaj, P., Borken-Kleefeld, J., and Schöpp, W. Global anthropogenic emissions of particulate matter including black carbon. *Atmospheric Chemistry and Physics* 17.14 (2017), pp. 8681–8723. DOI: 10.5194/acp-17-8681-2017 (cit. on p. 196).

[3] United Kingdom National Atmospheric Emissions Inventory. *Pollutant Information: PM_2.5*. https://naei.beis.gov.uk/overview/pollutants?pollutant_id=122. Accessed: 2024-05-17. 2021 (cit. on pp. 196, 197).

[4] United Kingdom National Atmospheric Emissions Inventory. *Pollutant Information: $PM_1$0*. https://naei.beis.gov.uk/overview/pollutants?pollutant_id=24. Accessed: 2024-05-17. 2021 (cit. on p. 196).

[5] World Health Organization. *WHO global air quality guidelines: particulate matter ($PM_{2.5}$ and PM_{10}), ozone, nitrogen dioxide, sulfur dioxide and carbon monoxide*. https://www.who.int/publications/i/item/9789240034228. Accessed: 2024-05-17. 2021 (cit. on p. 196).

[6] Department for Environment Food and Rural Affairs. *National Statistics: Particulate Matter*. https://www.gov.uk/government/statistics/air-quality-statistics/concentrations-of-particulate-matter-pm10-and-pm25#trends-in-concentrations-of-pm10-in-the-uk-1992-to-2023. Accessed: 2024-05-17. 2024 (cit. on p. 196).

[7] Marais, E. A., Kelly, J. M., Vohra, K., Li, Y., Lu, G., Hina, N., and Rowe, E. C. Impact of Legislated and Best Available Emission Control Measures on UK Particulate Matter Pollution, Premature Mortality, and Nitrogen-

Sensitive Habitats. *GeoHealth* 7.10 (2023), e2023GH000910. DOI: 10.1029/2023GH000910 (cit. on p. 196).

[8] Twigg, M. V. Controlling automotive exhaust emissions: Successes and underlying science. *Philosophical Transactions of the Royal Society A: Mathematical, Physical and Engineering Sciences* 363.1829 (2005), pp. 1013–1033. DOI: 10.1098/rsta.2005.1547 (cit. on pp. 197, 211).

[9] Giechaskiel, B., Joshi, A., Ntziachristos, L., and Dilara, P. European regulatory framework and particulate matter emissions of gasoline light-duty vehicles: A review. *Catalysts* 9.7 (2019), p. 586. DOI: 10.3390/cata19070586 (cit. on p. 197).

[10] Harrison, R. M. Airborne particulate matter. *Philosophical Transactions of the Royal Society A* 378.2183 (2020), p. 20190319. DOI: 10.1098/rsta.2019.0319 (cit. on p. 197).

[11] Monks, P., Carruthers, D., Carslaw, D., Dore, C., Harrison, R., Heal, M., Jenkin, M., Lewis, A., Stedman, J., Tomlin, A., et al. Mitigation of United Kingdom $PM_{2.5}$ Concentrations. *Air Quality Experts Group* (2015). URL: https://uk-air.defra.gov.uk/assets/documents/reports/cat11/1508060903_DEF-PB14161_Mitigation_of_UK_PM25.pdf (cit. on p. 198).

[12] Cummings, L. E., Stewart, J. D., Reist, R., Shakya, K. M., and Kremer, P. Mobile monitoring of air pollution reveals spatial and temporal variation in an urban landscape. *Frontiers in Built Environment* 7 (2021), p. 648620. DOI: 10.3389/fbuil.2021.648620 (cit. on p. 198).

[13] Apte, J. S., Messier, K. P., Gani, S., Brauer, M., Kirchstetter, T. W., Lunden, M. M., Marshall, J. D., Portier, C. J., Vermeulen, R. C., and Hamburg, S. P. High-resolution air pollution mapping with Google street view cars: exploiting big data. *Environmental science & technology* 51.12 (2017), pp. 6999–7008. DOI: 10.1021/acs.est.7b00891 (cit. on pp. 198, 207).

[14] Hu, S., Paulson, S. E., Fruin, S., Kozawa, K., Mara, S., and Winer, A. M. Observation of elevated air pollutant concentrations in a residential neighborhood

of Los Angeles California using a mobile platform. *Atmospheric environment* 51 (2012), pp. 311–319. DOI: 10.1016/j.atmosenv.2011.12.055 (cit. on p. 198).

[15] Wilde, S. E., Padilla, L. E., Farren, N. J., Alvarez, R. A., Wilson, S., Lee, J. D., Wagner, R. L., Slater, G., Peters, D., and Carslaw, D. C. Mobile monitoring reveals congestion penalty for vehicle emissions in London. *Atmospheric Environment: X* 21 (2024), p. 100241. DOI: 10.1016/j.aeaoa.2024.100241 (cit. on pp. 199, 200, 205, 206, 212, 233).

[16] Wagner, R. L., Farren, N. J., Davison, J., Young, S., Hopkins, J. R., Lewis, A. C., Carslaw, D. C., and Shaw, M. D. Application of a mobile laboratory using a selected-ion flow-tube mass spectrometer (SIFT-MS) for characterisation of volatile organic compounds and atmospheric trace gases. *Atmospheric Measurement Techniques* 14.9 (2021), pp. 6083–6100. DOI: 10.5194/amt-14-6083-2021 (cit. on p. 200).

[17] PALAS. *AQ Guard System Information*. https://www.palas.de/en/product/aq-guard?save=accept. Accessed: 2023-04-24. 2024 (cit. on p. 201).

[18] Airyx. *ICAD in situ NO_x monitor*. https://airyx.de/item/icad/. Accessed: 2023-04-24. 2024 (cit. on p. 202).

[19] Thermo Fischer Scientific. *Model 43i SO_2 analyzer*. https://www.thermofisher.com/order/catalog/product/43I. Accessed: 2023-04-24. 2024 (cit. on p. 202).

[20] The London Plan 2021. *Annex 2 - Inner and Outer London Boroughs*. https://www.london.gov.uk/programmes-strategies/planning/london-plan/the-london-plan-2021-online/annex-2-inner-and-outer-london-boroughs. Accessed: 2023-05-17. 2021 (cit. on p. 203).

[21] Padilla, L. E., Ma, G. Q., Peters, D., Dupuy-Todd, M., Forsyth, E., Stidworthy, A., Mills, J., Bell, S., Hayward, I., Coppin, G., et al. New methods to derive street-scale spatial patterns of air pollution from mobile monitoring. *Atmospheric environment* 270 (2022), p. 118851. DOI: 10.1016/j.atmosenv.2021.118851 (cit. on p. 204).

[22] Karagulian, F., Belis, C. A., Dora, C. F. C., Prüss-Ustün, A. M., Bonjour, S., Adair-Rohani, H., and Amann, M. Contributions to cities' ambient particulate matter (PM): A systematic review of local source contributions at global level. *Atmospheric environment* 120 (2015), pp. 475–483. DOI: 10.1016/j.atmosenv.2015.08.087 (cit. on pp. 206, 209).

[23] Elser, M., Bozzetti, C., El-Haddad, I., Maasikmets, M., Teinemaa, E., Richter, R., Wolf, R., Slowik, J. G., Baltensperger, U., and Prévôt, A. S. Urban increments of gaseous and aerosol pollutants and their sources using mobile aerosol mass spectrometry measurements. *Atmospheric Chemistry and Physics* 16.11 (2016), pp. 7117–7134. DOI: 10.5194/acp-16-7117-2016 (cit. on pp. 206, 209).

[24] Saha, P. K., Presto, A. A., Hankey, S., Murphy, B. N., Allen, C., Zhang, W., Marshall, J. D., and Robinson, A. L. National exposure models for source-specific primary particulate matter concentrations using aerosol mass spectrometry data. *Environmental Science & Technology* 56.20 (2022), pp. 14284–14295. DOI: 10.1021/acs.est.2c03398 (cit. on pp. 206, 209, 230).

[25] Harrison, R. M., Deacon, A. R., Jones, M. R., and Appleby, R. S. Sources and processes affecting concentrations of PM_{10} and $PM_{2.5}$ particulate matter in Birmingham (UK). *Atmospheric environment* 31.24 (1997), pp. 4103–4117. DOI: 10.1016/S1352-2310(97)00296-3 (cit. on p. 206).

[26] Latha, K. M. and Highwood, E. Studies on particulate matter (PM_{10}) and its precursors over urban environment of Reading, UK. *Journal of Quantitative Spectroscopy and Radiative Transfer* 101.2 (2006), pp. 367–379. DOI: 10.1016/j.jqsrt.2005.11.067 (cit. on p. 206).

[27] Jandacka, D. and Durcanska, D. Differentiation of particulate matter sources based on the chemical composition of PM_{10} in functional urban areas. *Atmosphere* 10.10 (2019), p. 583. DOI: 10.3390/atmos10100583 (cit. on p. 206).

[28] Matthaios, V. N., Lawrence, J., Martins, M. A., Ferguson, S. T., Wolfson, J. M., Harrison, R. M., and Koutrakis, P. Quantifying factors affecting contributions of roadway exhaust and non-exhaust emissions to ambient $PM1_{10-2.5}$ and

$PM_{2.5-0.2}$ particles. *Science of The Total Environment* 835 (2022), p. 155368. DOI: 10.1016/j.scitotenv.2022.155368 (cit. on pp. 206, 209, 210).

[29] Font, A., Baker, T., Mudway, I. S., Purdie, E., Dunster, C., and Fuller, G. W. Degradation in urban air quality from construction activity and increased traffic arising from a road widening scheme. *Science of the Total Environment* 497 (2014), pp. 123–132. DOI: 10.1016/j.scitotenv.2014.07.060 (cit. on p. 206).

[30] Schraufnagel, D. E. The health effects of ultrafine particles. *Experimental & molecular medicine* 52.3 (2020), pp. 311–317. DOI: 10.1038/s12276-020-0403-3 (cit. on p. 206).

[31] Harrison, R. M., Shi, J. P., Xi, S., Khan, A., Mark, D., Kinnersley, R., and Yin, J. Measurement of number, mass and size distribution of particles in the atmosphere. *Philosophical Transactions of the Royal Society of London. Series A: Mathematical, Physical and Engineering Sciences* 358.1775 (2000), pp. 2567–2580. DOI: doi.org/10.1098/rsta.2000.0669 (cit. on p. 206).

[32] Kumar, P., Robins, A., Vardoulakis, S., and Britter, R. A review of the characteristics of nanoparticles in the urban atmosphere and the prospects for developing regulatory controls. *Atmospheric Environment* 44.39 (2010), pp. 5035–5052. DOI: 10.1016/j.atmosenv.2010.08.016 (cit. on p. 206).

[33] Miller, D. J., Actkinson, B., Padilla, L., Griffin, R. J., Moore, K., Lewis, P. G. T., Gardner-Frolick, R., Craft, E., Portier, C. J., Hamburg, S. P., et al. Characterizing elevated urban air pollutant spatial patterns with mobile monitoring in Houston, Texas. *Environmental Science & Technology* 54.4 (2020), pp. 2133–2142. DOI: 10.1021/acs.est.9b05523 (cit. on p. 207).

[34] R Core Team. *R: A language and environment for statistical computing. R Foundation for Statistical Computing*. 2013 (cit. on p. 207).

[35] Wilde, S. *mobilemeasr: Tools to Perform Data Analysis on Mobile Measurements*. 2022 (cit. on p. 207).

[36] Watson, A. Y., Bates, R. R., and Kennedy, D. *Atmospheric transport and dispersion of air pollutants associated with vehicular emissions*. National Academies Press (US), 1988 (cit. on p. 207).

[37] Wood, S. N. *mgcv: Mixed GAM Computation Vehicle with Automatic Smoothness Estimation*. 2017 (cit. on p. 208).

[38] Song, R., Presto, A. A., Saha, P., Zimmerman, N., Ellis, A., and Subramanian, R. Spatial variations in urban air pollution: impacts of diesel bus traffic and restaurant cooking at small scales. *Air Quality, Atmosphere & Health* 14.12 (2021), pp. 2059–2072. DOI: 10.1007/s11869-021-01078-8 (cit. on pp. 209, 230).

[39] Department for Transport. *Transport and environment statistics: 2023*. https://www.gov.uk/government/statistics/transport-and-environment-statistics-2023/transport-and-environment-statistics-2023. Accessed: 2024-07-24. 2023 (cit. on p. 210).

[40] AECC. *Fuel quality and infrastructure legislation*. https://www.aecc.eu/legislation/fuel-quality-and-infrastructure-legislation. Accessed: 2024-03-01. 2020 (cit. on p. 219).

[41] Li, H., Zhang, Y., Li, C., Zhou, Z., Nie, X., Chen, Y., Cao, H., Liu, B., Zhang, N., Said, Z., et al. Extreme pressure and antiwear additives for lubricant: academic insights and perspectives. *The International Journal of Advanced Manufacturing Technology* 120.1 (2022), pp. 1–27. DOI: 10.1007/s00170-021-08614-x (cit. on p. 219).

[42] Tan, P., Li, Y., and Shen, H. Effect of lubricant sulfur on the morphology and elemental composition of diesel exhaust particles. *Journal of Environmental Sciences* 55 (2017), pp. 354–362. DOI: 10.1016/j.jes.2017.01.014 (cit. on pp. 219, 220).

[43] Lyu, X., Liang, X., Wang, Y., Wang, Y., Zhao, B., Shu, G., Tian, H., and Wang, K. Influence of lubricants on particulate matter emission from internal combustion engines: A review. *Fuel* 366 (2024), p. 131317. DOI: 10.1016/j.fuel.2024.131317 (cit. on p. 220).

[44] Plumley, M. J. Lubricant oil consumption effects on diesel exhaust ash emissions using a sulfur dioxide trace technique and thermogravimetry. PhD thesis. Massachusetts Institute of Technology, 2005 (cit. on p. 220).

[45] Driver and Vehicle Licensing Agency. *Get vehicle information from DVLA*. https://www.gov.uk/get-vehicle-information-from-dvla. Accessed: 2024-03-01. 2024 (cit. on p. 221).

[46] Ghaffarpasand, O., Ropkins, K., Beddows, D. C., and Pope, F. D. Detecting high emitting vehicle subsets using emission remote sensing systems. *Science of the Total Environment* 858 (2023), p. 159814. DOI: 10.1016/j.scitotenv.2022.159814 (cit. on p. 222).

[47] Wang, J., Jeong, C.-H., Zimmerman, N., Healy, R., Wang, D., Ke, F., and Evans, G. J. Plume-based analysis of vehicle fleet air pollutant emissions and the contribution from high emitters. *Atmospheric Measurement Techniques* 8.8 (2015), pp. 3263–3275. DOI: 10.5194/amt-8-3263-2015 (cit. on p. 222).

[48] Luan, T., Guo, X., Zhang, T., and Guo, L. Below-cloud aerosol scavenging by different-intensity rains in Beijing city. *Journal of Meteorological Research* 33.1 (2019), pp. 126–137. DOI: 10.1007/s13351-019-8079-0 (cit. on p. 226).

[49] Amato, F., Schaap, M., Gon, H. A. D. van der, Pandolfi, M., Alastuey, A., Keuken, M., and Querol, X. Effect of rain events on the mobility of road dust load in two Dutch and Spanish roads. *Atmospheric Environment* 62 (2012), pp. 352–358. DOI: 10.1016/j.atmosenv.2012.08.042 (cit. on p. 226).

[50] Greater London Authority. *London-Wide Ultra Low Emission Zone - One Year Report*. https://www.london.gov.uk/programmes-strategies/environment-and-climate-change/environment-and-climate-change-publications/london-wide-ultra-low-emission-zone-one-year-report. 2025 (cit. on p. 232).

[51] Zhai, M. and Wolff, H. Air pollution and urban road transport: Evidence from the world's largest low-emission zone in London. *Environmental Economics and Policy Studies* (2021), pp. 1–28. DOI: 10.1007/s10018-021-00307-9 (cit. on p. 232).

Chapter 5

Conclusion

5.1 Summary

Air pollution is a global issue that impacts nations at every stage of economic development and is attributable to 8.1 million deaths annually. Urban areas, where the majority of the world's population resides, are disproportionately affected due to a combination of high ambient pollutant concentrations and population density. Understanding and mitigating urban air pollution, therefore, remains one of the most important global challenges.

Road transport, while providing numerous societal benefits, is still a significant and complex contributor to urban air pollution. Although research-informed policy has led to reductions in vehicle emissions, no level of air pollution exposure is considered safe, and further reductions are necessary. This is especially true for regions where growing and ageing populations will see disproportionate benefits from future reductions and those that have yet to experience the full benefits of existing measures.

Ensuring the success of current and future mitigation strategies requires robust quantification and a deep understanding of the factors influencing road transport emissions. While many established techniques remain valuable, innovation and the next generation of research will be critical in shaping future policy decisions.

This thesis presents three interconnected research chapters unified by the overarching theme of extracting more information from fast-response individual vehicle emissions measurements to better understand the factors driving elevated pollutant concentrations in urban areas, from the local roadside environment to a national scale. A recurring theme is the positive impact of past efforts in reducing vehicle emissions while also identifying their shortcomings and new areas of focus as road transport emissions continue to decline. This process of understanding, refining, and advancing is what ultimately drives progress.

5.2 Contributions

The analysis of over 600,000 individual vehicle remote sensing measurements from more than 70 urban locations across the UK in Chapter 2 demonstrates the utility of this technique in quantifying and evaluating vehicle emissions at a national level. Aggregating these measurements to assess decade-long emissions trends had not been previously achieved. This work lays the foundation for such analysis, enabling the separation of emissions data from fleet composition information, which allows for modelling and comparing different scenarios to evaluate the impact of policy decisions.

The revealed emissions trends highlight the success of vehicle emission standards in reducing emissions from modern vehicles in the UK, with sufficient resolution to directly observe the impacts of policy changes and the introduction of nitrogen oxides (NO_x = NO + NO_2) specific after-treatment systems around 2015. Additionally, these trends provided an early indication of emerging concerns, such as rising passenger car ammonia (NH_3) emissions starting in the late 2010s, resulting from a shift towards gasoline and gasoline hybrid vehicles.

The evaluation of the promotion and subsequent decline of diesel fuel use highlights the importance of considering air quality in all related policy decisions. The promotion of diesel between 2001 and 2015 resulted in an additional 712 kt of total vehicular NO_x emissions in the UK. These excess NO_x emissions have caused a range of serious direct and indirect consequences that will persist far beyond the lifespan of the policy responsible. In addition to the local health impacts of increased NO_2 concentrations nationwide, the excess NO_x contributes to the formation of secondary PM and ozone (O_3) at a regional level (Section 1.2.3). Moreover, this quantity of NO_x is likely linked to various environmental impacts, such as eutrophication and reduced biodiversity caused by nitrogen deposition (Section 1.1.2). This work serves as a

clear example of how unintended consequences can arise when air quality is not adequately considered in policy design, leading to outcomes that may take decades to resolve.

While much attention is given to vehicle emissions at their source, understanding what happens between exhaust exit and human inhalation is essential for assessing exposure – the factor that ultimately determines health impacts. Using point sampling techniques and a recently developed plume regression approach, Chapter 3 explores how the physical characteristics of vehicles influence traffic-related air pollution (TRAP) concentrations near roads, namely exhaust position and aerodynamic properties.

Although the point sampling campaign used here was not originally designed to study these effects, the findings highlight the value of this novel technique, demonstrating that it is capable of extracting more than just emission rate information from passing vehicles. For example, the approximation of vehicle-induced turbulence from movement and technical information and the impact of this variable on near-road TRAP concentrations. The results show that dispersion effects driven by vehicle physical properties do impact near-road TRAP concentrations, and importantly, they suggest that non-emission interventions – such as exhaust relocation – could mitigate human exposure by reducing roadside TRAP concentration contributions from vehicles by up to a third. These insights emphasise the importance of considering near-road dispersion effects when developing future air quality strategies, broadening the focus beyond emission reduction alone.

This chapter also demonstrates the value of fast-response roadside measurements, with the increased understanding of roadside dispersion effects having implications for the thousands of near-road ambient air quality monitoring sites, despite their typically longer averaging times (Section 1.4.4). Moreover, this work suggests that upgrading these sites with faster-response instrumentation and the capacity to capture data on passing vehicles – read-

ily achievable with advances in automatic number plate recognition (ANPR) technology – could enable the development of a network of permanent point sampling monitoring sites, facilitating a more comprehensive evaluation of vehicle emissions.

An additional result from this work was the first evidence that vehicle electrification may offer local air quality benefits beyond emission reduction. The findings indicate that electric vehicles (EVs) reduce roadside TRAP concentrations. The turbulence generated by EVs acts to dilute the exhaust plumes from surrounding fossil-fuelled vehicles, improving air quality in the near-road environments that comprise the majority of urban areas. This result highlights a previously unrecognised benefit of fleet electrification.

Chapter 4 explores vehicle emissions using mobile monitoring to quantify the spatial distribution of two particulate matter (PM) size fractions in Central and Outer London. At both locations, measured concentration increments above background suggest that road-vehicle-derived fine (PM_{fine} = $PM_{2.5}$) and coarse (PM_{coarse} = PM_{10}- $PM_{2.5}$) particulate matter are well controlled. This finding reflects the widespread adoption of diesel particulate filters (DPFs) and gasoline particulate filters (GPFs) (Section 1.2.2). Unlike NO_x-specific after-treatment systems, DPF and GPF operation was found to be largely unaffected by the highly congested traffic conditions of Central London. Instead, the average condition of the vehicle fleet plays a more significant role, with the cleaner and newer vehicles inside the Ultra Low Emission Zone (ULEZ) contributing to lower measured PM_{fine} concentration increments.

Despite the generally well-controlled vehicular PM emissions, two important sources were identified for further reducing urban PM concentrations in London. The first was individual high-PM-emitting vehicles in Outer London, which were malfunctioning and burning engine lubricant during combustion, resulting in PM_{fine} concentration increments of up to

200 μg m^{-3}, 40 times higher than the average concentration increment at this location. Co-emission of sulfur dioxide (SO_2), a tracer of engine lubricant combustion, confirmed this source. Onboard camera footage from the mobile laboratory identified these vehicles as pre-GPF gasoline models, one of which subsequently failed its periodic technical inspection (PTI) in the months following the campaign (Section 1.3.3). The detection of two high-emitting vehicles during the study demonstrates the utility of mobile monitoring for identifying these vehicles in urban areas.

The second important source was construction activity. The spatial distributions of PM_{coarse} in Central and Outer London revealed two major construction sites, one at each location. Onboard camera footage confirmed the sites and a novel analytical technique was used to quantify the decline in their contribution to local ambient PM concentrations. Both sites were associated with maximum average PM_{coarse} concentration increments of 23 and 8 μg m^{-3} in Central and Outer London, respectively, which fell off within 500 m of the site centre. The PM_{coarse} contribution from the Central London site was highly weather-dependent, with the maximum average concentration increment declining by 62% in wet conditions. These findings highlight non-vehicular sources as increasingly important contributors to the controllable fraction of urban PM and demonstrate the value of mobile monitoring for identifying sources that are difficult to detect with more traditional stationary monitoring techniques.

Similar to Chapter 3, this work highlights the effectiveness of fast-response pollutant measurements in urban areas. In a single mobile monitoring campaign, the effectiveness of city-wide policy implementation was evaluated, individual high-emitting vehicles were detected, and previously unrecognised stationary non-vehicular PM sources were identified.

5.3 Future Directions

The work presented here offers a variety of opportunities for improvement and extension. The remote sensing analysis in Chapter 2 was primarily limited by the relatively small number of measurements of older and very new vehicles. As the technique becomes more widely adopted and the amount of available measurements increases, these limitations will diminish. The method presented in this thesis could, therefore, be applied to evaluate the emissions impact of other changes in the vehicle fleet, given its strength in determining emissions as a function of vehicle properties (fuel type in the case of this work). One example which was considered for exploration is the increasing presence of light goods vehicles (LGVs) in the UK fleet due to the rise of online shopping and fulfilment. The remote sensing technique provides a valuable tool to assess how this trend has influenced UK vehicle emissions. Portable emissions measurement system (PEMS) testing is also becoming more prevalent, increasing the availability of drive cycle data necessary for converting fuel-based emission factors into distance-based ones – an essential step in this analysis.

To build on this work and fully understand the implications of the additional 721 kt of NO_x emissions resulting from the promotion of diesel fuel in the UK – along with similar impacts in other European countries that implemented comparable policies – regional-scale air quality modelling could be performed. This approach could also offer an opportunity to evaluate the consequences of increasing NH_3 emissions from gasoline and gasoline-hybrid vehicles and how these compare with the reduction in NO_x emissions following the demise of diesel fuel use.

With respect to point sampling, the work presented in Chapter 3 is based on a relatively small number of local vehicle measurements and is exploratory in nature. As such, there are many ways future research could

build upon the findings. First, fast-response point sampling experiments using a tracer gas (such as methane) to simulate different exhaust positions and orientations could improve understanding of how exhaust position effects change with increasing lateral and vertical distance from the road. This work would provide insight into the effect of exhaust position on human exposure to TRAP in different urban environments. It could be extended with a dedicated real-world point sampling campaign focused on exhaust position, using a lower-positioned camera to better capture exhaust images or a thermal camera to enhance detection. Conducting measurements on both sides of the road would further strengthen the results.

Vehicle-induced turbulence and its effect on near-road TRAP concentrations could be better quantified by coupling point sampling with direct measurements of turbulent kinetic energy (TKE) using a sonic anemometer. Such studies would also help clarify the role of EVs in reducing roadside TRAP concentrations. Given the increasing share of EVs in the UK vehicle fleet, this is a particularly important area of research. Future work could investigate how this shift influences the magnitude of concentration reductions and whether these effects diminish as fossil-fuelled vehicles become less prevalent.

The mobile monitoring work in Chapter 4 did not include ultra-fine particulate matter ($PM_{0.1}$) measurements, which are linked to the most severe PM-related health effects and may not be as effectively reduced by diesel and gasoline particulate filters (DPFs and GPFs) (Section 1.1.2). A similar campaign that includes $PM_{0.1}$ measurements would help determine whether trends for ultra-fine PM align with those observed for PM_{fine} and PM_{coarse} and would help to identify sources to target.

Additionally, the influence of border effects, where emissions outside a low-emission zone (LEZ) change due to the presence of the zone, was not addressed in this thesis (Section 1.3.2). While comparing Central Lon-

don (inside the ULEZ) with Outer London (on the ULEZ border) provided valuable insights into fleet composition and congestion effects on PM emissions, a more robust study design could include an additional measurement site further from the ULEZ boundary to assess these border effects more comprehensively.

This thesis demonstrates the value of combining different measurement techniques to extract more from vehicle emissions data. While each method has stand-alone value, innovation can be derived by combining them. For example, mobile monitoring is effective for identifying high emission vehicles but is limited by the lack of individual vehicle information. Developing a mobile ANPR camera system to track vehicles near the mobile laboratory could provide technical information about nearby vehicles, adding a new dimension to the data. Combining this with a plume regression type analysis could create a more powerful vehicle emission quantification method, extending the applications of point sampling beyond a single stationary site.

5.4 Final Remarks

Vehicle emissions remain a significant contributor to urban air pollution. The last century has seen the mass adoption of road transport, the substantial benefits it has provided, and the realisation of the harm that it can cause. Decades of research have begun to uncover the complex role of vehicle emissions in urban air pollution, and this knowledge has been effectively applied to mitigate many of the associated health risks.

However, at the time of writing this thesis, the UK and global road vehicle fleet has never been larger, more diverse, or so rapidly changing. It is, therefore, essential to continue to measure and understand vehicle emissions to ensure that policy decisions are effective at sustained mitigation of the harmful effects of air pollution and that they do not incur additional unintended consequences. It is hoped that this thesis has demonstrated the value of such measurements and their associated analyses, and that future research will build upon them.

Appendix A

Vehicle Measurement Device

A.1 Design

Vehicle emission point sampling, described in Section 1.4.4 and Chapter 3, is a relatively new and developing technique. An important element of point sampling data is knowing when vehicles pass the emissions measurement apparatus and the properties of each vehicle. Since no commercial point sampling system currently exists, a custom Vehicle Measurement Device (VMD) was constructed to be used alongside emissions measurement instruments to facilitate point sampling measurements.

The VMD records the pass time for each vehicle, measures its movement (speed and acceleration), and captures a photograph of its registration number (license plate). The registration number is then cross-referenced with a technical database to obtain vehicle-specific details, including vehicle type, fuel type, emission standard, and model year. The system was deployed in a 2023 point sampling campaign in York, UK, where it recorded 11,264 vehicle passes. The VMD is comprised of three main components.

1. Sensor Unit: This powered component contains two retro-reflective photoelectric sensors (Sick GL10-R9811 dual lens), an Arduino Uno microcontroller, and a DC-DC converter (12V–24V).

2. Reflector Unit: This unpowered component houses two reflectors (Sick P250) aligned with the sensors of the sensor unit.

3. Camera Unit: This powered component (AXIS V5914 PTZ camera) captures images of vehicle registration numbers.

A diagram of the complete VMD setup is shown in Figure A.1. The system is operated by and records data to a single control laptop, which is also used to interface with the emissions measurement instruments.

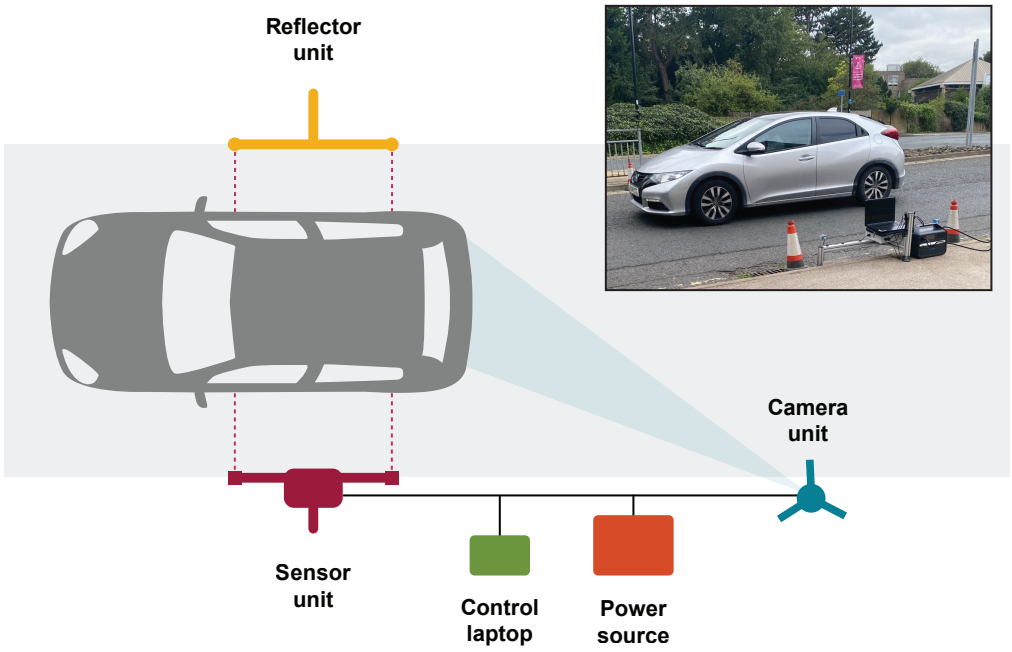

Figure A.1: Diagram and photograph of the VMD setup.

Hardware

The VMD was used across a single lane of road, with the sensor unit and camera system positioned on one side, approximately 5 m apart, and the reflector unit aligned on the opposite side of the lane. The sensor unit and camera system can be powered by a single 12 V DC source, such as those commonly found in vehicles or portable power stations.

Designed for full weather resistance, the VMD's electronic components are housed in an IP65-rated acrylonitrile butadiene styrene (ABS) enclosure, with threaded waterproof bulkhead connectors for wiring. The camera system is enclosed in a polypropylene housing with a transparent rain cover that can be fitted during adverse weather conditions. A schematic representation of the wiring diagram for the powered sensor unit and camera unit of the VMD is shown in Figure A.2.

The sensor and reflector units were designed to be highly adjustable, allowing for easy alignment at the roadside, accommodating raised curbs

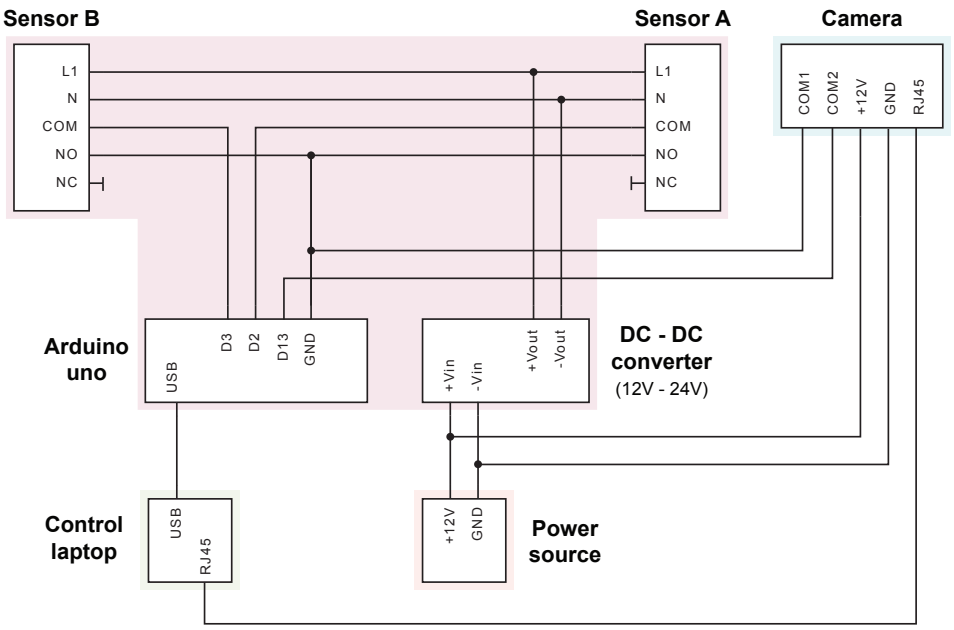

Figure A.2: Wiring diagram for the VMD sensor unit and camera unit.

and other urban features. The camera unit was mounted on a tripod approximately 5 m away from the sensor and reflector units and aligned to capture photographs of the rear of passing vehicles. The camera position and settings can be adjusted on the control laptop to minimise glare from sunlight and maximise registration number capture.

The sensors operate by emitting a beam of light that is reflected back to an integrated detector by the reflector unit when no vehicle is present. When a vehicle sequentially interrupted the beams, the Arduino microcontroller records the time of each interruption with millisecond accuracy, enabling the calculation of vehicle speed and acceleration using the equations of motion. The distance between the sensors is fixed at 1.37 m, and the sensor placement was approximately 0.25 m above the road surface. The maximum tested distance between the sensors and reflectors (effective road width) was 10 m. The Arduino microcontroller that records the sensor data relays it to a control laptop via a USB serial interface (baud rate 9600), where the data are

stored.

The camera unit is wired directly to the Arduino microcontroller, ensuring that a photo is taken at the exact moment a vehicle passes. Photos taken by the camera are transferred via a wired (RJ45) connection to a file transfer protocol (FTP) server on the control laptop, where they are stored alongside the sensor data.

Software

The script in Listing A.1 was written for the Arduino microcontroller in the C++ programming language. It records and relays sensor states with millisecond accuracy in real time to the control laptop, while simultaneously sending a trigger signal to the camera unit to capture a photograph.

```
// Assigning pins.
// Pin 2 used for sensor A (first in direction of trave).
int A=2;
// Pin 3 used for sensor B (second in direction of travel).
int B=3;
// Pin 13 used for camera trigger.
int C=13;
// Setting debounce interval in ms.
int debounceInterval=20;
// Setting camera trigger signal interval in ms.
int triggerInterval=100;
// Assigning strings to print.
String sensorAMade=",A0";
String sensorAUnmade=",A1";
String sensorBMade=",B0";
String sensorBUnmade=",B1";
void setup() {
// Setting up pins - input with pull up.
pinMode(A,INPUT_PULLUP);
pinMode(B, INPUT_PULLUP);
```

```
21 pinMode(C, OUTPUT);
22 // Establishing serial connection - baud rate 9600.
23 Serial.begin(9600);
24 // Setting up interrupt for sensor A.
25 // Mode set to CHANGE - will trigger interrupt whenever pin
       changes value.
26 attachInterrupt(digitalPinToInterrupt(A),isrSensorA,CHANGE);
27 attachInterrupt(digitalPinToInterrupt(B),isrSensorB,CHANGE);
28 }
29 // No code to loop.
30 void loop() {}
31 // Interrupt service routine for sensors.
32 // Triggers when pin changes value, checks time since last
       interrupt is greater
33 // than the debounce interval, checks the value of the pin,
       reports sensor state.
34 void isrSensorA() {
35 static unsigned long lastInterruptTimeA = 0;
36 unsigned long interruptTimeA = millis();
37 if (interruptTimeA - lastInterruptTimeA > debounceInterval)
38   {
39     if (digitalRead(A)==HIGH) {
40     Serial.print(millis());
41     Serial.println(sensorAUnmade);
42     digitalWrite(13, HIGH);
43   } else {
44     Serial.print(millis());
45     Serial.println(sensorAMade);
46     digitalWrite(13, LOW);
47   }
48   lastInterruptTimeA = interruptTimeA;
49   }
50 }
51 void isrSensorB() {
52 static unsigned long lastInterruptTimeB = 0;
```

```
53 unsigned long interruptTimeB = millis();
54 if (interruptTimeB - lastInterruptTimeB > debounceInterval)
55   {
56     if (digitalRead(B)==HIGH) {
57     Serial.print(millis());
58     Serial.println(sensorBUnmade);
59   } else {
60      Serial.print(millis());
61     Serial.println(sensorBMade);
62   }
63   lastInterruptTimeB = interruptTimeB;
64   }
65 }
```

Listing A.1: C++ Arduino microcontroller script for the VMD.

Vehicle Movement Calculation

The sensors are named A and B, with sensor A positioned first in the direction of travel of passing vehicles. When no vehicle is present and the sensor light beam is returned by the reflectors, both sensors have state 0. When a vehicle passes and the light beams are interrupted, both sensors have state 1. The four possible sensor state outputs from the VMD are therefore $A0$, $A1$, $B0$, and $B1$. Figure A.3 demonstrates the sensor state outputs at each stage of a typical vehicle pass.

The camera system is triggered to capture a photograph when the sensor state $A0$ is recorded, as this indicates the light beam being reformed at sensor A, corresponding to the rear of a vehicle being directly in line with the VMD. This setup enables simple camera alignment and ensures that photographs consistently captured the registration number of each passing vehicle.

The sensor state pattern for an ideal single vehicle pass is $A1$ $B1$ $A0$ $B0$. For each vehicle pass, the times t_1, t_2, and t_3 are defined as follows: t_1 represents the time taken for the vehicle to move the distance between

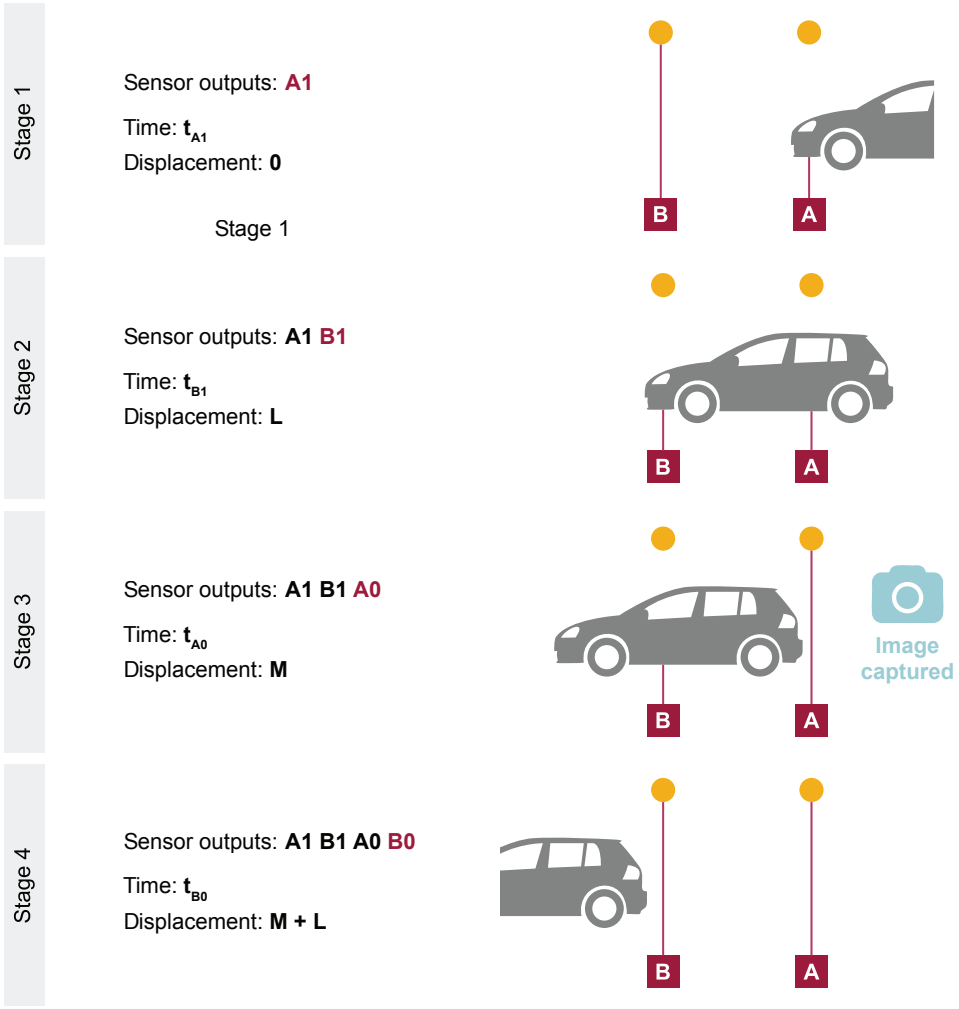

Figure A.3: Sensor state outputs for each stage of a typical vehicle pass.

sensors A and B, t_2 represents the time taken for the vehicle to fully pass sensor A, and t_3 represents the time taken for the vehicle to fully pass both sensors A and B. These times are shown with respect to the time of each sensor state in the pattern $A1\ B1\ A0\ B0$ in Equation A.1

$$\begin{aligned} t_1 &= t_{B1} - t_{A1} \\ t_2 &= t_{A0} - t_{A1} \\ t_3 &= t_{B0} - t_{A1} \end{aligned} \tag{A.1}$$

The equation of motion shown below in Equation A.2 can then be used to determine vehicle movement parameters.

$$s = u \cdot t + a \cdot \frac{t^2}{2}$$

$$\begin{aligned} s &= \text{displacement} \\ u &= \text{initial velocity} \\ a &= \text{acceleration} \\ t &= \text{time interval} \end{aligned} \tag{A.2}$$

The distance between sensors A and B is denoted as L, and the length of the vehicle as M. Therefore, for each of the times in Equation A.1, a corresponding equation of motion can be constructed where the displacement s is equal to L, M, and $L+M$ for t_1, t_2, and t_3 respectively. Constant acceleration a is assumed, and the initial velocity u taken to be the speed of the vehicle v as it first passes sensor A (t_{A1} is the start of all three time intervals). The three constructed equations of motion are shown in Equation A.3, where M, v, and a can be derived from solving the system for the measured values of t_1, t_2, and t_3 (the value of L is known).

$$\begin{aligned} L &= v \cdot t_1 + a \cdot \frac{t_1^2}{2} \\ M &= v \cdot t_2 + a \cdot \frac{t_2^2}{2} \\ L + M &= v \cdot t_3 + a \cdot \frac{t_3^2}{2} \end{aligned} \tag{A.3}$$

The system can be solved as shown in Equation A.4.

$$
\begin{aligned}
v \cdot t_1 + a \cdot \frac{t_1^2}{2} + v \cdot t_2 + a \cdot \frac{t_2^2}{2} &= v \cdot t_3 + a \cdot \frac{t_3^2}{2} \\
v \cdot (t_1 + t_2 - t_3) &= a \cdot \frac{t_3^2 - t_1^2 - t_2^2}{2} \\
v &= a \cdot \frac{t_3^2 - t_1^2 - t_2^2}{2 \cdot (t_1 + t_2 - t_3)} \\
L &= a \cdot \frac{t_3^2 - t_1^2 - t_2^2}{2 \cdot (t_1 + t_2 - t_3)} \cdot t_1 + a \cdot \frac{t_1^2}{2} \\
L &= a \cdot \frac{t_1 \cdot (t_3^2 - t_1^2 - t_2^2) + 2 \cdot t_1^2 \cdot (t_1 + t_2 - t_3)}{2 \cdot (t_1 + t_2 - t_3)} \\
a &= \frac{L \cdot 2 \cdot (t_1 + t_2 - t_3)}{t_1 \cdot (t_3^2 - t_1^2 - t_2^2) + 2 \cdot t_1^2 \cdot (t_1 + t_2 - t_3)}
\end{aligned}
\tag{A.4}
$$

For simplicity, the values of $(t_1 + t_2 - t_3)$ and $(t_3^2 - t_1^2 - t_2^2)$ can be defined as k_1 and k_2 respectively. The vehicle acceleration, speed, and length are then given by Equation A.5.

$$a = \frac{L \cdot 2 \cdot k_1}{(t_1 \cdot k_2) + (2 \cdot t_1^2 \cdot k_1)}$$

$$v = a \cdot \frac{k_2}{2 \cdot k_1} = \frac{L \cdot 2 \cdot k_1 \cdot k_2}{(2 \cdot t_1 \cdot k_2 \cdot k_1) + (4 \cdot t_1^2 \cdot k_1^2)} \tag{A.5}$$

$$M = v \cdot t_2 + a \cdot \frac{t_2^2}{2} = \frac{L \cdot 2 \cdot k_1 \cdot k_2 \cdot t_2}{(2 \cdot t_1 \cdot k_2 \cdot k_1) + (4 \cdot t_1^2 \cdot k_1^2)} + \frac{L \cdot 2 \cdot k_1 \cdot t_2^2}{(2 \cdot t_1 \cdot k_2) + (4 \cdot t_1^2 \cdot k_1)}$$

Vehicle motion calculations were performed during post-processing using the R programming language. In practice, a vehicle pass does not always follow the ideal sequence $A1$ $B1$ $A0$ $B0$. Gaps within the vehicle, such as those between a vehicle and an attached trailer, or between the wheels of vehicles with bodies elevated above the VMD sensors, can produce sensor state output patterns with additional states. However, the overall pattern remains consistent with the general form $A1...B0$.

The post-processing R script was designed to isolate individual vehicle passes based on a threshold time applied before the $A1$ sensor state and after the $B0$ sensor state. This threshold time represents the minimum possible duration between two consecutive vehicle passes. Setting the threshold too high may cause the script to incorrectly group two closely spaced vehicles as a single large vehicle, while setting it too low may split large vehicles into two smaller vehicles. A threshold of 0.5 s was suitable for the data collected during the 2023 York point sampling campaign, where the mean vehicle speed was $40.5\,\mathrm{km\,h^{-1}}$ and the mean gap between vehicles was 10.3 s.

Validity filters were applied to the calculated acceleration and speed values to exclude instances where pedestrians or cyclists passing the VMD produced sensor state patterns that led to erroneous calculations. The cut-off

values represent the extreme physical limits for each variable, as shown in Equation A.6.

$$\begin{aligned} -30\ km\ h^{-1}\ s^{-1} \ &< \ a \ < \ 30\ km\ h^{-1}\ s^{-1} \\ 0\ km\ h^{-1} \ &< \ v \ < \ 115\ km\ h^{-1} \end{aligned} \tag{A.6}$$

The vehicle pass end time (t_{A0}) was used to match the movement data with vehicle registration number photos. Automatic licence plate recognition (ALPR) software (Reckon CarCheck Plus) was used to extract registration numbers from the photos. Vehicle technical information was obtained from CDL Vehicle Information Services Limited, who source the data from the UK vehicle taxation system (DVLA) and the Society of Motor Manufacturers and Traders (SMMT) Motor Vehicle Registration Information System.

A.2 Operation

During the 2023 point sampling campaign, 11,264 vehicle passes were recorded, verified through manual review of footage from a separate camera. The VMD was able to successfully determine movement data for 11,151 vehicles (99 %), and automatically capture registration numbers and technical information for 10,624 vehicles (95 %), resulting in 9,687 vehicles (86 %) with complete movement and technical data.

Missing movement data (1 %) resulted from validity filters removing erroneously calculated values due to sensor output issues. The primary cause of these issues was cyclists passing the VMD simultaneously with the measured vehicle. Missing registration numbers (5 %) arose from various factors, including obscured or removed licence plates and glare from sunlight.

As a result of the validity filters, there were no false positive VMD vehicle pass measurements (non-vehicle sensor passes reported as vehicles).

Vehicle technical information contained dimension specifications, including exact vehicle length values, which enabled evaluation of the VMD movement calculations. The length differential was calculated as the difference between the VMD-calculated length and the technical information length. The mean length differential was 2 % for cars, 5 % for light goods vehicles (LGVs), and 4 % for buses, confirming the suitability of the movement calculation method and validating the calculated acceleration and speed values.

For heavy goods vehicles (HGVs), only 27 % of passes included length information in the technical data, with an average length discrepancy of 16 %. This larger discrepancy is likely because the VMD sensors are positioned at a height to optimize data capture for cars and LGVs. As a result, only the wheels of larger vehicles like HGVs are measured, rather than the full vehicle body referenced in the technical data.

The primary role of the VMD in point sampling is to provide vehicle pass times and technical data for the plume regression analysis in Chapter 3. However, the movement data also supports investigations into related factors, such as vehicle-induced turbulence or modelled instantaneous emission rates, and their impact on roadside pollutant concentrations, as discussed in Chapter 3. Additionally, the movement data has potential applications in other analyses. For example, speed and acceleration can indicate whether a vehicle has been travelling on the measurement road for an extended period or has recently joined from an adjoining road.

Since the 2023 York campaign, the VMD has been deployed in two further measurement campaigns: in Manchester, UK, in 2024, measuring approximately 20,000 vehicles, and in Sheffield, UK, in 2025, measuring approximately 25,000 vehicles.